# LOCAL CONTROL OF SYNAPTIC STRENGTH: NEUROTROPHIC AND DOPAMINERGIC MODULATION OF DENDRITIC PROTEIN SYNTHESIS

Thesis by

W. Bryan Smith

In Partial Fulfillment of the Requirements for the

degree of

Doctor of Philosophy

CALIFORNIA INSTITUTE OF TECHNOLOGY

Pasadena, California

2004

(Defended May 13, 2004)

# ACKNOWLEDGEMENTS

This work would not have been possible without the guidance and support of my advisor, Erin M. Schuman. Without her admonitions to focus my intellectual curiosity, and to stay on track with my projects, I would have never completed anything. I also owe a tremendous debt of gratitude to a number of professors, collaborators and colleagues: Girish Aakalu, Vivek Jayaraman, Bijan Pesaran, Shelley Starck, David Anderson, Mary Kennedy, Gilles Laurent, Henry Lester, Richard Roberts, the members of Dabney House, and members of the Schuman Lab. Their experiments, discussion, constructive criticism and support have made this work stronger and more complete than what I possibly could have accomplished on my own.

The late Norman Davidson deserves a great deal of credit for my development as a scientist. Every meeting with Norman was a tremendous learning experience, and his passion for rigor and desire to understand things at the most fundamental level will forever be an inspiration for me. In a single meeting, Norman permanently altered the degree to which I concern myself with the details of my experiments, as he berated me for something I had done: “That’s (expletive) capital D-U-M-B,” he told me. And of course, he was correct. What I was doing was idiotic, and I was not thinking carefully enough about the small details, which I have since learned makes all the difference.

My mom, Cynthia Smith, has been the most loving parent any aspiring scientist could ask for. Encouraging me as a child with books, chemistry kits, microscopes, and computers, she fostered my intellectual curiosity, and set the stage for my scientific drive.

Finally, this work is dedicated to Theodore and Holli. When frustrations mount, and the aggravations of daily life as a scientist begin to take their toll, Holli is a source of comfort and love that helps me keep it together, and continue on. Dealing with my moods and constant distraction, while accomplishing the task of raising our son, is more than I ever thought I would find in a person with whom I share my life.

# ABSTRACT

Understanding the cell biological mechanisms responsible for the plasticity of central neurons is key to our understanding of brain function. In an effort to better characterize the cell and molecular biology of individual neurons, we have studied the role of local, dendritic protein synthesis in hippocampal synaptic plasticity. Such a localized control of protein synthesis provides a means of achieving input-specificity, the observation that synapses on a given neuron are able to independently scale the strength of their connections. This property of synaptic enhancement is correlated with the encoding capacity of an individual cell: the greater the input specificity, the more information a cell can encode.

Here we show two pathways for inducing local protein synthesis, one mediated by the brain-derived neurotrophic factor, and another by the D1/D5 dopaminergic signaling system. Local protein synthesis stimulated by the dopaminergic pathway leads directly to an increase in synaptic strength by increasing production and synaptic localization of AMPA receptors, the glutamate-gated ion channels that mediate fast synaptic transmission at central synapses. We also present a set of software tools for quantitative analysis of 3-D colocalization and 2-D spatial correlation in immunofluorescence microscopy. These tools will greatly assist in exploratory data analysis of the dynamics of protein distributions in neurons and other cells.

# TABLE OF CONTENTS

# LIST OF ILLUSTRATIONS

# ABBREVIATIONS USED

| | |
|---|---|
| **5-HT** | 5-hydroxy tryptamine (serotonin) |
| **AMPA** | α-amino-3-hydroxy-5-methylsoxazole-4-propionate |
| **APV** | 2-amino-5-phosphonovaleric acid |
| **Arc** | activity-regulated cytoskeleton-associated protein |
| **BDNF** | brain-derived neurotrophic factor |
| **BGH** | bovine growth hormone |
| **CA1** | cornu ammonis 1 (a hippocampal subfield) |
| **CA3** | cornu ammonis 3 (a hippocampal subfield) |
| **CamKIIα** | calcium/calmodulin-dependent protein kinase α subunit |
| **cAMP** | cyclic adenosine monophosphate |
| **CNQX** | 6-cyano-7-nitroquinoxaline-2,3-dione |
| **CNS** | central nervous system |
| **CPE** | cytoplasmic polyadenylation element |
| **CPEB** | CPE binding protein |
| **CRE** | cAMP-responsive element |
| **DA** | dopamine |
| **DG** | dentate gyrus |
| **DHPG** | (RS)-3,5-dihydroxyphenylglycine |
| **DHX** | dihydrexidine |
| **EPSP** | excitatory postsynaptic potential |
| **F2P** | fluorescein-2-deoxycytidine-puromycin |
| **FMRP** | fragile-x mental retardation protein |
| **FRAP** | fluorescence recovery after photobleaching |
| **GAP43** | growth-associated protein 43 |
| **GFP** | green fluorescent protein |
| **HBS** | HEPES-buffered saline |
| **IRES** | internal ribosomal entry site |
| **kDa** | kilodaltons |
| **LPS** | local protein synthesis |
| **LTD** | long-term depression |
| **LTF** | long-term facilitation |
| **LTP** | long-term potentiation |
| **MAP2** | microtubule-associated protein 2 |
| **MECS** | maximum electroconvulsive shock |
| **mEPSC** | miniature excitatory postsynaptic current |

| | |
|---|---|
| **mRNA** | messenger ribonucleic acid |
| **mTOR** | mammalian target of rapamycin |
| **NMDA** | N-methyl-D-aspartate |
| **NT-3** | neurotrophin-3 |
| **PCR** | polymerase chain reaction |
| **PI** | propidium iodide |
| **PKA** | cAMP-dependent protein kinase |
| **PSD-95** | postsynaptic density protein of 95 kDa |
| **PVP** | poly-vinyl pyrolidone |
| **rRNA** | ribosomal ribonucleic acid |
| **SKF** | (R)-(+)-SKF-38393 hydrochloride |
| **SPRCs** | synapse-associated polyribosome clusters |
| **TTX** | tetrodotoxin |
| **UTR** | untranslated region |

*Chapter I*

# Introduction and

# Literature Review

# INTRODUCTION

The question of how an organism learns and remembers information essential for its survival has intrigued philosophers and scientists for hundreds of years. An old debate surrounding this issue as it relates to human beings is that of mind-body dualism, a concept first introduced in written form by the French philosopher and mathematician René Descartes. In his initial description of mental function, Descartes envisioned the mind and body as separate entities, with the soul — by way of the pineal gland — acting as the emissary between the two. Although the foundations of this argument were ultimately erroneous, Descartes made an important step toward describing something we now take for granted: the fact that physical events occurring inside the brain are responsible for all psychological phenomena.

While we now understand that the brain is the source of consciousness, it remains to be determined precisely how the brain is capable of storing and retrieving the information we describe as our thoughts, feelings and memories. Without a precise mechanistic description of the sequence of physiological events involved in storing or retrieving a memory, it may seem impossible to embark on studies of something so complicated as animal behavior. This has not, however, deterred the many scientists, philosophers and psychologists who have put forth their various theories on the subject over the course of time.

To a cellular and molecular biologist, perhaps the most influential of these theories was described in 1949 by Donald Hebb. The central premise of Hebb's postulate is as follows: When two neurons are connected to one another such that one neuron consistently and repeatedly causes the other neuron to fire, some growth process or metabolic change takes place that ultimately results in strengthening the connection between the two cells (Hebb, 1949). The essence of Hebbian plasticity has made its way into the thoughts of the general public, and is eloquently captured in the following quote by the popular novelist Tom Robbins:

> *The hand is the most wonderful instrument ever created, but it cannot act of its own accord; it is the servant of the brain. (Author's note: Well, that's the brain's story anyhow.) It reflects the kind of brain behind it by the manner and intelligence with which it performs its duties. The hand is the external reservoir of our most acute sensations. Sensations, when repeated frequently, have the capacity to mold and mark.*
>
> *Even Cowgirls Get the Blues*

**Long-Term Potentiation**

While it now seems intuitively obvious to a neuroscientist that repetitive, correlated activation of one neuron by another will enhance the communication between the two cells, direct experimental evidence of synaptic plasticity — the dynamic modification of synaptic strength between neurons of the central nervous system — was not described in a mammalian system until 1973, nearly 25 years after Hebb's insightful hypothesis. This seminal finding was the initial characterization of long-term potentiation (LTP). Working *in vivo* in the hippocampus, a region of the brain previously implicated in memory

formation, Bliss and Lømo induced LTP by delivering a series of high-frequency electrical pulses to the perforant path axons that innervate the dentate gyrus (Bliss and Gardner-Medwin, 1973). When the field excitatory postsynaptic potential (fEPSP) was measured following the high-frequency stimulus, Bliss and Lømo observed a sustained increase in the strength of activated synapses (shown schematically in Figure 1.1D).

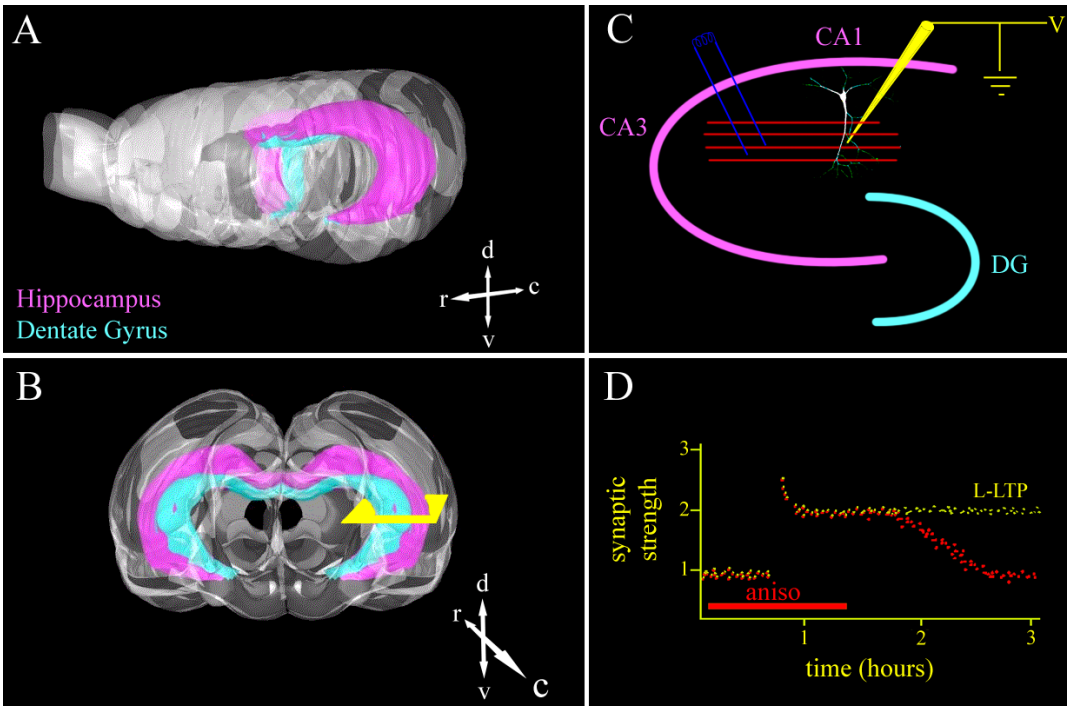


**Figure 1.1** The Hippocampus and Long-Term Potentiation

Panels A and B show two 3-D models of the rat brain in different orientations as described by the anatomical coordinate axes (r: rostral, c: caudal, d: dorsal, and v: ventral). The locations of the Dentate Gyrus and Hippocampal Formation are shown as cyan and magenta surfaces, respectively. A representative slice setup of the hippocampus for an LTP experiment, taken from the yellow plane in panel B, is show as a schematic in C. The three subfields are labeled as DG (dentate gyrus), CA1 and CA3 (*cornu ammonis* fields 1 and 3). A stimulating electrode (blue) and recording electrode (yellow) are also indicated. The protein synthesis-dependence of L-LTP is schematized in panel D: long-lasting synaptic enhancement, measured as an increase in synaptic strength above the baseline, can endure for several hours (yellow dots), but when LTP is induced in the presence of the protein synthesis inhibitor anisomycin (aniso), the LTP decays back to baseline within a couple hours (red dots).

The question of whether or not LTP is the mechanism employed in the brain for memory formation has not been confirmed, although it is a widely held belief that some form of synaptic plasticity is an important physical mechanism underlying learning and memory (Stevens, 1998). Several key attributes of LTP in hippocampal area CA1 make it an attractive candidate mechanism for memory encoding: cooperativity, associativity, temporal persistence, and input-specificity. Of these properties, the most obvious in terms of understanding the relevance of LTP to memory formation is that of temporal persistence. In order for synaptic plasticity, such as that seen in LTP, to be considered as a plausible cellular mechanism for memory formation, it must be true that the synaptic enhancement lasts sufficiently long for the memory to be encoded. Indeed, certain forms of late-phase LTP (L-LTP) in hippocampal slices will endure as long as the slice remains alive (Reymann et al., 1985), and LTP recorded in living animals lasts from several days to weeks (Bliss and Gardner-Medwin, 1973; Leung and Shen, 1995; Staubli and Lynch, 1987). While memories can easily last longer than LTP has ever been recorded, this does not discount LTP as a potential memory encoding device: it is possible that a separate mechanism is responsible for the long-term storage of a memory once it has been encoded (Bliss and Collingridge, 1993).

The properties of cooperativity and associativity result from the fact that LTP in some regions of the brain, including the Schaffer collateral/CA1 synapses, requires coordinated activity of pre- and post-synaptic neurons in order to activate the N-methyl-D-aspartate (NMDA) type of glutamate receptors (Collingridge et al., 1983). At normal resting membrane potentials, NMDA receptor ion channels do not conduct any current

because they are blocked by a $Mg^{2+}$ ion (Mayer et al., 1984). When a sufficiently large group of axons impinging on a given cell fire action potentials together (cooperativity) and/or when the postsynaptic neuron is sufficiently depolarized while receiving glutamatergic input (associativity), the $Mg^{2+}$ blockade of NMDA receptors is relieved, allowing depolarizing ionic current — and calcium ions in particular — to pass through the open channels.

**Silent Synapses**

The molecular cascades responsible for LTP induction and maintenance have been the focus of extensive research for the past 25 years. From this work has emerged the description of an interesting phenomenon that may provide a molecular mechanism for the increased synaptic communication observed in potentiated neurons. This idea, known as the silent synapse hypothesis, initially emerged in the LTP literature from experiments investigating action potential-evoked transmitter release. Because evoked release of a neurotransmitter quantum (presumed to be a single vesicle) is a probabilistic event, succeeding only 10–40% of the time (Rosenmund et al., 1993), it is possible to quantify the success and failure rates. Interestingly, a number of researchers have described a decrease in evoked failure rates after LTP induction, which initially lead researchers to conclude that LTP induces an increase in presynaptic release probability (reviewed in Kullmann and Siegelbaum, 1995).

Another possible explanation for silent synapses involves the dynamics of postsynaptic surface expression of another type of glutamate-gated ion channel, the α-

amino-3-hydroxy-5-methylsoxazole-4-propionate (AMPA) receptor. AMPA receptors mediate a majority of the fast, excitatory synaptic transmission in the brain, and unlike NMDA receptors, AMPA receptors are not blocked by $Mg^{2+}$ at resting membrane potentials. Because of this difference between the two receptor types, a synapse comprising exclusively NMDA receptors is functionally silent at a resting membrane potential whereas a synapse that contains both types of receptors is likely to generate an excitatory postsynaptic current (EPSC) in response to glutamate release.

Two independent reports (Isaac et al., 1995; Liao et al., 1995) identified postsynaptically silent synapses using whole-cell voltage clamp recordings. Under low-intensity stimulus conditions, some synapses failed to show a postsynaptic response when the neuron was held at -60 to -65 mV (potentials at which NMDARs are blocked), but responses were detected at +50 to +60 mV. The responses at positive holding potentials were blocked by APV, indicating an NMDAR origin. Furthermore, the proportion of synapses exhibiting EPSCs at -60 mV was increased after LTP induction. Since these initial electrophysiological characterizations of postsynaptically silent synapses, a number of groups have also identified 'morphological' silent synapses, or synapses that contain NMDARs but no AMPARs as determined by immunocytochemical labeling (Liao et al., 1999; Petralia et al., 1999). While these results clearly implicate postsynaptic silent synapses in LTP, a detailed account of the molecular mechanisms governing conversion into active, AMPAR-containing synapses, remains to be described.

**Input-Specificity**

An individual neuron in the mammalian CNS may contain up to ten thousand synaptic connections. Furthermore, small groups of synapses on each neuron can be independently regulated: synaptic enhancement induced at one location on the dendritic arbor does not spread throughout the entire neuron (Andersen et al., 1977; Bonhoeffer et al., 1989; Engert and Bonhoeffer, 1997; Nishiyama et al., 2000; Schuman and Madison, 1994; Tao et al., 2001). The precision with which a neuron is able to fine-tune its synaptic inputs is directly related to the encoding capacity of that individual cell: the greater the input-specificity, the more information the cell will be able to encode. In the absence of input-specificity, all inputs onto a given neuron would likely carry the same information. While the number of neurons in the brain may be sufficiently large that a single cell *could* be responsible for encoding just a single bit of information, input-specific synaptic enhancement has been observed in a number of systems, and is likely involved in the capacity of information a given network of neurons is capable of storing.

**Figure 1.2** Input-Specific Synaptic Enhancement

Shown is a simulated representation of a single hippocampal neuron during induction of synaptic plasticity. The region stimulated to induce plasticity is shown by the red plus sign in the full-scale image. As seen in the high-magnification inset image, the region of synaptic enhancement, as illustrated by the red color, is confined to only a small group of synapses in close proximity to the site of the plasticity-inducing stimulus.

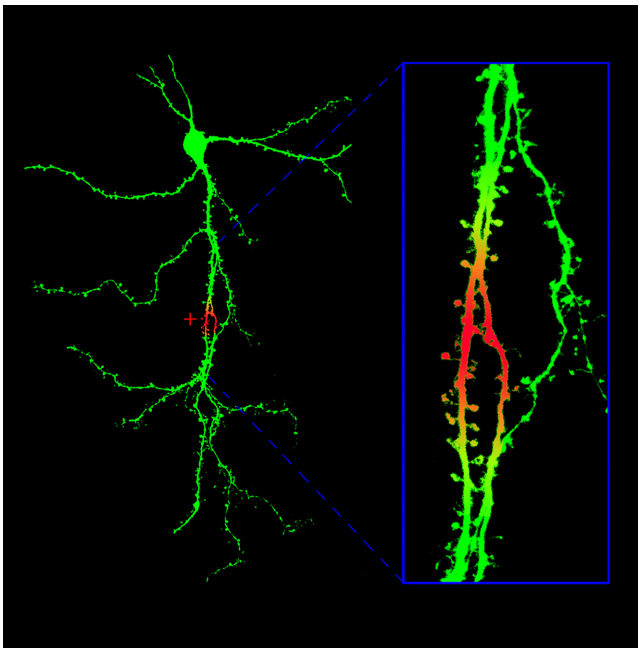

**Modulatory Transmitters and LTP**

It has been clearly established that NMDA receptor-mediated calcium influx is required for LTP induction, although a variety of modulatory signals have also been implicated in the induction and persistence of hippocampal synaptic plasticity. These include the peptide growth factors brain-derived neurotrophic factor (BDNF) and neurotrophin-3 (NT-3), as well as more classical neuromodulators such as acetylcholine, norepinephrine, and dopamine. While all of these transmitter systems likely function in a concerted, complex fashion to regulate plasticity in-vivo, my work has focused on the effects of dopaminergic signaling for the following reasons: dopamine receptor signaling can regulate levels of cyclic adenosine monophosphate (cAMP); dopaminergic signaling is critically involved in the late phase of LTP; certain forms of learning behavior require dopamine receptor activity.

The five cloned types of dopamine receptors are characterized by their G-protein-coupled effector molecules, with activation of the D1/D5 class eliciting increased cAMP production through stimulation of adenylyl cyclase (Figure 1.3). Cyclic AMP is a vital second messenger, activating the cAMP-dependent protein kinase (PKA), and the cAMP responsive element binding protein (CREB), a transcription factor that regulates the expression of genes involved in various forms of plasticity and learning and memory (Bito et al., 1996; Dash et al., 1995; Deisseroth et al., 1996; Pittenger et al., 2002).

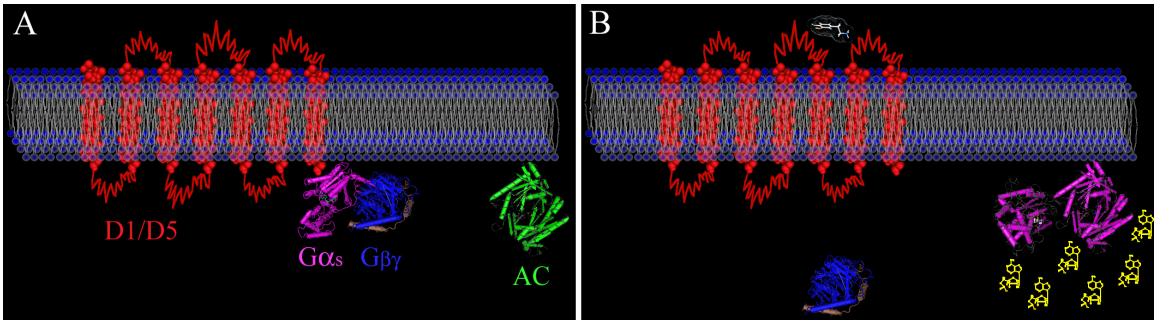


**Figure 1.3** D1/D5 Receptor Signaling

The G-protein-coupled D1/D5 receptor (shown in red as a 7-helix transmembrane protein) signals to adenylyl cyclase (AC) through the heterotrimeric G-protein complex. In the absence of Dopamine (panel A), the Gαs and Gβγ subunits are together in a complex, associated with the C-terminal end of the receptor. Upon dopamine binding (panel B), the Gαs subunit dissociates from the βγ subunit, and then stimulates the production of cAMP (yellow) via an interaction with adenylyl cyclase.

Activation of D1/D5 dopamine receptors in the hippocampus is both necessary and sufficient for the protein synthesis-dependent late phase of LTP (Frey et al., 1991; Huang and Kandel, 1995; Matthies et al., 1997). In the study by Huang and Kandel, bath application of SKF-38393, a D1/D5-selective agonist, was sufficient to induce a long-lasting form of LTP that was blocked by the protein synthesis inhibitor anisomycin (similar to the results shown in Figure 1.1D). In another study, the well-established decline in spatial memory performance observed in aged rats was attenuated by drugs that enhance the cAMP signaling pathway, including a dopamine D1/D5 agonist (Bach et al., 1999). In normal adult animals, dopamine appears to be involved in another interesting behavioral phenomenon (Li et al., 2003). In these experiments, exposure to a novel environment reduced the threshold for LTP induction in the rat hippocampus. Importantly, this decrease in the LTP threshold required dopaminergic signaling through the D1/D5 receptors, although the role of protein synthesis was not addressed. While other pathways are known

to activate cAMP signaling in neurons, such as the NMDA receptor-dependent activation of the alpha subunit of calcium/calmodulin-dependent kinase (CamKIIα; Chetkovich and Sweatt, 1993), the fact that dopamine receptor activity is both necessary and sufficient for L-LTP illustrates the importance of dopaminergic signaling in the protein synthesis-dependent phase of long-term synaptic enhancement.

Ultimately, changes in synaptic strength are achieved by modifying the complement, concentration and functional state of synaptic proteins. Such changes are affected by a variety of cellular processes, including trafficking and transport, buffering or sequestration, as well as protein synthesis and degradation. For example, in the presynaptic compartment, rapid axonal transport can provide many of the proteins and vesicles required to maintain and modulate synaptic function. In addition, the calcium-binding protein calmodulin can be buffered by the synaptic protein GAP43 (Baudier et al., 1991; Frey et al., 2000); the activity of some kinases is also effectively buffered by the binding of accessory subunits, such as the functional sequestration of PKA catalytic subunits by regulatory subunit binding. The most direct determinants of protein concentration, however, are protein synthesis and degradation. Translation and degradation are both critically involved in the regulation of protein expression; however the focus of the work described here is on the role of local protein synthesis in synaptic plasticity.

**Local Protein Synthesis in Neurons**

While there are forms of short-lasting plasticity that rely only on transient enzymatic cascades, long-lasting synaptic changes, as well as enduring memories, require

protein synthesis (Frey et al., 1988; Otani et al., 1989; Stanton and Sarvey, 1984). This requirement for protein synthesis, when considered in the context of the complexity of the dendritic tree and the input-specificity discussed above, poses an interesting question: How are newly synthesized proteins made available only at the synapses where they are needed?

At least three mechanisms may explain how neurons deliver the appropriate subset of proteins specifically to the modified synapses. In two of these, the proteins are synthesized in the cell body and then either shipped out to the correct synapses, or specifically sequestered at the enhanced synapses via an activity-dependent synaptic tag (Frey and Morris, 1997; Martin and Kosik, 2002; Schuman, 1999a). A more elegant solution to this problem, however, is provided by the local synthesis hypothesis. According to this idea, protein synthesis occurs specifically at or near synaptic sites where the new proteins are needed, thereby reducing the metabolic cost of activity-driven protein synthesis while simultaneously achieving region-specific protein delivery. Here I present the various studies that demonstrate the occurrence of local protein synthesis (LPS) and the possible roles for this cellular process in neural plasticity.

*Translation machinery*

One of the earliest hints at the existence of local protein synthesis in neuronal processes was the electron microscopic detection of polyribosomes in the dendrites of dentate granule cells in the hippocampus (Steward and Levy, 1982). In addition to observing these structures in the distal dendritic compartment, Steward and Levy noted the preferential localization of ribosomal clusters near dendritic spines. These synapse-

associated polyribosome clusters (SPRCs), situated in close proximity to the fundamental input units on CNS neurons, are positioned to respond rapidly to activity at nearby synapses.

Since Steward and Levy's initial characterization of SPRCs twenty years ago, the anatomical evidence supporting local synthesis in neurons has steadily accrued. In fact, an entire complement of translation machinery has been detected in mature neurites, including messenger RNAs, endoplasmic reticulum, and markers for Golgi membranes (Gardiol et al., 1999; Kacharmina et al., 2000; Pierce et al., 2001; Steward and Reeves, 1988; Torre and Steward, 1996). Polyribosomes found at great distances from the nucleus are typically packaged into RNA granules: aggregates of mRNA, translation initiation and elongation factors, and a host of other molecules (Ainger et al., 1993; Knowles et al., 1996; Krichevsky and Kosik, 2001). These granules, which are actively transported from the nucleus to the dendritic and axonal compartments, contain many of the components necessary to carry out regulated protein synthesis in the processes.

Of critical importance in understanding the role of LPS in synaptic plasticity has been the identification of mRNAs present in the dendrites and axons. Using standard *in situ* hybridization techniques, a number of mRNAs have been shown to exhibit somatodendritic localization (reviewed in Steward and Schuman, 2001). These include structural proteins such as MAP2 and β-actin, as well as plasticity-related proteins like CamKIIα and the NR1 subunit of the NMDA receptor. Not all of these messages, however, show identical subcellular distributions within the dendritic compartment. For

example, the NR1 mRNA appears to be limited to the proximal domain of dendrites in the hippocampus (Gazzaley et al., 1997; Miyashiro et al., 1994), whereas the mRNA for CamKIIα is seen throughout the dendritic arbor (Burgin et al., 1990; Mayford et al., 1996).

*mRNA trafficking*

A number of studies have illustrated that the subcellular distribution of some mRNA transcripts is dynamically regulated in response to neuronal activity. Using high-resolution *in situ* hybridization and immunofluorescence microscopy, Bassell and colleagues investigated β-actin mRNA dynamics in developing cortical neurons in culture. In these experiments, the mRNA appeared in distinct granules that colocalized with components of the translation machinery. Furthermore, these granules were rapidly translocated into the dendritic and axonal growth cones in response to cAMP stimulation (Bassell et al., 1998). In more mature cultured neurons, the mRNAs for BDNF and the TrkB receptor exhibited similar behavior: high potassium-induced depolarization of cultured hippocampal neurons resulted in a redistribution of these mRNA species from a proximal to a more distal dendritic localization (Tongiorgi et al., 1997).

Perhaps the most thoroughly studied example of mRNA redistribution is the dynamic regulation of the mRNA for Arc – the activity-regulated cytoskeleton-associated protein (Lyford et al., 1995; Steward et al., 1998; Wallace et al., 1998). This series of studies took advantage of an ideal hippocampal anatomy: axonal fibers innervating the dentate gyrus of the rat hippocampus are topographically distributed such that axons from a specific region of entorhinal cortex terminate in a specific layer of the dentate granule cell

dendrites. This laminar organization of the hippocampal formation allowed the authors to specifically stimulate one region of the entorhinal cortex resulting in Arc mRNA and protein accumulation precisely in the corresponding synaptic layer of the granule cell dendrites. Because these experiments were performed in mature animals in vivo, they provide very strong evidence for activity-dependent mRNA targeting to the dendrites. A caveat to this study, however, is the fact that maximum electroconvulsive shock (MECS) was used to induce the observed Arc redistribution. While this provided the authors with sufficient Arc signal to be detectable, the stimulation patterns associated with MECS may result in a pathological brain state more than the subtle stimuli that result in synaptic plasticity.

*Cis-acting RNA elements*

A considerable amount of research effort has been devoted to characterizing the cis-regulatory regions involved in dendritic transport of specific mRNA molecules. For example, sequences in the 3' untranslated region (UTR) of the CamKIIα mRNA are necessary and sufficient for dendritic RNA trafficking (Mayford et al., 1996). Transgenic mice were constructed in which the lacZ coding sequence was placed upstream of either the 3'UTR of CamKIIα or, in a control construct, the polyadenylation sequence for bovine growth hormone (BGH). In mice expressing the lacZ-CamK3'UTR, the lacZ mRNA and protein exhibited punctate distribution in the distal dendrites, while the control construct showed little or no dendritic localization. More recent data from the Mayford lab indicate that the 3'UTR of CamKIIα is necessary for sustained long-term potentiation (LTP) and memory consolidation (Miller et al., 2002). Using a targeted transgene approach, the

authors replaced the 3'UTR of CamKIIα in mice with the BGH 3'UTR. The mutant mice showed dramatically altered CamKIIα mRNA distribution, with a majority of the transcripts being confined to the cell body layers in hippocampus and cortex. Consequently, the dendritic localization of the CamKIIα protein was reduced by over 75 percent. Hippocampal slices prepared from these mutant mice exhibited decreased late-phase LTP. In addition, in an important step toward implicating LPS in behavior, the mutants in this study were impaired in spatial as well as non-spatial memory tasks.

The trafficking of mRNAs in dendrites and axons is likely as dynamic as the trafficking of proteins. In an elegant set of experiments, Kosik and colleagues labeled the 3'UTR of the CamKIIα mRNA using a GFP/MS2 bacteriophage tagging system (Bertrand et al., 1998; Rook et al., 2000). In cultured hippocampal neurons, the authors described three distinct types of motion of the GFP-tagged 3'UTR: oscillatory motion, anterograde transport and retrograde transport, with motion being skewed toward anterograde transport upon depolarization. Of particular interest in this study was the fact that the GFP-tagged CamKIIα 3'UTR was shown to colocalize with synaptic markers as determined by immunofluorescence microscopy. Taken together, these results demonstrate that depolarizing stimuli are capable of driving CamKIIα mRNA into synaptic sites.

*RNA-binding and transport proteins*

Given that all mRNA synthesis occurs in the cell nucleus, an important question regarding mRNA transport concerns the identity of the molecular machinery involved in exporting RNA granules from the soma out to the dendrites. A tremendous amount of

information from developmental biology has been particularly instructive in this regard. For example, in the early stages of *Drosophila* development, a number of RNA-binding proteins are involved in the asymmetric distribution of mRNA and protein in the fertilized oocyte, which ultimately results in establishment of the anterior-posterior axis of the organism. A critical protein in this developmental process is the RNA-binding protein Staufen, which binds the 3'UTR of maternal mRNAs and transports them throughout the oocyte and developing embryo in a microtubule-dependent manner (Ferrandon et al., 1994; St. Johnston et al., 1991).

The essential role of Staufen in *Drosophila* development prompted the cloning of mammalian Staufen homologues by three independent groups (DesGroseillers et al., 2001; Kiebler et al., 1999; Tang et al., 2001; Wickham et al., 1999). As one of these studies illustrates, the mammalian Staufen proteins are also intimately involved with RNA transport in neurons; overexpression of full-length Staufen results in an increase in total RNA in dendrites (Tang et al., 2001). Conversely, overexpressing the Staufen RNA-binding domain in the absence of the putative microtubule-binding region actually reduces the overall amount of RNA detectable in neuronal processes (Tang et al., 2001). This important observation indicates that Staufen is not only sufficient for RNA transport into dendrites, but that interfering with the function of Staufen can affect overall RNA transport in the cell. While the actual necessity of Staufen for RNA transport during synaptic enhancement remains to be shown, it is clear that the RNA-binding and transport functions of this molecule serve an important function in the maintenance of RNA distributions in neurons.

*Translation regulation*

If dendritic protein synthesis plays a meaningful role in input-specific synaptic enhancement, there must be translation regulation exerted on mRNAs that are shipped out to the neuronal processes. Without such control, the mRNA may be translated anywhere within the cell and at any point in time after the mRNA has been transcribed. The post-transcriptional modification and regulation of mRNA destined for export from the soma is therefore a very meaningful component of the LPS hypothesis.

Significant progress has recently been made in understanding the regulation of mRNA translation. Rapamycin, a protein synthesis inhibitor with immunosuppressant activity, has been a useful pharmacological agent aiding investigations of regulated protein synthesis. Perhaps hinting at the existence of multiple translation regulatory systems, it has been shown that only a subset of mRNAs inside a cell at a given time are sensitive to translation inhibition by rapamycin (Jefferies et al., 1994; Terada et al., 1994). At the Aplysia sensory-motor neuron synapse, serotonin-induced facilitation is completely blocked by the general protein synthesis inhibitor emetine but only partially inhibited by rapamycin (Casadio et al., 1999). In adult hippocampal neurons, the mammalian target of rapamycin (mTOR) and other proteins involved in cap-dependent translation initiation are localized to synaptic sites (Tang et al., 2002). Furthermore, Tang and colleagues showed that rapamycin treatment of hippocampal slices selectively attenuates late-phase LTP, while completely blocking BDNF-induced synaptic enhancement. In this case, the inhibition of synaptic plasticity observed in the presence of rapamycin was remarkably similar to that observed in the presence of a general protein synthesis inhibitor (Kang and

Schuman, 1996; Kang et al., 1997). Taken together, these findings suggest that rapamycin-sensitive translation plays an important role in synaptic plasticity.

*CPE and IRES sequences*

Another potentially crucial element of translation control is the cytoplasmic polyadenylation element (CPE) and the cognate binding protein CPEB (Wells et al., 2000). Polyadenylation of mRNA transcripts is generally required for efficient translation, making temporal control over this process a candidate regulatory point in activity-driven protein synthesis. A detailed molecular analysis of CPEB signaling has revealed a putative role for this biochemical pathway in activity-driven polyadenylation and translation of the CPE-containing CamKIIα mRNA (Wu et al., 1998). In this model, an mRNA containing CPE sequences in its 3'UTR is rendered translationally dormant through an intricate series of protein-protein interactions involving CPEB, maskin, and the rate-limiting translation initiation factor eIF4E (Stebbins-Boaz et al., 1999). These messages become translationally competent as a result of aurora kinase-catalyzed polyadenylation (Huang et al., 2002), and subsequent dissolution of the maskin-eIF4E interaction via the polyadenylation binding protein (Cao and Richter, 2002). While there is much that remains to be learned in terms of understanding precisely how this process is involved in synaptic plasticity, the evidence that cytoplasmic polyadenylation is a potentially important check point has been clearly established. Further investigations of the interactions between mTOR and CPEB-mediated cascades may provide the basis for an understanding of the complete series of reactions required to initiate translation of mRNAs in an activity-dependent fashion.

The stereotypical cap-dependent translation initiation through the CPEB pathway may only be part of the story, however. Another potentially interesting component of regulated protein synthesis is the cap-independent translation mediated by internal ribosome entry sites (IRESes) present in some mRNAs. Although traditionally associated with bicistronic messages found in viral genomes, IRES sequences may also serve as regulators of protein synthesis in eukaryotic mRNAs. Importantly, IRESes have been identified in a number of dendritically localized messages, including Arc, CamKIIα, and neurogranin (Pinkstaff et al., 2001). Of particular interest is the observation that the neurogranin IRES confers preferential cap-independent translation initiation in the dendrites, while protein synthesis regulation in the soma is mediated by a cap-dependent mechanism (Pinkstaff et al., 2001). This finding raises the possibility that distinct mechanisms may differentially regulate somatic versus dendritic translation of a single mRNA species.

**Demonstrations of Local Protein Synthesis**

With all of the components in place, and armed with the knowledge that mRNA granules containing translation machinery can be exported to the dendrites of living cells in an activity-dependent manner, it may seem a trivial leap to conclude that LPS is taking place in the dendritic compartment. However, the presence of mRNA and other requisite translation machinery does not necessarily indicate that all of these components are competent to produce functional proteins.

*Axonal LPS*

While most research in the field to date has focused on regulated translation in dendrites, the possible existence of axonal protein synthesis machinery has been described (Koenig and Giuditta, 1999). It has also been shown that protein synthesis in the presynaptic compartment of dorsal root ganglion neurons regulates axon regeneration in response to injury (Twiss et al., 2000; Zheng et al., 2001). More recent work has demonstrated a role for presynaptic LPS in growth cone responsiveness to local guidance cues during axon elongation (Brittis PA, 2002). Using a high-density retinal explant culture system, Brittis and colleagues determined that mechanically isolated axons continue to synthesize a GFP reporter. An important issue convincingly addressed in this study is the ability of distal processes to produce transmembrane proteins and deliver them to the cell surface. While it remains unclear whether axonal protein synthesis occurs in undamaged adult neurons, these data indicate that LPS plays a critical role in the presynaptic compartment during development and repair.

*Radiolabeled amino acid uptake*

One of the earliest studies providing compelling evidence that protein synthesis may take place in neuronal processes employed ventricular injection of $^{3}$H-leucine into adult rats and subsequent autoradiographic and electron microscopic analysis (Kiss, 1977). From these early experiments, Kiss observed that a majority of protein synthesis in dendrites was restricted to the proximal domain, although a small amount of [$^{3}$H]leucine incorporation could be seen throughout the dendrites. It was not clear from this study,

however, that the signal detected in distal processes was significantly higher than background levels. Furthermore, given the nature of these experiments, and the considerable delay between injection of the radioisotope and fixation of the sample for analysis, a somatic source of the proteins detected in the dendrites could not be ruled out.

A similar approach with analogous results was described in acute hippocampal slices (Feig and Lipton, 1993). Pairing electrical stimulation of Schaffer collateral axons with the cholinergic agonist carbachol resulted in increased $^{3}$H-leucine incorporation in the dendritic layers of hippocampal slices. While this further suggested the involvement of LPS in plasticity, it was unfortunate that the stimulation protocol used failed to elicit any type of synaptic modification. In addition, as with the study by Kiss, somatic protein synthesis as a source for the radiolabeled dendritic proteins could not be conclusively ruled out. Indeed, the fact that the cell body is such a large source of protein synthesis, with the neuronal processes being a relative sink, has present problems for researchers interested in the local protein synthesis hypothesis. In order to conclusively determine that the source of increased protein concentration in the dendrites cannot be attributed to proteins that were initially synthesized in the cell body, it is essential that the cell bodies and dendrites be somehow dissociated from one another.

*Synaptosome preparations*

Initial attempts at accomplishing this difficult task relied on subcellular fractionation techniques. Using a combination of biochemical tissue dissociation, filtration, and density gradient centrifugation of brain homogenates, it is possible to isolate small

membranous particles termed synaptosomes. These synaptosomes are pinched-off membranous structures which, when viewed through the electron microscope, appear to be presynaptic terminals and their associated postsynaptic structures. A number of groups have employed this method of synaptosome preparations as a means of addressing the local synthesis hypothesis without the confound of potential somatic contributions.

Perhaps unsurprisingly, the CamKIIα mRNA is enriched in synaptosomes. Upon NMDA receptor activation, CamKIIα protein is specifically upregulated in this biochemically-purified preparation, while overall translation is reduced (Scheetz et al., 2000). From this work, it is clear that synaptic stimulation is not simply activating translation of all proteins at random, but rather that a subset of proteins is preferentially increased. Other studies in synaptosomes have shown that activation of metabotropic glutamate receptors increases synthesis of the fragile-X mental retardation protein (FMRP) (Weiler et al., 1997). The RNA-binding properties of this protein are critically involved in neuronal development (Darnell et al., 2001), and deletion of the FMRP gene results in a dramatic loss of protein synthesis detected in synaptosomes (Greenough et al., 2001).

With sufficiently pure synaptosome fractions, it should be possible to evaluate the protein synthesis competence of these structures in the absence of cell bodies. There are, however, a number of complications involved in interpreting the synaptosome data (reviewed in Steward and Schuman, 2001). In particular, a number of mRNAs exist in synaptosomes that are entirely absent from the dendrites of neurons as determined by *in situ* hybridization (Steward and Schuman, 2001). These contaminants include the mRNA

encoding glial fibrillary acidic protein, a protein that is found exclusively in glial cells. The presence of such an impurity in synaptosomes warrants caution in the interpretation of data acquired with this technique.

*Acute hippocampal slices*

An important study providing very strong evidence of a direct link between LPS and synaptic enhancement used a brute-force method of removing principal cell bodies as a potential protein source: cell bodies in area CA1 of hippocampal slices were isolated from the synaptic neuropil by way of a microlesion with a dissecting knife (Kang and Schuman, 1996). Having previously demonstrated protein synthesis-dependent synaptic enhancement in hippocampal slices induced by neurotrophin treatment (Kang and Schuman, 1995a), Kang and Schuman used the microlesion technique to further demonstrate that this protein synthesis-dependent synaptic enhancement persisted even when the cell bodies were physically isolated from the dendrites. While this was the most convincing evidence to date, the argument could be made that the protein synthesis required for neurotrophin-induced enhancement was taking place in glial cells, interneurons or axons – all of which are present in the dendritic layer of the hippocampus.

In addition to long-term potentiation, neurons in hippocampal slices exhibit long-term depression, or LTD. This form of synaptic modification can be induced in slices by bath application of the group 1 metabotropic glutamate receptor agonist DHPG [(RS)-3,5-dihydroxyphenylglycine](Huber et al., 2000). Using a microlesion approach similar to that employed by Kang and Schuman, Huber and colleagues convincingly demonstrated that

DHPG-induced LTD in area CA1 is blocked by bath applied inhibitors of protein synthesis. Further strengthening the claim of LPS in the dendritic compartment, the authors also showed that inclusion of a protein synthesis inhibitor in the postsynaptic whole-cell recording pipette blocked mGluR-induced LTD. Because the net electrophysiological consequences of LTP and LTD are effectively opposite, it will be interesting to learn what proteins are differentially upregulated in response to these two forms of synaptic plasticity.

*Dissociated culture systems*

The dissociated cell culture system has provided the most definitive data illustrating the ability of neurites to synthesize proteins. In a beautiful series of experiments, Martin and colleagues used cultured Aplysia neurons to examine the possibility that LPS contributes to long-term facilitation (LTF) in these neurons (Martin et al., 1997). Given the large size and relatively robust nature of Aplysia neurons, the authors were able to culture a single bifurcating sensory neuron synapsing onto two spatially separated motor neurons. Taking great care to avoid the cell body, serotonin was locally perfused onto one of the connections, leaving the other sensory-motor connection unperturbed. The result of this precise serotonin application was input-specific LTF: only the synapses treated with serotonin exhibited synaptic enhancement. Importantly, the LTF was blocked by injection of a protein synthesis inhibitor into the presynaptic sensory neuron. Finally, to assess the ability of isolated neurites to synthesize proteins, 30-40 sensory neurons were cultured, their cell bodies removed, and then tested for their ability to incorporate $^{35}$S-methionine.

Even in the absence of cell bodies, these isolated sensory neuron processes incorporated the radiolabeled amino acid in a protein synthesis-dependent manner.

These exciting results provided the first definitive proof that neurites, independent of the cell body, can produce proteins in response to synaptic enhancement-inducing stimuli. While intriguing, the results of Martin and colleagues may be limited due to the differences between vertebrate and invertebrate neurons. A presynaptic locus of protein synthesis-dependent synaptic enhancement is also inconsistent with the ultrastructural anatomical data in vertebrate neurons: SPRCs are present in dendrites but have not been detected in axons of mature vertebrate neurons in the CNS.

In order to conclusively demonstrate the occurrence of local, dendritic protein synthesis in mammalian neurons, we expressed a GFP-based protein synthesis reporter in cultured hippocampal neurons and monitored the GFP signal in real time using confocal microscopy (Aakalu et al., 2001). As detailed in Chapter 2, the GFP construct was translated in isolated dendrites in response to BDNF, and the highest intensity GFP signal was found near synaptic sites. Having developed a useful system for examining local translation, we next turned our attention to the effects of dopaminergic signaling on LPS. The results of these experiments, the focus of Chapter 3, show convincingly that D1/D5 dopamine receptor activity converts silent into active synapses by increasing surface GluR1 at synaptic sites in a protein synthesis-dependent manner.

In the course of these studies, it became apparent that more rigorous tools for analysis of colocalization and spatial correlation of immunolabeled proteins were required.

In Chapter 4, I present and provide a detailed methodology for the quantitative analysis of 3-D colocalization and 2-D correlation of protein clusters within the dendrites of cultured hippocampal neurons. The algorithms take into account important issues of image analysis including thresholding, signal quantity, and sensitivity of the results to user bias. Code for implementation of the algorithms in the MATLAB environment is provided in Appendices A and B.

Finally, while considerable progress has been made in the study of local protein synthesis, a number of intriguing questions remain. For example, relatively little is known about the degree to which input-specificity is expressed at the level of small groups of synapses. Furthermore, the role of local protein synthesis in establishing and maintaining input-specificity remains to be determined. Another issue concerns the relationship between NMDA receptors and dopaminergic signaling in the protein synthesis-dependent conversion of silent into active synapses. These questions, as well as a discussion of the potential future directions for this line of research, are discussed in Chapter 5.

*Chapter II*

# Dynamic Visualization of Local Protein Synthesis in Hippocampal Neurons

## Summary

Using pharmacological approaches, several recent studies suggest that local protein synthesis is required for synaptic plasticity. Convincing demonstrations of bona fide dendritic protein synthesis in mammalian neurons are rare, however. We developed a protein synthesis reporter in which the coding sequence of green fluorescent protein is flanked by the 5′ and 3′ untranslated regions from CamKIIα, conferring both dendritic mRNA localization and translational regulation. In cultured hippocampal neurons, we show that BDNF, a growth factor involved in synaptic plasticity, stimulates protein synthesis of the reporter in intact, mechanically, or "optically" isolated dendrites. The stimulation of protein synthesis is blocked by anisomycin and not observed in untreated neurons. In addition, dendrites appear to possess translational hot spots, regions near synapses where protein synthesis consistently occurs over time.

## Introduction

The discovery that polyribosomes are located near the base of many spines (Steward and Levy, 1982) in the hippocampus suggested the possibility that neuronal proteins can be synthesized in dendrites. In theory, the synthesis of proteins in dendrites provides a mechanism by which synapses can independently control their strength, circumventing the need for precisely addressed protein transport from the soma (Schuman, 1999). In the context of synaptic plasticity, then, the ability to locally synthesize proteins allows synapses to solve the problem of maintaining "specificity" and obtaining the newly

synthesized proteins required for long-term synaptic plasticity (Frey et al., 1988; Kang et al., 1997; Nguyen et al., 1994; Otani et al., 1989; Stanton and Sarvey, 1984).

In the past 5 years, several studies have shown that locally synthesized proteins likely contribute to long-lasting synaptic plasticity (reviewed in Schuman, 1999; Steward and Schuman, 2001; Wells et al., 2000). In hippocampal slices, BDNF-induced synaptic plasticity is blocked by inhibitors of protein synthesis (Kang and Schuman, 1996). In the same study, Schaffer-collateral CA1 synapses that were isolated from their pre- and postsynaptic cell bodies still exhibited protein synthesis-dependent plasticity, suggesting a local, dendritic source of protein synthesis. A similar dependence on dendritic protein synthesis has been observed for metabotropic receptor-induced LTD at Schaffer-collateral CA1 synapses in the hippocampus (Huber et al., 2000). Long-term facilitation induced by 5-HT at cultured sensory motoneuron synapses in Aplysia also shows a requirement for local protein synthesis in the sensory neuron (Casadio et al., 1999; Martin et al., 1997). In addition, 5-HT application to isolated sensory neurites results in new protein synthesis (Martin et al., 1997). Most demonstrations of dendritic protein synthesis have relied on biochemical fractionation techniques to isolate fragments of dendrites and postsynaptic spines (e.g., the synaptoneurosome). In these studies, the incorporation of radiolabeled amino acids into new proteins demonstrated that synthesis can clearly occur in these dendritically derived fractions (Rao and Steward, 1991; Weiler and Greenough, 1991, 1993). The use of a cell culture system in which the cell bodies are separated from the dendrites also showed that isolated dendrites can synthesize proteins (Torre and Steward, 1992) and glycosylate proteins (Torre and Steward, 1996). The drawbacks of the above

techniques include the possibility of contamination by nondendritic fractions, the removal from a physiological context, and the lack of temporal resolution. Here we describe the development of a high-fidelity dendritic protein synthesis reporter and show unequivocally that protein synthesis can be stimulated in dendrites by BDNF, a growth factor involved in synaptic plasticity.

## Results

### BDNF Stimulates Protein Synthesis of a GFP Reporter in Hippocampal Neurons

In order to examine dendritic protein synthesis dynamically in living neurons, we constructed a green fluorescent protein (GFP) reporter, flanked by the 5′ and 3′ untranslated regions (UTR) from the Ca2+/calmodulin-dependent kinase II-α subunit (CamKIIα) (5′GFP3′). Previous work has shown that the 3′UTR of the CamKIIα mRNA contains information sufficient for its dendritic localization (Mayford et al., 1996; Mori et al., 2000). In initial experiments, the 5′GFP3′ reporter was introduced into cultured neurons using Biolistics. In expressing neurons, GFP was present in the soma and the dendrites, as indicated by immunolabeling for the dendritic marker MAP2 (Figure 2.1A). In most untreated neurons, expression of the reporter was robust in the cell bodies and relatively weak in the associated dendritic processes (Figure 2.1B). We examined whether exposure to BDNF modified the levels and/or pattern of GFP expression in neurons; 6 hr after transfection, dishes were exposed to either BDNF (50 ng/ml) or a control (HBS) solution for 4 hr. Neurons that were exposed to BDNF exhibited an increase in GFP synthesis that was evident in both the cell body and the dendrites (Figure 2.1B). The analysis of total

fluorescence in the dendrites revealed that BDNF-treated neurons had significantly greater quantities of GFP throughout the length of the dendritic process (Figure 2.1C). These experiments demonstrate that BDNF can stimulate protein synthesis in hippocampal neurons but do not indicate the cellular compartment (e.g., dendrites and/or soma) where the synthesis is occurring.

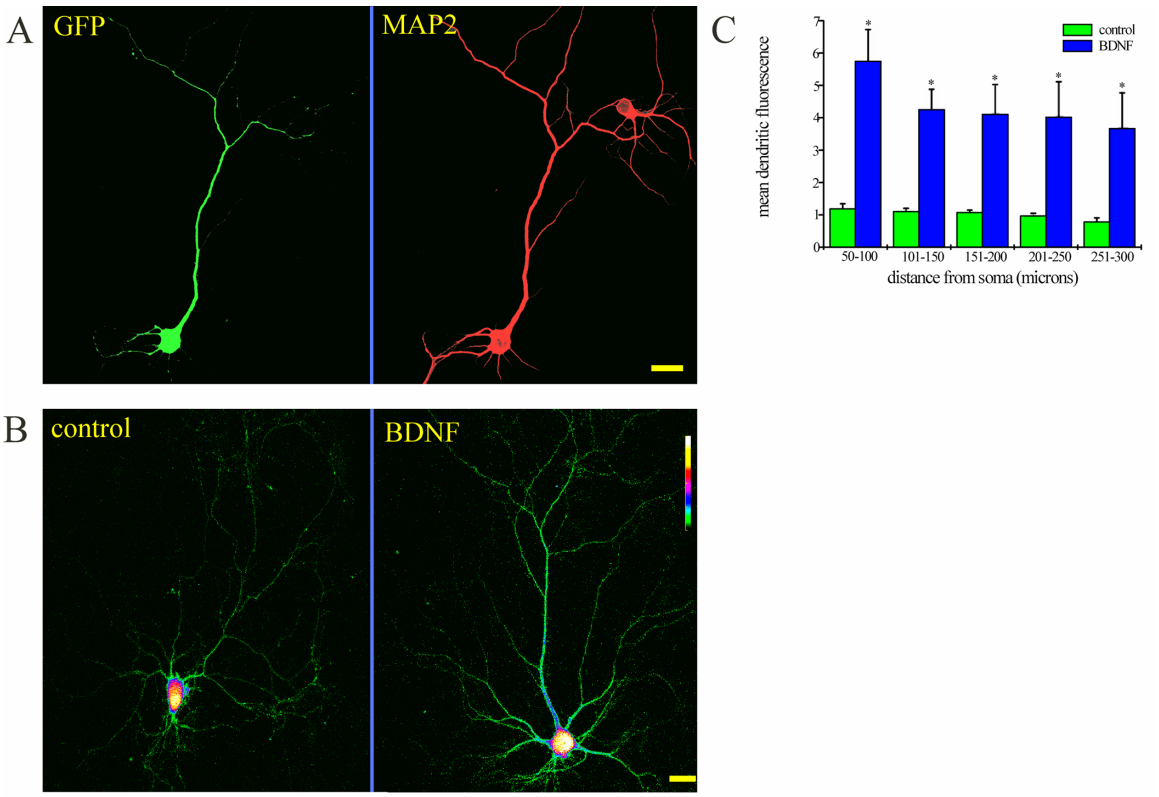


**Figure 2.1** BDNF Stimulates Protein Synthesis of the GFP Reporter in Hippocampal Neurons

(A) Shown is a cultured hippocampal neuron expressing the GFP reporter and immunostained for the dendritic marker MAP2. The majority of the GFP signal occurs in the dendrites, as indicated by the coincident MAP2 signal. Scale bar = 15 µm.

(B) Shown are an untreated and BDNF-treated neuron expressing the GFP reporter. The BDNF-treated cell shows enhanced fluorescence in the cell body and dendrites when compared to the untreated cell. Color lookup bar shows that the absence of GFP signal is indicated by black, increasing fluorescence is indicated by transitions to green, blue, red, and yellow, and saturated fluorescence is indicated by white. Scale bar = 15 µm.

(C) Summary data for all untreated (n = 7) and BDNF-treated (n = 10) dendrites. BDNF-treated neurons showed significantly greater fluorescence ($p < 0.01$) in all dendritic compartments (e.g., 50–300 µm from the soma).

## Time-Lapse Imaging of BDNF-Stimulated Translation

In an effort to ascertain the source of the increased GFP synthesis apparent in the above experiments, we conducted time-lapse imaging. We monitored the localization and

levels of the GFP reporter over time in individual neurons before and after BDNF treatment. To facilitate the expression of the reporter in a larger population of neurons, we incorporated the reporter construct into a Sindbis virus system (see Experimental Procedures.) We used a destabilized version of GFP, dGFP, in order to decrease the cumulative fluorescence that ultimately contributes to signal saturation. Dishes of cultured hippocampal neurons were infected with Sin-5′dGFP3′; initial images were collected 12 hr after infection, at a time when the fluorescence had reached steady-state levels. Untreated neurons, imaged over a 4 hr period, showed stable or declining fluorescence in the dendrites and cell body over time (Figures 2A and 2B). In contrast, neurons that were treated with BDNF showed increases in GFP fluorescence that were evident within 60 min of BDNF addition (Figures 2A and 2B). BDNF-induced increases in fluorescence were apparent in both the dendritic and somatic compartments. Of particular interest was the observation of increases in fluorescence in remote aspects of the dendrites (see boxed regions in Figure 2.2A); these increases were detected as early as the increases observed in the cell body, consistent with the notion that GFP is synthesized locally. Overall, when the total length of the dendrite was analyzed, we found that only BDNF-treated neurons showed significant increases in dendritic GFP fluorescence; the average increase in fluorescence was roughly 60%. This is likely a very conservative estimate of BDNF's actions since the analysis includes both synaptic and nonsynaptic areas of the dendrite. For example, our analysis of changes at individual “hot spots,” which may correspond to synaptic sites (see below), indicates that BDNF-induced increases in GFP fluorescence ranged from ~1- to 8-fold. Untreated neurons showed no significant increase in dendritic fluorescence when examined over the same time periods (Figure 2.2C). In addition, the

BDNF-induced increases were prevented by coapplication of the protein synthesis inhibitor anisomycin (Figure 2.2C). In BDNF-treated neurons, we also observed, however, what appeared to be the diffusion of GFP from the soma into the dendrite. This observation prevented us from concluding, unambiguously, that all of the increases in dendritic GFP we observed were due to local synthesis.

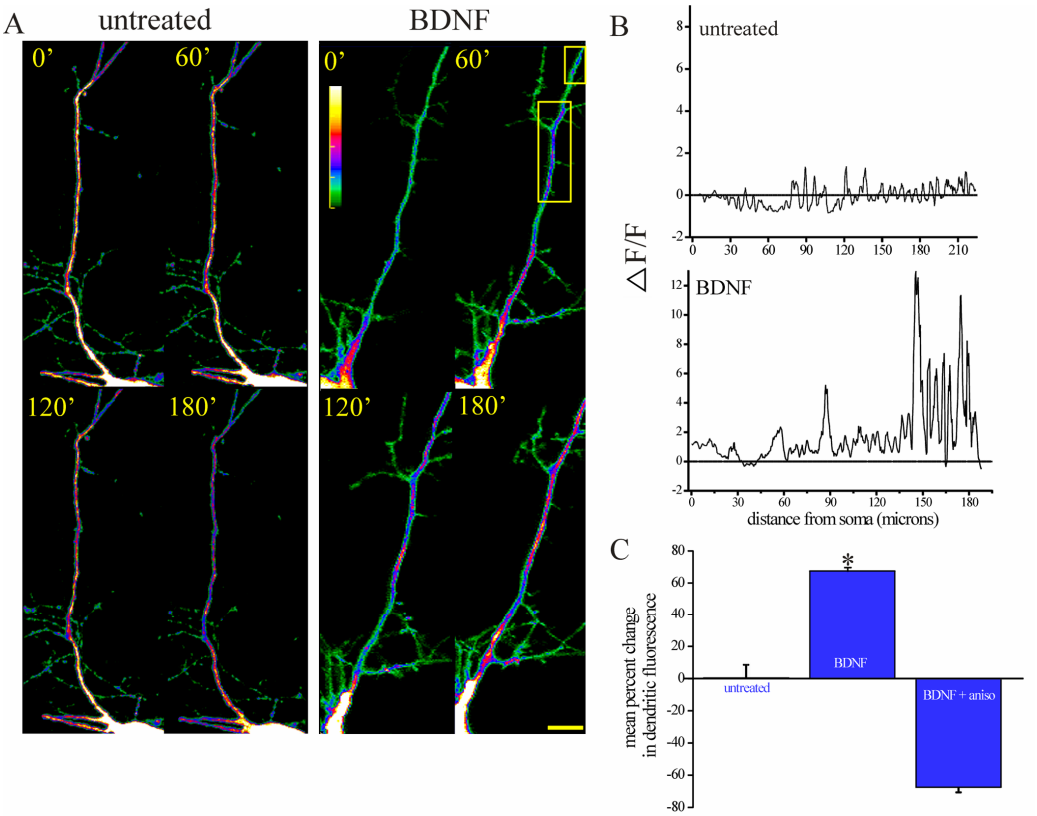


**Figure 2.2** Time-Lapse Imaging of BDNF-Stimulated Translation

(A) Repeated images of a control neuron and BDNF-treated neuron. BDNF was added immediately after the 0 min image was acquired. The BDNF-treated neuron showed increased fluorescence in the dendrite whereas the control neuron was relatively stable over time. Scale bar = 15 μm.

(B) Analysis of the individual neurons shown in (A). ΔF/F was calculated using the data from the 0 and 120 min images (see Experimental Procedures).

(C) Summary data for analysis of total dendritic length showing that only dendrites treated with BDNF exhibited significant ($p < 0.01$) increases in fluorescence.

**BDNF Stimulates Protein Synthesis in Healthy, Mechanically Isolated Dendrites**

In order to remove the cell body as a potential source of GFP signal, we performed dendritic transections in which the dendrites were physically isolated from the cell bodies using a micropipette. Ensuring neuron health and viability following such transections was a major concern. Of approximately 300 transections performed over a 2-year period, only 10 transected neurons fulfilled the health and viability criteria we established for use in experiments (see Experimental Procedures). Technical difficulty aside, the transected dendrite can provide the most unambiguous proof of local protein synthesis. As before, neurons were infected with Sin-5′dGFP3′. Transected dendrites that were not treated with BDNF usually showed declining fluorescence when monitored over time (Figure 2.3). In contrast, transected dendrites treated with BDNF exhibited increases in fluorescence in the isolated dendrites (Figure 2.4). As would be expected, BDNF-induced increases in fluorescence were also observed in the soma and the intact dendrites. The BDNF-induced increases in GFP fluorescence observed in the dendrites were blocked by cotreatment with anisomycin, indicating that the enhanced fluorescence was due to new protein synthesis (Figure 2.5). Plotting the distribution of changes in pixel intensity over time demonstrated that most regions of transected dendrites treated with BDNF showed increases in intensity (Figure 2.5C). In contrast, most regions of untreated dendrites or those treated with anisomycin plus BDNF tended to decrease in intensity. (Note that the small number of pixels that increased in intensity in the presence of anisomycin must represent the redistribution of pixels from adjacent areas of the dendrite or the contribution of synthesized, but not yet fluorescent GFP, e.g., Cubitt et al., 1995.) Taken together, these

data clearly show that BDNF can stimulate protein synthesis in isolated dendrites. The local dendritic protein synthesis we observed was robust and stable over time.

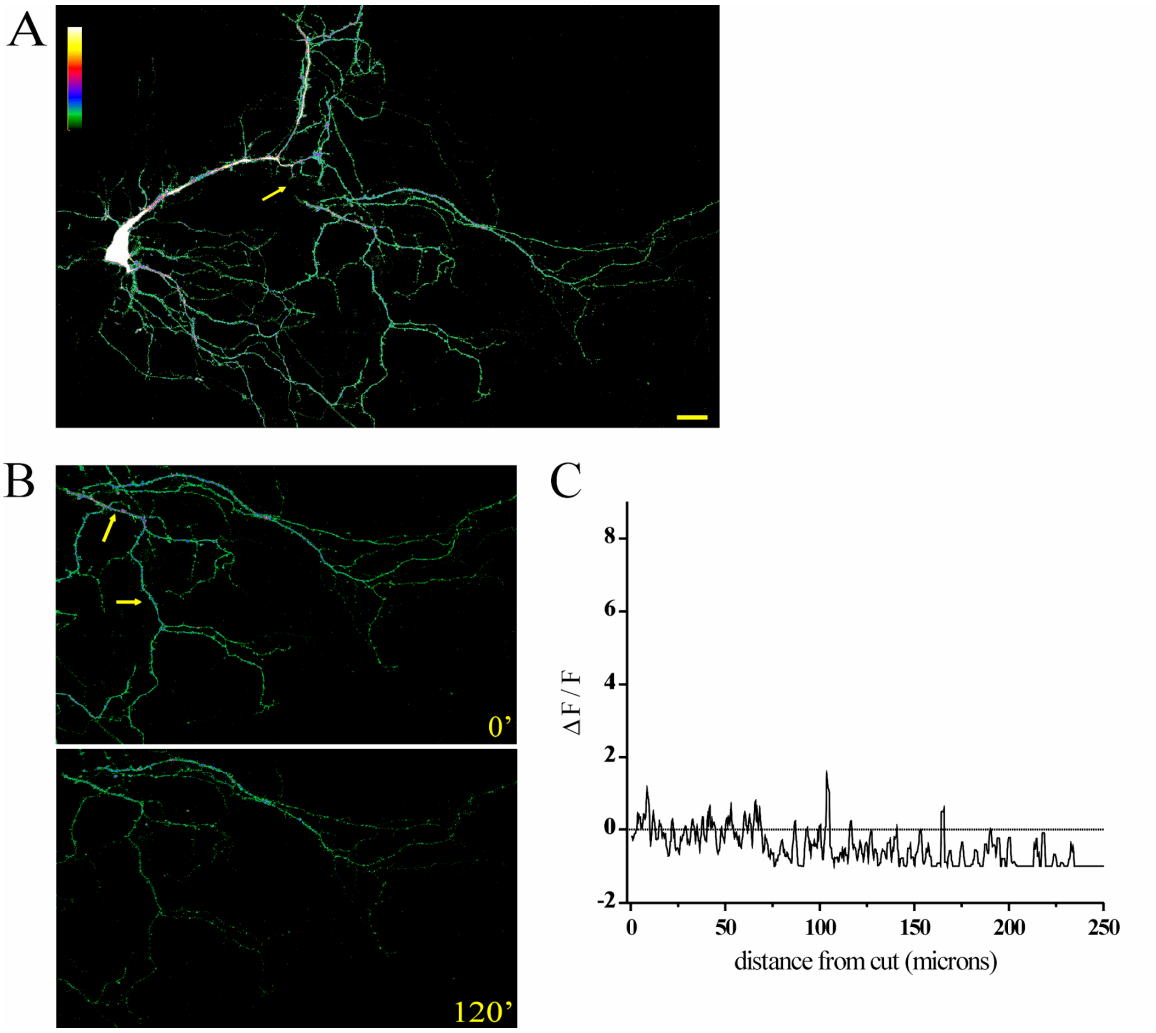


**Figure 2.3** Untreated, Transected Dendrites Do Not Show Increases in Protein Synthesis

(A) Image of an infected neuron; arrow points to the region of transection. Scale bar = 15 μm.

(B) Images of the isolated region of the dendrite immediately following transection and 120 min later. The fluorescent signal in the dendrite decreases over time. Arrows point to the dendrite chosen for analysis in (C). The top dendrite was also analyzed and included in the group analysis (Figure 2.5).

(C) Analysis of the transected dendrite shown in (A) and (B). ΔF/F was calculated using the data from the 0 and 120 min images (see Experimental Procedures).

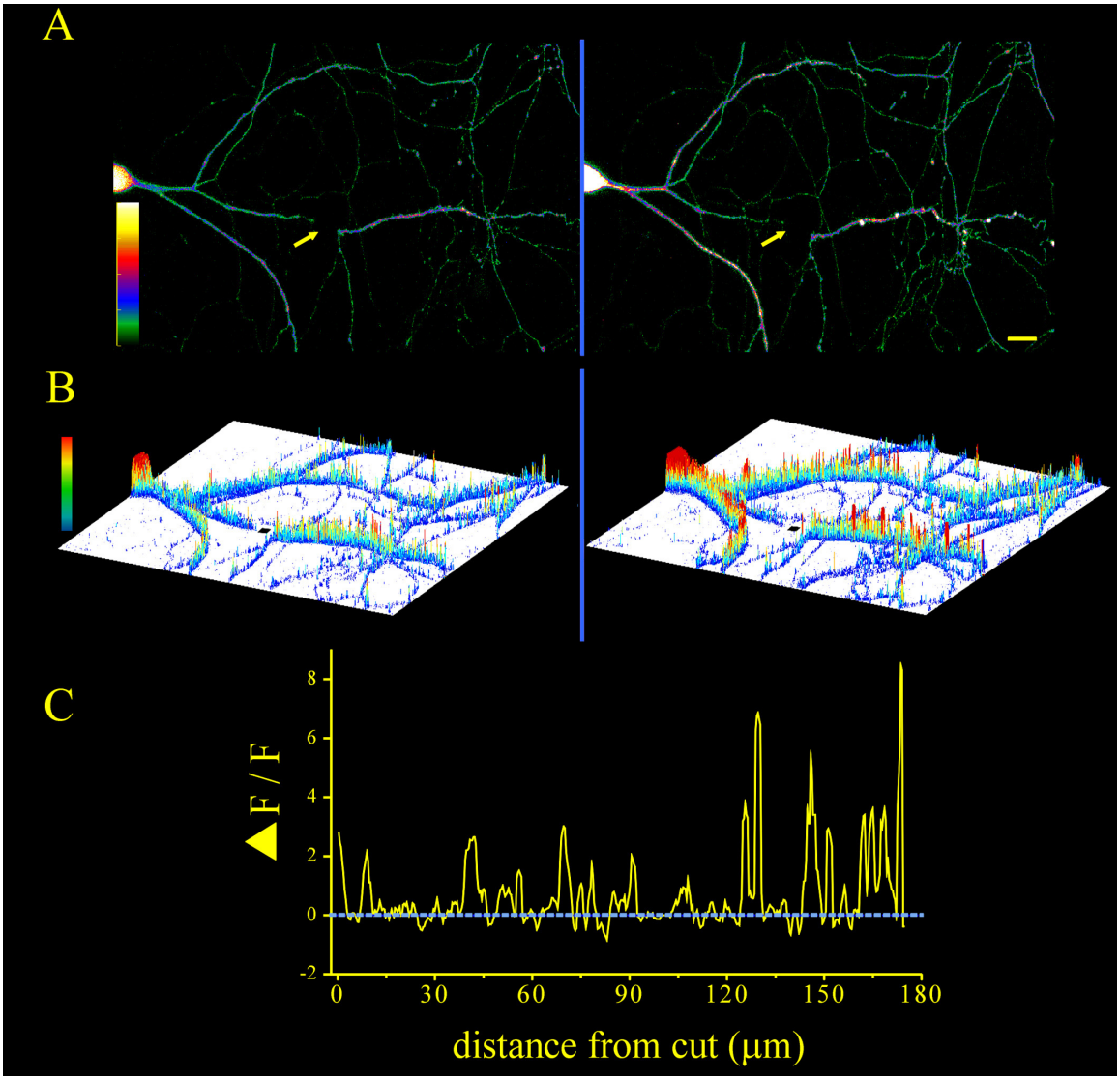


**Figure 2.4** BDNF Stimulates Protein Synthesis in Healthy, Mechanically Isolated Dendrites

(A) Images of transected neuron before (left) and 120 min after (right) BDNF treatment; arrow points to the region of transection. The fluorescent signal in the transected dendrite increases following BDNF treatment. Scale bar = 15 μm.

(B) Surface plot of the neuron shown in (A) in which changes in fluorescence are indicated by both changes in color and changes in the height of the pixels shown.

(C) Analysis of the transected dendrite shown in (A) and (B). ΔF/F was calculated using the data from the 0 and 120 min images (see Experimental Procedures).

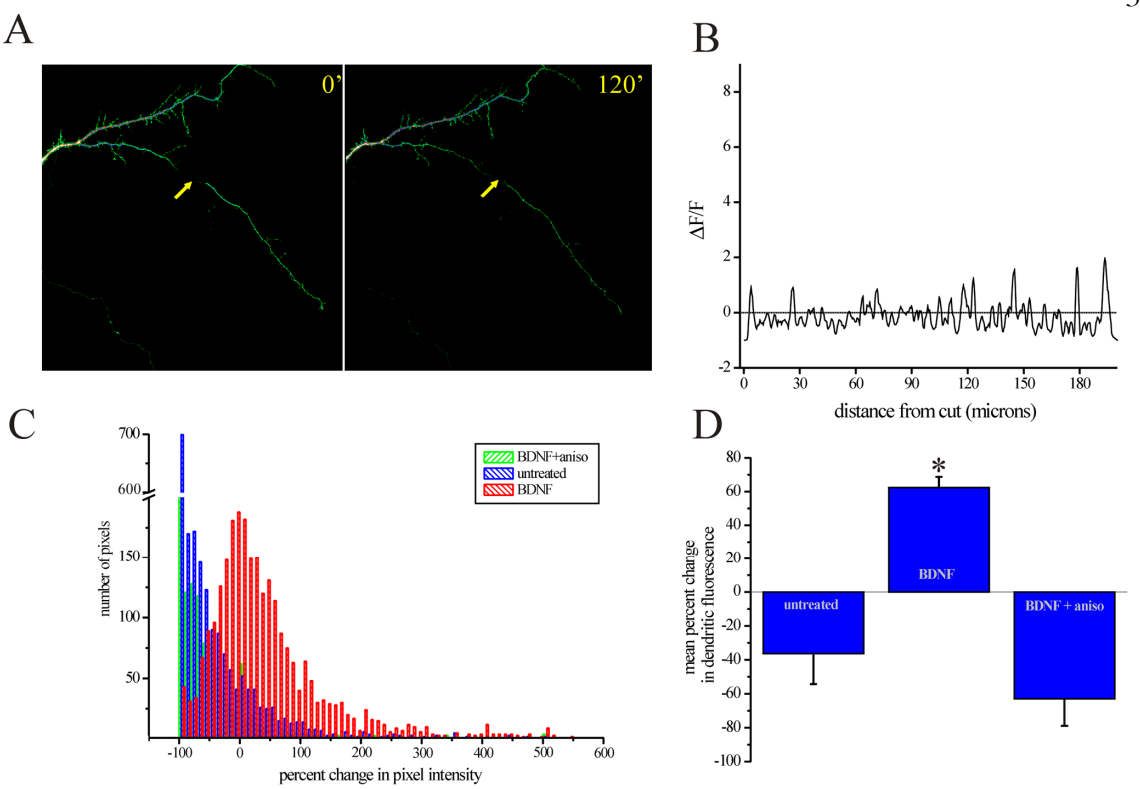


**Figure 2.5** Anisomycin Prevents BDNF-Induced Increases in Protein Synthesis in Transected Dendrites

(A) Images of a transected dendrite before and 120 min after coapplication of BDNF and anisomycin; arrow points to the region of transection. The fluorescent signal in the transected dendrite decreased over time. Arrows indicate the site of transection. Scale bar = 15 μm.

(B) Analysis of the transected dendrite shown in (A). ΔF/F was calculated using the data from the 0 and 120 min images (see Experimental Procedures).

(C) Summary histogram indicating the pixel intensity distributions for all untreated, BDNF-treated, and BDNF plus anisomycin-treated transected dendrites.

(D) Summary diagram indicating the mean percent change in pixel intensity for the three groups. Only the BDNF-treated dendrites showed a significant increase in fluorescence intensity over time ($p \leq 0.01$). N (cells, dendrites) for each group are as follows: untreated (3, 4); BDNF (4, 5); BDNF + aniso (3, 4).

**A Membrane-Anchored GFP Reporter Exhibits Extremely Limited Diffusion**

Because of technical difficulty and the potential for compromising long-term neuronal health, the transection experiments are not a viable option for extensive explorations of local protein synthesis. We reasoned that modifications to the protein synthesis reporter that limited its diffusion would also decrease the potential contribution of somatically synthesized GFP to the signal observed in dendrites. Toward this end, we conferred membrane localization to the reporter by adding a myristoylation consensus sequence (Patrick et al., 1999) at the N terminus of the GFP molecule and expressed this construct, Sin-5′myrdGFP3′, in neurons using Sindbis virus. We compared the diffusion of Sin-5′dGFP3′ and Sin-5′myr dGFP3′ by conducting FRAP (fluorescence recovery after photobleaching) experiments in dendrites. Note that the recovery of reporter fluorescence in dendrites following photobleaching is due to both diffusion from the adjacent (nonbleached) compartment as well as new synthesis of the reporter in the bleached domain. To monitor the contribution of diffusion exclusively, we included anisomycin in the bath. In the nonmembrane anchored version of the reporter (Sin-5′dGFP3′), there was substantial recovery of fluorescence in the bleached dendrite within 60 min (Figure 2.6A). We found that the addition of the myr sequence, however, severely retarded the diffusion of the modified (Sin-5′myrdGFP3′) reporter (Figure 2.6A). Negligible recovery from the photobleached state was observed in the 120 min following the photobleaching episode. These data indicate that the myristoylated reporter exhibits limited diffusion (see Experimental Procedures), suggesting that it can be used to faithfully report local protein synthesis in intact dendrites.

**BDNF Stimulates Protein Synthesis in Healthy, "Optically Isolated" Dendrites**

We next used the diffusion-restricted reporter (Sin-5′myrdGFP3′) in combination with photobleaching to examine dendritic protein synthesis in intact neurons. In these experiments, we continuously photobleached the cell body in order to abolish the contribution of somatically synthesized GFP to the dendritic signal; in this way we "optically isolated" the dendrites of interest. The continuous photobleaching of the soma did not compromise neuronal health: propidium iodide labeling of bleached cells revealed no incorporation of the dye (see Experimental Procedures). When we analyzed untreated, optically isolated dendrites, we found that the fluorescence of the reporter decreased over time at most dendritic sites (Figures 6B and 6C). We occasionally observed small (e.g., 0- to 5-fold) fluorescence increases at some sites. These small increases in signal reflect either the redistribution of GFP from adjacent dendritic sites or bona fide new protein synthesis. The fact that both untreated and anisomycin-treated dendrites showed similar average fluorescence change profiles (Figure 2.8) suggests that most of these small increases reflect redistribution from adjacent portions of the dendrite.

In contrast to untreated neurons, the addition of BDNF to optically isolated dendrites resulted in a robust stimulation of protein synthesis. As shown in Figure 2.7, increases in reporter translation ranging from 1- to 17-fold were observed at many sites along optically isolated dendrites. Sites of decreased fluorescence were not common in BDNF-treated dendrites. The coapplication of anisomycin completely prevented the BDNF-induced increases in GFP fluorescence, confirming that the observed effects of BDNF were due to new protein synthesis (Figure 2.8). Dendrites that were treated with

anisomycin alone or anisomycin plus BDNF usually showed decreases in fluorescence along the length of the dendrite interspersed with very small increases that likely represented redistribution of GFP molecules from adjacent regions of the dendrites (Figure 2.8).

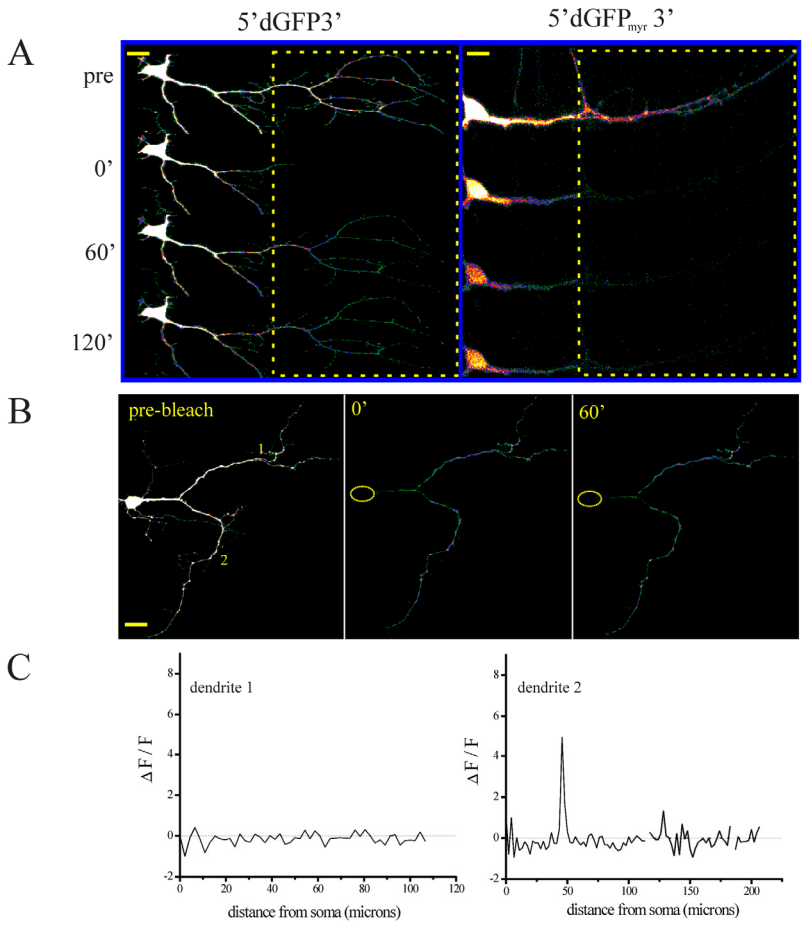


**Figure 2.6** A Membrane-Anchored GFP Reporter Exhibits Limited Diffusion

(A) Shown are two neurons infected with either 5′dGFP3′ or the membrane-anchored 5′$_{myr}$dGFP3′. Neurons were treated with anisomycin for 1 hr prior to the initiation of photobleaching (boxed region shows bleached area). FRAP was monitored in each neuron over time. The neuron infected with the diffusible reporter (5′dGFP3′) showed significant recovery of fluorescence within 60 min of the photobleaching. In contrast, the myristoylated reporter showed negligible recovery within 2 hr following photobleaching. Scale bars: 5′dGFP3′, 15 μm; 5′$_{myr}$dGFP3′, 10 μm.

(B) Time-lapse images of a 5′$_{myr}$dGFP3′-expressing neuron that was subjected to somatic photobleaching for the duration of the experiment. The prebleached neuron is shown at the right and two consecutive time points following photobleaching are shown in the middle and left. In this untreated neuron there was an overall decline in dendritic fluorescence during the experiment. Scale bar = 15 μm.

(C) Profile of fluorescence changes between 0 and 60 min for dendrites 1 and 2 (labeled in [B]). In the profiles shown, the mean change in fluorescence between t = 0 and t = 60 was −15.4% and −12.3% for dendrite 1 and 2, respectively.

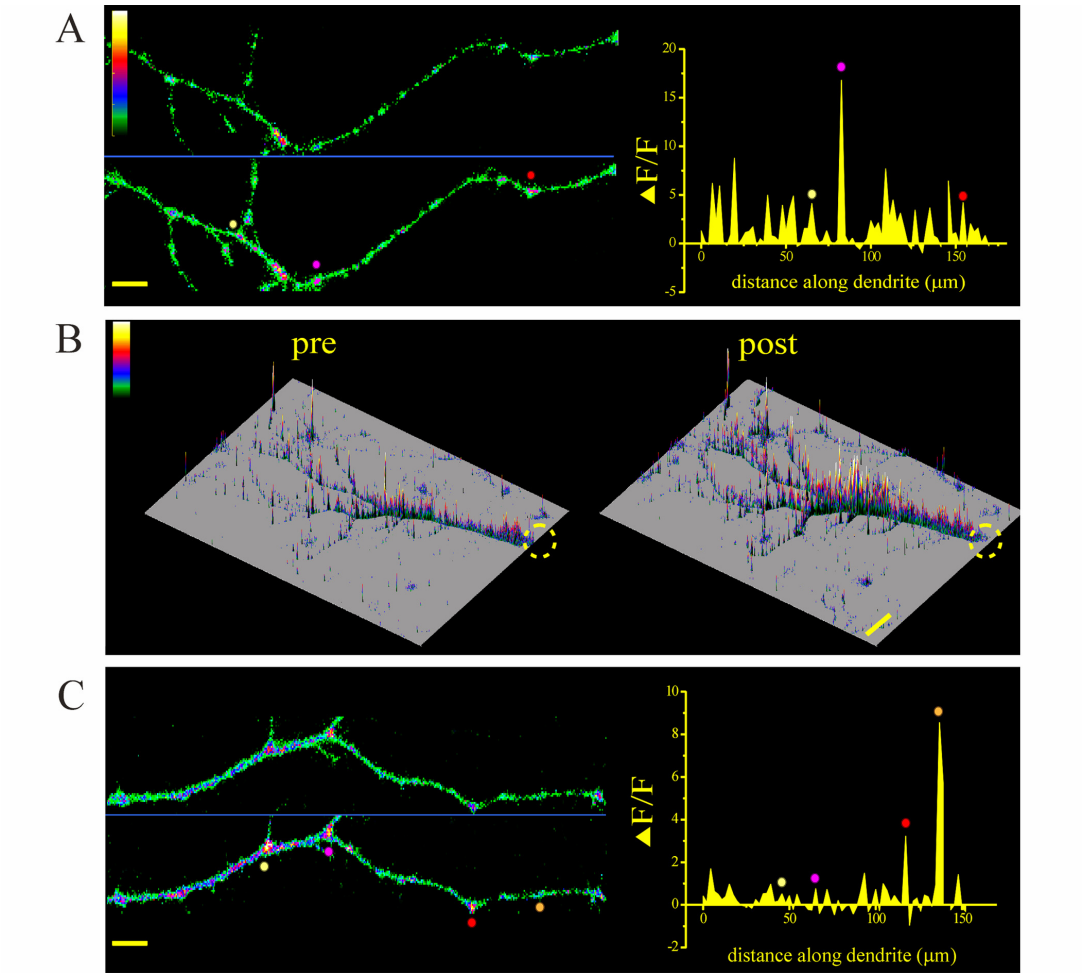


**Figure 2.7** BDNF Stimulates Protein Synthesis in Healthy, "Optically Isolated" Dendrites

(A) Shown is BDNF-induced enhancement of GFP translation in an optically isolated dendrite at two consecutive time points. The profile of fluorescence change between the two time points shown is plotted on the right. Individual hot spots are identified by colored circles on the image and the corresponding profile. Scale bar = 5 μm.

(B) A surface plot of a different neuron in which the dendrites were optically isolated. The region of the bleached soma is shown by the dashed circle. The effects of BDNF are evident in comparing the dendritic fluorescence in the pre and post images. Scale bar = 15 μm.

(C) An isolated dendritic segment from the neuron shown in (B) at two different time points. The profile of fluorescence change between the two time points shown is plotted on the right. Individual hot spots are identified by colored circles on the image and the corresponding profile. Scale bar = 5 μm.

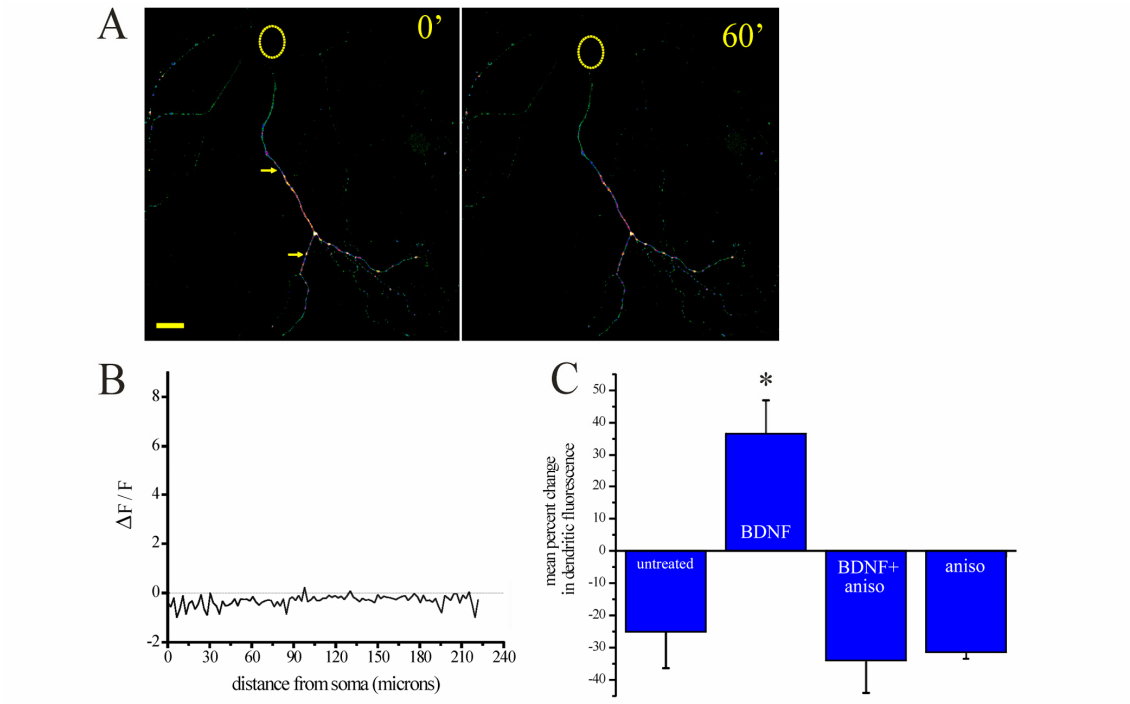


**Figure 2.8** Anisomycin Blocks BDNF-Induced Increases in Protein Synthesis in Optically Isolated Dendrites

(A) Time-lapse images of an optically isolated dendrite that was treated with BDNF plus anisomycin. The optically isolated dendrites are shown at two consecutive time points. There was an overall decline in dendritic fluorescence during the experiment. The area occupied by the photobleached soma is shown by the yellow circle. Scale bar = 15 μm.

(B) Profile of fluorescence changes between 0 and 60 min for dendrite indicated by the arrow in (A). The mean change in fluorescence between t = 0 and t = 60 was −25.7%.

(C) Summary diagram indicating the mean percent change in pixel intensity for all untreated, BDNF-, and BDNF plus anisomycin-, and anisomycin-treated optically isolated dendrites. Only the BDNF-treated dendrites showed a significant increase in fluorescence intensity over time ($p \leq 0.01$). N (cells, dendrites) for each group are as follows: untreated (4, 6); BDNF (5, 8); BDNF + aniso (4, 5); aniso (3, 5).

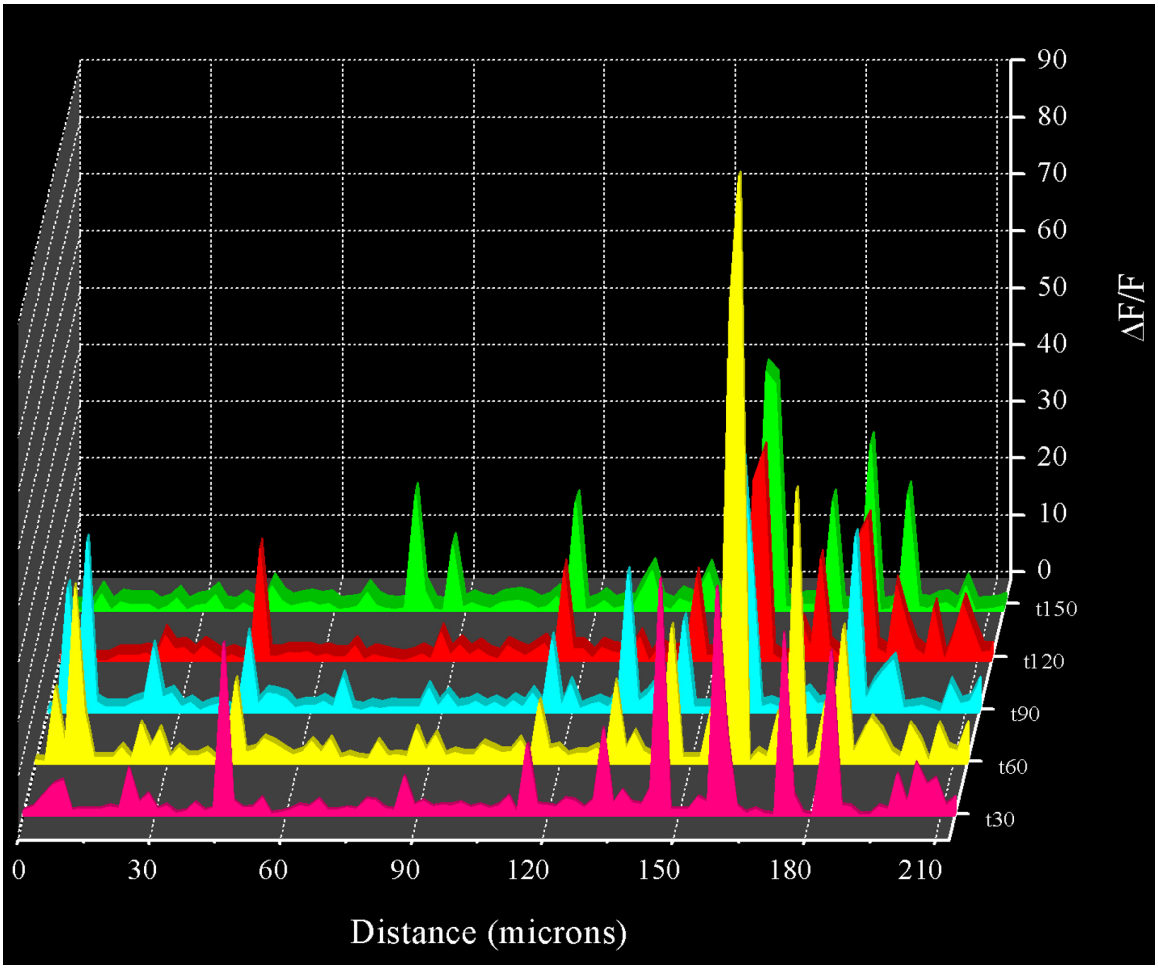


**Figure 2.9** GFP Reporter Signals Are Spatially and Temporally Persistent

Shown are the ΔF/F profiles for a single optically isolated dendrite at several time points (t30 – t150 minutes). The increased GFP signal is concentrated at relatively stable sites along the length of the dendrites. These sites also appear to be temporally stable over a 2 hr time period.

## The Protein Synthesis Reporter Is Concentrated near Sites of Translation and Synapses

Repeated imaging of optically isolated dendrites allowed us to examine the location of GFP signals over time. When the fluorescence intensity profiles derived from time-lapse imaging of an individual dendrite were plotted together, it became clear that the GFP signals appeared to be spatially concentrated at hot spots that were stationary over time

(Figure 2.9). The increases and occasional decreases in GFP signal that were observed over time tended to appear at the same locations along the dendrite. We next examined whether these reporter hot spots were in the vicinity of synaptic sites and/or sites of protein translation. We immunolabeled 5′myrdGFP3′-expressing cells with an antibody to the postsynaptic marker PSD-95, the presynaptic marker synapsin I, or rRNA (Y10B; Koenig et al., 2000; Lerner et al., 1981). We found that the GFP hot spots often were near ribosomes or synaptic regions as indicated by the proximity of the PSD-95, synapsin, or Y10B signal to GFP (Figure 2.10). The colabeling for PSD-95 also revealed that the myristoylated reporter appeared not to enter synaptic spines to an appreciable extent and appeared more concentrated in dendritic shafts. As such, we did not expect to observe strict "colocalization" of the GFP signal with the synaptic markers. We did observe, however, that GFP was, much more often than not, in the vicinity of ribosomes and synapses. To quantify this relationship, we calculated the mean fluorescence for each signal across the dendritic width (thus obtaining mean fluorescence values for the entire length of each dendrite), and calculated the pairwise cross-correlation of GFP and PSD-95, synapsin, or Y10B. A cross-correlation measures the spatial coincidence of the two signals, with the lag value representing the distance one signal must be shifted in order to spatially correlate with the other signal. Analysis of the GFP/Y10B, GFP/synapsin, or GFP/PSD-95 (data not shown) signals revealed a significant cross-correlation between the two signals (Figure 2.10). The peaks at zero lag for both the GFP/Y10B and GFP/synapsin analysis (Figures 10F and 10G) indicate that the two signals are highly correlated. The observation that locally synthesized GFP is concentrated in the vicinity of ribosomes and synapses suggests that there are local hot spots of translation that are near synaptic sites.

These data are predicted to some extent by previous anatomical observations of ribosomes at or near the bases of dendritic spines (Steward and Levy, 1982). The spatially and temporally stable sites of translation that we have identified provide evidence for a central tenet of the local protein synthesis hypothesis—the notion that locally synthesized proteins might be selectively made available to their associated synapses, thus providing a mechanism for synapse specificity (Schuman, 1999a; Steward, 1997; Steward and Schuman, 2001). Whether these observations hold true for other types of locally synthesized proteins (e.g., nonmyristoylated) is an important issue for future studies.

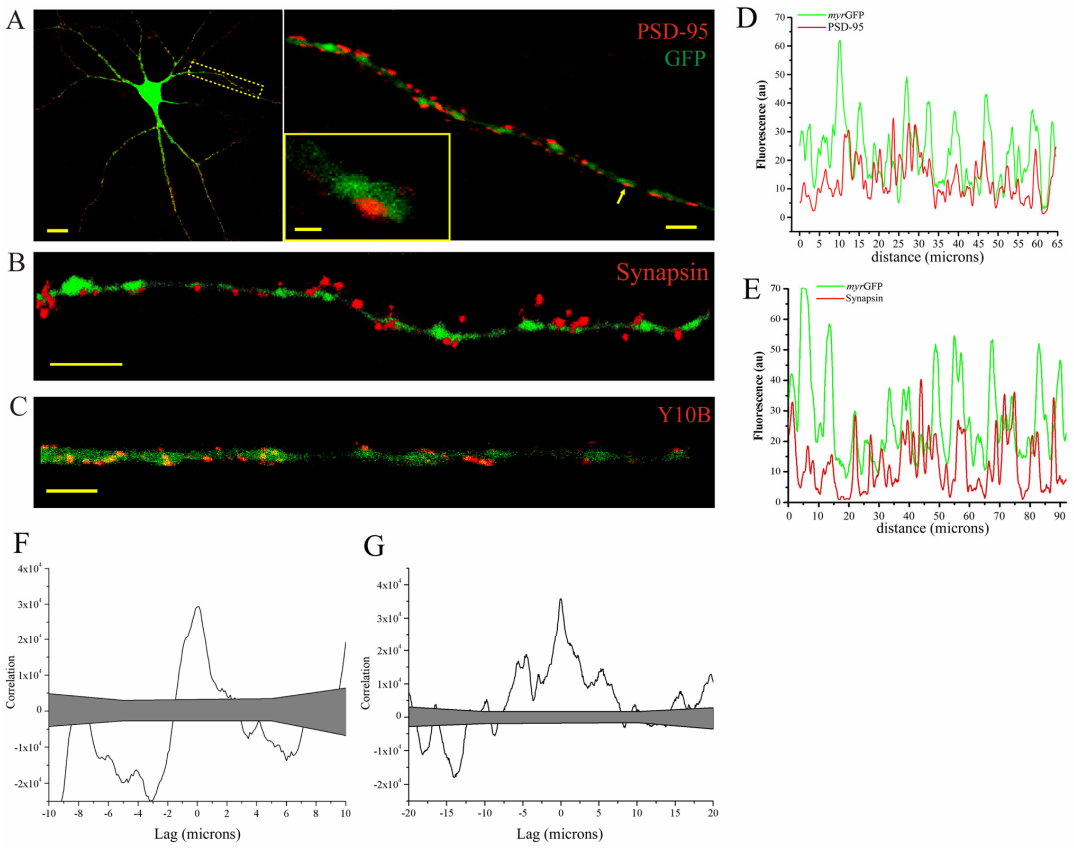


**Figure 2.10** GFP Reporter Signals Colocalize with Ribosomes and Synaptic Markers

(A) Low- (left) and high-power (right) images of a GFP reporter-expressing neuron immunostained with an antibody against the synaptic marker PSD-95. The inset shows the GFP signal that forms a cloud around the punctate PSD-95 signal. Scale bars = 15, 5, and 1 μm, for low-, high-power, and inset images, respectively.

(B) High-power image of a GFP reporter-expressing neuron immunostained with an antibody against the presynaptic protein synapsin I, showing that the GFP signal is often in the vicinity of the presynaptic marker.

(C) High-power image of a GFP reporter-expressing neuron immunostained with an antibody against the ribosomal marker Y10B.

(D) Fluorescence intensity plots for the GFP and PSD-95 signals of the dendrite shown in (A). The mean fluorescence along the width of the dendrite was calculated.

(E) Fluorescence intensity plots for the GFP and synapsin signals of the dendrite shown in (B). The mean fluorescence along the width of the dendrite was calculated.

(F) The cross-correlation functions for GFP and synapsin is shown for the dendrite in (B). The shaded area indicates the results of 100 cross-correlations computed on randomized versions of the data. The upper and lower bounds of the shaded area define the 95% confidence interval.

(G) The cross-correlation functions for GFP and Y10B is shown for the dendrite in (C). The shaded area indicates the results of 100 cross-correlations computed on randomized versions of the data. The upper and lower bounds of the shaded area define the 95% confidence interval.

## Discussion

We have described the visualization of dendritic protein synthesis in mature cultured hippocampal neurons. We report a robust stimulation of local protein synthesis by the growth factor BDNF. In the last 5 years, several studies have used clever applications of protein synthesis inhibitors to demonstrate roles for locally synthesized proteins in different forms of synaptic plasticity (Kang and Schuman, 1996; Martin et al., 1997; Casadio et al., 1999; Huber et al., 2000). In Aplysia sensory neurons, serotonin application to isolated neurites results in detectable protein synthesis (Casadio et al., 1999). Direct demonstrations of protein synthesis in mature mammalian dendrites are scarce, however. Using radiolabeling, Feig and Lipton (1993) showed that newly synthesized proteins could be detected in dendrites of hippocampal slices—the timing was such that the cell body was unlikely to be the source of protein synthesis. Nevertheless, the difficulty associated with the radiolabeling procedure as well as the troublesome identification of dendritic compartments limits the appeal of this approach. In contrast, the approach we have developed allows the visualization of dendritic protein synthesis in living neurons over time. Ultimately, we combined the use of a membrane-anchored, destabilized GFP with somatic photobleaching to be sure that reporter signals observed in the dendrite were synthesized in the dendrite. Given the limited diffusion of the myristoylated dGFP (e.g., Figure 2.6), a case could certainly be made for using the myristoylated reporter alone (without somatic photobleaching) in future investigations of dendritic protein synthesis in slice preparations as well as in vivo.

The BDNF-induced increases in GFP fluorescence we observed were completely blocked by anisomycin. Since BDNF does not slow the degradation rate of the GFP reporter (our unpublished data), these data indicate that the fluorescence increases were due to new protein synthesis. In addition, BDNF-induced dendritic protein synthesis was not accompanied by any obvious or systematic changes in cell morphology. We observed increases in GFP reporter within 45–60 min of BDNF application (e.g., Figure 2.2). Preceding its ability to fluoresce, GFP possesses posttranslational requirements for cyclization and oxidation (Cubitt et al., 1995). As such, GFP is not an optimal reporter for addressing how quickly protein synthesis can occur in dendrites. Previous studies using developing neurons reported that a combination of BDNF and NT-3 (Crino and Eberwine, 1996) or a metabotropic receptor agonist (Kacharmina et al., 2000) could stimulate translation of a myc epitope in transected growth cones between 1 and 4 hr after transfection. In addition to participating in synaptic plasticity, a role for BDNF-stimulated dendritic protein synthesis might also be imagined in other contexts where BDNF clearly plays an important neurotrophic role in development and the morphology of neurons (McAllister et al., 1999; Schuman, 1999b).

The regulated synthesis of our reporter may mimic the translation of endogenous CamKIIα since our reporter contains both the 5′ and 3′UTR from the CamKIIα gene. Indeed, a stimulation of dendritic CamKIIα translation by LTP has been suggested by immunohistochemical studies (Ouyang et al., 1997, 1999). The 5′UTR may contain translational regulatory elements: we noticed that GFP fluorescence in neurons transfected with a construct lacking the 5′UTR (GFP3′) appeared to be greater than that observed in

cells expressing a construct containing both the 5′ and 3′UTR (data not shown). The 3′UTR was included primarily to confer dendritic localization of the GFP mRNA (Mayford et al., 1996; Mori et al., 2000), although this was likely not necessary in the present study given the abundance of the mRNA produced by viral infection. The 3′UTR of CamKIIα also contains elements for regulation of translation, namely the CPE (cytoplasmic polyadenylation element) and polyadenylation signal (Wu et al., 1998). We have not addressed whether the BDNF-stimulated translation we observe requires these elements, although others have clearly shown regulation of CamKIIα translation via these and other regulatory elements (Sheetz et al., 2000; Wu et al., 1998).

In addition to its effects on hippocampal slices, BDNF can also facilitate synaptic transmission in cultured hippocampal neurons (Levine et al., 1995; Li et al., 1998a, 1998b). Both pre- and postsynaptic (Levine et al., 1997) mechanisms have been proposed for BDNF's actions on synaptic transmission. In the present experiments, the stimulation of protein synthesis could be due to activation of postsynaptic TrkB receptors and subsequent stimulation of local translation machinery, potentially through the rapamycin-sensitive m-TOR kinase pathway (e.g., Brown and Schreiber, 1996; Casadio et al., 1999). Alternatively, BDNF could enhance glutamate release from presynaptic terminals (e.g., Li et al., 1998a, 1998b), which could then stimulate postsynaptic protein synthesis through glutamate receptor signaling.

In sum, these data clearly show that dendrites of mammalian neurons can synthesize proteins. The demonstration that dendrites that are in a synaptic network can

synthesize proteins provides support for the idea that locally synthesized proteins contribute to synaptic function. The observation that there are spatially and temporally consistent hot spots for translation suggests that local synthesis might play a role in maintaining the specificity of synaptic connections.

## Experimental Procedures

### Cultured Neurons

Dissociated hippocampal neuron cultures are prepared from postnatal 2- and 3-day rat pups as described (Banker and Goslin, 1990). Neurons are plated at a density of 15,000–45,000 cells/cm2 onto poly-L-lysine and laminin-coated coverslips. The cultures are maintained and allowed to mature in growth medium (Neurobasal-A supplemented with B27 and Gluta MAX-1) for 14–21 days before use. In Biolistic experiments, dissociated P2 hippocampal neurons were transfected with the pcDNA3.1-5′GFP3′ construct according to the manufacturer's protocol (Bio-Rad). DNA-gold complexes were generated with the following parameters: 50 μg plasmid DNA, 17 mg 1.6 μm diameter gold particles, and 0.01% PVP. In viral infection experiments, dissociated P2 hippocampal neurons were infected for 12 hr in growth medium containing the Sindbis virus of choice. Six hours post initial transfection or 10–12 hr post initial infection, growth medium was removed and replaced with HEPES-buffered solution (HBS) (Malgaroli and Tsien, 1992; without glycine or picrotoxin) for imaging. All neurons used in our experiments had a pyramidal neuron-like morphology with one or two major dendrites emanating from the cell body. For immunolabeling, neurons were fixed at room temperature with 4%

paraformaldehyde for 20 min. Fixed cultures were then treated sequentially with PBS, PBT (1× PBS, 2 mg/mL BSA, 0.1% Triton X-100), preblock (20% normal goat serum in PBT), primary Ab in preblock at 4°C overnight, preblock, Cy3-conjugated secondary Ab in preblock, preblock, and PBS. Immunostained specimens were imaged in PBS. The sources of the antibodies were as follows: MAP2 (Chemicon), PSD-95 (Upstate Biotechnology), Y10B (generous gift from Jeff Twiss, UCLA), synapsin I (Novus).

**Constructs**

pcDNA3.1-5′dGFP3′: The CamKIIα 3′UTR sequence obtained from plasmid (Mayford et al., 1996) was PCR amplified (forward primer: 5′-ttatatttgcggccgcggtcgctac-cattaccagtt-3′; reverse primer: 5′-ggcgctctctcgagtttaaatttgtagct-3′) and cloned into the NotI and XhoI sites of the pcDNA3.1 vector (Invitrogen). The resulting vector was then cleaved with BamHI and NotI for insertion of the destabilized EGFP ORF (from pd2EGFP, Clontech). The CamKIIα 5′UTR was released from a plasmid (obtained from J. Fallon) and inserted at the HindIII-BamHI sites, yielding pcDNA-5′dGFP3′. pSinRep5-5′dGFP3′: The 5′dGFP3′ fragment was released with PmeI-ApaI (blunted) and ligated into pSinRep5 (Invitrogen). pcDNA3.1-5′myrdGFP3′: The d2EGFP ORF (from pd2EGFP, Clontech) was PCR amplified (forward primer: 5′-cgactctagagtgagcaagggcgaggagctg-3′; reverse primer: 5′-tctagagtcgcggccgcatctacaca-3′), digested, and inserted into the XbaI-NotI sites of pBSK. To generate the myristoylation signal, two oligos corresponding to the N-terminal 10 amino acids of p10 were annealed (myr1: 5′-gatccatgggcacggtgctgtccctgtctcccagct-3′; myr2: 5′-ctagagctgggagacagggacagcaccgtgcccatg-3′), digested, and inserted into the BamHI-XbaI sites of pBSK-d2EGFP. The myrdGFP was subcloned into the BamHI-NotI sites of

pcDNA3.1-5′dGFP3′. pSinRep5-5′myrdGFP3′: The 5′myr3 dGFP3′ fragment was released with PmeI-ApaI and subcloned into the StuI-ApaI sites of pSinRep5 (Invitrogen). Sindbis viroids were produced according to the Experimental Procedures provided by Invitrogen. Contrary to observations in other cell types, it appears that single-stranded RNA viruses of the α family do not shut down protein synthesis in neurons (K. Lundstrom, personal communication, Hoffmann-LaRoche, Basel, Switzerland).

**Microscopy**

Confocal images were acquired in 0.3 μm sections; image analysis was conducted on z-compressed image stacks that contained the entire neuron of interest. GFP was excited at 488 nm and emitted light was collected between 510–550 nm. Images were acquired with parameters that maximized the dynamic range of pixel intensity for the dendritic signal. Using these parameters, the cell body fluorescence intensity was necessarily, occasionally, saturated. In all experiments, identical acquisition parameters and settings were used for both control and BDNF-treated dendrites on a given experimental day. In time-lapse experiments, the cultured neurons were maintained in an incubator (36.5°C) between image acquisition episodes. Images were acquired at room temperature. The acquisition of images at individual time points took less than 3 min.

**Transections**

Cells were preincubated in HBS for 2 hr before the start of transection experiments. Transection was carried out as follows: GFP-expressing neurons were oriented such that the dendritic segment to be cut was in line with the long axis of the microelectrode. The

glass microelectrode was then carefully lowered onto the dendrite until a spot of no GFP signal was seen, indicating that the dendrite had been pinched at that point. After allowing the microelectrode to rest in this position for 1-2 min, the electrode was slowly moved down vertically, allowing the tip to flex and push the proximal aspect of the dendrite toward the soma and away from the more distal dendrites. Complete transection of the dendrite as well as the integrity of the dendritic arbor was verified by DIC images. In order to be included in experiments, transected neurons were required to meet the following criteria: (1) both the transected process and the neuron from which it was cut must remain morphologically intact and healthy for the duration of the experiment; (2) no signs of varicosity formation or blebbing; (3) some detectable fluorescence signal must be observed in the transected process 2 hr post transection.

**Photobleaching**

In FRAP experiments, an infected neuron was selected and a dendrite from that neuron was scanned for 1 hr with a 488 nm, 5 mW laser. Complete volumetric data of the dendrite to be studied were acquired at regular intervals before and after the bleaching. In optical isolation experiments, an infected neuron was selected, and its soma was continuously scanned to photobleach the somatic GFP. Propidium iodide (PI) exclusion experiments were conducted to insure neuronal viability during optical isolation experiments. After ~90 min somatic photobleaching, the cell was stained with PI solution (50 μg/ml). The cell was then assessed for PI staining. Positive control experiments utilizing glutamate-induced toxicity (250 μM) were also carried out. No PI staining was evident after somatic photobleaching whereas the glutamate-induced toxicity in the same

cells led to strong PI staining. Pilot experiments indicated that complete somatic photobleaching was obtained within 120 min of the initiation of photobleaching. In all experiments, data analysis began with this (complete somatic photobleaching) time point and hence was designated as t = 0. Using data from FRAP experiments, we estimate the membrane tethered reporter's diffusion coefficient to be $1 \times 10{-}8$ $cm^{2/s}$, which is only slightly greater than the diffusion coefficient of rhodopsin ($\sim 5 \times 10{-}9$ $cm^{2/s}$) (Wey et al., 1981) and glycine receptors ($\sim 1 \times 10{-}9$ $cm^{2/s}$) (Srinivasan et al., 1990). This difference is expected since rhodopsin and glycine receptors are integral membrane proteins that may be bound to elements in the cytoskeleton and therefore would be more diffusion limited than a myristoylated protein. This estimate of the reporter's diffusion coefficient may include the simultaneous effects of degradation on the reporter. Indeed, there are examples of FRAP experiments where the rate of degradation of the reporter exceeded the rate of diffusion of the reporter.

**Analysis**

To analyze the GFP of individual dendrites, we calculated the mean pixel intensity for each dendrite along its length (NIH Image, or ImageJ), thus controlling for changes in the width of the dendrite. In time-lapse experiments, we calculated a normalized difference score, $\Delta F/F(y - x/x)$, that indicates the change in dendritic fluorescence as a function of time and, when appropriate, treatment with BDNF. In plotting $\Delta F/F$, the data were binned into 1–2 μm sections. In regular time-lapse and dendritic transection experiments, x was

the baseline (first) fluorescence measurement and y was the brightest time point following the baseline (typically 120 min). In "optical isolation" experiments, x was chosen as the lowest time point following somatic photobleaching and y was usually taken 60 min later. All untreated cells were "yoked" to experimental cells. That is, they were infected at the same time, imaged at equivalent time points, and the analysis was calculated using the same time points as their BDNF-treated "sister" neurons. For analysis of colocalization, horizontal dendritic segments were analyzed by obtaining the mean fluorescence signal across the width of the dendritic segment. A cross-correlation was calculated for the myrdGFP and PSD-95, synapsin, or Y10B: the mean fluorescence across the width of a dendritic segment was calculated, generating a one-dimensional representation of the relative amplitudes of the red and green signals. A cross-correlation was calculated on these two data sets. To calculate the significance of the cross-correlation, one hundred cross-correlations of the randomized data were performed to yield a 95% confidence level. In other experiments, Student's t tests were performed to assess statistical differences between groups. We chose for analysis the brightest (usually principal) dendrite from each neuron in each group. When a single neuron possessed two bright, principal dendrites, both were used in the analysis.

*Chapter III*

# Dopaminergic Stimulation of Local Protein Synthesis Enhances Surface GluR1 Expression and Synaptic Transmission in Hippocampal Neurons

## Introduction

The use-dependent modification of synapses is strongly influenced by the actions of the neuromodulator dopamine, a transmitter that participates in both the physiology and pathophysiology of animal behavior. In the hippocampus, dopaminergic signaling acting via the cAMP-PKA pathway is thought to play a key role in protein synthesis-dependent forms of synaptic plasticity ( Frey et al., 1993; Huang and Kandel, 1995; Bach et al., 1999). The molecular mechanisms by which dopamine influences synaptic function, however, are not well understood. Using a green fluorescent protein (GFP)-based reporter of translation, as well as a novel, small-molecule reporter of endogenous protein synthesis, we show that dopamine D1/D5 receptor activation stimulates local protein synthesis in the dendrites of cultured hippocampal neurons. Furthermore, we identify the GluR1 subunit of AMPA receptors as one protein upregulated by dopamine receptor activation. In addition to enhancing GluR1 synthesis, dopamine receptor agonists increase the incorporation of surface GluR1 at synaptic sites. The insertion of new GluRs is accompanied by an increase in the frequency, but not the amplitude, of miniature synaptic events. Together, these data suggest a local protein synthesis-dependent activation of previously silent synapses as a result of dopamine receptor stimulation.

## Results

In initial experiments, we examined the ability of a dopamine D1/D5 receptor agonist (SKF-38393) to stimulate protein synthesis by visualizing a GFP protein synthesis reporter molecule (Aakalu et al., 2001) in cultured hippocampal neurons. We compared the levels of GFP signal in control (untreated) neurons to neurons that had been exposed to bath application of the dopamine agonist. Relative to controls, neurons treated with SKF (100 μM for 15 min) showed significantly enhanced protein synthesis in both the soma and dendrites (Figure 3.1A,C). Similar results were obtained with a different D1/D5 receptor agonist, dihydrexidine (DHX; data not shown). The stimulation of protein synthesis by SKF was completely prevented by the co-application of a D1/D5 receptor antagonist (SCH-23390; 10 μM), confirming that the observed effects are due to dopamine receptor activation [mean percent inhibition of SKF-stimulated protein synthesis: 97.3 ± 5.1%; n = 12]. We next examined the time course of SKF-induced protein synthesis using time-lapse imaging of dendrites. Control dendrites exhibited relatively stable levels of GFP fluorescence over a 60-minute imaging period (Figure 3.1B). In contrast, a brief (15 min) exposure to SKF increased the GFP signal in dendrites within 60 minutes (Figure 3.1B,D). In both sets of experiments, the effects of SKF were completely prevented by co-application of the protein synthesis inhibitor anisomycin (Figure 3.1C,D), indicating that D1/D5 receptor activation stimulates protein synthesis in hippocampal neurons.

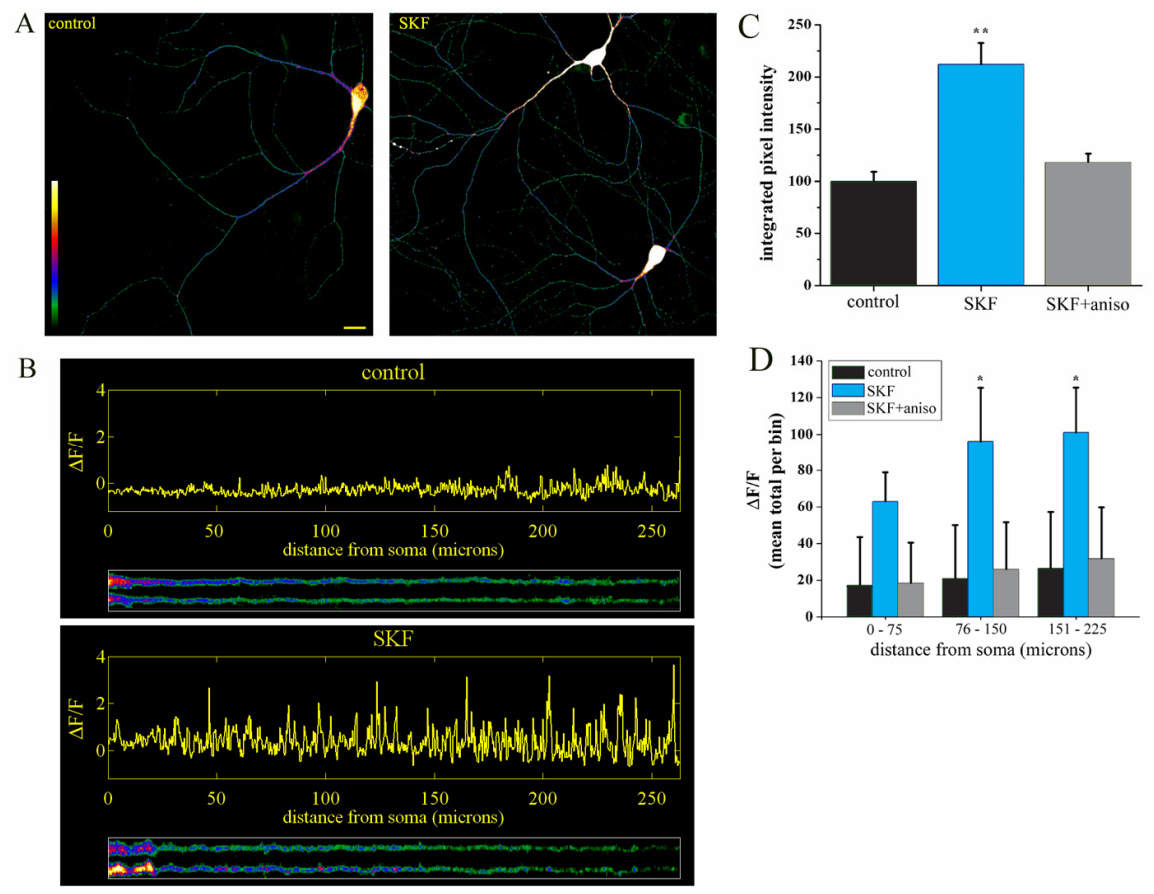


**Figure 3.1** Dopamine D1/D5 Receptor Activation Stimulates Protein Synthesis in Hippocampal Neurons

**(**A) P2 cultured hippocampal neurons infected with a sindbis virus encoding a GFP reporter. Shown are a control neuron (left) and neurons treated for 15 minutes with the D1/D5-selective agonist SKF-38393 (right). The pseudocolor scale at left in the control image indicates GFP fluorescence levels. Scale bar = 15 μm.

**(**B) Time-lapse imaging of a control neuron (top panel) shows a small decrease in GFP signal as seen in the ΔF/F plot for images before and 60 minutes after vehicle treatment. In contrast, a neuron treated with SKF for 15 minutes (bottom panel) shows an overall increase in GFP signal, with small hotspots of high-intensity fluorescence throughout the dendrite. Images of the dendrites before (top) and 60 minutes after vehicle or SKF treatment (bottom) are shown in the white box beneath each ΔF/F plot, which is aligned to the dendrite shown.

**(**C) Between-dish (A) summary data showing a significant increase in GFP fluorescence in the dendrites of SKF-treated neurons relative to control neurons ($n$ = 28 dendrites per condition, $p < 0.01$).

**(**D) Time-lapse (B) summary data 60 minutes after agonist application showing a significant increase in GFP signal at distances greater than 75 microns from the cell soma ($n$ = 12 dendrites per condition, asterisk indicates $p < 0.05$).

The above data show that dopamine agonists can stimulate the synthesis of a fluorescent protein synthesis reporter that contains the 5' and 3' untranslated regions from CaMKIIα (Aakalu et al., 2001). To determine whether D1/D5 receptors activate the translation of endogenous mRNAs in living neurons, we used fluorescein-dC-puromycin (F2P), a novel protein synthesis reporter based on the peptidyl transferase inhibitor puromycin (Starck and Roberts, 2002). Because puromycin is a structural analog of an amino-acyl tRNA molecule, it enters ribosomes actively engaged in translation where it becomes covalently attached to the carboxy-terminus of nascent proteins through a peptide linkage (Nathans, 1964). Initially, we examined whether F2P can serve as a protein synthesis reporter in cultured hippocampal neurons (Figure 3.2A,B). A brief (~15 min) bath application of F2P resulted in fluorescence detected in both the cell body and the dendrites (Figure 3.2A). The majority of the fluorescence observed in the dendrites reflects basal protein synthesis as it was significantly attenuated by co-application of anisomycin or unlabeled puromycin (data not shown). When neurons were treated with the dopamine agonist SKF in the presence of F2P, a dramatic stimulation of protein synthesis in the cell body, dendrites and spines was observed [mean percent increase in F2P signal relative to control: 91.3 ± 11.2 %; n = 14] (Figure 3.2B). These data indicate that dopamine agonists can stimulate the synthesis of endogenous protein(s) in hippocampal neurons.

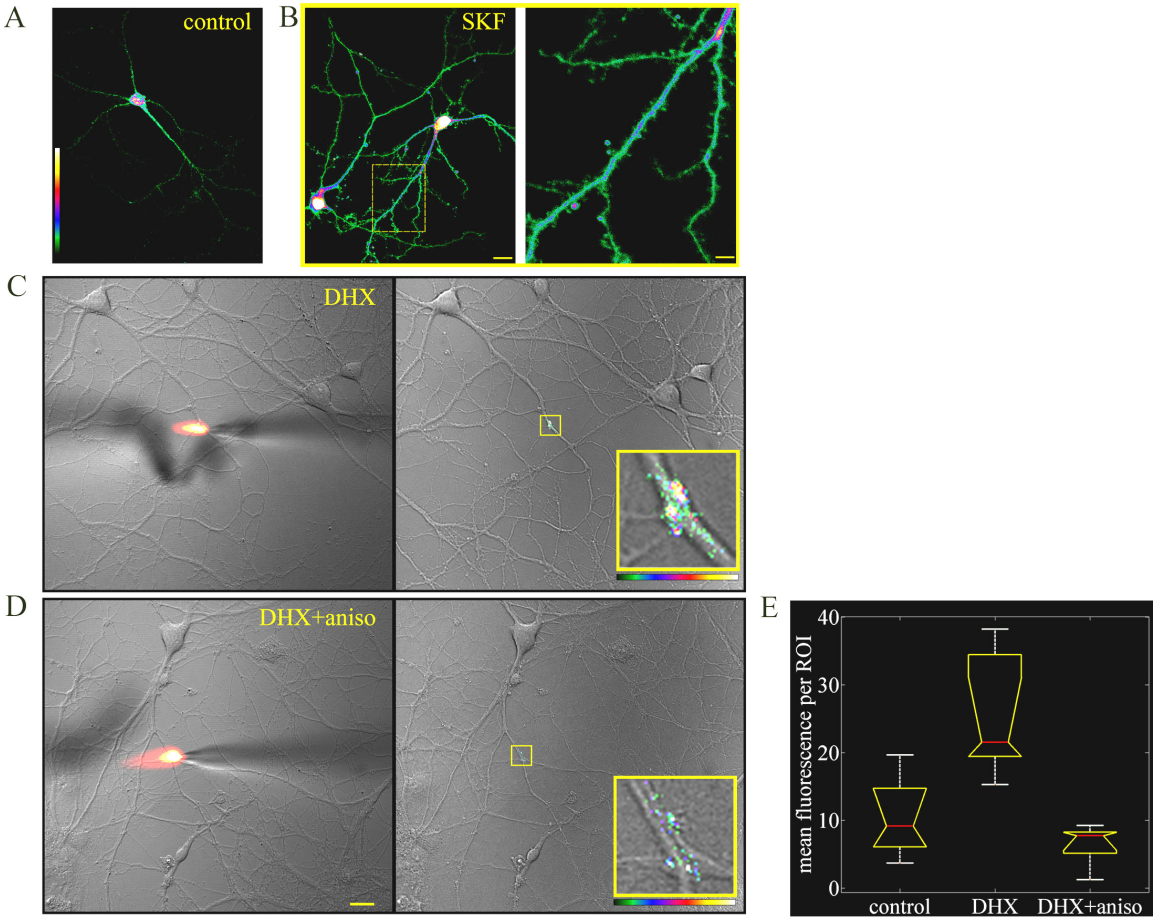


**Figure 3.2** A Dopamine Agonist Stimulates the Local Translation of Endogenous Proteins as Indicated by Novel Puromycin-Based Reporter of Protein Synthesis

(A) A control neuron incubated for 15 minutes in F2P (left) exhibits moderate levels of fluorescence primarily due to basal rates of protein synthesis in the unstimulated cell.

(B) Neurons treated with the dopamine agonist SKF for 15 minutes in F2P show markedly higher fluorescence, with signal apparent throughout the dendritic arbor. The region boxed in yellow is shown at high power (right), where signal in the spines is clearly evident. Scale bars = 20 (left), and 5 μm (right).

(C) A solution containing dihydrexidine (DHX), F2P, and the dye Alexa 568 (to mark solution flow) was perfused for 15 minutes onto a small dendritic segment of a cultured hippocampal pyramidal cell (left; shown is dye spot) resulting in a strong dendritic F2P signal (right). The high-power image (right, inset) shows high levels of F2P incorporation indicating local protein synthesis in the stimulated dendrite.

(D) Pretreatment and perfusion with a solution containing anisomycin abolished most of the DHX-induced F2P incorporation in the dendrite (compare high-power insets at right).

(E) The average F2P pixel intensity in each perfused region of interest (ROI, defined by the area of dendrite beneath the Alexa 568 dye) is shown as a series of box plots (see methods for a description of box plots). Perfusion of dendrites with DHX resulted in significantly greater F2P incorporation when compared to control dendrites ($p < 0.05$). The enhancement produced by DHX was completely blocked by preincubation and perfusion with anisomycin ($p < 0.01$, $n = 8$ dendrites for each condition).

Local, dendritic protein synthesis (Steward and Levy, 1982; Torre and Steward, 1992) is required for some forms of synaptic plasticity (Huber et al., 2000; Kang and Schuman, 1996; Martin et al., 1997). We directly examined whether dopamine receptor activation stimulates local protein synthesis by restricting the F2P application to a small (3-10 μm) region of the dendrite (Figure 3.2C). Using a red fluorescent dye to monitor the size and location of the perfusion spot, we locally delivered a continuous stream of both F2P and the D1/D5 agonist DHX (Figure 3.2C) to dendritic regions at least 100 μm from the cell body. A 15-minute exposure to DHX caused a dramatic stimulation of local protein synthesis (Figure 3.2C,E) that was completely prevented when anisomycin was included in the perfusate (Figure 3.2D,E). Because the perfusate was delivered only to a small region of dendrite, remote from the cell body, the F2P signal detected is the result of local protein synthesis. These data firmly establish that D1/D5 agonists stimulate protein synthesis in dendrites.

The above data indicate that dopamine agonists can stimulate the dendritic synthesis of endogenous proteins, but do not establish which particular protein(s) are the targets of dopamine receptor activation. Since dopamine has been shown to enhance synaptic transmission at hippocampal synapses (Bouron and Reuter, 1999; Frey et al., 1993; Huang and Kandel, 1995; Otmakhova and Lisman, 1996), we considered the possibility that a glutamate receptor subunit might be a target for local, dopamine-stimulated translation. We first examined the effect of dopamine agonist treatment on total GluR1 protein detected by Western blot analysis of lysates prepared from hippocampal neurons. We found that a brief (20 min) exposure to DHX resulted in a significant increase

in GluR1 levels relative to untreated controls (Figure 3.3A). In individual experiments, we observed a 9–20% increase in GluR1 levels following D1/D5 receptor activation, which was blocked by anisomycin (Figure 3.3A). A DHX-stimulated increase in dendritic GluR1 was also observed in a parallel set of experiments in which quantitative immunocytochemical labeling was conducted on cultured hippocampal neurons (Figure 3.3B). We next examined whether the new synthesis of GluR1 alters the population of receptors on the cell surface at synaptic sites. Using an antibody that recognizes the GluR1 extracellular domain, we conducted live immunolabeling for surface GluR1 (Figure 3.3C). To determine the location of surface-expressed GluR1 relative to synaptic sites, presynaptic compartments were labeled with an anti-synaptophysin antibody (Figure 3.3C). In control conditions we observed 24 synaptophysin-positive puncta per 10 μm; on average, 21.6% of these puncta colocalized with the surface GluR1. Neurons briefly exposed to DHX (15 min) showed a large, anisomycin-sensitive increase in surface GluR1 (Figure 3.3C-E; Table 1). This increase was evident in both the number and average size of GluR1 puncta detected on the surface; the average intensity of GluR1 puncta was not changed (Table 1). The DHX-stimulated increase in GluR1 was accompanied by an increase in the overlap of GluR1-positive puncta with synaptophysin (Figure 3.3C-E). To analyze the overlap, the number of colocalized (GluR1 and synaptophysin) particles was divided by the number of synaptophysin particles; the result estimates the fraction of synaptic sites that are associated with GluR1 puncta. This analysis revealed that DHX treatment also increased the colocalization of the surface pool of GluR1 and synaptophysin. Importantly, the observed increase in colocalization cannot be attributed to a decrease in the number of synaptophysin particles (Figure 3.3E). Both the increased surface GluR1 expression and the increased

synaptic localization were prevented by anisomycin (Figure 3.3C-E), indicating that protein synthesis is required for these changes.

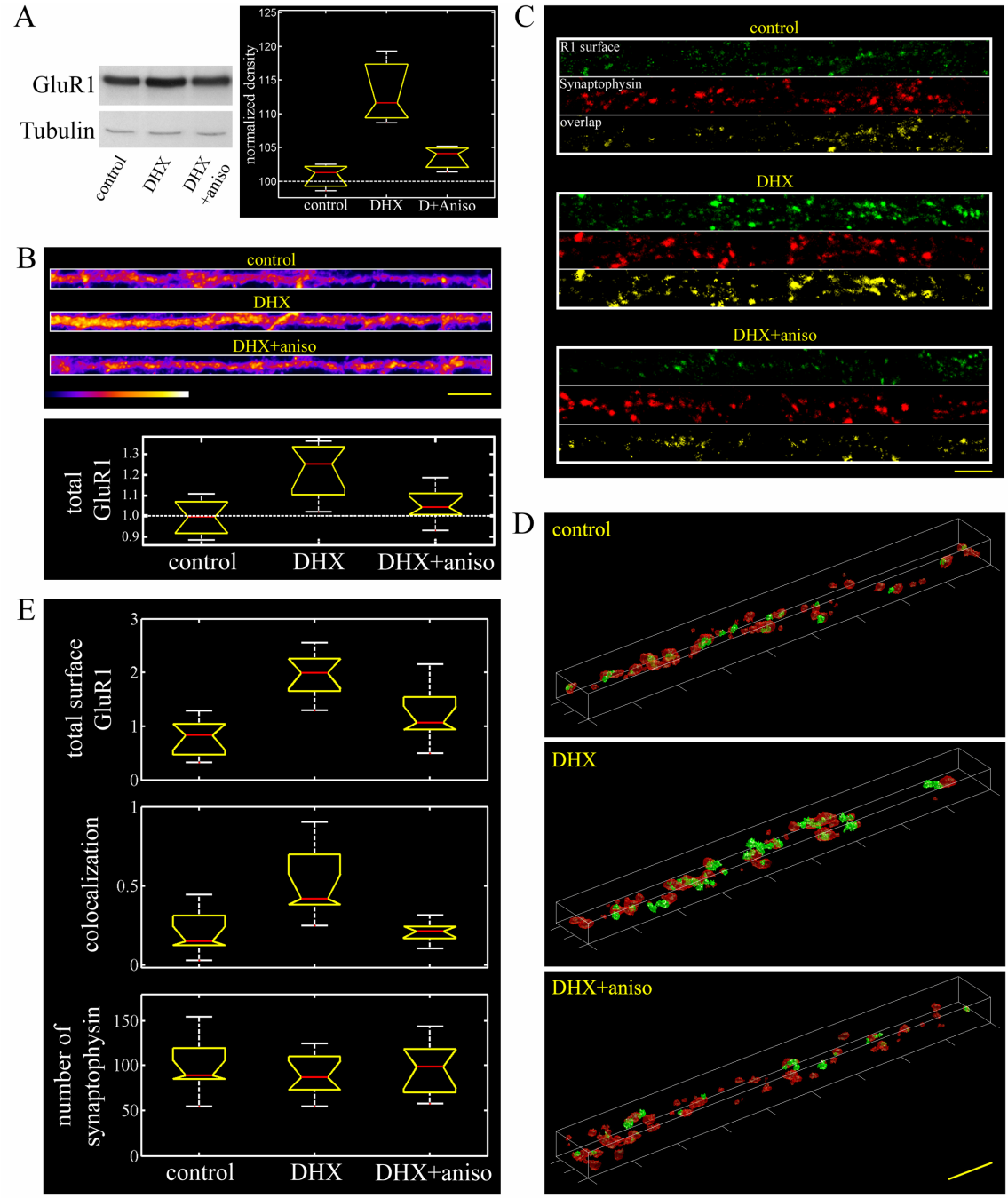


**Figure 3.3** Treatment With a Dopamine Agonist Produces a Protein Synthesis-Dependent Increase in Total and Surface GluR1 Expression at Synaptic Sites

(A) Western blot of whole-cell lysates prepared from cultured hippocampal neurons treated for 20 minutes with DMSO (control), dihydrexidine (DHX), or DHX plus anisomycin (DHX+aniso). Blots were probed with antibodies against GluR1 (top), and β-Tubulin as a loading control (bottom). A box plot summary of GluR1 band densities normalized to the Tubulin band in each lane (control mean = 100%) shows significantly higher levels of GluR1 protein in neurons treated with DHX, which is blocked by anisomycin ($n = 3$, $p < 0.05$).

(B) Neurons treated with DMSO (control), dihydrexidine (DHX), or dihydrexidine in the presence of anisomycin (DHX+aniso) show significantly increased levels of total GluR1 protein detected in the dendrites by immunofluorescence labeling ($n = 12$ dendrites per condition, $p < 0.05$). As shown in the box plot summary, the effect is blocked by anisomycin, with no significant difference detected between control and DHX+aniso groups. The pseudocolor scale ranging from dark blue to white is shown at bottom left. Scale bar = 15 μm.

(C) Neurons treated as in (B) were immunostained under nonpermeabilizing conditions with antibodies recognizing extracellular epitopes of GluR1 (green), and synaptophysin (red), and are shown as 2-D projections. The yellow image (overlap) of each 2-D set represents the colocalization between GluR1 and synaptophysin. Increased surface GluR1 as well as increased colocalization of GluR1 with synaptophysin is evident in dendrites treated with DHX. Scale bar = 5 μm.

(D) Representative examples of immunostained dendritic segments are shown as 3-D surface renderings. In these images, only those GluR particles that overlap with synaptophysin are shown whereas all synaptophysin particles are shown. Scale bar = 5μm.

(E) Analysis of 3-D immunostaining data shows significantly increased surface GluR1 and GluR1/synaptophysin colocalization in dendrites treated with DHX ($n = 15$ dendrites per condition, $p < 0.01$). DHX-induced increases were blocked by anisomycin ($p < 0.01$), with no significant difference in synaptophysin labeling between groups.

Given the increase in the total and synaptic GluR1 population, we next examined the effects of dopamine agonists on synaptic transmission. To monitor synaptic strength before and after exposure to a dopamine agonist, we recorded miniature excitatory postsynaptic currents (mEPSCs) in cultured hippocampal neurons. After a baseline recording period (Figure 3.4$A_i$,$B_i$) neurons were treated with DHX (Figure 3.4A) or DHX in the presence of anisomycin (Figure 3.4B). We observed that DHX induced a rapid increase in mEPSC frequency that was completely prevented when protein synthesis was inhibited. On average, DHX induced a 2-fold increase in mEPSC frequency (Figure 3.4C). There was, however, no change in mEPSC amplitude elicited by the dopamine agonist

(Figure 3.4D). To determine whether the mEPSC frequency increase was due to a pre- or postsynaptic mechanism, we included the membrane impermeant PKA inhibitor peptide $PKI_{6-22}$ in the recording pipette. Blocking the activity of PKA postsynaptically completely prevented the DHX-induced increase in mEPSC frequency (Figure 3.4C). These data indicate that activation of D1/D5 receptors induces a postsynaptically-driven increase in the frequency, but not amplitude, of mEPSCs.

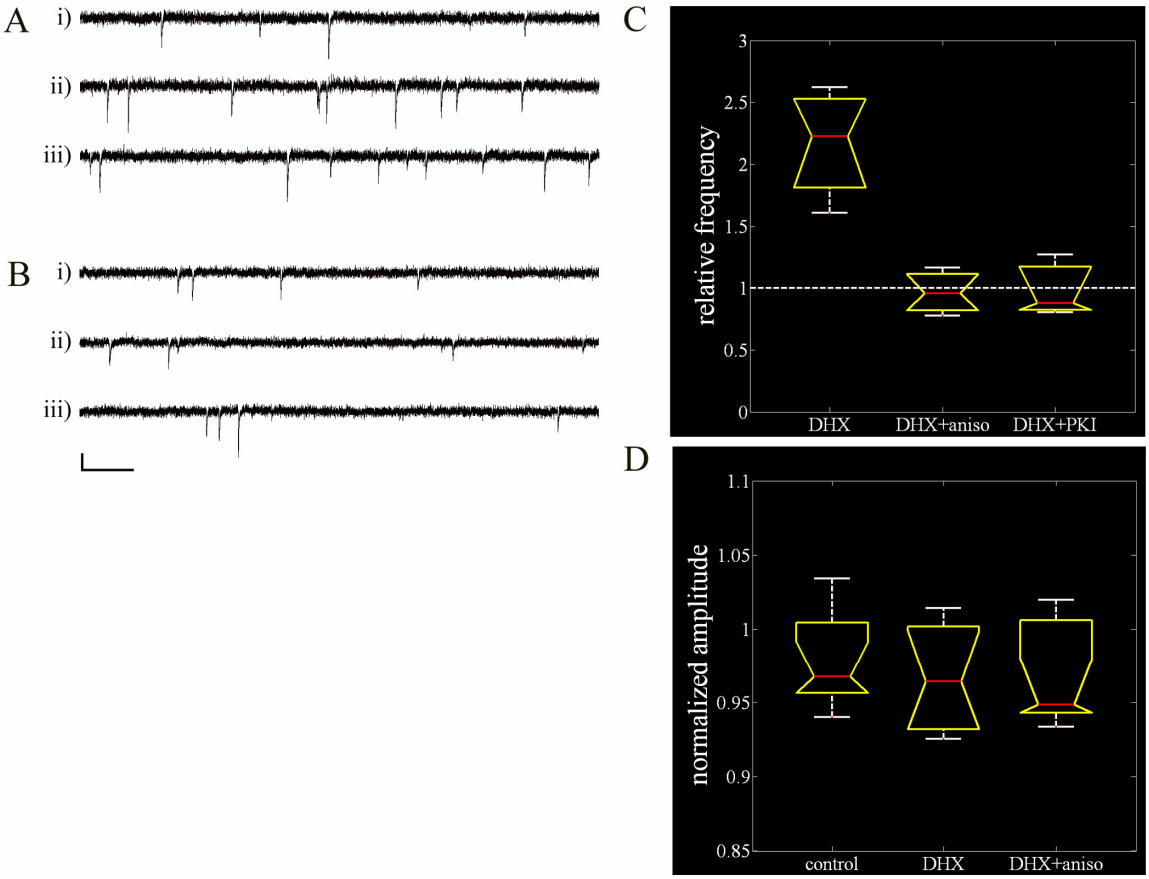


**Figure 3.4** A Dopamine Agonist Increases the Frequency, but Not the Amplitude, of Miniature Excitatory Postsynaptic Currents in a Protein Synthesis-Dependent Manner

(A) Whole-cell voltage clamp recording from a cultured hippocampal neuron during a baseline period (i), and 10-12 minutes after bath application of dihydrexidine (ii and iii) shows a rapid increase in mini frequency after agonist application.

(B) Whole-cell voltage clamp recording from a neuron pretreated with anisomycin for 30 minutes shows no difference in mini frequency between the baseline recording period (i) and 10-12 minutes after bath application of dihydrexidine (ii and iii). Scale bar = 10 pA, 333 ms.

(C) Summary analysis illustrating a 2-fold increase in mini frequency in neurons treated with dihydrexidine (DHX), which is completely blocked by preincubation with anisomycin (DHX+aniso, $n$ = 10 cells per condition, $p < 0.01$). Relative frequency is plotted as the mean frequency 10-12 minutes after agonist application, normalized to the mean frequency during the final 2 minutes of the baseline recording period for each experiment.

(D) Analysis of mini amplitudes shows no significant difference between groups. Normalized amplitudes are plotted as the mean amplitude 10-12 minutes after agonist application, normalized to the mean amplitude during the final 2 minutes of the baseline recording period for each experiment.

Using both a GFP-based reporter of local translation and a novel, small molecule reporter, we observed the stimulation of local protein synthesis in the dendrites of cultured hippocampal neurons by dopamine receptor agonists. We identify GluR1 as one synaptic protein whose synthesis is stimulated by dopamine receptor activation; dopamine agonists also induced an increase in surface GluR1, as has been observed in the nucleus accumbens (Chao et al., 2002; Mangiavacchi S, 2004). The agonist-stimulated increase in surface GluR1 required new protein synthesis and increased the fraction of synapses that possess a surface GluR1 cluster. The stimulated synthesis and surface expression of GluR1 was accompanied by a dopamine agonist-stimulated increase in the frequency, but not amplitude, of mEPSCs. Because these changes occur rapidly (10-15 minutes), our data are most consistent with the idea that GluR1 is locally synthesized. Indeed, two recent studies have demonstrated that glutamate receptors can be locally synthesized in dendrites (Ju et al., 2004; Kacharmina et al., 2000). Taken together, these data suggest that D1/D5 receptor activation stimulates a local protein synthesis-dependent increase in surface GluR1 at synaptic sites that did not previously possess functional postsynaptic GluRs, consistent with

the activation of postsynaptically silent synapses (Isaac et al., 1995; Liao et al., 1999; Liao et al., 1995; Petralia et al., 1999).

Our data provide a potential cellular mechanism for the dopaminergic modulation of long-lasting plasticity at hippocampal synapses. Others have reported that dopamine or activators of the cAMP/PKA pathway can induce a long-lasting protein synthesis-dependent form of potentiation in hippocampal slices (Frey et al., 1993; Huang and Kandel, 1995). It has also been shown that late-phase long-term potentiation (LTP) is diminished in hippocampal slices treated with dopamine receptor antagonists (Frey et al., 1991; Frey et al., 1990; Swanson-Park et al., 1999) or prepared from D1 receptor knock-outs (Matthies et al., 1997). In addition, a PKA-dependent increase in GluR1 synthesis has been observed during the late (3hr post-induction) phase of LTP (Nayak et al., 1998). The data presented here indicate that dopamine may exert its effects on plasticity, at least in part, by local regulation of protein synthesis.

| 3D particles analysis summary data | | | | | | | | | | |
|---|---|---|---|---|---|---|---|---|---|---|
| | R1 num | R1 vol | R1 intensity | R1 total | Syn num | Syn vol | Syn intensity | Coloc num | Coloc /R1 | Coloc /Syn |
| control | 91.70 | 20.77 | 35.60 | 0.7e5 | 101.1 | 65.24 | 4.0e5 | 26.70 | 0.254 | 0.216 |
| DHX | 183.5 | 33.10 | 31.93 | 1.9e5 | 98.60 | 61.18 | 2.8e5 | 53.30 | 0.334 | 0.492 |
| DHX+aniso | 111.9 | 24.34 | 38.83 | 1.1e5 | 97.90 | 61.34 | 3.0e5 | 32.10 | 0.294 | 0.227 |
| Statistical comparison between groups (ANOVA) | | | | | | | | | | |
| ctrl/DHX | * | * | | * | | | | * | | * |
| DHX/aniso | * | * | | * | | | | * | | * |

**Table 3.1**: 3D particle analysis values

Shown are summary data for the 3D particles analysis on surface GluR1 staining (R1) and synaptophysin (Syn) colocalization (Coloc). The variables are: number of particles (num), mean particle volume (vol), mean pixel intensity per particle (intensity), and integrated pixel intensity (total). An asterisk in the bottom portion of the table indicates statistical significance at $p < 0.05$. No significant differences were observed between the control and DHX+aniso groups.

## Methods

### Cultured hippocampal neurons

Dissociated hippocampal neurons were prepared and maintained as previously described (4). Briefly, hippocampi from postnatal day 2 Sprague-Dawley rat pups were enzymatically and mechanically dissociated and plated into poly-lysine coated glass-bottom petri dishes (Mattek). Neurons were maintained for 14-21 days at 37º C in growth medium (Neurobasal A supplemented with B27 and Glutamax-1, Invitrogen).

### Microscopy and image analysis

All images were acquired with an Olympus IX-70 confocal laser scanning microscope running Fluoview software (Olympus America, Inc). GFP, Alexa 488, and F2P were excited with the 488 nm line of an argon ion laser, and emitted light was collected between 510 and 550 nm. Alexa 568 was excited with the 568 nm line of a krypton ion laser, and emitted light was collected above 600 nm. In experiments where two channels were acquired simultaneously, settings were chosen to ensure no signal bleed-through between channels. For between-dish comparisons on a given day, all images were acquired at the same settings, without knowledge of the experimental condition during image acquisition. All post-acquisition processing and analysis was carried out with ImageJ (NIH) and MATLAB (The MathWorks, Inc.). To facilitate the analysis of fluorescence signal as a function of distance from the soma, dendrites were linearized and extracted from the full-frame image using a modified version of the Straighten plugin for ImageJ.

Dendrites were analyzed for time lapse as follows: fluorescence was averaged across the width of linearized dendrites, generating a vector of mean pixel intensities equal to the length of the dendrite. $\Delta F/F$ ($F_{tn}$-$F_{t0}/F_{t0}$) was then computed at each pixel along the dendritic length. A value of one was added to every pixel in the linearized dendrite image, to a maximum of 255, which sets the minimum mean pixel intensity across the width of the dendrite equal to one. This prevents artificially large $\Delta F/F$ values that result from fractional mean pixel values due to zeros in the initial image. For time-lapse summary data, the sum of $\Delta F/F$ values in 75 μm bins was computed for each dendrite, and the mean ± standard error for all dendrites in a given experimental condition was plotted. 3-D colocalization and particle analysis was performed using custom-written functions in Matlab. Of particular concern in such measurements is the issue of selecting appropriate threshold values to isolate the punctate data of interest from background noise in the raw images. In order to avoid potential biases in selecting thresholds, we have relied on the *graythresh* command in Matlab. This function generates an optimal threshold based on Ostu's method, which sets a threshold that minimizes the intraclass variance of the black and white pixels. To further ensure that the experimental effects we observed were robust to threshold settings, the colocalization and particle analysis was performed with a series of 7 to 11 thresholds, using the output of graythresh as the median threshold value. All reported results were unaffected by such a range of threshold settings.

**Box plots**

Box plots were used because they capture a number of properties about the distribution of the data in a single graph. In each box plot, the red line indicates the median of the data, the diagonal lines leading away from the median (notches) are robust estimates of the uncertainty about the median, the horizontal white lines show the interquartile range, and the vertical whiskers represent the entire extent of the data. In general, a visual comparison of data shown in a box plot can be used to determine statistical significance by comparing the notches between groups; if the notches do not overlap, the two data sets are significantly different from one another.

**GFP experiments**

The GFP construct and Sindbis virus used were described previously (Aakalu et al., 2001). Neurons 14-21 days in vitro were infected for 15-20 minutes with the virus, and allowed to incubate for 12-14 hours at 37º C before imaging commenced. After the incubation period, cells were transferred from growth medium into a HEPES-based imaging medium (HBS), containing (in mM): 119 NaCl, 5 KCl, 2 $CaCl_2 \cdot 2H_20$, 2 $MgCl_2 \cdot 6H_20$, 30 glucose, 20 HEPES. Dishes were maintained at 37º C in HBS for a minimum of 1 hour prior to imaging. For between-dish experiments (Fig 1A), neurons were treated for 15 minutes with 100 μM SKF-38393 (Sigma), rinsed with HBS, incubated at 37º C for an additional 45 minutes, and then fixed in 4% formaldehyde / 4% sucrose for 20 minutes at 4º C. For time-lapse experiments (Fig 1B), 3 baseline images were acquired at 30-minute intervals before drug treatment in order to ensure relatively stable

fluorescence in un-manipulated neurons. At time t=0, neurons were treated for 15 minutes with HBS (control) or 100 μM SKF. The next image (t=30 minutes) was acquired 15 minutes after drug washout, and images were acquired every 30 minutes thereafter. Neurons were maintained at 37º C between imaging periods, with image acquisition periods lasting no longer than three minutes at room temperature. In an effort to control for possible non-specific mechanical effects of adding or removing solution from the dishes, the number of solution exchanges was held constant across all experimental conditions.

**F2P experiments**

Fluorescein-dC-puromycin was synthesized using standard phosphoramidite chemistry at the California Institute of Technology oligonucleotide synthesis facility and desalted via OPC cartridge chromatography (Glen Research) and on Sephadex G-10 (Sigma). For bath application experiments, F2P was added to HBS for a final working concentration of 40-60 μM. Cells were pre-loaded with F2P for 5 minutes and then incubated in SKF (100 μM) or HBS (control) for 15 minutes in the presence of F2P at 37° C. F2P was washed out with 4x 2 ml of HBS before neurons were fixed for fluorescence microscopy. Local perfusion experiments were done for 15 minutes without pre-loading the neurons with F2P. Flow rates were manually regulated using syringes attached to patch pipettes. The was no significant difference in perfusion spot size between groups (data not shown). In experiments using anisomycin to inhibit F2P incorporation, equimolar concentrations of anisomycin were added to the neurons 30 minutes before and for the entire duration of the experiment.

**Immunocytochemistry and Western blot analysis**

For surface GluR1/Synaptophysin colocalization experiments, cultured neurons were pre-treated for 20 minutes at 37 º C with DMSO or 40 μM anisomycin and then treated for 15 minutes at 37º C with DMSO (control), 10 μM dihydrexidine (DHX), or DHX+anisomycin. Immunolabeling of cultured hippocampal neurons to detect total as well as surface GluR1 was done as previously described (Patrick et al., 2003; Richmond et al., 1996). For surface labeling experiments, neurons were live-labeled for 10 minutes at 37º C with an antibody against the extracellular domain of GluR1 immediately following drug treatment, and then fixed and processed for immunocytochemistry using conventional techniques. For Western blot experiments, three dishes of high-density neurons were used for each experimental condition, and samples for each condition were loaded in triplicate on each gel. Anisomycin-treated dishes were pretreated for 30 minutes with 40 μM anisomycin; control and DHX-treated dishes were pretreated with DMSO. After the preincubation period, dishes were then treated with DMSO (control), 10 μM DHX, or DHX+40μM anisomycin for 20 minutes. The analysis represents the mean GluR1 band density normalized to the β-Tubulin band for all three lanes in a given experiment. A total of three experiments (9 lanes per condition) were analyzed. The following antibodies were used: rabbit anti-β-Tubulin (1:200, Santa Cruz Biotechnology), rabbit anti-GluR1 N-terminal domain (1:10, Oncogene Research Products), rabbit anti-GluR1 for Western blot (1:1,000, Upstate), mouse anti-synaptophysin (1:1000, Sigma), goat anti-mouse Alexa 568 (1:300), goat anti-rabbit Alexa 488 (1:300, Molecular Probes).

**Whole-cell recordings**

Whole-cell recordings in voltage clamp mode were performed on cultured neurons 14-21 days in vitro using a whole-cell solution containing (in mM): 100 gluconic acid, 0.2 EGTA, 5 $MgCl_2 \cdot 6H20$, 40 HEPES, 2 Mg ATP, 0.3 Li GTP, pH adjusted to 7.2 with CsOH. Cells were held at a membrane potential of -60 to -65 mV with holding currents that did not exceed -250 pA. Baseline recordings from cells were acquired for 5-8 minutes for each cell, and for at least 10 minutes after drug application. For anisomycin experiments, cells were pretreated with 40 μM aniso for 30-45 minutes, and anisomycin was added to the recording pipette. The $PKI_{6-22}$ peptide was used at 20 μM in the patch pipette. Neither anisomycin, nor $PKI_{6-22}$ significantly affected baseline frequency or amplitude (data not shown). Cells with a change in series resistance that exceeded 15% were excluded from analysis.

*Chapter IV*

# Quantitative Analysis of 3-D Colocalization and 2-D Correlation of Two-Color Fluorescence Images

## Introduction

The trend in neuroscience and other fields of biology over the past 10 years to rely upon images produced by advanced microscopy techniques has not been met with an availability of tools for the careful quantitation of such images. All too frequently, an image is shown in a publication as being a 'representative example' of a reported effect, yet no statistical summary accompanies the image. In certain cases, the effect is sufficiently obvious that an analysis of the image may not provide additional information. However, given the tremendous variability in biological systems, it is very important that the beauty and stunning detail captured at the subcellular level with today's microscopes is substantiated with a rigorous analysis of properties of interest within the images.

Of particular relevance in this regard is the analysis of the spatial co-distributions of two or more proteins within a cell as identified through fluorescence immunocytochemical techniques. In neurons, for example, it is frequently reported that a given protein, which may exhibit a punctate or particulate distribution, tends to colocalize with markers of synaptic sites. The clustering of a particular protein at a synapse could be biologically meaningful since, presumably, in order to affect the function of the synapse in some way, the protein should be located in close proximity to synaptic sites. Furthermore, the distribution of proteins may change as a function of the state of the neuron (e.g. the well-characterized movement of AMPA receptors into and out of the membrane in response to synaptic plasticity), and it is useful to understand quantitatively how the colocalization properties of sets of proteins may differ across a range of experimental conditions.

A number of commercially and freely available programs provide the ability to analyze colocalization in two dimensions, employing a simple scatter plot of the pixel intensities of two-color immunostained images, with the colocalization index represented as a regression fit to the scatter plot. This method of quantifying colocalization is certainly a step in the right direction, but potentially interesting spatial information in the original images is lost in the final output of this type of analysis. Also, with the prevalence of confocal and multi-photon microscopy, it has become necessary to analyze colocalization in three dimensions rather than two. One software package exists with such capabilities (Volocity, from Improvision), although at a cost of more than $10,000.00, it is not practical for many users. Furthermore, at last assessment, the Volocity program was very slow to perform a colocalization analysis on images of dimensions 512x512x10, a routine image size. In order to facilitate the analysis of 3-D colocalization, and to make the technology accessible to all researchers, I have developed a program using MATLAB (The Mathworks), which has been compiled as a stand-alone application to run on any Microsoft Windows-based computer. While the program is very useful for quantifying the colocalization properties of protein particles in two-color fluorescence images, there are a number of limitations to the program in this early stage. The MATLAB source code, which can be compiled using MATLAB or run as a graphical user interface from within the MATLAB framework, is included in Appendix A. The program, including an assessment of its limitations, is discussed in the 3DParticles section below.

In addition to colocalization, clusters of proteins may exhibit biologically relevant spatial correlation. Even if the signals for two proteins never colocalize, it is interesting in

many instances to characterize and quantify the spatial codistributions of the particles. This case is illustrated by considering the ultrastructural detail of dendrites on central mammalian neurons, with the main dendritic shaft containing small protrusions called spines onto which a majority of excitatory synapses are made (see, for example, Figure 1.2). Due to rapid rates of active transport in neurons, measured at up to 5 μm/s (Brown, 2003), it is not necessary for a protein to be located within the spine in order to affect synaptic function on a rapid timescale. Indeed, the movement of proteins and cellular machinery such as ribosomes to the base of dendritic spines has been postulated as a molecular mechanism underlying synaptic plasticity (Ostroff et al., 2002; Shi et al., 2001; Shi et al., 1999; Steward and Levy, 1982). The quantitation of the 2-D spatial correlation of synaptic markers and postsynaptic proteins of interest, however, is lacking.

We have developed a strategy for a normalized 2-D cross-correlation analysis that greatly facilitates the quantitative description of the spatial codistributions of clusters of proteins within linear segments of dendrites and axons. Because there exists some random probability that two punctate signals exhibit spatial correlation, our algorithm estimates the random correlation that would be expected in a given image pair, and then subtracts the magnitude of that random correlation from the raw 2-D cross-correlation signal. The result is a 2-D correlation output that quantitatively describes the spatial coincidence of protein clusters in the cell, normalized to the correlation that might be randomly present simply due to the abundance of "on" signal in each thresholded image. The algorithm, as well as examples of the output of the Matlab script on simple test images, are illustrated in the 2DXcorr section below.

**3-D Particles Analysis**

3DParticles is a simple program for the quantitative analysis of colocalization in three-dimensional confocal or two-photon micrographs of fluorescently-immunolabeled biological specimens. A number of assumptions about the images must be true if the results of the program are to be meaningful. These considerations are to be taken into account for any high-resolution immunofluorescence microscopy experiments, and have been discussed in detail elsewhere, but some mention of the more relevant points is in order. Of primary concern is the optical thickness of each section for each color in the sample to be analyzed. Due to the differential chromatic aberrations from different wavelengths of fluorophores used in immunolabeling experiments (typically red and green fluorescent markers are used), the thickness of an optical section for each color will vary for a given confocal pinhole aperture. On systems with a continuously variable confocal pinhole, this can easily be circumvented by selecting an appropriate pinhole for each channel that results in optical slices of equal thickness. With some older confocal systems, however, it may be necessary to pre-process the images in order to negate any pixel shift before running the colocalization analysis. In general, if the user is comparing between experimental and control groups, such chromatic aberrations should average out between groups, but it is always best to ensure that the images are, as accurately as possible with light microscopy, representing the true positions of the proteins being analyzed. A generalized method for detecting and correcting chromatic aberrations in lateral as well as axial planes has been previously published (Kozubek and Matula, 2000), and will not be discussed further here.

Another issue of interest with regards to the fidelity of colocalization analysis in general is that of signal cross-talk, or bleedthrough. Because the excitation and emission spectra of fluorophores used in immunocytochemistry typically have some degree of overlap, it is important that the user select fluorophores, filter sets, and image acquisition parameters that minimize or eliminate signal bleedthrough from one channel to another. Using advanced microscopy systems such as the Zeiss Meta detector, or the Leica AOBS system, it is possible to completely separate the fluorophores based on their spectral characteristics. However, even in the absence of such high-tech spectral detectors, the experimenter should take care that appropriate filter sets and detector settings are used to minimize bleedthrough, which can create spurious colocalization signal even if the proteins in the cell never occupy the same general space. In any case, the amount of bleedthrough should be measured, and the amount of signal in each channel that results from such bleedthrough must be subtracted from the image, or a threshold must be set that does not include pixel intensity values within the range of the cross-talk.

One potential limitation of the 3DParticles program is the need to threshold the images in order to run the analysis. While this is an inevitable consequence of the morphological analysis performed by the algorithm, issues of thresholding are to be taken seriously. Morphological image analysis, almost by necessity, involves thresholding the images in order to define particles or other objects of interest. While it is possible to perform such segmentation without the use of direct thresholding techniques (for example, using the watershed segmentation algorithm), it is standard practice to convert a grayscale image into a thresholded binary image as the first step in many analysis routines. In the

best case scenario, thresholding will simply remove the noise, leaving behind the real data of interest in the image. In most instances, however, what is considered to be real is subjectively determined. While it may be true that the human eye is an exquisitely tuned machine for picking out the relevant objects of data in a noisy image, it is unsatisfying to use such subjective criteria in an analysis algorithm as "it looks good." Not only does it lack rigor, but it requires more user interaction with the analysis procedure, which ultimately increases the probability that user bias will interfere with the result. This is likely one reason for the vast body of literature on the subject of image thresholding in the computer science and electrical engineering communities.

Fortunately, there is a widely accepted method for analytically determining the optimal threshold in a grayscale image. This is an iterative technique known as Otsu's Method (Otsu, 1979), and is the basis for the initial threshold settings applied to the images when they are first loaded into the 3DParticles. While this is certainly not the only method for image segmentation, it is built in to MATLAB, so it is convenient. An interesting and highly-educational several hours may be spent on the internet by searching Google with the terms:

"image thresholding" otsu

Although not perfect, Otsu's method does at least provide an analytical starting point for defining image threshold cutoffs. Some limitations to the method involve the fact that it assumes a bimodal pixel intensity distribution, with one mode being the noise and the other being the data of interest. In images with high signal to noise ratio, such as tends

to be the case in confocal microscopy where the background is frequently equal to zero, the bimodal intensity assumption may not hold. This is why the 3DParticles program is equipped with a means of altering the threshold values (i.e., the sliders beneath each axis). There is still a subjective component to the routine as written, but one can simply chose to use the automatically generated threshold settings if an entire lack of subjectivity is desired. At the very least, this method provides some consistency in the threshold determination.

**Running 3DParticles**

Launching the program from within the Matlab environment opens a program window as shown in Figure 4.1A. The user loads 3-D image stacks by clicking on the "Load 3D Images" button. The program assumes the image stacks are saved as TIFF files. Once both images are loaded, three-dimensional surface renderings of each image are plotted into the two axes, with the top axis showing the first image that was loaded. As a starting point, the images are initially plotted using Otsu's method to generate a threshold. If desired, the user may then change the threshold for each image using the sliders beneath each image axis, or by entering a value between aero and one in the box to the left of each slider. For a quick look at a two-dimensional representation of the images, which may be useful in determining an appropriate threshold setting, the user may click on the "2D Projections" button.

The image in each axis may be rotated, zoomed, and panned across the screen using the left, right, and middle mouse buttons, respectively. This can prove to be useful when there are particles very close to one another, and complete separation is desired. By

rotating and zooming into the images, it is possible to set a threshold that effectively separates closely packed particles while maintaining as much image data as possible. If, after rotating the image, the orientation of the image becomes unclear, the default position can be reset with the "Reset Axes" button. The reset button functions only to restore the axes to the default 3-D position, and does not affect the zoom level.

Selection of three different colocalization plots is possible by selecting the desired output using the various radio buttons in the "Colocalization Plots" panel. The default setting, Colocalization Only, generates a plot showing only the particles in each image that are overlapping with one another. The other two options allow the user to plot all of the particles of one image or the other, along with the colocalized particles from the other image. Such a plot is useful in the case where a neuronal process has been filled with GFP or some other soluble dye, and the user is interested in only visualizing the particles from the other channel that are colocalized with the filled process. Once the appropriate plot style is selected, the routine is completed by clicking the "Save and Run" button, which results in the display of some progress indicator windows followed by the selected colocalization plot.

In addition to the graphical output as shown in Figure 4.1, 3DParticles generates a tab-delimited text file named "rowdat.txt" located in the directory where the original images were stored. This file contains 25 variables that describe a number of the properties of particles in each image, as well as some information about the colocalization of those particles. If the analysis is run multiple times on a given image pair, or if there are

multiple image pairs in any given directory, the results of each analysis will be appended to the end of the rowdat.txt file. Below is a list of the 25 variables, along with brief definitions of each:

1. TH1: the threshold used for image 1
2. TH2: the threshold used for image 2
3. MeanV1: average particle volume for image 1
4. TotalV1: total amount of signal in the thresholded version of image 1
5. MeanPix1: average pixel intensity of particles in image 1
6. TotalPix1: total pixel intensity of particles in image 1
7. NumP1: number of particles in image 1
8. MeanP1frac: average fractional volume of particles in image 1 contributing to overlap
9. MeanV2: average particle volume for image 2
10. TotalV2: total amount of signal in the thresholded version of image 2
11. MeanPix2: average pixel intensity of particles in image 2
12. TotalPix2: total pixel intensity of particles in image 2
13. NumP2: number of particles in image 2
14. MeanP2frac: average fractional volume of particles in image 2 contributing to overlap
15. MeanVOL: average volume of overlapping particles
16. TotalVOL: total amount of signal in the overlapping image
17. NumPOL: number of particles in the overlapping image
18. TotalPixOL1: total intensity from image1 of particles that overlap
19. MeanPixOL1: mean intensity (per particle) from image1 of particles that overlap
20. NumOLdivTot1: NumPOL/NumP1
21. VOLdivTotV1: total overlap volume as fraction of total image 1 particle volumes
22. TotalPixOL2: total intensity from image2 of particles that overlap
23. MeanPixOL2: mean intensity (per particle) from image2 of particles that overlap
24. NumOLdivTot2: NumPOL/NumP2
25. VOLdivTotV2: total overlap volume as fraction of total image 2 particle volumes

The output format of rowdat.txt is suitable for import into Matlab or a spreadsheet program such as Excel for further statistical analysis.

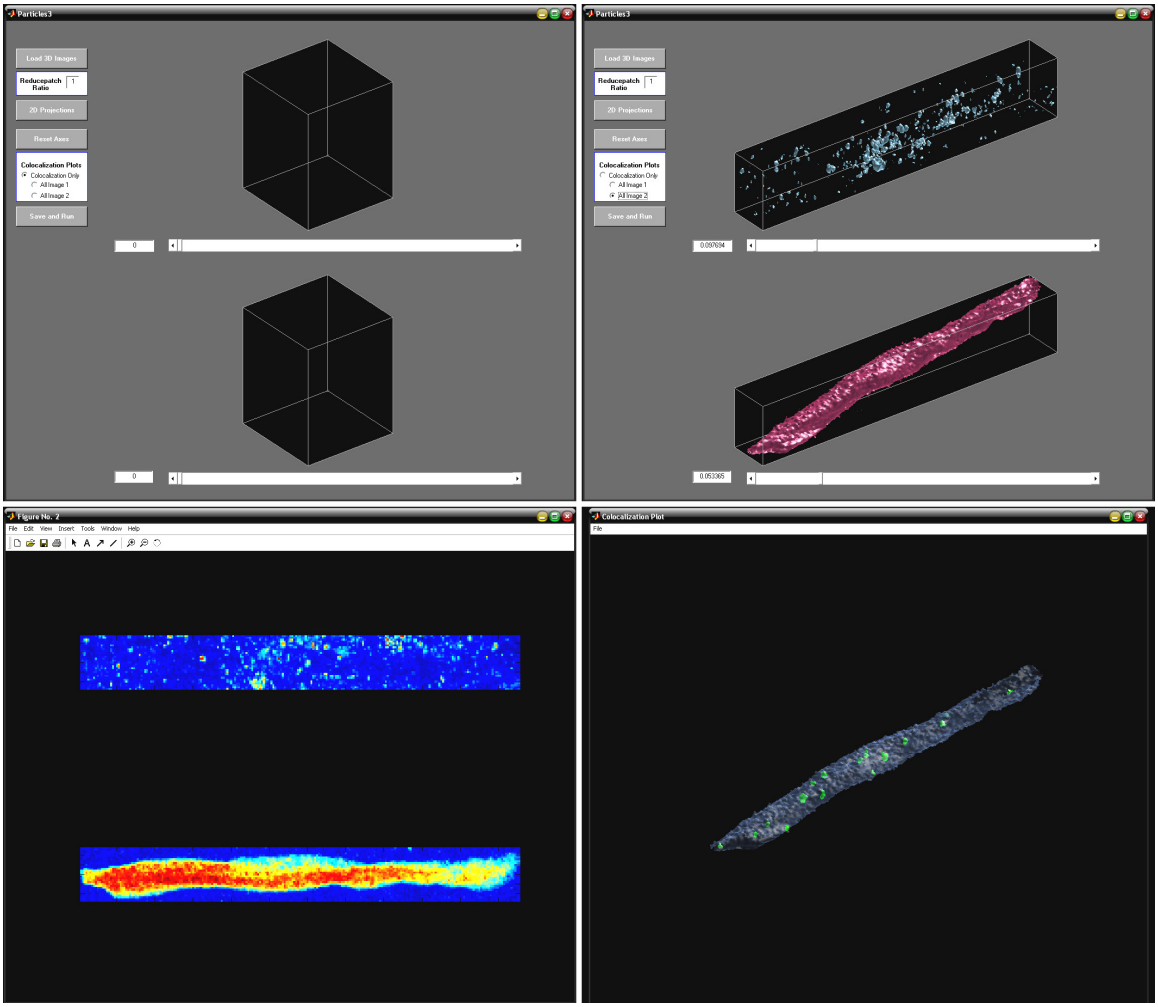


**Figure 4.1** Screenshots of the 3DParticles Application

The program window is shown immediately after launching the application (top, left), and after images are loaded and thresholds adjusted (top, right). Also shown are 2-D projections of the loaded images (bottom, left), and the colocalization image generated using the "all image 2" option (bottom, right).

**2-D Cross-Correlation**

In our previous work (see Figure 2.10), we used a normalized one-dimensional cross-correlation routine to argue that GFP hotspots (or puncta) seen in the dendrites of cultured hippocampal neurons were correlated with the presence of synaptic markers and ribosomal proteins. This analysis bolstered our claim that the GFP was locally synthesized in the dendrites, near synaptic sites. Given the potential loss of information in taking the mean pixel intensity across the width of the dendrites, for example, due to the fact that some regions of the dendrite may have a synapse on either side while others have only a single synapse, we devised a routine to analyze the correlation in 2-D space.

The amount of correlation detected between two images using a standard two-dimensional cross-correlation algorithm is a function of the spatial distributions of particles within each image, as well as the total amount of signal detectable in each image. The effect of signal abundance on the expected correlation is most obvious at the upper limit: if one image or the other is completely filled with signal, there will be perfect 2-D correlation (as well as colocalization) between the images. Even in real biological samples, where the signal of interest frequently occupies less than one third of the image area, there is some probability that any correlation measured between a pair of images is simply due to the amount of space filled by the signal in each image. Here we describe an algorithm that normalizes the 2-D correlation by removing the average correlation detected when the particles from each image are randomly redistributed within the image frame. The result gives an estimate of the likelihood that the correlation detected is due to randomness, or if it is in fact due to some underlying process that is potentially more meaningful.

**Methodology**

Here I describe, in detail, the steps involved in the 2DXcorr routine. Because the MATLAB code is included in Appendix B, the discussion here will be limited to a more intuitive description of the process. The specifics of each step, and the computation involved, are clearly identified in the comments of the code.

The routine begins by loading the images into the MATLAB workspace. The images are assumed to be in the TIFF format. It is also assumed that the images represent two independent signals (red and green fluorescent signal derived from two different proteins, for example) from a single, horizontal, linear dendritic segment. While the routine is easily generalized to cases in which these constraints are not met, the linearization of a single neuronal process greatly facilitates the analysis for two important reasons: first, there is no ambiguity about the orientation of the principal x and y axes, and second, much less memory is required for images pre-processed in this manner.

In order to fully understand the 2DXcorr algorithm, it is necessary to first review the general 2-D correlation function. Briefly, the 2-D correlation in the frequency domain is computed in MATLAB using the following code:

```
Fa = fft2(rot90(a,2));
Fb = fft2(b);
cor = real(ifft2(Fa .* Fb));
```

where the 2-D Fourier transform (fft2) is computed on each image, **a** (rotated 180 degrees) and **b**. The final output, **cor**, is equal to the real component of the inverse 2-dimensional

FFT of the product of the transformed images. If the images are identical, the result is a special case of correlation known as the autocorrelation, shown graphically in Figure 4.2. The autocorrelation determines the maximum possible correlation for a given image.

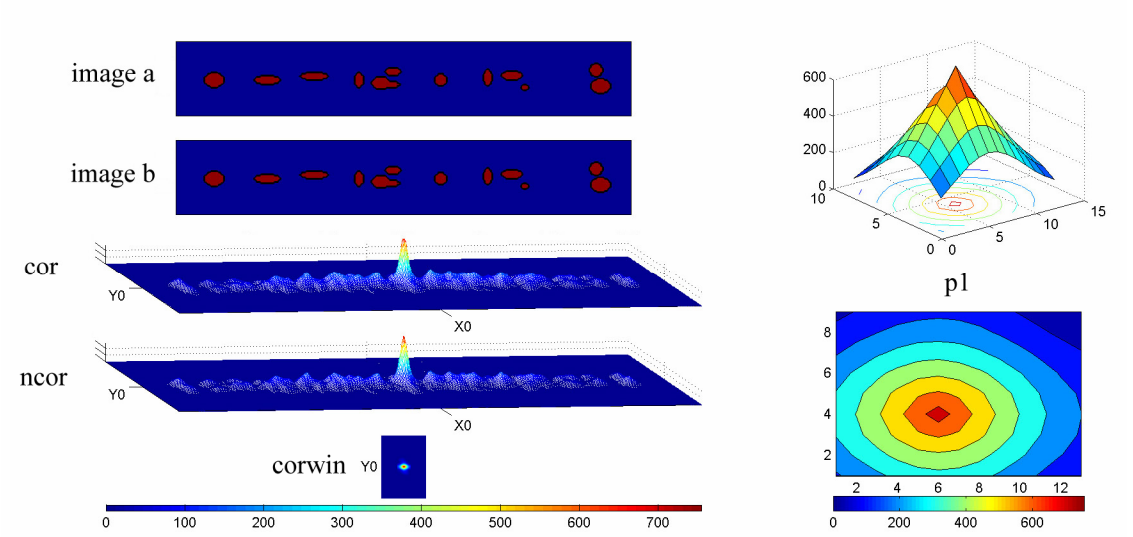


**Figure 4.2** The Autocorrelation Function

Shown at left are two identical simulated images (*image a* and *image b*), the raw 2-D autocorrelation output (*cor*), and the correlation after subtraction of the randomized correlations (*ncor*, see text). The correlation window (*corwin*) around the X=0 lag position is also shown, and the correlation peak (p1) extracted from corwin is plotted as a surface (top, right) and a filled contour plot (bottom, right).

As seen in Figure 4.2, plotting the 2-D autocorrelation output as a surface generates a large peak in the middle of the 2-D correlation space. If the dimensions of the original images are defined as (x,y), the dimensions of the correlation space are equal to ((2*x)-1,(2*y)-1). Intuitively, this is because the correlation operation considers one image as a template, and then shifts the other image in 2-D space over the template, measuring the correlation at each point. The correlation axes are expressed in units of *lag*, where (X0,Y0) in the correlation space is the midpoint of each axis. The maximum-

amplitude peak of the autocorrelation, located at (X0,Y0), indicates that the images do not need to be shifted in either dimension in order to generate the maximum correlation.

In the case where the images are not identical, although very highly correlated, the correlation function output becomes more complicated. Figure 4.3 shows the case where the test correlation images have been generated with the intent of emulating signal in the shaft of a dendrite (image a), and signal marking synapses in spines (image b). While the particles in each image are identical, the fact that the particles in image b are distributed away from the y-axis midline results in a correlation output that differs from the autocorrelation case. Specifically, given that the particles in image b are distributed on both sides of the y-axis midline, with the particles in image a largely confined to the midline, the 2-D correlation results in two distinct peaks, one on either side of the Y0 lag position.

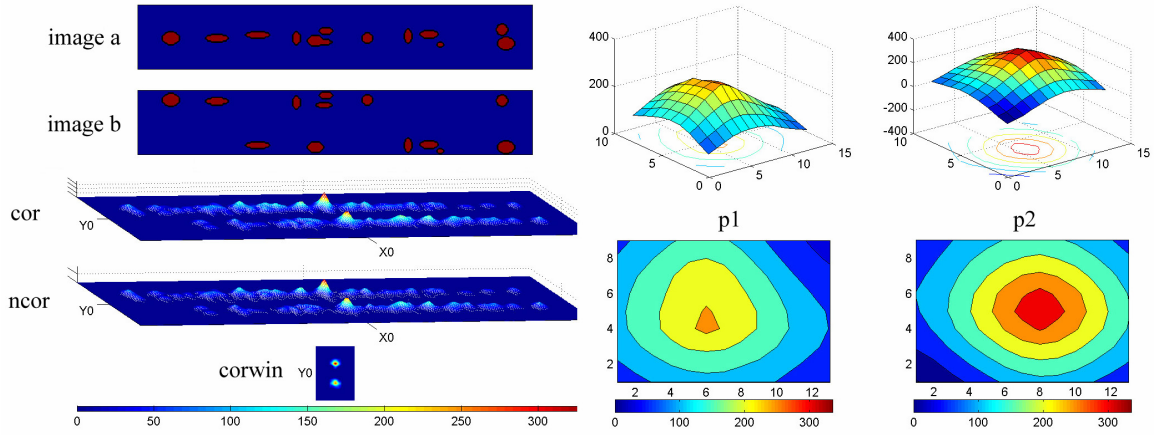


**Figure 4.3** Highly Correlated Test Images

Shown are simulated test images, with *image a* representative of protein signal in the shaft of a dendrite, and image b designed to emulate protein signal at synapses on spines. Because particles in *image b* lie on either side of particles in *image a* (in the y-axis), the correlation function (cor) results in two peaks: *p1* at (X0,-Y) and *p2* at (X0,+Y).

To illustrate the importance of the correlation window (*corwin*), Figure 4.4 shows an example where the particles are uncorrelated, as defined by our criteria. Because we are interested only in correlating particles in the dendritic shaft with synaptic signal that is nearby, we limit our analysis of the correlation output to a small window centered around (X0,Y0). We have chosen a method that defines *corwin* based on the measured linear distances between adjacent particles. As specified in the code found in Appendix B, the dimensions of *corwin* in the X-lag axis are limited to $2\times(\text{mean}(d)+\text{std}(d))$, where $d$ is the linear distance between adjacent particle centroids, and *std* is the standard deviation of that mean. For example, if the mean distance were 10 pixels, with a standard deviation of 3, *corwin* would be set at (X0−13,X0+13). Because the images are preprocessed for this routine such that only a single neuronal process occupies the image, the Y-lag window is self-limiting.

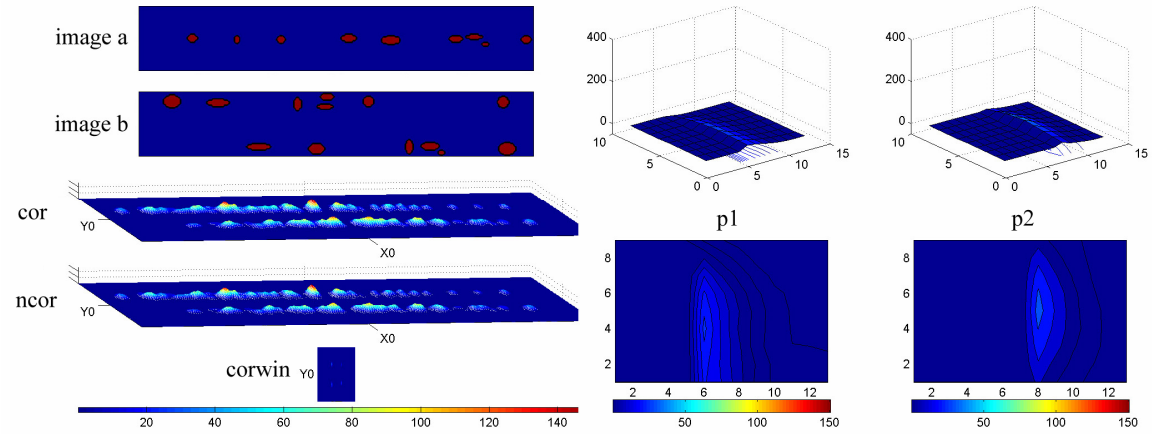


**Figure 4.4** Uncorrelated Test Images

Shown are two images (*image a* and *image b*), designed to show the effect of limiting the analysis to *corwin*. In this case, the images are uncorrelated as defined by the algorithm, because each particle in *image a* is directly in between particles in *image b*. The result is a set of correlation peaks that fall outside the dimensions of the *corwin* X-lag.

The results of an analysis on real image data are shown in Figure 4.5. The images in this case are the same as those used in Figure 1.10, where *image a* is the GFP signal, and *image b* shows synaptic locations as determined by PSD-95 staining. As a reference, a sample of the randomized versions of each image is plotted in Figure 4.6. From analysis of the 2DXcorr output, it is clear that a substantial portion of the raw correlation (*cor*) is attributable to the abundance of the two signals, which can be seen in the amount of correlation signal that has been subtracted as a result of the normalization routine (cf. *cor* to *ncor*). However, within the specified window of the normalized correlation (*corwin*), there are two significant peaks remaining (*p1win, p2win*). The sum of the two peaks, divided by the autocorrelation of the GFP image, gives a correlation score of 0.40. While this number by itself carries little meaning, further analysis reveals that of the randomized correlations, analysis from repeated trials of the correlation that ranks as the upper limit of the $95^{th}$ percentile produces correlation scores ranging from 0.08 to 0.12.

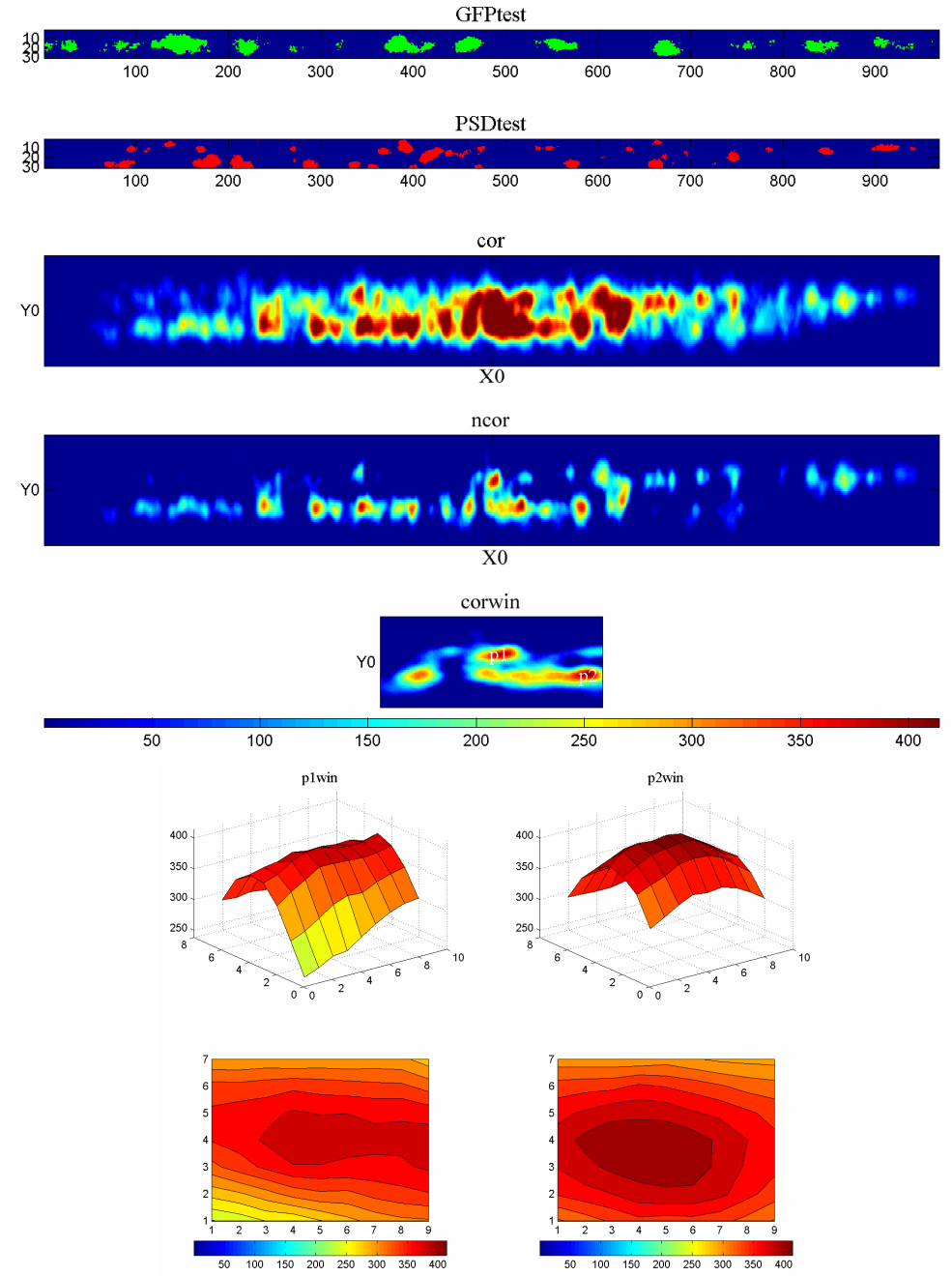


**Figure 4.5** *myr*dGFP / PSD-95 Cross-Correlation

Brief visual inspection shows that a large amount of the correlation signal (*cor*) has been subtracted away in the process of generating the normalized correlation (*ncor*). Integration of the two correlation peaks (*p1win* and *p2win*) gives a correlation score of 0.40. Refer to text for further details.

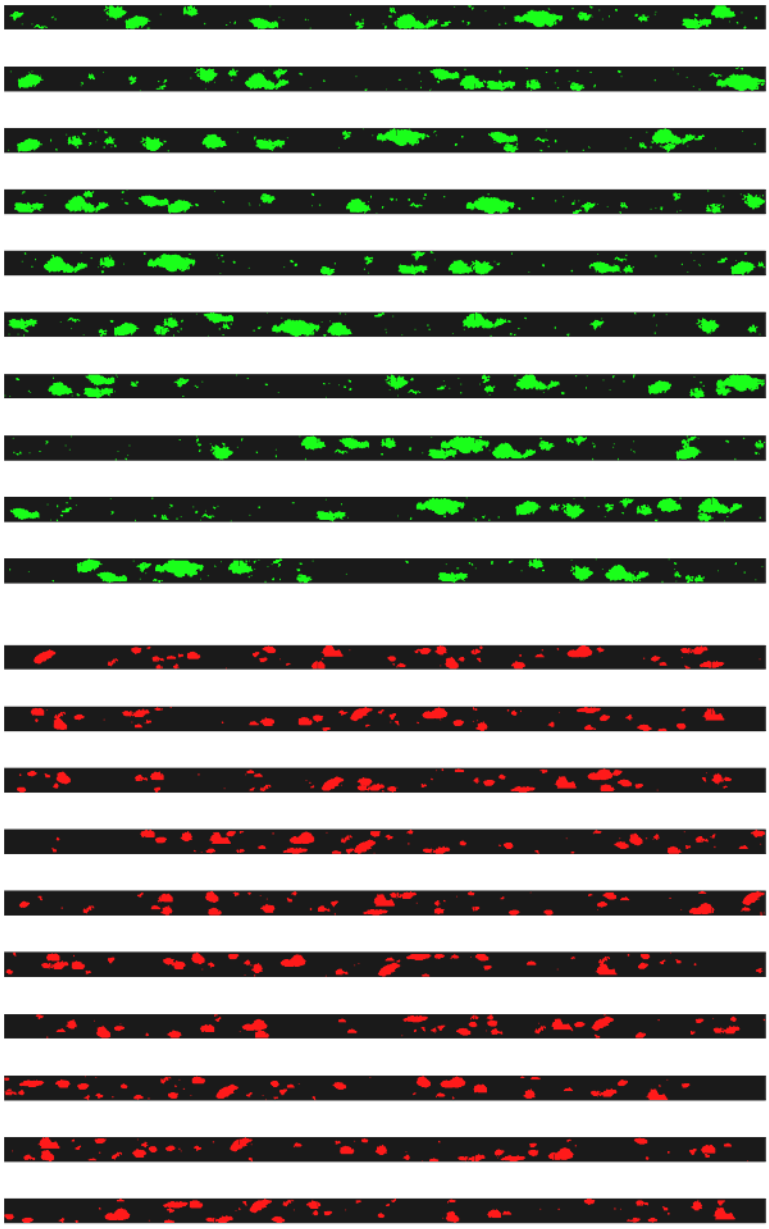

**Figure 4.6** Examples of Randomized GFP Puncta (top) and PSD-95 Puncta (bottom).

**Conclusions**

The routines presented here, for quantitative analysis of 3-D colocalization and 2-D correlation, provide a simple, intuitive means of measuring and summarizing the most frequently-reported properties of immunostained particles. These programs are a good starting point for such analyses, although some refinement will improve the algorithms. Currently, the need to threshold the images is the greatest limitation. Developing methods that permit similar analyses while maintaining the full bit-depth of the original images will dramatically improve the robustness of these algorithms. Such modifications will further reduce the potential for user bias in the analysis process. Another benefit would be to allow for direct comparisons of colocalized and spatially correlated particles of similar intensities between the two images. Such comparisons may provide further information about the dynamics of the system.

The 2DXcorr program will also benefit from more a more advanced statistical analysis of the distributions of particles in the real versus the random data sets. For example, with an appropriately large set of randomized images (generating on the order of $10^5$ randomized correlations), it may be possible to assign significance values to individual correlations using a statistical measure that computes the distance between the actual correlation and the distribution of random correlations. This will, in turn, further facilitate the between-group comparisons required in experiments using this routine.

*Chapter V*

# Summary, Discussion and Future Directions

**Summary of Results**

Our work, described in detail in Chapter 2, provided the first direct visualization of dendritic protein synthesis dynamics in living hippocampal neurons (Aakalu et al., 2001). Taking advantage of the visible fluorescence signal provided by GFP, we flanked a membrane-tethered GFP coding sequence with the 3' and 5' UTRs of CamKIIα to both target the mRNA to the dendrites, and endow it with translation control elements. Neurons expressing this construct showed increased GFP production in response to brain-derived neurotrophic factor (BDNF). Increases in the distal dendrites were seen within 30 minutes of BDNF application, suggesting a local origin of the GFP signal. In an effort to rule out the cell body as a source of GFP signal detected in the distal dendrites, we successfully isolated dendrites using mechanical and optical techniques. In both cases, isolated dendrites continued to show increased GFP signal that was completely blocked in the presence of a protein synthesis inhibitor. Lending additional support to the putative synaptic localization of the increased GFP, we quantitatively demonstrated that GFP hotspots in the dendrites were spatially persistent over time, and were correlated with ribosomal and synaptic markers.

In more recent experiments, we investigated the role of dopaminergic signaling in LPS (Chapter 3). Given the similar temporal profiles of L-LTP inhibition by dopamine receptor agonists and protein synthesis inhibitors, we examined the ability of D1/D5 agonists to stimulate protein synthesis in the dendrites of cultured hippocampal neurons. In addition to direct observation of LPS stimulation by the agonists, our work provides a

possible mechanistic understanding of how dopamine may exert its effects on long-lasting synaptic enhancement: An important consequence of D1/D5-stimulated protein synthesis is the conversion of silent synapses into active synapses. This postsynaptic conversion was detected as increased surface GluR1 at synaptic sites, as well as an increase in the frequency, but not amplitude, of miniature excitatory postsynaptic currents. These results mark the first established connection between dopaminergic signaling, local protein synthesis, and silent synapse activation.

We have also provided the first freely available software tools for quantitative analysis of 3-D colocalization and 2-D spatial correlation (Chapter 4). While qualitative properties of colocalized signals in fluorescent images are frequently reported, they are rarely quantified. The method we have presented permits fully automated analysis of colocalization in 3-D image sets, as well as descriptive statistics about the particles from each image, regardless of their colocalization status. For cases in which spatial correlation may be of interest, for example, when proteins do not share the same space but may cluster in the same region of the cell, we have provided an analysis routine that quantifies this correlation, and expresses the result in a normalized fashion that facilitates between-group comparisons. Both programs include the ability for objective threshold determination and batch analysis, which will greatly reduce the potential of erroneous results due to user bias. These programs, when used within the constraints of the limitations addressed in Chapter 4, have the potential to create a consensus method for describing properties of colocalization and spatial correlation in immunofluorescence image data.

## Discussion and Future Directions

While our work, along with the work of other researchers in the field (reviewed in Martin et al., 2000; Steward and Schuman, 2001; Steward and Schuman, 2003), has begun to define the importance of local protein synthesis in hippocampal neurons, the precise physiological function of this phenomenon remains largely unknown. Here I present a few of the outstanding issues related to LPS in synaptic plasticity, as well as some experiments that will help to address these questions.

### *Input-Specificity and LPS*

A problem that has received considerable attention is the issue of input-specific synaptic enhancement, as briefly introduced in Chapter 1. Although it is generally accepted that some degree of input-specificity is maintained in neurons, the lower spatial limits of this specificity, as well as the role of LPS in this effect, have not been convincingly addressed. If plasticity is induced at just a few synapses on a distal dendritic segment, how far does that plasticity spread to adjacent synapses? In one study, this lower limit was determined to be approximately 70 μm from the site of LTP induction (Engert and Bonhoeffer, 1997). In these experiments, synaptic transmission was globally inhibited by bathing the cells in a cadmium-containing solution, which blocks the voltage-gated $Ca^{++}$ channels responsible for evoked neurotransmitter release. Synaptic enhancement was induced by pairing whole-cell depolarization with local perfusion of a solution containing high $Ca^{++}$ without cadmium.

A limitation to this experimental approach is that Engert and Bonhoeffer determined the spatial resolution of their stimulation and measurement technique to be approximately 30 μm, as estimated by visual inspection of a blue food coloring dye used in the perfusion solution. The use of this dye, when compared to a soluble fluorescent dye, gives a relatively poor estimate of the extent to which a perfused solution is spatially restricted (W. B. Smith, unpublished observations), raising the possibility that the authors were stimulating a much larger area than estimated. Even if this were a perfect assessment of the limit of their perfusate, a 30 μm section of dendrite could be too large an area to accurately assess the question of input-specificity. This result is further confounded by the fact that whole-cell depolarization, using an electrode at the cell soma, was used to induce plasticity. This may have disrupted voltage-gated ion channels in non-stimulated regions of the dendrite that under normal conditions could serve some critical function in maintaining input specificity.

More recently, an interesting set of experiments has examined, at a very crude spatial resolution, the role of LPS in input specificity (Bradshaw et al., 2003). In these experiments, Bradshaw and colleagues measured high frequency-induced L-LTP in two separate subfields of the hippocampal slice — stratum radiatum and stratum oriens — which are separated from one another by hundreds of microns of dendritic length, and are on opposite sides of the cell soma. The authors found that locally perfusing emetine, a protein synthesis inhibitor, selectively blocked L-LTP in the subfield where the drug was applied (for example, in radiatum), without altering potentiation in the other subfield (oriens). While this result successfully implicates LPS in input specificity, the scale at

which input specificity was examined is considerably larger than what has previously been reported.

To address the actual lower limit on the spatial restrictions of LPS-dependent input specific plasticity, it may be necessary to examine the process in cultured hippocampal neurons rather than using acute slices or slice cultures. There are certainly disadvantages to this approach, given the potential differences in synapse density and connectivity between the dissociated culture system and slice. However, the advantages of spatial precision and temporal control over drug application make the dissociated culture system ideal for investigations of this nature. Cultured neurons expressing GluR1 tagged with an extracellular pH-sensitive GFP molecule could be used to investigate the spatial limits of stimulus-induced AMPA receptor surface expression dynamics. With such a construct, surface GluR1 expression could be followed in near real-time as follows: an image acquired in the presence of a mildly acidic bath solution would be subtracted from a previously acquired image at pH 7.4. With an appropriate GFP tag, such as the pHluorin GFP molecule (Miesenbock et al., 1998), this subtraction will yield an image of the surface population of GluR-containing AMPA receptors. This imaging protocol, used in combination with local perfusion of a dopamine agonist, glutamate, or high $K^+$, would facilitate the rapid visualization of activity-regulated GluR1 surface dynamics, a phenomenon that has been correlated with synaptic plasticity (reviewed in Malenka, 2003).

Because an experiment monitoring receptor dynamics would be correlative in nature, direct demonstration of the input specificity limit would require combining this imaging approach with whole-cell or perforated patch recordings. By measuring evoked responses at a number of locations on the dendritic arbor, both before and after local perfusion at one location with a drug that induces plasticity, it should be possible to measure the spread of synaptic enhancement from one location to another. Ultimately, the merging of these two experimental approaches would provide the most accurate estimate of the degree to which synaptic enhancement is truly input-specific, and whether or not LPS is critically involved in this specificity.

*Role of Dopaminergic Signaling*

A number of interesting questions remain unanswered with regards to the dopamine studies. In particular, the necessity of this pathway for LPS induction has not been addressed. It has previously been shown that D1/D5 dopamine receptors can converge with various signaling systems via physical interactions with GABA and NMDA receptors (Lee et al., 2002; Liu et al., 2000; Pei et al., 2004). Given the critical involvement of NMDA receptors in various forms of synaptic plasticity, it will be interesting to examine the relationship between NMDA-R signaling and the effects of D1/D5 agonists we have described. It is possible that the D1/D5 receptors simply play a permissive role, somehow enhancing NMDA-R signaling to produce the observed increases in GluR1 surface expression and synaptic transmission. Alternatively, the dopaminergic signaling pathway may serve as a necessary and sufficient mechanism for the conversion of postsynaptic

silent synapses. A relatively simple set of experiments, in which the effects of D1/D5 agonists on GluR1 expression and synaptic transmission are examined in the presence of APV, should be sufficient to resolve this issue.

The source of the GluRs that are increased on the cell surface in response to dopamine receptor activation also remains to be determined. While we show that the increase is sensitive to protein synthesis inhibitors, as well as showing a small increase in total cellular levels of GluR1, we have not conclusively demonstrated that the newly synthesized receptors are the same receptors that appear on the surface. Distinguishing between the three possibilities (i.e., whether some, all, or none of the new receptors on the surface were synthesized in response to the agonist), will be an interesting topic to explore. There are a variety of ways to answer this question. One experiment involves $^{35}$S-methionine/cysteine labeling followed by surface biotinylation and combined streptavidin/GluR1 immunoprecipitation. If D1/D5 agonists simulate synthesis and insertion of newly-synthesized GluRs, agonist treatment should result in higher levels of biotinylated $^{35}$S-GluR1 as compared to control samples. Because there may be significant loss of the GluR1 product in the various steps of such a complex procedure, the $^{35}$S pulse could instead be followed by chymotryptic digestion of surface proteins. Because the chymotrypsin is not membrane permeant, subsequent immunoprecipitation of GluR1 and autoradiography will show a reduced molecular weight GluR1 band if the $^{35}$S-labeled receptors are inserted into the plasma membrane.

**Concluding Remarks**

The localized control of complex cellular processes, such as the regulation of protein synthesis at synaptic sites, is an important mechanism for achieving subcellular specificity in a variety of biological systems. In the single-celled yeast *Saccharomyces cerevisiae*, precise targeting of specific mRNA species from the mother to the daughter cell during budding is important for successful asexual reproduction (Beach and Bloom, 2001; Bertrand et al., 1998). The partitioning of mRNA and proteins is also a key component of developing embryos in *Drosophila*: when the normal spatial distributions of these factors are disrupted, proper development of the organism may fail (Berleth et al., 1988; Ding et al., 1993; Lieberfarb et al., 1996).

Here we have presented evidence that local protein synthesis takes place in the dendrites of mature hippocampal neurons, and that D1/D5-mediated dopaminergic signaling affects GluR1 receptor dynamics in a protein synthesis-dependent manner. Because dopamine is an important neuromodulator, playing a critical role in such diverse phenomena as drug addiction, Parkinson's disease, schizophrenia, and learning and memory, implicating the dopaminergic system in regulation of local protein synthesis opens up a large potential field for research. If it can be determined that the effects of dopamine in any of these behavioral or pathological conditions are mediated through protein synthesis-dependent pathways, new therapies may de developed to help treat addiction, and improve cognitive performance in both abnormal and normal brains.

# *Work Cited*

Aakalu, G., Smith, W. B., Nguyen, N., Jiang, C., and Schuman, E. M. (2001). Dynamic visualization of local protein synthesis in hippocampal neurons. *Neuron* 30, 489-502.

Ainger, K., Avossa, D., Morgan, F., Hill, S. J., Barry, C., Barbarese, E., and Carson, J. H. (1993). Transport and localization of exogenous myelin basic protein mRNA microinjected into oligodendrocytes. *J. Cell. Biol.* 123, 431-441.

Andersen, P., Sundberg, S. H., Sveen, O., and Wigstrom, H. (1977). Specific long-lasting potentiation of synaptic transmission in hippocampal slices. *Nature* 266, 736-737.

Bach, M. E., Barad, M., Son, H., Zhuo, M., Lu, Y. F., Shih, R., Mansuy, I., Hawkins, R. D., and Kandel, E. R. (1999). Age-related defects in spatial memory are correlated with defects in the late phase of hippocampal long-term potentiation in vitro and are attenuated by drugs that enhance the cAMP signaling pathway. *Proc. Natl. Acad. Sci. USA* 96, 5280-5285.

Banker, G., and Goslin, K. (1990). *Culturing nerve cells*. (Cambridge, MA, MIT Press).

Bassell, G. J., Zhang, H., Byrd, A. L., Femino, A. M., Singer, R. H., Taneja, K. L., Lifshitz, L. M., Herman, I. M., and Kosik, K. S. (1998). Sorting of beta-actin mRNA and protein to neurites and growth cones in culture. *J. Neurosci.* 18, 251-265.

Baudier, J., Deloulme, J. C., Van Dorsselaer, A., Black, D., and Matthes, H. W. (1991). Purification and characterization of a brain-specific protein kinase c substrate, neurogranin (p17). Identification of a consensus amino acid sequence between neurogranin and neuromodulin (*GAP43*) that corresponds to the protein kinase c phosphorylation site and the calmodulin-binding domain. *J. Biol. Chem.* 266, 229-237.

Beach, D. L., and Bloom, K. (2001). Ash1 mRNA localization in three acts. *Mol. Biol. Cell* 12, 2567-2577.

Berleth, T., Burri, M., Thoma, G., Bopp, D., Richstein, S., Frigerio, G., Noll, M., and Nusslein-Volhard, C. (1988). The role of localization of bicoid rna in organizing the anterior pattern of the *Drosophila* embryo. *EMBO J.* 7, 1749-1756.

Bertrand, E., Chartrand, P., Schaefer, M., Shenoy, S. M., Singer, R. H., and Long, R. M. (1998). Localization of ash1 mRNA particles in living yeast. *Mol. Cell* 2, 437-445.

Bito, H., Deisseroth, K., and Tsien, R. W. (1996). Creb phosphorylation and dephosphorylation: A ca2+- and stimulus duration-dependent switch for hippocampal gene expression. *Cell* 87, 1203-1214.

Bliss, T. V. P., and Collingridge, G. L. (1993). A synaptic model of memory: Long-term potentiation in the hippocampus. *Nature* 361, 31-39.

Bliss, T. V. P., and Gardner-Medwin, A. R. (1973). Long-lasting potentiation of synaptic transmission in the dentate area of the anaesthetized rabbit following stimulation of the perforant path. *J. Physiol. (London)* 232, 357-374.

Bonhoeffer, T., Staiger, V., and Aertsen, A. (1989). Synaptic plasticity in rat hippocampal slice cultures: Local "hebbian" conjuction of pre- and postsynaptic stimulation leads to distributed synaptic enhancement. *Proc. Natl. Acad. Sci. USA* 86, 8113-8117.

Bouron, A., and Reuter, H. (1999). The D1 dopamine receptor agonist SKF-38393 stimulates the release of glutamate in the hippocampus. *Neuroscience* 94, 1063-1070.

Bradshaw, K. D., Emptage, N. J., and Bliss, T. V. (2003). A role for dendritic protein synthesis in hippocampal late ltp. *Eur. J. Neurosci.* 18, 3150-3152.

Brittis PA, L. Q., Flanagan JG (2002). Axonal protein synthesis provides a mechanism for localized regulation at an intermediate target. *Cell* 110, 223-235.

Brown, A. (2003). Axonal transport of membranous and nonmembranous cargoes: A unified perspective. *J. Cell. Biol.* 160, 817-821.

Brown, E. J., and Schreiber, S. L. (1996). A signaling pathway to translational control. *Cell* 86, 517-520.

Burgin, K. E., Waxham, M. N., Rickling, S., Westgate, S. A., Mobley, W. C., and Kelly, P. T. (1990). *In situ* hybridization histochemisty of Ca/calmodulin dependent protein kinase in developing rat brain. *J. Neurosci.* 10, 1788-1789.

Cao, Q., and Richter, J. D. (2002). Dissolution of the maskin-eif4e complex by cytoplasmic polyadenylation and poly(A)-binding protein controls Cyclin b1 mRNA translation and oocyte maturation. *EMBO J.* 21, 3852-3862.

Casadio, A., Martin, K. C., Giustetto, M., Zhu, H., Chen, M., Bartsch, D., Bailey, C. H., and Kandel, E. R. (1999). A transient, neuron-wide form of CREB-mediated long-term faciliation can be stablized at specific synapses by local protein synthesis. *Cell* 99, 221-237.

Chao, S. Z., Ariano, M. A., Peterson, D. A., and Wolf, M. E. (2002). D1 dopamine receptor stimulation increases GluR1 surface expression in nucleus accumbens neurons. *J. Neurochem.* 83, 704-712.

Chetkovich, D. M., and Sweatt, J. D. (1993). NMDA receptor activation increases cyclic AMP in area CA1 of the hippocampus via calcium/calmodulin stimulation of adenylyl cyclase. *J. Neurochem.* 61, 1933-1942.

Collingridge, G. L., Kehl, S. J., and McLennon, H. (1983). Excitatory amino acids in synaptic transmission in the schaffer collateral-commissural pathway of the rat hippocampus. *J. Physiol. (London)* 334, 33-46.

Crino, P. B., and Eberwine, J. (1996). Molecular characterization of the dendritic growth cone: Regulated mRNA transport and local protein synthesis. *Neuron* 17, 1173-1187.

Cubitt, A. B., Heim, R., Adams, S. R., Boyd, A., and Gross, L. A. (1995). Understanding, improving and using green fluorescent proteins. *Trends Biochem. Sci.* 20, 448-455.

Darnell, J. C., Jensen, K. B., Jin, P., Brown, V., Warren, S. T., and Darnell, R. B. (2001). Fragile X mental retardation protein targets G quartet mRNAs important for neuronal function. *Cell* 107, 489-499.

Dash, P. K., Moore, A. N., and Dixon, C. E. (1995). Spatial memory deficits, increased phosphorylation of the transcription factor CREB, and induction of the AP-1 complex following experimental brain injury. *J. Neurosci.* 15, 2030-2039.

Deisseroth, K., Bito, H., and Tsien, R. W. (1996). Signalling from synapse to nucleus: Postsynaptic CREB phosphorylation during multiple forms of hippocampal synaptic plasticity. *Neuron* 16, 89-101.

DesGroseillers, L., Kuhl, D., Richter, D., and Kindler, S. (2001). Two rat brain Staufen isoforms differentially bind RNA. *J. Neurochem.* 76: 155-165.

Ding, D., Parkhurst, S. M., and Lipshitz, H. D. (1993). Different genetic requirements for anterior RNA localization revealed by the distribution of adducin-like transcripts during *Drosophila* oogenesis. *Proc. Natl. Acad. Sci. USA* 90, 2512-2516.

Engert, F., and Bonhoeffer, T. (1997). Synapse specificity of long-term potentiation breaks down at short distances. *Nature* 388, 279-284.

Feig, S., and Lipton, P. (1993). Pairing the cholinergic agonist carbachol with patterned schaffer collateral stimulation initiates protein synthesis in hippocampal CA1 pyramidal cell dendrites via a muscarinic, NMDA-dependent mechanism. *J. Neurosci.* 13, 1010-1021.

Ferrandon, D., Elphick, L., Nusslein-Volhard, C., and St Johnston, D. (1994). Staufen protein associates with the 3'UTR of bicoid mRNA to form particles that move in a microtubule-dependent manner. *Cell* 79, 1221-1232.

Frey, D., Laux, T., Xu, L., Schneider, C., and Caroni, P. (2000). Shared and unique roles of cap23 and *GAP43* in actin regulation, neurite outgrowth, and anatomical plasticity. *J. Cell Biol.* 149, 1443-1454.

Frey, U., Huang, Y. Y., and Kandel, E. R. (1993). Effects of cAMP simulate a late stage of LTP in hippocampal CA1 neurons. *Science* 260, 1661-1664.

Frey, U., Krug, M., Reymann, K. G., and Matthies, H. (1988). Anisomycin, an inhibitor of protein synthesis, blocks late phases of LTP phenomena in the hippocampal CA region in vitro. *Brain Res.* 452, 57-65.

Frey, U., Matthies, H., and Reymann, K. G. (1991). The effect of dopaminergic D1 receptor blockade during tetanization on the expression of long-term potentiation in the rat CA1 region in vitro. *Neurosci. Lett.* 129, 111-114.

Frey, U., and Morris, R. G. (1997). Synaptic tagging and long-term potentiation. *Nature* 385, 533-536.

Frey, U., Schroeder, H., and Matthies, H. (1990). Dopaminergic antagonists prevent long-term maintenance of posttetanic LTP in the CA1 region of rat hippocampal slices. *Brain Res.* 522, 69-75.

Gardiol, A., Racca, C., and Triller, A. (1999). Dendritic and postsynaptic protein synthetic machinery. *J. Neurosci.* 19, 168-179.

Gazzaley, A. H., Benson, D. L., Huntley, G. W., and Morrison, J. H. (1997). Differential subcellular regulation of NMDAR1 protein and mRNA in dendrites of dentate gyrus granule cells after perforant path transection. *J. Neurosci.* 17, 2006-2017.

Greenough, W. T., Klintsova, A. Y., Irwin, S. A., Galvez, R., Bates, K. E., and Weiler, I. J. (2001). Synaptic regulation of protein synthesis and the Fragile X protein. *Proc. Natl. Acad. Sci. USA* 98, 7101-7106.

Hebb, D. O. (1949). *The Organization of Behavior*, John Wiley & Sons.

Huang, Y. S., Jung, M. Y., Sarkissian, M., and Richter, J. D. (2002). N-methyl-d-aspartate receptor signaling results in aurora kinase- catalyzed CPEB phosphorylation and alpha CamKII mRNA polyadenylation at synapses. *EMBO J.* 21, 2139-2148.

Huang, Y. Y., and Kandel, E. R. (1995). D1/D5 receptor agonists induce a protein synthesis-dependent late potentiation in the CA1 region of the hippocampus. *Proc. Natl. Acad. Sci. USA* 92, 2446-2450.

Huber, K. M., Kayser, M. S., and Bear, M. F. (2000). Role for rapid dendritic protein synthesis in hippocampal mGluR-dependent long-term depression. *Science* 288, 1254-1256.

Isaac, J. T., Nicoll, R. A., and Malenka, R. C. (1995). Evidence for silent synapses: Implications for the expression of LTP. *Neuron* 15, 427-434.

Jefferies, H. B., Reinhard, C., Kozma, S. C., and Thomas, G. (1994). Rapamycin selectively represses translation of the "polypyrimidine tract" mRNA family. *Proc. Natl. Acad. Sci. USA* 91, 4441-4445.

Ju, W., Morishita, W., Tsui, J., Gaietta, G., Deerinck, T. J., Adams, S. R., Garner, C. C., Tsien, R. Y., Ellisman, M. H., and Malenka, R. C. (2004). Activity-dependent regulation of dendritic synthesis and trafficking of AMPA receptors. *Nat. Neurosci.* 7, 244-253.

Kacharmina, J. E., Job, C., Crino, P., and Eberwine, J. (2000). Stimulation of glutamate receptor protein synthesis and membrane insertion within isolated neuronal dendrites. *Proc. Natl. Acad. Sci. USA* 97, 11545-11550.

Kang, H., and Schuman, E. M. (1995a). Long-lasting neurotrophin-induced enhancment of synaptic transmission in the adult hippocampus. *Science* 267, 1658-1662.

Kang, H., and Schuman, E. M. (1996). A requirement for local protein synthesis in neurotrophin-induced synaptic plasticity. *Science* 273, 1402-1406.

Kang, H., Welcher, A. A., Shelton, D., and Schuman, E. M. (1997). Neurotrophins and time: Different roles for TRK-B signaling in hippocampal long-term potentiation. *Neuron* 19, 653-664.

Kiebler, M. A., Hemraj, I., Verkade, P., Kohrmann, M., Fortes, P., Marion, R. M., Ortin, J., and Dotti, C. G. (1999). The mammalian Staufen protein localizes to the somatodendritic domain of cultured hippocampal neurons: Implications for its involvement in mRNA transport. *J. Neurosci.* 19, 288-297.

Kiss, J. (1977). Synthesis and transport of newly formed proteins in dendrites of rat hippocampal pyramid cells. An electron microscope autoradiographic study. *Brain Res.* 124, 237-250.

Knowles, R. B., Sabry, J. H., Martone, M. E., Deerinck, T. J., Ellisman, M. H., Bassell, G. J., and Kosik, K. S. (1996). Translocation of RNA granules in living neurons. *J. Neurosci.* 16, 7812-7820.

Koenig, E., and Giuditta, A. (1999). Protein-synthesizing machinery in the axon compartment. *Neuroscience* 89, 5-15.

Koenig, E., Martin, R., Titmus, M., and Sotelo-Silveira, J. R. (2000). Cryptic peripheral ribosomal domains distributed intermittently along mammalian myelinated axons. *J. Neurosci.* 20, 8390-8400.

Kozubek, M., and Matula, P. (2000). An efficient algorithm for measurement and correction of chromatic aberrations in fluorescence microscopy. *J. Microsc.* 200 Pt 3, 206-217.

Krichevsky, A. M., and Kosik, K. S. (2001). Neuronal RNA granules: A link between RNA localization and stimulation-dependent translation. *Neuron* 32, 683-696.

Kullmann, D. M., and Siegelbaum, S. A. (1995). The site of expression of NMDA receptor-dependent LTP: New fuel for an old fire. *Neuron* 15, 997-1002.

Lee, F. J., Xue, S., Pei, L., Vukusic, B., Chery, N., Wang, Y., Wang, Y. T., Niznik, H. B., Yu, X. M., and Liu, F. (2002). Dual regulation of NMDA receptor functions by direct protein-protein interactions with the dopamine D1 receptor. *Cell* 111, 219-230.

Lerner, E. A., Lerner, M. R., Janeway, C. A., and Steitz, J. A. (1981). Monoclonal antibodies to nucleic acid-containing cellular constituents: Probes for molecular biology and autoimmune disease. *Proc. Natl. Acad. Sci. USA* 78, 2737-2741.

Leung, L. S., and Shen, B. (1995). Long-term potentiation at the apical and basal dendritic synapses of CA1 after local stimulation in behaving rats. *J. Neurophysiol.* 73, 1938-1946.

Levine, E. S., Dreyfus, C. F., Black, I. B., and Plummer, M. R. (1995a). Brain-derived neurotrophic factor rapidly enhances synaptic transmission in hippocampal neurons via postsynaptic tyrosine kinase receptors. *Proc. Natl. Acad. Sci. USA* 92, 8074-8078.

Levine, E. S., Dreyfus, C. F., Black, I. B., and Plummer, M. R. (1995b). Differential effects of NGF and BDNF on voltage-gated calcium currents in embryonic basal forebrain neurons. *J. Neurosci.* 15(4), 3084-3091.

Li, S., Cullen, W. K., Anwyl, R., and Rowan, M. J. (2003). Dopamine-dependent facilitation of LTP induction in hippocampal CA1 by exposure to spatial novelty. *Nat. Neurosci.* 6, 526-531.

Li, Y. X., Xu, Y., Ju, D., Lester, H. A., Davidson, N., and Schuman, E. M. (1998). Expression of a dominant negative TRK B receptor, T1, reveals a requirement for presynaptic signaling in BDNF-induced synaptic potentiation in cultured hippocampal neurons. *Proc. Natl. Acad. Sci. USA* 95, 10884-10889.

Li, Y. X., Zhang, Y., Lester, H.A., Schuman, E.M., Davidson, N. (1998). Enhancement of excitatory neurotransmitter release induced by BDNF in cultured hippocampal neurons. *J. Neurosci.* 18, 10231-10240.

Liao, D., Zhang, X., O'Brien, R., Ehlers, M. D., and Huganir, R. L. (1999). Regulation of morphological postsynaptic silent synapses in developing hippocampal neurons. *Nat. Neurosci.* 2, 37-43.

Liao, S., Hessler, N. A., and Malinow, R. (1995). Activation of postsynaptically silent synapses during pairing-induced ltp in ca1 region of hippocampal slice. *Nature* 375, 400-404.

Lieberfarb, M. E., Chu, T., Wreden, C., Theurkauf, W., Gergen, J. P., and Strickland, S. (1996). Mutations that perturb poly(A)-dependent maternal mRNA activation block the initiation of development. *Development* 122, 579-588.

Liu, F., Wan, Q., Pristupa, Z. B., Yu, X. M., Wang, Y. T., and Niznik, H. B. (2000). Direct protein-protein coupling enables cross-talk between dopamine D5 and gamma-aminobutyric acid A receptors. *Nature* 403, 274-280.

Lyford, G. L., Yamagata, K., Kaufmann, W. E., Barnes, C. A., Sanders, L. K., Copeland, N. G., Gilbert, D. J., Jenkins, N. A., Lanahan, A. A., and Worley, P. F. (1995). Arc, a growth factor and activity-regulated gene, encodes a novel cytoskeleton-associated protein that is enriched in neuronal dendrites. *Neuron* 14, 433-445.

Malenka, R. C. (2003). Synaptic plasticity and AMPA receptor trafficking. *Ann. N. Y. Acad. Sci.* 1003, 1-11.

Malgaroli, A., and Tsien, R. W. (1992). Glutamate-induced long-term potentiation of the frequency of miniature synaptic currents in cultured hippocampal neurons. *Nature* 357, 134-139.

Mangiavacchi S, W. M. (2004). D1 dopamine receptor stimulation increases the rate of AMPA receptor insertion onto the surface of cultured nucleus accumbens neurons through a pathway dependent on protein kinase A. *J. Neurochem.* 88, 1261-1271.

Martin, K. C., Barad, M., and Kandel, E. R. (2000). Local protein synthesis and its role in synapse-specific plasticity. *Curr. Op. Neurobiol.* 10, 587-592.

Martin, K. C., Casadio, A., Zhu, H., E, Y., Rose, J. C., Chen, M., Bailey, C. H., and Kandel, E. R. (1997). Synapse-specific, long-term facilitation of aplysia sensory to motor synapses: A function for local protein synthesis in memory storage. *Cell* 91, 927-938.

Martin, K. C., and Kosik, K. S. (2002). Synaptic tagging - who's it? *Nat. Rev. Neurosci.* 3, 813-820.

Matthies, H., Becker, A., Schroeder, H., Kraus, J., Hollt, V., and Krug, M. (1997). Dopamine D1-deficient mutant mice do not express the late phase of hippocampal long-term potentiation. *Neuroreport* 8, 3533-3535.

Mayer, M. L., Westbrook, G. L., and Guthrie, P. B. (1984). Voltage-dependent block by $Mg^{2+}$ of NMDA responses in spinal cord neurones. *Nature* 309, 261-263.

Mayford, M., Baranes, D., Podsypanina, K., and Kandel, E. R. (1996). The 3'-untranslated region of CamKII-alpha is a cis-acting signal for the localization and translation of mRNA in dendrites. *Proc. Natl. Acad. Sci. USA* 93, 13250-13255.

McAllister, A. K., Katz, L. C., and Lo, D. C. (1999). Neurotrophins and synaptic plasticity. *Ann. Rev. Neurosci.* 22, 295-318.

Miesenbock, G., De Angelis, D. A., and Rothman, J. E. (1998). Visualizing secretion and synaptic transmission with pH-sensitive green fluorescent proteins. *Nature* 394, 192-195.

Miller, S., Yasuda, M., Coats, J. M., Jones, Y., Martone, M. E., and Mayford, M. (2002). Disruption of dendritic translation of CamKII-alpha impairs stabilizaiton of synaptic plasticity and memory consolidation. *Neuron* 36, 507-519.

Miyashiro, K., Dichter, M., and Eberwine, J. (1994). On the nature and differential distribution of mRNAs in hippocampal neurites: Implications for neuronal functioning. *Proc. Natl. Acad. Sci. USA* 91, 10800-10804.

Mori, Y., Imaizumi, K., Katayama, T., Yoneda, T., and Tohyama, M. (2000). Two cis-acting elements in the 3' untranslated region of the alpha-CamKII regulate its dendritic targeting. *Nat. Neurosci.* 3, 1079-1084.

Nathans, D. (1964). Puromycin inhibition of protein synthesis: Incorporation of puromycin into peptide chains. *Proc. Natl. Acad. Sci. USA* 51, 585-592.

Nayak, A., Zastrow, D. J., Lickteig, R., Zanister, N. R., and Browning, M. D. (1998). Maintenance of late-phase LTP is accompanied by PKA-dependent increase in AMPA receptor synthesis. *Nature* 394, 690-683.

Nguyen, P. V., Abel, T., and Kandel, E. R. (1994). Requirement of a critical period of transcription for induction of a late phase of LTP. *Science* 265, 1104-1107.

Nishiyama, M., Hong, K., Mikoshiba, K., Poo, M. M., and Kato, K. (2000). Calcium stores regulate the polarity and input specificity of synaptic modification. *Nature* 408, 584-588.

Ostroff, L. E., Fiala, J. C., Allwardt, B., and Harris, K. M. (2002). Polyribosomes redistribute from dendritic shafts into spines with enlarged synapses during LTP in developing rat hippocampal slices. *Neuron* 35, 535-545.

Otani, S., Marshall, C. J., Tate, W. P., Goddard, G. V., and Abraham, W. C. (1989). Maintenance of long-term potentiation in rat dentate gyrus requires protein synthesis but not messenger RNA synthesis immediately post-tetanization. *Neuroscience* 28, 519-526.

Otmakhova, N. A., and Lisman, J. E. (1996). D1/D5 dopamine receptor activation increases the magnitude of early long-term potentiation at CA1 hippocampal synapses. *J. Neurosci.* 16, 7478-7486.

Otsu, N. (1979). A threshold selection method from gray-level histograms. *IEEE Trans. Sys., Man, and Cyb.* 9, 62-66.

Ouyang, Y., Kantor, D. B., Harris, K. M., Schuman, E. M., and Kennedy, M. B. (1997). Visualization of the distribution of autophosphorylated calcium/calmodulin-dependent protein kinase II after tetanic stimulation in the CA1 area of the hippocampus. *J. Neurosci.* 17, 5416-5427.

Ouyang, Y., Rosenstein, A., Kreiman, G., Schuman, E. M., and Kennedy, M. B. (1999). Tetanic stimulation leads to increased accumulation of ca(2+)/calmodulin-dependent protein kinase II via dendritic protein synthesis in hippocampal neurons. *J. Neurosci.* 19, 7823-7833.

Patrick, G. N., Bingol, B., Weld, H. A., and Schuman, E. M. (2003). Ubiquitin-mediated proteasome activity is required for agonist-induced endocytosis of GluRs. *Curr. Biol.* 13, 2073-2081.

Patrick, G. N., Zukerberg, L., Nikolic, M., de la Monte, S., Dikkes, P., and Tsai, L. H. (1999). Conversion of p35 to p25 deregulates cdk5 activity and promotes neurodegeneration. *Nature* 402, 615-622.

Pei, L., Lee, F. J., Moszczynska, A., Vukusic, B., and Liu, F. (2004). Regulation of dopamine D1 receptor function by physical interaction with the NMDA receptors. *J. Neurosci.* 24, 1149-1158.

Petralia, R. S., Esteban, J. A., Wang, Y. X., Partridge, J. G., Zhao, H. M., Wenthold, R. J., and Malinow, R. (1999). Selective acquisition of  receptors over postnatal development suggests a molecular basis for silent synapses. *Nat. Neurosci.* 2, 31-36.

Pierce, J. P., Mayer, T., and McCarthy, J. B. (2001). Evidence for a satellite secretory pathway in neuronal dendritic spines. *Curr. Biol.* 11, 351-355.

Pinkstaff, J. K., Chappell, S. A., Mauro, V. P., Edelman, G. M., and Krushel, L. A. (2001). Internal initiation of translation of five dendritically localized neuronal mRNAs. *Proc. Natl. Acad. Sci. USA* 98, 2770-2775.

Pittenger, C., Huang, Y. Y., Paletzki, R. F., Bourtchouladze, R., Scanlin, H., Vronskaya, S., and Kandel, E. R. (2002). Reversible inhibition of CREB/ATF transcription factors in region CA1 of the dorsal hippocampus disrupts hippocampus-dependent spatial memory. *Neuron* 34, 447-462.

Rao, A., and Steward, O. (1991). Evidence that protein constituents of postsynaptic membrane are locally synthesized: Analysis of proteins synthesized within synaptosomes. *J. Neurosci.* 11, 2881-2895.

Reymann, K. G., Malisch, R., Schulzeck, K., Brodemann, R., Ott, T., and Matthies, H. (1985). The duration of long-term potentiation in the CA1 region of the hippocampal slice preparation. *Brain. Res. Bull.* 15, 249-255.

Richmond, S. A., Irving, A. J., Molnar, E., McIlhinney, R. A., Michelangeli, F., Henley, J. M., and Collingridge, G. L. (1996). Localization of the glutamate receptor subunit GluR1 on the surface of living and within cultured hippocampal neurons. *Neuroscience* 75, 69-82.

Rook, M. S., Lu, M., and Kosik, K. S. (2000). CamkII-alpha 3' untranslated region-directed mRNA translocation in living neurons: Visualization by GFP linkage. *J. Neurosci.* 20, 6385-6393.

Scheetz, A. J., Nairn, A. C., and Constantine-Paton, M. (2000). NMDA receptor-mediated control of protein synthesis at developing synapses. *Nat. Neurosci.* 3, 211-216.

Schuman, E. M. (1999a). mRNA trafficking and local protein synthesis at the synapse. *Neuron* 23, 645-648.

Schuman, E. M. (1999b). Neurotrophin regulation of synaptic transmission. *Curr. Opin. Neurobiol.* 9, 105-109.

Schuman, E. M., and Madison, D. V. (1994). Locally distributed synaptic potentiation in the hippocampus. *Science* 263, 532-536.

Shi, S., Hayashi, Y., Esteban, J. A., and Malinow, R. (2001). Subunit-specific rules governing AMPA receptor trafficking to synapses in hippocampal pyramidal neurons. *Cell* 105, 331-343.

Shi, S. H., Hayashi, Y., Petralia, R. S., Zaman, S. H., Wenthold, R. J., Svoboda, K., and Malinow, R. (1999). Rapid spine delivery and redistribution of AMPA receptors after synaptic NMDA receptor activation. *Science* 284, 1811-1816.

Srinivasan, Y., Guzikowski, A. P., Haugland, R. P., and Angelides, K. J. (1990). Distribution and lateral mobility of glycine receptors on cultured spinal cord neurons. *J. Neurosci.* 10, 985-995.

St. Johnston, D., Beuchle, D., and Nusslein-Volhard, C. (1991). Staufen, a gene required to localize maternal RNAs in the *Drosophila* egg. *Cell* 66, 51-63.

Stanton, P. K., and Sarvey, J. M. (1984). Blockade of long-term potentiation in rat hippocampal CA1 region by inhibitors of protein synthesis. *J. Neurosci.* 4, 3080-3084.

Starck S. R., and Roberts R. W. (2002). Puromycin oligonucleotides reveal steric restrictions for ribosome entry and multiple modes of translation inhibition. *RNA* 8, 890-903.

Staubli, U., and Lynch, G. (1987). Stable hippocampal long-term potentiation elicited by 'theta' pattern stimulation. *Brain Res.* 435, 227-234.

Stebbins-Boaz, B., Cao, Q., de Moor, C. H., Mendez, R., and Richter, J. D. (1999). Maskin is a CPEB-associated factor that transiently interacts with eIF-4e. *Mol. Cell* 4, 1017-1027.

Stevens, C. F. (1998). A million dollar question: Does LTP = memory? *Neuron* 20, 1-2.

Steward, O. (1997). mRNA localization in neurons: A multipurpose mechanism? *Neuron* 18, 9-12.

Steward, O., and Levy, W. B. (1982). Preferential localization of polyribosomes under the base of dendritic spines in granule cells of the dentate gyrus. *J. Neurosci.* 2, 284-291.

Steward, O., and Reeves, T. M. (1988). Protein-synthesis machinery beneath postsynaptic sites on CNS neurons: Association between polyribosomes and other organelles at the synaptic site. *J. Neurosci.* 8, 176-184.

Steward, O., and Schuman, E. M. (2001). Protein synthesis at synaptic sites on dendrites. *Ann. Rev. Neurosci.* 24, 299-325.

Steward, O., and Schuman, E. M. (2003). Compartmentalized synthesis and degradation of proteins in neurons. *Neuron* 40, 347-359.

Steward, O., Wallace, C. S., Lyford, G. L., and Worley, P. F. (1998). Synaptic activation causes the mRNA for the IEG Arc to localize selectively near activated postsynaptic sites on dendrites. *Neuron* 21, 741-751.

Swanson-Park, J. L., Coussens, C. M., Mason-Parker, S. E., Raymond, C. R., Hargreaves, E. L., Dragunow, M., Cohen, A. S., and Abraham, W. C. (1999). A double dissociation within the hippocampus of dopamine D1/D5 receptor and beta-adrenergic receptor contributions to the persistence of long-term potentiation. *Neuroscience* 92, 485-497.

Tang, S. J., Meulemans, D., Vasquez, L., Colaco, N., and Schuman, E. M. (2001). A role for Staufen in the delivery of RNA to neuronal dendrites. *Neuron* 8, 463-475.

Tang, S. J., Reis, G., Kang, H., Gingras, A. C., Sonenberg, N., and Schuman, E. M. (2002). A rapamycin-sensitive signaling pathway contributes to long-term synaptic plasticity. *Proc. Natl. Acad. Sci. USA* 99, 467-472.

Tao, H. W., Zhang, L. I., Engert, F., and Poo, M. (2001). Emergence of input specificity of LTP during development of retinotectal connections in vivo. *Neuron* 31, 569-580.

Terada, N., Patel, H. R., Takase, K., Kohno, K., Nairn, A. C., and Gelfand, E. W. (1994). Rapamycin selectively inhibits translation of mRNAs encoding elongation factors and ribosomal proteins. *Proc. Natl. Acad. Sci. USA* 91, 11477-11481.

Tongiorgi, E., Righi, M., and Cattaneo, A. (1997). Activity-dependent dendritic targeting of BDNF and TRKB mRNAs in hippocampal neurons. *J. Neurosci.* 17, 9492-9505.

Torre, E. R., and Steward, O. (1996). Protein synthesis within dendrites: Glycosylation of newly synthesized proteins in dendrites of hippocampal neurons in culture. *J. Neurosci.* 16, 5967-5978.

Torre, E. R., and Steward, O. (1992). Demonstration of local protein synthesis within dendrites using a new cell culture system that permits the isolation of living axons and dendrites from their cell bodies. *J. Neurosci.* 12, 762-772.

Twiss, J. L., Smith, D. S., Chang, B., and Shooter, E. M. (2000). Translational control of ribosomal protein l4 mRNA is required for rapid neurite regeneration. *Neurobiol. Dis.* 7, 416-428.

Wallace, C. S., Lyford, G. L., Worley, P. F., and Steward, O. (1998). Differential intracellular sorting of immediate early gene mRNAs depends on signals in the mRNA sequence. *J. Neurosci.* 18, 26-35.

Weiler, I. J., and Greenough, W. T. (1991). Potassium ion stimulation triggers protein translation in synaptoneurosomal polyribosomes. *Mol. Cell. Neurosci.* 2, 305-314.

Weiler, I. J., and Greenough, W. T. (1993). Metabotropic glutamate receptors trigger postsynaptic protein synthesis. *Proc. Natl. Acad. Sci. USA* 90, 7168-7171.

Weiler, I. J., Irwin, S. A., Klintsova, A. Y., Spencer, C. M., Brazelton, A. D., Miyashiro, K., Comery, T. A., Patel, B., Eberwine, J., and Greenough, W. T. (1997). Fragile X mental retardation protein is translated near synapses in response to neurotransmitter activation. *Proc. Natl. Acad. Sci. USA* 94, 5395-9400.

Wells, D. G., Richter, J. D., and Fallon, J. R. (2000). Molecular mechanisms for activity-regulated protein synthesis in the synapto-dendritic compartment. *Curr. Opin. Neurobiol.* 10, 132-137.

Wey, C. L., Cone R.A., and A., E. M. (1981). Lateral diffusion of rhodopsin in photoreceptor cells measured by fluorescence photobleaching and recovery. *Biophys. J.* 33, 225-232.

Wickham, L., Duchaine, T., Luo, M., Nabi, I. R., and DesGroseillers, L. (1999). Mammalian Staufen is a double-stranded RNA- and tubulin-binding protein which localizes to the rough endoplasmic reticulum. *Mol. Cel. Biol.* 19, 2220-2230.

Wu, L., Wells, D., Tay, J., Mendis, D., Abbott, M. A., Barnitt, A., Quinlan, E., Heynen, A., Fallon, J. R., and Richter, J. D. (1998). CPEB-mediated cytoplasmic polyadenylation and the regulation of experience-dependent translation of alpha-CamKII mRNA at synapses. *Neuron* 21, 1129-1139.

Zheng, J. Q., Kelly, T. K., Chang, B., Ryazantsev, S., Rajasekaran, A. K., Martin, K. C., and Twiss, J. L. (2001). A functional role for intra-axonal protein synthesis during axonal regeneration from adult sensory neurons. *J. Neurosci.* 21, 9291-9303.

*Appendix A*

**MATLAB Code for 3-D Particles Analysis:**

Lines marked with the % are comments in the code, and are not required for running the program, but should be left in place in order help users understand the various components. The function depends on a few other MATLAB files, including "getstacks," "timebar" (written and provided by Chad English), and "dlview" (written and provided by David Liebowitz). All the dependent functions are also shown below. In order for the program to run properly, all the functions must be copied into a text editor and then saved as a .m file into a directory on the MATLAB path. The files should be saved according to the function name, such as "Particles3.m" and "dlview.m". This version has been tested on MATLAB version 6, releases 12, 13, and 13.1.

```
function varargout = Particles3(varargin)
% Particles3 - graphical interface for running 3D particle analysis.
%
% Calling Particles3 opens a new window with two axes displayed in 3 dimensions.
% To load images (in TIFF format only), click the "Load 3D Images" button.
% If you need to use some other image format, you can modify the GETSTACKS
% function, which is called for opening the image stacks.  Once images have
% been loaded, isosurfaces of each image are plotted in the axes.  The initial
% isovalue is set to the maximum value of GRAYTHRESH for each image.  You
% can adjust the threshold settings using the sliders beneath each axis,
% or by entering threshold values (between zero and one) in the text boxes
% to the left of each slider.
%
% Left-click and drag on each axis to rotate the image in 3D.
% Right-click and drag on each axis to zoom in and out of the image.
% Middle-click and drag to pan left or right in the image.
%
% The idea is to set a threshold level that will isolate the particles in
% your image data without losing any 'real' information.  Of course what is
% real is very subjective, so you may wish to set several thresholds for any
% given analysis.  You may then run your image processing routine with the
% various threshold settings to see if any effect you observe is due to an
% artifact of your threshold settings, or if it is truly something real in
% your data.  An intensity-coded 2D version of the images will be plotted
% into a new window if the 2D Projections button is pressed.
%
% Once a threshold is set, clicking the "Save and Run" button will complete
% the analysis and plot the 3D render of the overlapping particles in a new
% figure.  Depending on your data, you may want to only plot the particles
% that colocalize, or you may choose to plot all of one image or the other.
% These selections can be made with the Colocalization Plots radio buttons.
% If you do not want to plot the data, uncheck the "Colocalization Only"
% button, which is checked by default.
%
% If you have a slow video card, you can use the Reducepatch command by
```

```
% entering a value less than one in the Reducepatch Ratio text box.  This
% will increase the computation time required to render the surface, but
% will make the real-time 3D rotation much faster.  By default, the ratio
% is set to 1, which renders all surfaces.  Changing the value to something
% less than 1 will reduce the number of surfaces rendered.  For example,
% entering 0.2 will result in rendering 20% of the total number of surfaces
% for the image.
%
% See Also IMREAD, GETSTACKS, ISOSURFACE, REDUCEPATCH, GRAYTHRESH, DLVIEW

% Last Modified by GUIDE v2.5 03-Apr-2004 22:25:41

% Begin initialization code - DO NOT EDIT
gui_Singleton = 1;
gui_State = struct('gui_Name',       mfilename, ...
                   'gui_Singleton',  gui_Singleton, ...
                   'gui_OpeningFcn', @Particles3_OpeningFcn, ...
                   'gui_OutputFcn',  @Particles3_OutputFcn, ...
                   'gui_LayoutFcn',  @Particles3_LayoutFcn, ...
                   'gui_Callback',   []);
if nargin & isstr(varargin{1})
   gui_State.gui_Callback = str2func(varargin{1});
end

if nargout
   [varargout{1:nargout}] = gui_mainfcn(gui_State, varargin{:});
else
   gui_mainfcn(gui_State, varargin{:});
end
% End initialization code - DO NOT EDIT


% --- Executes just before Particles3 is made visible.
function Particles3_OpeningFcn(hObject, eventdata, handles, varargin)
set(gcf,'Color',[.3 .3 .3]);
set(gcf,'toolbar','none');
%s = wgetname(gcf);
%seticon(s,'C:\MATLAB6p5\p3icon.ico');

% Choose default command line output for Particles3
handles.output = hObject;

% Update handles structure
guidata(hObject, handles);

% --- Outputs from this function are returned to the command line.
function varargout = Particles3_OutputFcn(hObject, eventdata, handles)

% Get default command line output from handles structure
varargout{1} = handles.output;

% --- Executes during object creation, after setting all properties.
function figure1_CreateFcn(hObject, eventdata, handles)
dlview on;
```

```
% --- Plots isosurface of image1
function surf1
handles = guidata(gcbo);
[r c z] = size(handles.img1);
if str2double(get(handles.edit3,'String')) == 1;
   axes(handles.img1plot); cla;
   p1 = patch(isosurface(handles.img1,get(handles.slider1,'Value'))); axis([0 c 0 r 0 z]);
   set(p1,'FaceColor',[.4 .6 .7],'FaceAlpha',1,'EdgeColor',[.4 .6 .7],'EdgeAlpha',.01);
   axis vis3d; light; light; light('Position', [-1 -1 -3]); lighting gouraud;
   set(gca,'Color','black');
else str2double(get(handles.edit3,'String')) ~= 1;
   axes(handles.img1plot); cla;
   p1 = patch(isosurface(handles.img1,get(handles.slider1,'Value'))); axis([0 c 0 r 0 z]);
   reducepatch(p1, str2double(get(handles.edit3,'String')));
   set(p1,'FaceColor',[.4 .6 .7],'FaceAlpha',1,'EdgeColor',[.4 .6 .7],'EdgeAlpha',.01);
   axis vis3d; light; light; light('Position', [-1 -1 -3]); lighting gouraud;
   set(gca,'Color','black');
end

% --- Plots isosurface of image2
function surf2
handles = guidata(gcbo);
[r c z] = size(handles.img2);
if str2double(get(handles.edit3,'String')) == 1;
   axes(handles.img2plot); cla;
   p2 = patch(isosurface(handles.img2,get(handles.slider2,'Value'))); axis([0 c 0 r 0 z]);
   set(p2,'FaceColor',[.7 .2 .4],'FaceAlpha',1,'EdgeColor',[.7 .2 .4],'EdgeAlpha',.01);
   axis vis3d; light; light('Position', [-1 -1 -3]); lighting gouraud;
else str2double(get(handles.edit3,'String')) ~= 1;
   axes(handles.img2plot); cla;
   p2 = patch(isosurface(handles.img2,get(handles.slider2,'Value'))); axis([0 c 0 r 0 z]);
   reducepatch(p2, str2double(get(handles.edit3,'String')));
   set(p2,'FaceColor',[.7 .2 .4],'FaceAlpha',1,'EdgeColor',[.7 .2 .4],'EdgeAlpha',.01);
   axis vis3d; light; light('Position', [-1 -1 -3]); lighting gouraud;
end

% --- Executes on button press in pushbutton3.
function pushbutton3_Callback(hObject, eventdata, handles)
[img1,img2] = getstacks;
handles.img1 = img1;
handles.img2 = img2;
guidata(hObject,handles);
set(handles.slider1, 'Min', min(min(min(img1))));
set(handles.slider1, 'Max', max(max(max(img1))));
set(handles.slider2, 'Min', min(min(min(img2))));
set(handles.slider2, 'Max', max(max(max(img2))));
set(handles.slider1, 'Value', max(graythresh(img1)));
set(handles.slider2, 'Value', max(graythresh(img2)));
set(handles.edit1, 'String', num2str(get(handles.slider1,'Value')));
set(handles.edit2, 'String', num2str(get(handles.slider2,'Value')));
surf1;
surf2;
```

```
% --- Executes on button press in pushbutton4.
function pushbutton4_Callback(hObject, eventdata, handles)
figure, subplot(211), imagesc(flipud(max(handles.img1,[],3))), axis image;
      subplot(212), imagesc(flipud(max(handles.img2,[],3))), axis image;
      set(gcf,'Color','Black');

% --- Executes on button press in pushbutton5.
function pushbutton5_Callback(hObject, eventdata, handles)
axes(handles.img1plot); view(3);
axes(handles.img2plot); view(3);

% --- Executes on slider1 movement.
function slider1_Callback(hObject, eventdata, handles)
set(handles.edit1,'String',num2str(get(handles.slider1,'Value')));
surf1;

% --- Executes when user enters values in edit1 textbox
function edit1_Callback(hObject, eventdata, handles)
set(handles.slider1,'Value',str2double(get(handles.edit1,'String')));
surf1;

% --- Executes on slider2 movement.
function slider2_Callback(hObject, eventdata, handles)
set(handles.edit2,'String',num2str(get(handles.slider2,'Value')));
surf2;

% --- Executes when user enters values in edit2 textbox
function edit2_Callback(hObject, eventdata, handles)
img2 = handles.img2;
set(handles.slider2,'Value',str2double(get(handles.edit2,'String')));
surf2;

% --- Executes when user enters values in edit3 textbox
function edit3_Callback(hObject, eventdata, handles)
[r c z] = size(handles.img1);
if isfield(handles,'img1') == 1;
   surf1;
   surf2;
else isfield(handles,'img1') == 0;
   str2num(get(hObject,'String'));
end

% --- Executes on radiobutton1 activation.
function radiobutton1_Callback(hObject, eventdata, handles)
if get(handles.radiobutton1,'Value') == 1;
   set(handles.radiobutton2,'Value',0);
   set(handles.radiobutton3,'Value',0);
end

% --- Executes on radiobutton2 activation.
function radiobutton2_Callback(hObject, eventdata, handles)
if get(handles.radiobutton2,'Value') == 1;
   set(handles.radiobutton1,'Value',0);
   set(handles.radiobutton3,'Value',0);
```

```
end

% --- Executes on radiobutton3 activation.
function radiobutton3_Callback(hObject, eventdata, handles)
if get(handles.radiobutton3,'Value') == 1;
   set(handles.radiobutton1,'Value',0);
   set(handles.radiobutton2,'Value',0);
end

% --- Executes on button press in pushbutton2.
% This code does most of the work (lines 195-318)
function pushbutton2_Callback(hObject, eventdata, handles)

% Make Image1 Binary
[r c z] = size(handles.img1);
for i = 1:z;
   [img1th(:,:,i)] = im2bw([handles.img1(:,:,i)],get(handles.slider1, 'Value'));
end
img1th = bwareaopen(img1th,4,26);
img1thlabel = bwlabeln(img1th,26);

% Make Image2 Binary
for i = 1:z;
   [img2th(:,:,i)] = im2bw([handles.img2(:,:,i)],get(handles.slider2, 'Value'));
end
img2th = bwareaopen (img2th,4,26);
img2thlabel = bwlabeln (img2th,26);

handles.img1th = img1th; handles.img1thlabel = img1thlabel;
handles.img2th = img2th; handles.img2thlabel = img2thlabel;

% Find Overlap
ol = (img1th&img2th);
ollabel = bwlabeln (ol,26);

% Find particle volumes in each image
props1 = regionprops (img1thlabel,'Area','PixelList');
vols1 = [props1.Area];
props2 = regionprops (img2thlabel,'Area','PixelList');
vols2 = [props2.Area];
propsol = regionprops (ollabel,'Area','PixelList');
volsol = [propsol.Area];

% Find sum, mean, max, and min pixel intensity values
% for image1
pixlist1 = {props1.PixelList};
h = timebar('Finding Image1 Pixel Properties','Computation Progress');
%seticon(h,'C:\MATLAB6p5\p3icon.ico');
for i = 1:length(vols1)
   for j = 1:length(pixlist1{i}(:,1))
      [mpval(j)] = im2uint8(handles.img1(pixlist1{i}(j,2),pixlist1{i}(j,1),pixlist1{i}(j,3)));
   end
   [sumpixvals1(i)] = sum(mpval);
   [meanpixvals1(i)] = mean(mpval);
```

```
   [maxpixvals1(i)] = max(mpval);
   [minpixvals1(i)] = min(mpval);
   timebar(h,i/length(vols1));
   clear mpval;
end
close(h);
clear i j mpval;
p1pixmean = mean(meanpixvals1);
p1pixtot = sum(sumpixvals1);

% Find sum, mean, max, and min pixel intensity values
% for image2
pixlist2 = {props2.PixelList};
h = timebar('Finding Image2 Pixel Properties','Computation Progress');
%seticon(h,'C:\MATLAB6p5\p3icon.ico');
for i = 1:length(vols2)
   for j = 1:length(pixlist2{i}(:,1))
      [mpval(j)] = im2uint8(handles.img2(pixlist2{i}(j,2),pixlist2{i}(j,1),pixlist2{i}(j,3)));
   end
   [sumpixvals2(i)] = sum(mpval);
   [meanpixvals2(i)] = mean(mpval);
   [maxpixvals2(i)] = max(mpval);
   [minpixvals2(i)] = min(mpval);
   timebar(h,i/length(vols2));
   clear mpval;
end
close(h);
clear i j mpval;
p2pixmean = mean(meanpixvals2);
p2pixtot = sum(sumpixvals2);

% Compute total volume of particles in each image (and the overlaps)
vp1tot = length(find(img1th));
vp2tot = length(find(img2th));
voltot = length(find(ol));

% Compute number and mean volume of particles in each image
nump1 = length(vols1);              % Number of particles in img1
meanp1 = mean(vols1);               % Mean volume of particles in img1
nump2 = length(vols2);              % Number of particles in img2
meanp2 = mean(vols2);               % Mean volume of particles in img2
numol = length(volsol);             % Number of particles in overlap image
meanols = mean(volsol);             % Mean volume of particles in overlap image

% Compute fraction of overlaping volumes (for the whole image)
volsolp1 = sum(volsol)/sum(vols1);    % Overlaps as fraction of total img1 particle volumes
volsolp2 = sum(volsol)/sum(vols2);    % Overlaps as fraction of total img2 particle volumes

% Compute fraction of particles (number) that overlap (for the whole image)
numolp1 = numol/nump1;              % Number of overlap particles/number of particles in img1
numolp2 = numol/nump2;              % Number of overlap particles/number of particles in img2

% Compute fraction of EACH particle that contributes to overlap
olp = zeros (length(volsol),3);
```

```
for i = 1:length(volsol)
   olp(i,:) = [propsol(i).PixelList(1,:)];
end

set(0,'Units','Pixels');

% Sub-Volume Calculations (finding properties of particles iff they
% have any overlap)
volsp1sub = zeros(size(volsol));
volsp2sub = zeros(size(volsol));
h = timebar('Finding Sub-Volumes','Computation Progress');
%seticon(h,'C:\MATLAB6p5\p3icon.ico');
for i = 1:length(volsol)
   volsp1sub(i) = length(find(img1thlabel == img1thlabel((olp(i,2)),(olp(i,1)),(olp(i,3)))));
   volsp2sub(i) = length(find(img2thlabel == img2thlabel((olp(i,2)),(olp(i,1)),(olp(i,3)))));
   volsp1subidx(i) = img1thlabel((olp(i,2)),(olp(i,1)),(olp(i,3)));
   volsp2subidx(i) = img2thlabel((olp(i,2)),(olp(i,1)),(olp(i,3)));
   for j=1:length(propsol(i).PixelList(:,1))
      [pixol1(j)] = im2uint8(handles.img1((propsol(i).PixelList(j,2)), (propsol(i).PixelList(j,1)),
(propsol(i).PixelList(j,3))));
      [pixol2(j)] = im2uint8(handles.img2((propsol(i).PixelList(j,2)), (propsol(i).PixelList(j,1)),
(propsol(i).PixelList(j,3))));
   end
   [spixol1(i)] = sum(pixol1);
   [spixol2(i)] = sum(pixol2);
   clear pixol1;
   clear pixol2;
   timebar(h,i/length(volsol));
end
close(h);
p1fract = volsol./volsp1sub;
p2fract = volsol./volsp2sub;
sumpixol1 = sum(spixol1);
sumpixol2 = sum(spixol2);
meanpixol1 = mean((spixol1./volsol));
meanpixol2 = mean((spixol2./volsol));

for i = 1:z
   [img1thlabelsub(:,:,i)] = ismember(img1thlabel(:,:,i), volsp1subidx);
   [img2thlabelsub(:,:,i)] = ismember(img2thlabel(:,:,i), volsp2subidx);
end

varids = {'TH1','TH2','MeanV1','TotalV1','MeanPix1','TotalPix1','NumP1','MeanP1frac'...
      'MeanV2','TotalV2','MeanPix2','TotalPix2','NumP2','MeanP2frac'...
      'MeanVOL','TotalVOL','NumPOL','TotalPixOL1', 'MeanPixOL1','NumOLdivTot1','VOLdivTotV1',...
      'TotalPixOL2','MeanPixOL2','NumOLdivTot2','VOLdivTotV2'};
% Make data row vector
[data(1,:)] = [get(handles.slider1,'Value'), get(handles.slider2,'Value'),...
      meanp1, vp1tot, p1pixmean, p1pixtot, nump1, mean(p1fract),...
      meanp2, vp2tot, p2pixmean, p2pixtot, nump2, mean(p2fract),...
      meanols, voltot, numol,...
      sumpixol1, meanpixol1, numolp1, volsolp1,...
      sumpixol2, meanpixol2, numolp2, volsolp2];
% dlmwrite('rowdat.xls',data,'\t');
```

```
if isempty(dir('rowdat.txt')) == 1;
   fid = fopen('rowdat.txt','at+');
   fprintf(fid,'%s\t',varids{:});
   fprintf(fid,'\r');
   fprintf (fid,'%g\t',data);
   fclose(fid);
else isempty(dir('rowdat.txt')) == 0;
   fid = fopen('rowdat.txt','at+');
   fseek(fid,0,'eof');
   fprintf(fid,'\r');
   fprintf (fid,'%g\t',data);
   fclose (fid);
end

save alldat;

% Plot Colocalization isosurfaces
if (get(handles.radiobutton1,'Value'))+(get(handles.radiobutton2,'Value'))+...
  (get(handles.radiobutton3,'Value')) == 1;
   if get(handles.radiobutton1,'Value') == 1;
      fig2 = figure('numbertitle','off','name','Colocalization Plot');
      set(gcf,'InvertHardCopy', 'off','PaperPositionMode','Auto','Renderer','OpenGL');
      m = uimenu('Label','File');
         uimenu(m,'Label','Export...','Callback','print -dtiff -r300 Coloc');
      %seticon(gcf,'C:\MATLAB6p5\p3icon.ico');
      figure(fig2);
      p1 = patch(isosurface(img1thlabelsub,0));
      set(p1,'FaceColor','green','EdgeColor','none','FaceAlpha',1), lighting gouraud;
      hold on;
      p2 = patch(isosurface(img2thlabelsub,0));
      set(p2,'FaceColor','red','EdgeColor','none','FaceAlpha',0.4),
      light; light; light('Position', [-1 -1 -3]); lighting gouraud;
      set (gcf,'menubar','none','Color','Black','Units','Normalized','Position',[.1 .05 .8 .85]);
      view(3), axis([0 c 0 r 0 z]), grid off, box off; axis off;axis vis3d;
      set(gca,'DataAspectRatio',[1,1,1]);
      dlview on;
   elseif get(handles.radiobutton2,'Value') == 1;
      fig2 = figure('numbertitle','off','name','Colocalization Plot');
      set(gcf,'InvertHardCopy', 'off','PaperPositionMode','Auto','Renderer','OpenGL');
      m = uimenu('Label','File');
         uimenu(m,'Label','Export...','Callback','print -dtiff -r300 Coloc');
      %seticon(gcf,'C:\MATLAB6p5\p3icon.ico');
      figure(fig2);
      p1 = patch(isosurface(img1thlabel,0));
      set(p1,'FaceColor',[.3,.4,.6],'EdgeColor','none','FaceAlpha',0.3), lighting gouraud;
      hold on;
      p2 = patch(isosurface(img2thlabelsub,0));
      set(p2,'FaceColor','green','EdgeColor','none','FaceAlpha',1),
      light; light; light('Position', [-1 -1 -3]); lighting gouraud;
      set (gcf,'menubar','none','Color','Black','Units','Normalized','Position',[.1 .05 .8 .85]);
      view(3), axis([0 c 0 r 0 z]), grid off, box off; axis off;axis vis3d;
      set(gca,'DataAspectRatio',[1,1,1]);
      dlview on;
   else get(handles.radiobutton3,'Value') == 1;
```

```
        fig2 = figure('numbertitle','off','name','Colocalization Plot');
        set(gcf,'InvertHardCopy', 'off','PaperPositionMode','Auto','Renderer','OpenGL');
        m = uimenu('Label','File');
           uimenu(m,'Label','Export...','Callback','print -dtiff -r300 Coloc');
        %seticon(gcf,'C:\MATLAB6p5\p3icon.ico');
        figure(fig2);
        p1 = patch(isosurface(img1thlabelsub,0));
        set(p1,'FaceColor','green','EdgeColor','none','FaceAlpha',1), lighting gouraud;
        hold on;
        p2 = patch(isosurface(img2thlabel,0));
        set(p2,'FaceColor',[.3,.4,.6],'EdgeColor','none','FaceAlpha',0.3),
        light; light; light('Position', [-1 -1 -3]); lighting gouraud;
        set (gcf,'menubar','none','Color','Black','Units','Normalized','Position',[.1 .05 .8 .85]);
        view(3), axis([0 c 0 r 0 z]), grid off, box off; axis off;axis vis3d;
        set(gca,'DataAspectRatio',[1,1,1]);
        dlview on;
    end
else (get(handles.radiobutton1,'Value'))+(get(handles.radiobutton2,'Value'))+...
     (get(handles.radiobutton3,'Value')) == 0;
end

% --- Executes when user attempts to close figure1.
function figure1_CloseRequestFcn(hObject, eventdata, handles)
delete(hObject);

% --- Creates and returns a handle to the GUI figure.
function h1 = Particles3_LayoutFcn(policy)
% policy - create a new figure or use a singleton. 'new' or 'reuse'.

persistent hsingleton;
if strcmpi(policy, 'reuse') & ishandle(hsingleton)
    h1 = hsingleton;
    return;
end

h1 = figure(...
'Units','characters',...
'BackingStore','off',...
'CloseRequestFcn','Particles3("figure1_CloseRequestFcn",gcf,[],guidata(gcf))',...
'Color',[0.87843137254902 0.874509803921569 0.890196078431373],...
'Colormap',[0 0 0.5625;0 0 0.625;0 0 0.6875;0 0 0.75;0 0 0.8125;0 0 0.875;0 0 0.9375;0 0 1;0 0.0625 1;0
0.125 1;0 0.1875 1;0 0.25 1;0 0.3125 1;0 0.375 1;0 0.4375 1;0 0.5 1;0 0.5625 1;0 0.625 1;0 0.6875 1;0 0.75
1;0 0.8125 1;0 0.875 1;0 0.9375 1;0 1 1;0.0625 1 1;0.125 1 0.9375;0.1875 1 0.875;0.25 1 0.8125;0.3125 1
0.75;0.375 1 0.6875;0.4375 1 0.625;0.5 1 0.5625;0.5625 1 0.5;0.625 1 0.4375;0.6875 1 0.375;0.75 1
0.3125;0.8125 1 0.25;0.875 1 0.1875;0.9375 1 0.125;1 1 0.0625;1 1 0;1 0.9375 0;1 0.875 0;1 0.8125 0;1 0.75
0;1 0.6875 0;1 0.625 0;1 0.5625 0;1 0.5 0;1 0.4375 0;1 0.375 0;1 0.3125 0;1 0.25 0;1 0.1875 0;1 0.125 0;1
0.0625 0;1 0 0;0.9375 0 0;0.875 0 0;0.8125 0 0;0.75 0 0;0.6875 0 0;0.625 0 0;0.5625 0 0],...
'DoubleBuffer','on',...
'IntegerHandle','off',...
'InvertHardcopy',get(0,'defaultfigureInvertHardcopy'),...
'MenuBar','none',...
'ToolBar','figure',...
'Name','Particles3',...
'NextPlot','replace',...
```

```
'NumberTitle','off',...
'PaperPosition',get(0,'defaultfigurePaperPosition'),...
'Position',[17.8 5.23076923076923 209 67.6153846153846],...
'Renderer','OpenGL',...
'RendererMode','manual',...
'WindowButtonDownFcn','dlview("down")',...
'WindowButtonUpFcn','dlview("up")',...
'CreateFcn','Particles3("figure1_CreateFcn",gcbo,[],guidata(gcbo))',...
'HandleVisibility','callback',...
'Tag','figure1',...
'UserData',[]);

setappdata(h1, 'GUIDEOptions',struct(...
'active_h', 141.000366210938, ...
'taginfo', struct(...
'figure', 2, ...
'axes', 3, ...
'slider', 3, ...
'pushbutton', 7, ...
'text', 6, ...
'edit', 4, ...
'radiobutton', 4, ...
'frame', 3), ...
'override', 1, ...
'release', 13, ...
'resize', 'simple', ...
'accessibility', 'callback', ...
'mfile', 1, ...
'callbacks', 1, ...
'singleton', 1, ...
'syscolorfig', 1, ...
'lastSavedFile', 'C:\MATLAB6p5\work\3dparticles\Particles3.m'));


h2 = axes(...
'Parent',h1,...
'View',[-37.5 30],...
'Box','on',...
'CameraPosition',[-4.47536790582704 -5.98402569409362 4.27491721763537],...
'CameraPositionMode',get(0,'defaultaxesCameraPositionMode'),...
'Color',[0 0 0],...
'ColorOrder',get(0,'defaultaxesColorOrder'),...
'DataAspectRatio',[1 1 0.8],...
'DataAspectRatioMode','manual',...
'DrawMode','fast',...
'GridLineStyle','--',...
'Position',[0.189473684210526 0.562002275312856 0.71866028708134 0.399317406143345],...
'XColor',[0.501960784313725 0.501960784313725 0.501960784313725],...
'XGrid','on',...
'XTick',[],...
'XTickMode','manual',...
'YColor',[0.501960784313725 0.501960784313725 0.501960784313725],...
'YGrid','on',...
'YTick',[],...
```

```
'YTickMode','manual',...
'ZColor',[0.501960784313725 0.501960784313725 0.501960784313725],...
'ZGrid','on',...
'ZTick',[],...
'ZTickMode','manual',...
'Tag','img1plot');


h3 = get(h2,'title');

set(h3,...
'Parent',h2,...
'Color',[0 0 0],...
'HorizontalAlignment','center',...
'Position',[0.292601242303295 0.238059871974735 1.5086149558603],...
'VerticalAlignment','bottom',...
'HandleVisibility','off');

h4 = get(h2,'xlabel');

set(h4,...
'Parent',h2,...
'Color',[0.501960784313725 0.501960784313725 0.501960784313725],...
'HorizontalAlignment','right',...
'Position',[0.0810430988934279 -0.838978817227471 0.14616899281302],...
'HandleVisibility','off');

h5 = get(h2,'ylabel');

set(h5,...
'Parent',h2,...
'Color',[0.501960784313725 0.501960784313725 0.501960784313725],...
'HorizontalAlignment','center',...
'Position',[-0.794096904613886 -0.151447703705669 0.163771653834303],...
'HandleVisibility','off');

h6 = get(h2,'zlabel');

set(h6,...
'Parent',h2,...
'Color',[0.501960784313725 0.501960784313725 0.501960784313725],...
'HorizontalAlignment','center',...
'Position',[-0.557043331997765 0.332777628167659 0.896042352319665],...
'Rotation',90,...
'VerticalAlignment','bottom',...
'HandleVisibility','off');

h7 = axes(...
'Parent',h1,...
'View',[-37.5 30],...
'Box','on',...
'CameraPosition',[-4.47536790582704 -5.98402569409362 4.27491721763537],...
'CameraPositionMode',get(0,'defaultaxesCameraPositionMode'),...
'Color',[0 0 0],...
```

```
'ColorOrder',get(0,'defaultaxesColorOrder'),...
'DataAspectRatio',[1 1 0.8],...
'DataAspectRatioMode','manual',...
'DrawMode','fast',...
'Position',[0.189473684210526 0.0705346985210466 0.71866028708134 0.399317406143345],...
'XColor',[0.501960784313725 0.501960784313725 0.501960784313725],...
'XTick',[],...
'XTickMode','manual',...
'YColor',[0.501960784313725 0.501960784313725 0.501960784313725],...
'YTick',[],...
'YTickMode','manual',...
'ZColor',[0.501960784313725 0.501960784313725 0.501960784313725],...
'ZTick',[],...
'ZTickMode','manual',...
'Tag','img2plot');


h8 = get(h7,'title');

set(h8,...
'Parent',h7,...
'Color',[0 0 0],...
'HorizontalAlignment','center',...
'Position',[0.292601242303296 0.238059871974735 1.5086149558603],...
'VerticalAlignment','bottom',...
'HandleVisibility','off');

h9 = get(h7,'xlabel');

set(h9,...
'Parent',h7,...
'Color',[0.501960784313725 0.501960784313725 0.501960784313725],...
'HorizontalAlignment','right',...
'Position',[0.0810430988934288 -0.838978817227471 0.14616899281302],...
'HandleVisibility','off');

h10 = get(h7,'ylabel');

set(h10,...
'Parent',h7,...
'Color',[0.501960784313725 0.501960784313725 0.501960784313725],...
'HorizontalAlignment','center',...
'Position',[-0.794096904613886 -0.151447703705669 0.163771653834303],...
'HandleVisibility','off');

h11 = get(h7,'zlabel');

set(h11,...
'Parent',h7,...
'Color',[0.501960784313725 0.501960784313725 0.501960784313725],...
'HorizontalAlignment','center',...
'Position',[-0.557043331997765 0.332777628167659 0.896042352319665],...
'Rotation',90,...
'VerticalAlignment','bottom',...
```

```
'HandleVisibility','off');

h12 = uicontrol(...
'Parent',h1,...
'Units','normalized',...
'CData',[],...
'ForegroundColor',[0 0 1],...
'ListboxTop',0,...
'Position',[0.0172248803827751 0.622298065984073 0.126315789473684 0.103526734926052],...
'String',{  '' },...
'Style','frame',...
'Tag','frame1',...
'UserData',[]);


h13 = uicontrol(...
'Parent',h1,...
'Units','normalized',...
'Callback','Particles3("slider1_Callback",gcbo,[],guidata(gcbo))',...
'ListboxTop',0,...
'Position',[0.286124401913876 0.517633674630262 0.62200956937799 0.0261660978384528],...
'String','slider1',...
'Style','slider',...
'SliderStep',[0.01 0.01],...
'TooltipString','move to adjust image1 threshold',...
'Tag','slider1');


h14 = uicontrol(...
'Parent',h1,...
'Units','normalized',...
'Callback','Particles3("slider2_Callback",gcbo,[],guidata(gcbo))',...
'ListboxTop',0,...
'Position',[0.286124401913876 0.0307167235494881 0.62200956937799 0.0261660978384528],...
'String',{  '' },...
'Style','slider',...
'SliderStep',[0.004 0.004],...
'TooltipString','move to adjust image2 threshold',...
'Tag','slider2');


h15 = uicontrol(...
'Parent',h1,...
'Units','normalized',...
'BackgroundColor',[0.501960784313725 0.501960784313725 0.501960784313725],...
'Callback','Particles3("pushbutton2_Callback",gcbo,[],guidata(gcbo))',...
'FontWeight','bold',...
'ForegroundColor',[0.901960784313726 0.901960784313726 0.901960784313726],...
'ListboxTop',0,...
'Position',[0.0172248803827751 0.569965870307167 0.126315789473684 0.0420932878270762],...
'String','Save and Run',...
'Tag','pushbutton2');
```

```
h16 = uicontrol(...
'Parent',h1,...
'Units','normalized',...
'BackgroundColor',[0.501960784313725 0.501960784313725 0.501960784313725],...
'Callback','Particles3("pushbutton3_Callback",gcbo,[],guidata(gcbo))',...
'FontWeight','bold',...
'ForegroundColor',[0.901960784313726 0.901960784313726 0.901960784313726],...
'ListboxTop',0,...
'Position',[0.0172248803827751 0.899886234357224 0.126315789473684 0.0420932878270762],...
'String','Load 3D Images',...
'Tag','pushbutton3');


h17 = uicontrol(...
'Parent',h1,...
'Units','normalized',...
'BackgroundColor',[1 1 1],...
'Callback','Particles3("edit1_Callback",gcbo,[],guidata(gcbo))',...
'ListboxTop',0,...
'Position',[0.190430622009569 0.517633674630262 0.0698564593301435 0.025028441410694],...
'String','0',...
'Style','edit',...
'Tag','edit1');


h18 = uicontrol(...
'Parent',h1,...
'Units','normalized',...
'BackgroundColor',[1 1 1],...
'Callback','Particles3("edit2_Callback",gcbo,[],guidata(gcbo))',...
'ListboxTop',0,...
'Position',[0.19043062200957 0.0352673492605233 0.0679425837320574 0.025028441410694],...
'String','0',...
'Style','edit',...
'Tag','edit2');


h19 = uicontrol(...
'Parent',h1,...
'Units','normalized',...
'BackgroundColor',[0.501960784313725 0.501960784313725 0.501960784313725],...
'Callback','Particles3("pushbutton4_Callback",gcbo,[],guidata(gcbo))',...
'FontWeight','bold',...
'ForegroundColor',[0.901960784313726 0.901960784313726 0.901960784313726],...
'ListboxTop',0,...
'Position',[0.0172248803827751 0.791808873720137 0.126315789473684 0.0420932878270762],...
'String','2D Projections',...
'Tag','pushbutton4');


h20 = uicontrol(...
'Parent',h1,...
'Units','normalized',...
'Callback','Particles3("radiobutton1_Callback",gcbo,[],guidata(gcbo))',...
```

```
'ListboxTop',0,...
'Position',[0.0258373205741627 0.667804323094426 0.109090909090909 0.0182025028441411],...
'String','Colocalization Only',...
'Style','radiobutton',...
'Value',1,...
'Tag','radiobutton1');


h21 = uicontrol(...
'Parent',h1,...
'Units','normalized',...
'Callback','Particles3("radiobutton2_Callback",gcbo,[],guidata(gcbo))',...
'ListboxTop',0,...
'Position',[0.0430622009569378 0.648464163822526 0.0755980861244019 0.0170648464163823],...
'String','All Image 1',...
'Style','radiobutton',...
'Tag','radiobutton2');


h22 = uicontrol(...
'Parent',h1,...
'Units','normalized',...
'Callback','Particles3("radiobutton3_Callback",gcbo,[],guidata(gcbo))',...
'ListboxTop',0,...
'Position',[0.0430622009569378 0.625711035267349 0.0755980861244019 0.0170648464163823],...
'String','All Image 2',...
'Style','radiobutton',...
'Tag','radiobutton3');


h23 = uicontrol(...
'Parent',h1,...
'Units','normalized',...
'FontWeight','bold',...
'ListboxTop',0,...
'Position',[0.0181818181818182 0.688282138794084 0.123444976076555 0.0182025028441411],...
'String','Colocalization Plots',...
'Style','text',...
'Tag','text4');


h24 = uicontrol(...
'Parent',h1,...
'Units','normalized',...
'BackgroundColor',[0.501960784313725 0.501960784313725 0.501960784313725],...
'Callback','Particles3("pushbutton5_Callback",gcbo,[],guidata(gcbo))',...
'FontWeight','bold',...
'ForegroundColor',[0.901960784313726 0.901960784313726 0.901960784313726],...
'ListboxTop',0,...
'Position',[0.0172248803827751 0.731513083048919 0.126315789473684 0.0420932878270762],...
'String','Reset Axes',...
'Tag','pushbutton5');
```

```
h25 = uicontrol(...
'Parent',h1,...
'Units','normalized',...
'ForegroundColor',[0 0 1],...
'ListboxTop',0,...
'Position',[0.0172248803827751 0.844141069397042 0.126315789473684 0.0500568828213879],...
'String',{  '' },...
'Style','frame',...
'Tag','frame2');


h26 = uicontrol(...
'Parent',h1,...
'Units','normalized',...
'FontWeight','bold',...
'ListboxTop',0,...
'Position',[0.0181818181818182 0.845278725824801 0.0861244019138756 0.037542662116041],...
'String',{  'Reducepatch'; 'Ratio' },...
'Style','text',...
'Tag','text5');


h27 = uicontrol(...
'Parent',h1,...
'Units','normalized',...
'BackgroundColor',[1 1 1],...
'Callback','Particles3("edit3_Callback",gcbo,[],guidata(gcbo))',...
'ListboxTop',0,...
'Position',[0.105263157894737 0.857792946530148 0.0239234449760766 0.0273037542662116],...
'String','1',...
'Style','edit',...
'Tag','edit3');



hsingleton = h1;


% --- Handles default GUIDE GUI creation and callback dispatch
function varargout = gui_mainfcn(gui_State, varargin)




gui_StateFields =  {'gui_Name'
                    'gui_Singleton'
                    'gui_OpeningFcn'
                    'gui_OutputFcn'
                    'gui_LayoutFcn'
                    'gui_Callback'};
gui_Mfile = '';
for i=1:length(gui_StateFields)
   if ~isfield(gui_State, gui_StateFields{i})
      error('Could not find field %s in the gui_State struct in GUI M-file %s', gui_StateFields{i}, gui_Mfile);
```

```
    elseif isequal(gui_StateFields{i}, 'gui_Name')
        gui_Mfile = [getfield(gui_State, gui_StateFields{i}), '.m'];
    end
end

numargin = length(varargin);

if numargin == 0
    % PARTICLES3
    % create the GUI
    gui_Create = 1;
elseif numargin > 3 & ischar(varargin{1}) & ishandle(varargin{2})
    % PARTICLES3('CALLBACK',hObject,eventData,handles,...)
    gui_Create = 0;
else
    % PARTICLES3(...)
    % create the GUI and hand varargin to the openingfcn
    gui_Create = 1;
end

if gui_Create == 0
    varargin{1} = gui_State.gui_Callback;
    if nargout
        [varargout{1:nargout}] = feval(varargin{:});
    else
        feval(varargin{:});
    end
else
    if gui_State.gui_Singleton
        gui_SingletonOpt = 'reuse';
    else
        gui_SingletonOpt = 'new';
    end

    % Open fig file with stored settings.  Note: This executes all component
    % specific CreateFunctions with an empty HANDLES structure.

    % Do feval on layout code in m-file if it exists
    if ~isempty(gui_State.gui_LayoutFcn)
        gui_hFigure = feval(gui_State.gui_LayoutFcn, gui_SingletonOpt);
    else
        gui_hFigure = local_openfig(gui_State.gui_Name, gui_SingletonOpt);
        % If the figure has InGUIInitialization it was not completely created
        % on the last pass.  Delete this handle and try again.
        if isappdata(gui_hFigure, 'InGUIInitialization')
            delete(gui_hFigure);
            gui_hFigure = local_openfig(gui_State.gui_Name, gui_SingletonOpt);
        end
    end

    % Set flag to indicate starting GUI initialization
    setappdata(gui_hFigure,'InGUIInitialization',1);

    % Fetch GUIDE Application options
```

```
gui_Options = getappdata(gui_hFigure,'GUIDEOptions');

if ~isappdata(gui_hFigure,'GUIOnScreen')
   % Adjust background color
   if gui_Options.syscolorfig
      set(gui_hFigure,'Color', get(0,'DefaultUicontrolBackgroundColor'));
   end

   % Generate HANDLES structure and store with GUIDATA
   guidata(gui_hFigure, guihandles(gui_hFigure));
end

% If user specified 'Visible','off' in p/v pairs, don't make the figure
% visible.
gui_MakeVisible = 1;
for ind=1:2:length(varargin)
   if length(varargin) == ind
      break;
   end
   len1 = min(length('visible'),length(varargin{ind}));
   len2 = min(length('off'),length(varargin{ind+1}));
   if ischar(varargin{ind}) & ischar(varargin{ind+1}) & ...
         strncmpi(varargin{ind},'visible',len1) & len2 > 1
      if strncmpi(varargin{ind+1},'off',len2)
         gui_MakeVisible = 0;
      elseif strncmpi(varargin{ind+1},'on',len2)
         gui_MakeVisible = 1;
      end
   end
end

% Check for figure param value pairs
for index=1:2:length(varargin)
   if length(varargin) == index
      break;
   end
   try, set(gui_hFigure, varargin{index}, varargin{index+1}), catch, break, end
end

% If handle visibility is set to 'callback', turn it on until finished
% with OpeningFcn
gui_HandleVisibility = get(gui_hFigure,'HandleVisibility');
if strcmp(gui_HandleVisibility, 'callback')
   set(gui_hFigure,'HandleVisibility', 'on');
end

feval(gui_State.gui_OpeningFcn, gui_hFigure, [], guidata(gui_hFigure), varargin{:});

if ishandle(gui_hFigure)
   % Update handle visibility
   set(gui_hFigure,'HandleVisibility', gui_HandleVisibility);

   % Make figure visible
   if gui_MakeVisible
```

```
            set(gui_hFigure, 'Visible', 'on')
            if gui_Options.singleton
               setappdata(gui_hFigure,'GUIOnScreen', 1);
            end
         end

         % Done with GUI initialization
         rmappdata(gui_hFigure,'InGUIInitialization');
      end

      % If handle visibility is set to 'callback', turn it on until finished with
      % OutputFcn
      if ishandle(gui_hFigure)
         gui_HandleVisibility = get(gui_hFigure,'HandleVisibility');
         if strcmp(gui_HandleVisibility, 'callback')
            set(gui_hFigure,'HandleVisibility', 'on');
         end
         gui_Handles = guidata(gui_hFigure);
      else
         gui_Handles = [];
      end

      if nargout
         [varargout{1:nargout}] = feval(gui_State.gui_OutputFcn, gui_hFigure, [], gui_Handles);
      else
         feval(gui_State.gui_OutputFcn, gui_hFigure, [], gui_Handles);
      end

      if ishandle(gui_hFigure)
         set(gui_hFigure,'HandleVisibility', gui_HandleVisibility);
      end
   end

   function gui_hFigure = local_openfig(name, singleton)
   try
      gui_hFigure = openfig(name, singleton, 'auto');
   catch
      % OPENFIG did not accept 3rd input argument until R13,
      % toggle default figure visible to prevent the figure
      % from showing up too soon.
      gui_OldDefaultVisible = get(0,'defaultFigureVisible');
      set(0,'defaultFigureVisible','off');
      gui_hFigure = openfig(name, singleton);
      set(0,'defaultFigureVisible',gui_OldDefaultVisible);
   end
```

```
function [img1,img2,img1sum,img2sum,r,c,z] = getstacks;
% GETSTACKS User interface for interactively loading 3D image stacks into
% the MATALAB workspace
%
% [img1,img2,img1sum,img2sum,r,c,z] = getstacks;
%
% Calling GETSTACKS with all the output arguments will generate 7 variables
% in the MATLAB workspace: the two images (img1 and img2), 2D projections
% of each image (img1sum, img2sum), and the coordinate dimensions of the
% images (r,c,z).  By default, the script only opens TIFF images, but any
% image type supported by MATLAB will work.  You can simply delete the
% '*.tif' option call from lines 19 and 38, and MATLAB should be able to
% determine all supported image types.
%
% NOTE that the function converts the images into DOUBLE format, even if
% the original data are only 8-bit.
%
% See Also UIGETFILE, IMREAD, IM2DOUBLE, IMFINFO

% Load First Image Stack

[stack1,direct1] = uigetfile('*.tif', 'Select First Stack');
cd (direct1)
info1 = imfinfo (stack1);
r1 = max([info1.Height]);
c1 = max([info1.Width]);
stacksize1 = length([info1.FileSize]);
img1 = zeros (r1,c1,stacksize1);

for i = 1:stacksize1;
   [img1(:,:,i)] = flipud(im2double(imread(stack1,i)));
end

img1sum = sum(img1,3);

% define image dimensions
[r c z] = size (img1);
clear i;

% Load Second Image Stack
[stack2,direct2] = uigetfile('*.tif', 'Select Second Stack');
cd (direct2)
info2 = imfinfo (stack2);
r2 = max([info2.Height]);
c2 = max([info2.Width]);
stacksize2 = length([info2.FileSize]);
img2 = zeros (r2,c2,stacksize2);

for i = 1:stacksize2;
   [img2(:,:,i)] = flipud(im2double(imread(stack2,i)));
end

img2sum = sum(img2,3);
```

```
function dlview(inp)
persistent last_pt

switch inp
	case 'on'
		last_pt = [];
		set(gcf, 'windowbuttondownfcn', 'dlview("down")')
		set(gcf, 'windowbuttonupfcn',  'dlview("up")')
		set(gcf, 'windowbuttonmotionfcn', '')
	case 'off'
		set(gcf, 'windowbuttondownfcn', '');
		set(gcf, 'windowbuttonupfcn',  '');
		set(gcf, 'windowbuttonmotionfcn', '');
	case 'down'
		set(gcf, 'windowbuttonmotionfcn', 'dlview("motion")');
		last_pt = get_pixel_pt(gcf);
	case 'up'
		set(gcf, 'windowbuttonmotionfcn', '');
		last_pt = [];
	case 'motion'
		new_pt = get_pixel_pt(gcf);
		d = new_pt - last_pt;
		last_pt = new_pt;
		switch lower(get(gcf,'SelectionType'))
			case 'normal'
				camorbit(-d(1), -d(2), 'camera')
			case 'alt'
				q = max(-.9, min(.9, sum(d)/70));
				camzoom(1+q);
			case 'extend'
				pan_d = d*camva(gca)/500;
				campan(-pan_d(1), -pan_d(2), 'camera');
			otherwise
		end
end

function pt = get_pixel_pt(figh)
p_units = get(figh, 'Units');
set(figh, 'Units', 'Pixels');
pt = get(figh, 'CurrentPoint');
pt = pt(1,1:2);
set(figh, 'Units', p_units);
```

```
function h = timebar(message,name,update_rate)

% TIMEBAR Progress bar with estimated time remaining
%   H = TIMEBAR('message','name') creates and displays a progress
%   bar with alphanumeric progress percentage and estimated time
%   time remaining.  A user input message ('message') is displayed,
%   typically to distinguish what process is being monitored, and
%   'name' is an optional figure name.  The figure handle H is
%   returned.
%
%   TIMEBAR(H,X) will update the length of the progress bar, the
%   percentage complete, and the estimated time remaining, where
%   X is a fractional progress between 0 (initial) and 1 (complete).
%   (Note that the order of H,X is opposite to waitbar.)
%
%   TIMEBAR(H,X,RATE) will update the progress bar and information
%   at a rate given by RATE in seconds.  Default is 0.1 seconds.
%
%   The estimated time remaining is linear using the initial time
%   (when TIMEBAR is first opened), the current time, and the percent
%   complete.
%
%   TIMEBAR is typically used inside a FOR loop or during numerical
%   simulation.  A sample for loop is shown below:
%
%     h = timebar('Loop counter','Progress')
%     for i = 1:100
%       % computation here %
%       timebar(h,1/100)
%     end
%     close(h)
%
%   A sample for numerical integration is shown below:
%
%     % script file
%     t0 = 0;
%     tf = 60;
%     h = timebar('Simulation integration','Progress')
%     [tt,xx] = ode45('states.m',[t0 tf],initial_conditions);
%     close(h)
%
%     % states.m
%     function xdot = states(t,x)
%     xdot(1) = ...;
%     xdot(2) = ...;
%     ...
%     timebar(h,(t-t0)/(tf-t0))
%
%   Version: 2.0
%   Version History:
%   1.0   2002-01-18   Initial release
%   2.0   2002-01-21   Added update rate option
%
%   Copyright 2002, Chad English
```

```
%    cenglish@myrealbox.com

if nargin < 3                                   % If update rate is not input
   update_rate = 0.1;                           %    set it to 0.1 seconds
end

if ~ishandle(message)                           % If first input is not a timebar handle,
                                                %    treat as new timebar

   % SET WINDOW SIZE AND POSITION
   winwidth = 300;                              % Width of timebar window
   winheight = 75;                              % Height of timebar window
   screensize = get(0,'screensize');            % User's screen size [1 1 width height]
   screenwidth = screensize(3);                 % User's screen width
   screenheight = screensize(4);                % User's screen height
   winpos = [0.5*(screenwidth-winwidth), ...
     0.5*(screenheight-winheight), winwidth, winheight];  % Position of timebar window origin

   % END SET WINDOW SIZE AND POSITION

   % OPEN FIGURE AND SET PROPERTIES
   if nargin < 2
      name = '';                                % If timebar name not input, set blank
   end

   wincolor = 0.75*[1 1 1];                     % Define window color
   est_text = 'Estimated time remaining: ';     % Set static estimated time text

   h = figure('menubar','none',...              % Turn figure menu display off
      'numbertitle','off',...                   % Turn figure numbering off
      'name',name,...                           % Set the figure name to input name
      'position',winpos,...                     % Set the position of the figure as above
      'color',wincolor,...                      % Set the figure color
      'resize','off',...                        % Turn of figure resizing
      'tag','timebar');                         % Tag the figure for later checking

   userdata.text(1) = uicontrol(h,'style','text',...   % Prepare message text (set the style to text)
      'pos',[10 winheight-30 winwidth-20 20],...       % Set the textbox position and size
      'hor','center',...                        % Center the text in the textbox
      'backgroundcolor',wincolor,...            % Set the textbox background color
      'foregroundcolor',0*[1 1 1],...           % Set the text color
      'string',message);                        % Set the text to the input message

   userdata.text(2) = uicontrol(h,'style','text',...   % Prepare static estimated time text
      'pos',[10 5 winwidth-20 20],...           % Set the textbox position and size
      'hor','left',...                          % Left align the text in the textbox
      'backgroundcolor',wincolor,...            % Set the textbox background color
      'foregroundcolor',0*[1 1 1],...           % Set the text color
      'string',est_text);                       % Set the static text for estimated time

   userdata.text(3) = uicontrol(h,'style','text',...   % Prepare estimated time
      'pos',[135 5 winwidth-145 20],...         % Set the textbox position and size
      'hor','left',...                          % Left align the text in the textbox
      'backgroundcolor',wincolor,...            % Set the textbox background color
```

```
    'foregroundcolor',0*[1 1 1],...                % Set the text color
    'string','');                                  % Initialize the estimated time as blank

  userdata.text(4) = uicontrol(h,'style','text',...  % Prepare the percentage progress
    'pos',[winwidth-35 winheight-50 25 20],...     % Set the textbox position and size
    'hor','right',...                              % Left align the text in the textbox
    'backgroundcolor',wincolor,...                 % Set the textbox background color
    'foregroundcolor',0*[1 1 1],...                % Set the textbox foreground color
    'string','');                                  % Initialize the progress text as blank

  userdata.axes = axes('parent',h,...              % Set the progress bar parent to the figure
    'units','pixels',...                           % Provide axes units in pixels
    'pos',[10 winheight-45 winwidth-50 15],...     % Set the progress bar position and size
    'xlim',[0 1],...                               % Set the range from 0 to 1
    'box','on',...                                 % Turn on axes box (to see where 100% is)
    'color',[1 1 1],...                            % Set plot background color to white
    'xtick',[],'ytick',[]);                        % Turn off axes tick marks and labels

  userdata.bar = patch([0 0 0 0 0],[0 1 1 1 0 0],'r');  % Initialize progress bar to zero area
  userdata.time = clock;                           % Record the current time
  userdata.inc = clock;                            % Set incremental clock to current time
  set(h, 'userdata', userdata)                     % Allow access to the text and axes settings
                                                   %    by including them with the timebar data
  % END OPEN FIGURE AND SET PROPERTIES

else                                               % If first input is a timebar handle, update
                                                   %    the window
  % GET HANDLE AND PROGRESS
  pause(10e-100)                                   % Message, bar, and static text won't display
                                                   %    without arbitrary pause (don't know why)
  h = message;                                     % Set handle to first input
  progress = name;                                 % Set progress to second input

  if ~strcmp(get(h,'tag'), 'timebar')              % Check object tag to see if it is a timebar
    error('Handle is not to a timebar window')     % If not a timebar, report error and stop
  end
  % END GET HANGLE AND PROGRESS

  % CALCULATE ESTIMATED TIME REMAINING
  userdata = get(h,'userdata');                    % Get the userdata included with the timebar
  inc = clock-userdata.inc;                        % Calculate time increment since last update
  inc_secs = inc(3)*3600*24 + inc(4)*3600 + ...
    inc(5)*60 + inc(6);                            % Convert the increment to seconds

  if [inc_secs > update_rate] | [progress == 1]    % Only update at update rate or 100% complete
    userdata.inc = clock;                          % If updating, reset the increment clock
    set(h,'userdata',userdata)                     % Update userdata with the new clock setting
    tpast = clock-userdata.time;                   % Calculate time since timebar initialized
    seconds_past = tpast(3)*3600*24 + tpast(4)*3600 + ...
      tpast(5)*60 + tpast(6);                      % Transform passed time into seconds
    estimated_seconds = seconds_past*(1/progress-1);  % Estimate the time remaining in seconds
    hours = floor(estimated_seconds/3600);         % Calculate integer hours of estimated time
    minutes = floor((estimated_seconds-3600*hours)/60); % Calculate integer minutes of estimated time
    seconds = floor(estimated_seconds-3600*hours- ...
```

```
      60*minutes);                                % Calculate integer seconds of estimated time
    tenths = floor(10*(estimated_seconds - ...
      floor(estimated_seconds)));                 % Calculate tenths of seconds (as integer)
    % END CALCULATE ESTIMATED TIME REMAINING

    % UPDATE ESTIMATED TIME AND PROGRESS TO TIMEBAR
    if progress > 1                               % Check if input progress is > 1
      time_message = ' Error!  Progress > 1!';    % If >1, print error to estimated time
      time_color = 'r';                           %    in red
    else
      if hours < 10; h0 = '0'; else h0 = '';end   % Put leading zero on hours if < 10
      if minutes < 10; m0 = '0'; else m0 = '';end % Put leading zero on minutes if < 10
      if seconds < 10; s0 = '0'; else s0 = '';end % Put leading zero on seconds if < 10
      time_message = strcat(h0,num2str(hours),':',m0,...
        num2str(minutes),':',s0,num2str(seconds),...
        '.',num2str(tenths),' (hh:mm:ss.t)');     % Format estimated time as hh:mm:ss.t
      time_color = 'k';                           % Format estimated time text as black
    end

    set(userdata.bar,'xdata',[0 0 progress progress 0]) % Update progress bar
    set(userdata.text(3),'string',time_message,...
      'foregroundcolor',time_color);              % Update estimated time
    set(userdata.text(4),'string',...
      strcat(num2str(floor(100*progress)),'%'));  % Update progress percentage
  end
  % END UPDATE ESTIMATED TIME AND PROGRESS TO TIMEBAR
end

% TIMEBAR HANDLE
if nargout == 0                                   % If handle not asked for
  clear h                                         %    do not output it
end
% END TIMEBAR HANDLE
```

*Appendix B*

## MATLAB Code for 2-D Correlation Analysis:

The function for normalized 2-D correlation is included below. The output variables are identified by comments in the code. Three dependent functions, rnda, rndb, and fastxcor2 which randomize the particles for each image, and calculate the correlation, are included at the end of this code. This script also requires the 'timebar' function included in Appendix A.

```
function [NcorDat, NcorRnd, coloc] = xc2d

% 2DXcorr script for calculating normalized
% 2D correlation between two images.  The output
% variables are defined as:
%
% NcorDat: normalized correlation between images (a) and (b), computed as
%
% NcorDat = (corwin-meanrndcor)/corNNwin
%
% where corwin is the raw 2D correlation in a defined lag window,
% meanrndcorr is the mean of 1024 correlations generated from random
% versions of the real image data, and corNNwin is the autocorrelation
% of the image with the greatest amount of signal.  For example,
% if length(find(a)) > length(find(b)), corNNwin == coraawin.
%
%
% NcorRnd: normalized 95th percentile correlation from randomized data.
%
% coloc: colocalization value, determined as the zero-lag correlation,
% divided by the autocorrelation of the image with the greatest amount
% of signal.
%
% note that, by default, these are the only three output variables
% generated by this function.  If desired, all the output data will
% remain in the workspace by simply comenting out the 'function' line
% above and running the routine as a script.
%
% Last modified by W. Bryan Smith, Caltech, March 28, 2004.

[a1,direct1] = uigetfile('*.tif', 'Select First Image');
cd (direct1)
info1 = imfinfo (a1);
r = max([info1.Height]);
c = max([info1.Width]);
a = zeros (r,c);
a = flipud(im2double(imread(a1)));

[b1,direct2] = uigetfile('*.tif', 'Select Second Image');
cd (direct2)
```

```
info2 = imfinfo (b1);
b = zeros (r,c);
b = flipud(im2double(imread(b1)));

abw = im2bw(a, graythresh(a));
bbw = im2bw(b, graythresh(b));

% Compute real data cross-correlation
cor = fastxcor2(a,b);
[szcory,szcorx] = size(cor);

% Find properties of data particles
alabel = bwlabeln (abw,8);
blabel = bwlabeln (bbw,8);
aprops = regionprops (alabel, 'Area', 'Centroid', 'MajorAxisLength', 'MinorAxisLength');
bprops = regionprops (blabel, 'Area', 'Centroid', 'MajorAxisLength', 'MinorAxisLength');

clear *label

%% Extract properties of image 'a' particles
aarea = mean ([aprops(find([aprops.Area]>2)).Area]);
aep = std([aprops.MajorAxisLength])/2;
acentr = [aprops.Centroid];
acentrx = mean(acentr(find(diff(acentr(1:2:length(acentr)-1))  >= aep )));
amajor = round(mean([aprops.MajorAxisLength]));
aminor = round(mean([aprops.MinorAxisLength]));

%% Extract properties of image 'b' particles
barea = mean ([bprops(find([bprops.Area]>2)).Area]);
bep = std([bprops.MajorAxisLength])/2;
bcentr = [bprops.Centroid];
bcentrx = mean(bcentr(find(diff(bcentr(1:2:length(bcentr)-1))  >= bep )));
bmajor = round(mean([bprops.MajorAxisLength]));
bminor = round(mean([bprops.MinorAxisLength]));

clear m n i *props


if aminor > bminor
   winy = aminor;
elseif aminor < bminor
   winy = bminor;
else aminor = bminor
   winy = aminor;
end
if amajor > bmajor
   winx = bmajor;
elseif amajor < bmajor
   winx = amajor;
else amajor = bmajor
   winx = amajor;
end
```

```
%% Define limit of x-lag for peak search
%% based on the max mean distance between data particles
if acentrx == bcentrx
   xlim = acentrx;
elseif acentrx < bcentrx
   xlim = bcentrx;
else acentrx > bcentrx
   xlim = acentrx;
end

% Make xlim smaller, based on half the major axis length
% of the largest particle set because we used centroids
% to calculate the distance between particles
xlim = round ((xlim/2) - (0.5*winx));

% Randomize particles in each image 32 times
h = timebar('Generating Randomized Images','Progress');
rnda = zeros(r,c,32);
rndb = zeros(r,c,32);
for i = 1:32
   rnda(:,:,i) = rnda2(a);
   rndb(:,:,i) = rndb2(b);
   timebar(h,i/32);
end
close (h);

% Compute 1024 random cross-correlations
rndcor = zeros(szcory,(2*xlim)+1,1024);
h = timebar('Computing Random Correlations','Progress');
i = 0;
for n = 1:32
   for m = 1:32
      i = i+1;
      randcor = fastxcor2(rnda(:,:,n),rndb(:,:,m));
      rndcor(:,:,i) = randcor(:,c-xlim:c+xlim);
      timebar(h,i/1024);
   end
end
close(h);

% compute mean of random correlations,
meanrnd = mean(rndcor,3);

% Find 95th percentile random correlation
sumrnds = squeeze(sum(sum(rndcor)));
[sumrnds, sortidx] = sort(sumrnds);
rndcor95 = (rndcor(:,:,find(sortidx == 973)))-meanrnd;

% calculate normalized correlation window
corlim = cor(:,c-xlim:c+xlim);
corwin = corlim-meanrnd;
[szcorwiny,szcorwinx] = size(corwin);

filla = length(find(abw))/(r*c);
```

```
fillb = length(find(bbw))/(r*c);

%% Compute Properties of Autocorrelation of image a
coraa = fastxcor2(abw,abw);
coraawin = [coraa(:,c-xlim:c+xlim)] - meanrnd;
coraaPwin = coraawin(floor(r-(0.5*(winy))):ceil(r+(0.5*(winy))),...
   (floor(0.5*(szcorwinx-winx)):ceil(0.5*(szcorwinx+winx))));
coraamax = sum(sum(coraaPwin));

%% Compute Properties of Autocorrelation of image b
corbb = fastxcor2(bbw,bbw);
corbbwin = [corbb(:,c-xlim:c+xlim)] - meanrnd;
corbbPwin = corbbwin(floor(r-(0.5*(winy))):ceil(r+(0.5*(winy))),...
   (floor(0.5*(szcorwinx-winx)):ceil(0.5*(szcorwinx+winx))));
corbbmax = sum(sum(corbbwin));

%% Compute Properties of Peaks p1 and p2

% Find peak at -ylag
p1 = max(max(corwin(1:r,:)));
p1r = max(max(rndcor95(1:r,:)));
% Find peak at +ylag
p2 = max(max(corwin((r+1):szcorwiny,:)));
p2r = max(max(rndcor95((r+1):szcorwiny,:)));

[p1y,p1x] = find (corwin(1:r,:) == p1);
[p1ry,p1rx] = find(rndcor95(1:r,:) == p1r);
[p2y,p2x] = find (corwin((r+1):szcorwiny,:) == p2);
[p2ry,p2rx] = find (rndcor95((r+1):szcorwiny,:) == p2r);
p2y = p2y + r;
p2ry = p2ry +r;

if (p1x-(round(0.5*(winx)))) < 0;
   p1win = corwin((p1y-(round(0.5*(winy))):p1y+(round(0.5*(winy)))),...
      (1:p1x+(round(0.5*(winx)))));
elseif (p1x+(round(0.5*(winx)))) > szcorwinx;
   p1win = corwin((p1y-(round(0.5*(winy))):p1y+(round(0.5*(winy)))),...
      (p1x-(round(0.5*(winx))):(szcorwinx)));
else (p1x-(round(0.5*(winx)))) >= 0;
   if (p1x-(round(0.5*(winx)))) == 0
      p1win = corwin((p1y-(round(0.5*(winy))):p1y+(round(0.5*(winy)))),...
         (1+(p1x-(round(0.5*(winx)))):p1x+(round(0.5*(winx)))));
   elseif (p1x-(round(0.5*(winx)))) > 0
      p1win = corwin((p1y-(round(0.5*(winy))):p1y+(round(0.5*(winy)))),...
         (p1x-(round(0.5*(winx))):p1x+(round(0.5*(winx)))));
   end
end

if (p1rx-(round(0.5*(winx)))) < 0;
   p1rwin = corwin((p1ry-(round(0.5*(winy))):p1ry+(round(0.5*(winy)))),...
      (1:p1rx+(round(0.5*(winx)))));
elseif (p1rx+(round(0.5*(winx)))) > szcorwinx;
   p1rwin = corwin((p1ry-(round(0.5*(winy))):p1ry+(round(0.5*(winy)))),...
      (p1rx-(round(0.5*(winx))):(szcorwinx)));
```

```
else (p1rx-(round(0.5*(winx)))) >= 0;
   if (p1rx-(round(0.5*(winx)))) == 0
      p1rwin = corwin((p1ry-(round(0.5*(winy))):p1ry+(round(0.5*(winy)))),...
         (1+(p1rx-(round(0.5*(winx)))):p1rx+(round(0.5*(winx))));
   elseif (p1rx-(round(0.5*(winx)))) > 0
      p1rwin = corwin((p1ry-(round(0.5*(winy))):p1ry+(round(0.5*(winy)))),...
         (p1rx-(round(0.5*(winx))):p1rx+(round(0.5*(winx))));
   end
end

if (p2x-(round(0.5*(winx)))) < 0;
   p2win = corwin((p2y-(round(0.5*(winy))):p2y+(round(0.5*(winy)))),...
      (1:p2x+(round(0.5*(winx))));
elseif (p2x+(round(0.5*(winx)))) > szcorwinx;
   p2win = corwin((p2y-(round(0.5*(winy))):p2y+(round(0.5*(winy)))),...
      (p2x-(round(0.5*(winx))):(szcorwinx));
else (p2x-(round(0.5*(winx)))) >= 0;
   if (p2x-(round(0.5*(winx)))) == 0
      p2win = corwin((p2y-(round(0.5*(winy))):p2y+(round(0.5*(winy)))),...
         (1+(p2x-(round(0.5*(winx)))):p2x+(round(0.5*(winx))));
   elseif (p2x-(round(0.5*(winx)))) > 0
      p2win = corwin((p2y-(round(0.5*(winy))):p2y+(round(0.5*(winy)))),...
         (p2x-(round(0.5*(winx))):p2x+(round(0.5*(winx))));
   end
end

if (p2rx-(round(0.5*(winx)))) < 0;
   p2rwin = corwin((p2ry-(round(0.5*(winy))):p2ry+(round(0.5*(winy)))),...
      (1:p2rx+(round(0.5*(winx))));
elseif (p2rx+(round(0.5*(winx)))) > szcorwinx;
   p2rwin = corwin((p2ry-(round(0.5*(winy))):p2ry+(round(0.5*(winy)))),...
      (p2rx-(round(0.5*(winx))):(szcorwinx));
else (p2rx-(round(0.5*(winx)))) >= 0;
   if (p2rx-(round(0.5*(winx)))) == 0
      p2rwin = corwin((p2ry-(round(0.5*(winy))):p2ry+(round(0.5*(winy)))),...
         (1+(p2rx-(round(0.5*(winx)))):p2rx+(round(0.5*(winx))));
   elseif (p2rx-(round(0.5*(winx)))) > 0
      p2rwin = corwin((p2ry-(round(0.5*(winy))):p2ry+(round(0.5*(winy)))),...
         (p2rx-(round(0.5*(winx))):p2rx+(round(0.5*(winx))));
   end
end


% Integrate +/- ylag peaks
% Add them together to get the total correlation
p1sum = sum(sum(p1win));
p1rsum = sum(sum(p1rwin));

p2sum = sum(sum(p2win));
p2rsum = sum(sum(p2rwin));

corsum = p1sum+p2sum;
corsumr = p1rsum+p2rsum;
```

```
if filla == fillb
   cormax = max(max(coraa));
   NcorDat = corsum/coraamax;
   NcorRnd = corsumr/coraamax;
elseif filla > fillb;
   cormax = max(max(coraa));
   NcorDat = corsum/coraamax;
   NcorRnd = corsumr/coraamax;
else fillb > filla;
   cormax = max(max(corbb));
   NcorDat = corsum/corbbmax;
   NcorRnd = corsumr/corbbmax;
end
disp('Normalized corr score = '), disp(NcorDat)
disp('95th percentile randcor score = '), disp(NcorRnd)

% Express Colocalization as fraction of overlapping pixels
coloc = (max(cor(r,c)))/cormax;


% Plot the data
cmin = 0;
cmax = max(max(corwin));
r2 = 2^nextpow2(r);
c2 = 2^nextpow2(c);
subplot (411), imagesc (a),axis image, title(a1(1:length(a1)-4),'fontname','Times New Roman',...
   'fontsize',14,'VerticalAlignment','baseline');
subplot (412), imagesc (b),axis image, title(b1(1:length(b1)-4),'fontname','Times New Roman',...
   'fontsize',14,'VerticalAlignment','baseline');
subplot (413), imagesc (cor), set(gca,'XTickLabel',{'X0','c2'}), set(gca,'XTick',c2),...
   set(gca,'YTickLabel',{'Y0','r2'}), set(gca,'YTick',r2), caxis([cmin cmax]),axis tight,...
   title('cor','fontname','Times New Roman','fontsize',14,'VerticalAlignment','baseline');
subplot (414), imagesc (corwin),axis square,...
   set(gca,'XTick',[]),...
   set(gca,'YTickLabel',{'Y0','r2'}), set(gca,'YTick',r2),caxis([cmin cmax]),...
   title('corwin','fontname','Times New Roman','fontsize',14,'VerticalAlignment','baseline');
   text(p2x,p2y,'p2','color','white','FontSize',12,'HorizontalAlignment','center','fontname','Times New Roman');
   text(p1x,p1y,'p1','color','white','FontSize',12,'HorizontalAlignment','center','fontname','Times New Roman');
colorbar('horiz');

figure, subplot (221), surf (p1win), zlim([min(min(p1win)),max(max(corwin))]), caxis([cmin cmax]),...
   title('p1win','fontname','Times New Roman','fontsize',14);
subplot (222), surf (p2win), zlim([min(min(p2win)),max(max(corwin))]), caxis([cmin cmax]),...
   title('p2win','fontname','Times New Roman','fontsize',14);
subplot (223), contourf (p1win),caxis([cmin cmax]), colorbar('horiz'), axis image;
subplot (224), contourf (p2win),caxis([cmin cmax]), colorbar('horiz'), axis image;

% % clear s* w* xlim fill* h i* p1x p1y p2x p2y d* f* coraa corbb ans c c2 cmax cmin m n r r2
% % clear aarea acentr acentrx aep amajor aminor barea bcentr bcentrx bep bmajor bminor
```

```
function rnda = rnda2(a)
rand ('state',sum(100*clock));
rnda = zeros(size(a));
abw = im2bw(a,graythresh(a));
[albl,aobj] = bwlabeln (abw,8);

for objnum = 1:aobj
   [r,c]=find(albl==objnum);
   validated = 0;
   while validated == 0
      newloc = ([ceil(rand*size(abw,1)), ceil(rand*size(abw,2))]);
      rshift = newloc(1) - r(1);
      cshift = newloc(2) - c(1);
      newrows = r + rshift;
      newcols = c + cshift;
      if ~isempty(find(newrows < 1))
         newrows = newrows - min(newrows) + 1;
      end
      if ~isempty(find(newcols < 1))
         newcols = newcols - min(newcols) + 1;
      end
      if ~isempty(find(newrows > size(abw,1)))
         newrows = newrows-(max(newrows)-size(abw,1));
      end
      if ~isempty(find(newcols > size(abw,2)))
         newcols = newcols-(max(newcols)-size(abw,2));
      end
      val = [];
      for pix = 1:length(r)
         val = [val rnda(newrows(pix),newcols(pix))];
         if rnda(newrows(pix),newcols(pix))~=0
            break
         end
      end
      if length(find(val)) == 0
         validated = 1;
      end
   end
   for pix = 1:length(r)
      rnda(newrows(pix),newcols(pix)) = abw(r(pix),c(pix));
   end
end
```

```
function rndb = rndb2(b)
rand ('state',sum(100*clock));
rndb = zeros(size(b));
bbw= im2bw(b,graythresh(b));
[blbl,bobj] = bwlabeln (bbw,8);

for objnum = 1:bobj
   [r,c]=find(blbl==objnum);
   validated = 0;
   while validated == 0
      newloc = ([ceil(rand*size(bbw,1)), ceil(rand*size(bbw,2))]);
      rshift = newloc(1) - r(1);
      cshift = newloc(2) - c(1);
      newrows = r + rshift;
      newcols = c + cshift;
      if ~isempty(find(newrows < 1))
         newrows = newrows - min(newrows) + 1;
      end
      if ~isempty(find(newcols < 1))
         newcols = newcols - min(newcols) + 1;
      end
      if ~isempty(find(newrows > size(bbw,1)))
         newrows = newrows-(max(newrows)-size(bbw,1));
      end
      if ~isempty(find(newcols > size(bbw,2)))
         newcols = newcols-(max(newcols)-size(bbw,2));
      end
      val = [];
      for pix = 1:length(r)
         val = [val rndb(newrows(pix),newcols(pix))];
         if rndb(newrows(pix),newcols(pix))~=0
            break
         end
      end
      if length(find(val)) == 0
         validated = 1;
      end
   end
   for pix = 1:length(r)
      rndb(newrows(pix),newcols(pix)) = bbw(r(pix),c(pix));
   end
end


function cor = fastxcor2(a,b);

T_size = size(a);
A_size = size(b);
outsize = A_size + T_size - 1;
outsize = [2^nextpow2(outsize(1)),2^nextpow2(outsize(2))];
Fa = fft2(rot90(a,2),outsize(1),outsize(2));
Fb = fft2(b, outsize(1),outsize(2));
cor = real(ifft2(Fa .* Fb));
```

*Appendix C*

# Reprints of Published Articles

Neuron, Vol. 30, 489–502, May, 2001, Copyright ©2001 by Cell Press

# Dynamic Visualization of Local Protein Synthesis in Hippocampal Neurons

**Girish Aakalu,[2] W. Bryan Smith,[2] Nhien Nguyen, Changan Jiang, and Erin M. Schuman[1]**
Caltech
Howard Hughes Medical Institute
Division of Biology 216-76
Pasadena, California 91125

## Summary

**Using pharmacological approaches, several recent studies suggest that local protein synthesis is required for synaptic plasticity. Convincing demonstrations of bona fide dendritic protein synthesis in mammalian neurons are rare, however. We developed a protein synthesis reporter in which the coding sequence of green fluorescent protein is flanked by the 5′ and 3′ untranslated regions from CAMKII-α, conferring both dendritic mRNA localization and translational regulation. In cultured hippocampal neurons, we show that BDNF, a growth factor involved in synaptic plasticity, stimulates protein synthesis of the reporter in intact, mechanically, or "optically" isolated dendrites. The stimulation of protein synthesis is blocked by anisomycin and not observed in untreated neurons. In addition, dendrites appear to possess translational hot spots, regions near synapses where protein synthesis consistently occurs over time.**

## Introduction

The discovery that polyribosomes are located near the base of many spines (Steward and Levy, 1982) in the hippocampus suggested the possibility that neuronal proteins can be synthesized in dendrites. In theory, the synthesis of proteins in dendrites provides a mechanism by which synapses can independently control their strength, circumventing the need for precisely addressed protein transport from the soma (Schuman, 1999a). In the context of synaptic plasticity, then, the ability to locally synthesize proteins allows synapses to solve the problem of maintaining "specificity" *and* obtaining the newly synthesized proteins required for long-term synaptic plasticity (Frey et al., 1988; Kang et al., 1997; Nguyen et al., 1994; Otani et al., 1989; Stanton and Sarvey, 1984).

In the past 5 years, several studies have shown that locally synthesized proteins likely contribute to long-lasting synaptic plasticity (reviewed in Schuman, 1999a; Steward and Schuman, 2001; Wells et al., 2000). In hippocampal slices, BDNF-induced synaptic plasticity is blocked by inhibitors of protein synthesis (Kang and Schuman, 1996). In the same study, Schaffer-collateral CA1 synapses that were isolated from their pre- and postsynaptic cell bodies still exhibited protein synthesis-dependent plasticity, suggesting a local, dendritic source of protein synthesis. A similar dependence on dendritic protein synthesis has been observed for metabotropic receptor-induced LTD at Schaffer-collateral CA1 synapses in the hippocampus (Huber et al., 2000). Long-term facilitation induced by 5-HT at cultured sensory motoneuron synapses in *Aplysia* also shows a requirement for local protein synthesis in the sensory neuron (Casadio et al., 1999; Martin et al., 1997). In addition, 5-HT application to isolated sensory neurites results in new protein synthesis (Martin et al., 1997). Most demonstrations of dendritic protein synthesis have relied on biochemical fractionation techniques to isolate fragments of dendrites and postsynaptic spines (e.g., the synaptoneurosome). In these studies, the incorporation of radiolabeled amino acids into new proteins demonstrated that synthesis can clearly occur in these dendritically derived fractions (Rao and Steward, 1991; Weiler and Greenough, 1991, 1993). The use of a cell culture system in which the cell bodies are separated from the dendrites also showed that isolated dendrites can synthesize proteins (Torre and Steward, 1992) and glycosylate proteins (Torre and Steward, 1996). The drawbacks of the above techniques include the possibility of contamination by nondendritic fractions, the removal from a physiological context, and the lack of temporal resolution. Here we describe the development of a high-fidelity dendritic protein synthesis reporter and show unequivocally that protein synthesis can be stimulated in dendrites by BDNF, a growth factor involved in synaptic plasticity.

## Results

### BDNF Stimulates Protein Synthesis of a GFP Reporter in Hippocampal Neurons

In order to examine dendritic protein synthesis dynamically in living neurons, we constructed a green fluorescent protein (GFP) reporter, flanked by the 5′ and 3′ untranslated regions (UTR) from the $Ca^{2+}$/calmodulin-dependent kinase II-α subunit (CAMKII-α) (5′GFP3′). Previous work has shown that the 3′UTR of the CAMKII-α mRNA contains information sufficient for its dendritic localization (Mayford et al., 1996; Mori et al., 2000). In initial experiments, the 5′GFP3′ reporter was introduced into cultured neurons using Biolistics. In expressing neurons, GFP was present in the soma and the dendrites, as indicated by immunolabeling for the dendritic marker MAP2 (Figure 1A). In most untreated neurons, expression of the reporter was robust in the cell bodies and relatively weak in the associated dendritic processes (Figure 1B). We examined whether exposure to BDNF modified the levels and/or pattern of GFP expression in neurons; 6 hr after transfection, dishes were exposed to either BDNF (50 ng/ml) or a control (HBS) solution for 4 hr. Neurons that were exposed to BDNF exhibited an increase in GFP synthesis that was evident in both the cell body and the dendrites (Figure 1B). The analysis of total fluorescence in the dendrites revealed that BDNF-treated neurons had significantly greater quantities of

[1] Correspondence: schumane@its.caltech.edu
[2] These authors contributed equally to this work.

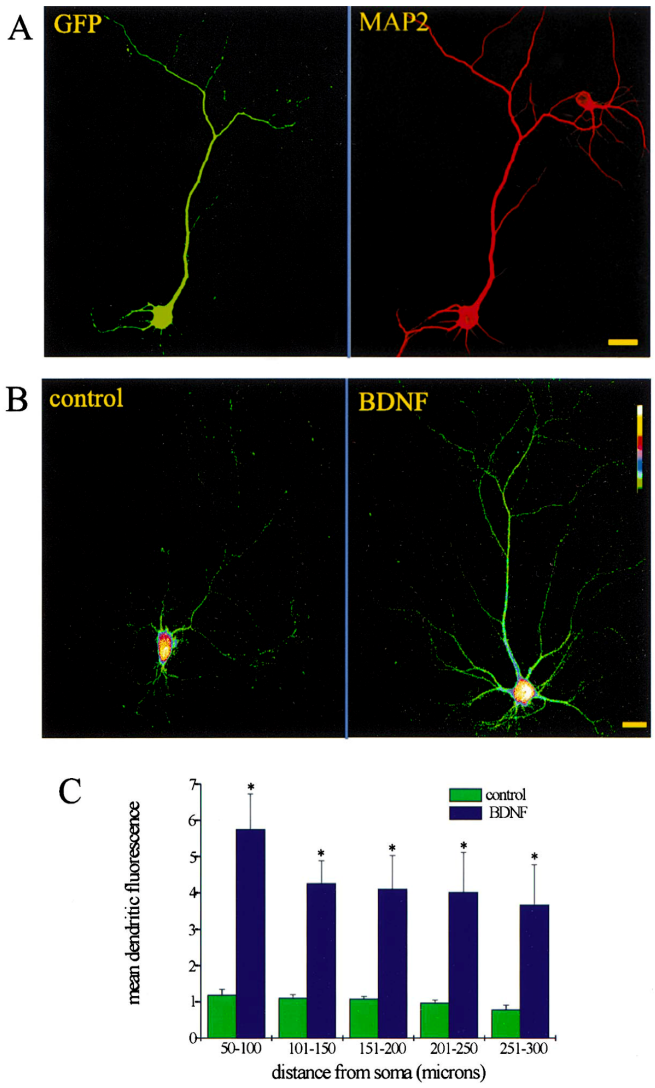


Figure 1. BDNF Stimulates Protein Synthesis of the GFP Reporter in Hippocampal Neurons

(A) Shown is a cultured hippocampal neuron expressing the GFP reporter and immunostained for the dendritic marker MAP2. The majority of the GFP signal occurs in the dendrites, as indicated by the coincident MAP2 signal. Scale bar = 15 μm.

(B) Shown are an untreated and BDNF-treated neuron expressing the GFP reporter. The BDNF-treated cell shows enhanced fluorescence in the cell body and dendrites when compared to the untreated cell. Color lookup bar shows that the absence of GFP signal is indicated by black, increasing fluorescence is indicated by transitions to green, blue, red, and yellow, and saturated fluorescence is indicated by white. Scale bar = 15 μm.

(C) Summary data for all untreated (n = 7) and BDNF-treated (n = 10) dendrites. BDNF-treated neurons showed significantly greater fluorescence ($p < 0.01$) in all dendritic compartments (e.g., 50–300 μm from the soma).

GFP throughout the length of the dendritic process (Figure 1C). These experiments demonstrate that BDNF can stimulate protein synthesis in hippocampal neurons but do not indicate the cellular compartment (e.g., dendrites and/or soma) where the synthesis is occurring.

**Time-Lapse Imaging of BDNF-Stimulated Translation**

In an effort to ascertain the source of the increased GFP synthesis apparent in the above experiments, we conducted time-lapse imaging. We monitored the localization and levels of the GFP reporter over time in individual neurons before and after BDNF treatment. To facilitate the expression of the reporter in a larger population of neurons, we incorporated the reporter construct into a Sindbis virus system (see Experimental Procedures). (We used a destabilized version of GFP, dGFP, in order to decrease the cumulative fluorescence that ultimately contributes to signal saturation.) Dishes of cultured hippocampal neurons were infected with Sin-5′dGFP3′; initial images were collected 12 hr after infection, at a time when the fluorescence had reached steady-state levels. Untreated neurons, imaged over a 4 hr period, showed stable or declining fluorescence in the dendrites and cell body over time (Figures 2A and 2B). In contrast, neurons that were treated with BDNF showed increases in GFP fluorescence that were evident within 60 min of BDNF addition (Figures 2A and 2B). BDNF-induced increases in fluorescence were apparent in both the dendritic and somatic compartments. Of particular interest was the observation of increases in fluorescence in remote aspects of the dendrites (see boxed regions in Figure 2A); these increases were detected as early as

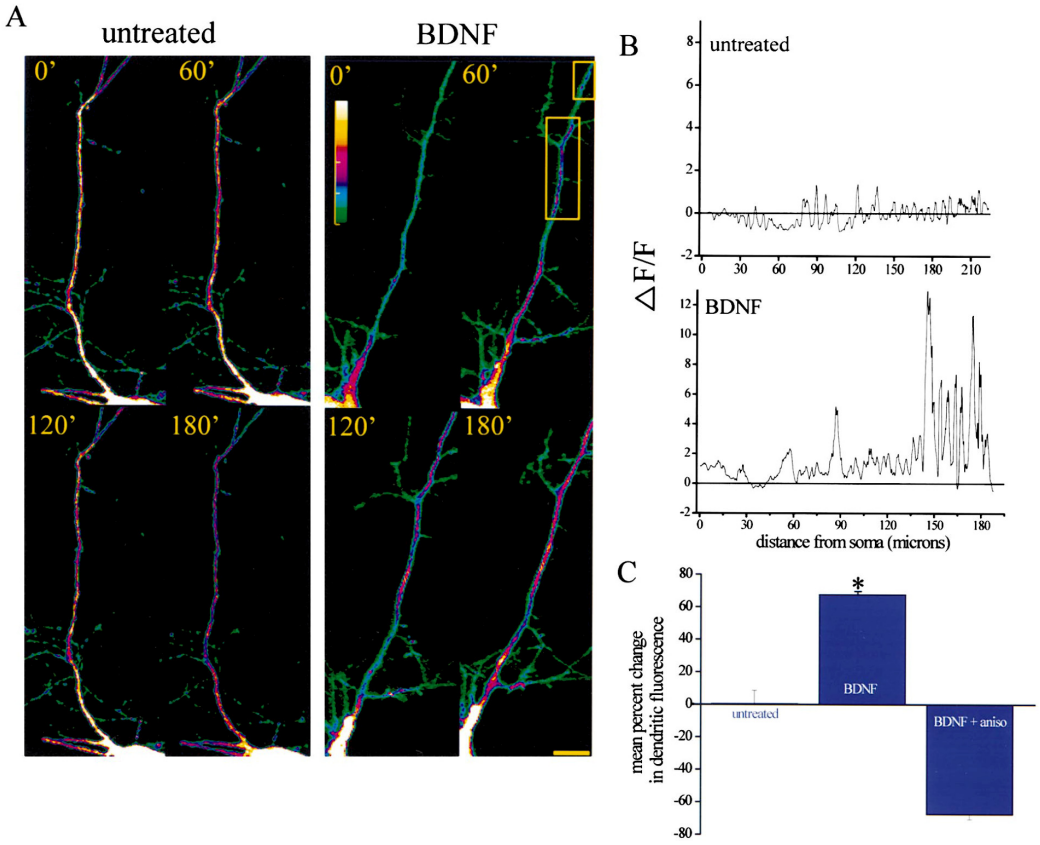


Figure 2. Time-Lapse Imaging of BDNF-Stimulated Translation

(A) Repeated images of a control neuron and BDNF-treated neuron. BDNF was added immediately after the 0 min image was acquired. The BDNF-treated neuron showed increased fluorescence in the dendrite whereas the control neuron was relatively stable over time. Scale bar = 15 μm.

(B) Analysis of the individual neurons shown in (A). ΔF/F was calculated using the data from the 0 and 120 min images (see Experimental Procedures).

(C) Summary data for analysis of total dendritic length showing that only dendrites treated with BDNF exhibited significant ($p < 0.01$) increases in fluorescence.

the increases observed in the cell body, consistent with the notion that GFP is synthesized locally. Overall, when the total length of the dendrite was analyzed, we found that only BDNF-treated neurons showed significant increases in dendritic GFP fluorescence; the average increase in fluorescence was roughly 60%. This is likely a very conservative estimate of BDNF's actions since the analysis includes both synaptic and nonsynaptic areas of the dendrite. For example, our analysis of changes at individual "hot spots," which may correspond to synaptic sites (see below), indicates that BDNF-induced increases in GFP fluorescence ranged from ~1- to 8-fold. Untreated neurons showed no significant increase in dendritic fluorescence when examined over the same time periods (Figure 2C). In addition, the BDNF-induced increases were prevented by coapplication of the protein synthesis inhibitor anisomycin (Figure 2C). In BDNF-treated neurons, we also observed, however, what appeared to be the diffusion of GFP from the soma into the dendrite. This observation prevented us from concluding, unambiguously, that all of the increases in dendritic GFP we observed were due to local synthesis.

### BDNF Stimulates Protein Synthesis in Healthy, Mechanically Isolated Dendrites

In order to remove the cell body as a potential source of GFP signal, we performed dendritic transections in which the dendrites were physically isolated from the cell bodies using a micropipette. Ensuring neuron health and viability following such transections was a major concern. Of approximately 300 transections performed over a 2 year period, only 10 transected neurons fulfilled the health and viability criteria we established for use in experiments (see Experimental Procedures). Technical difficulty aside, the transected dendrite can provide the

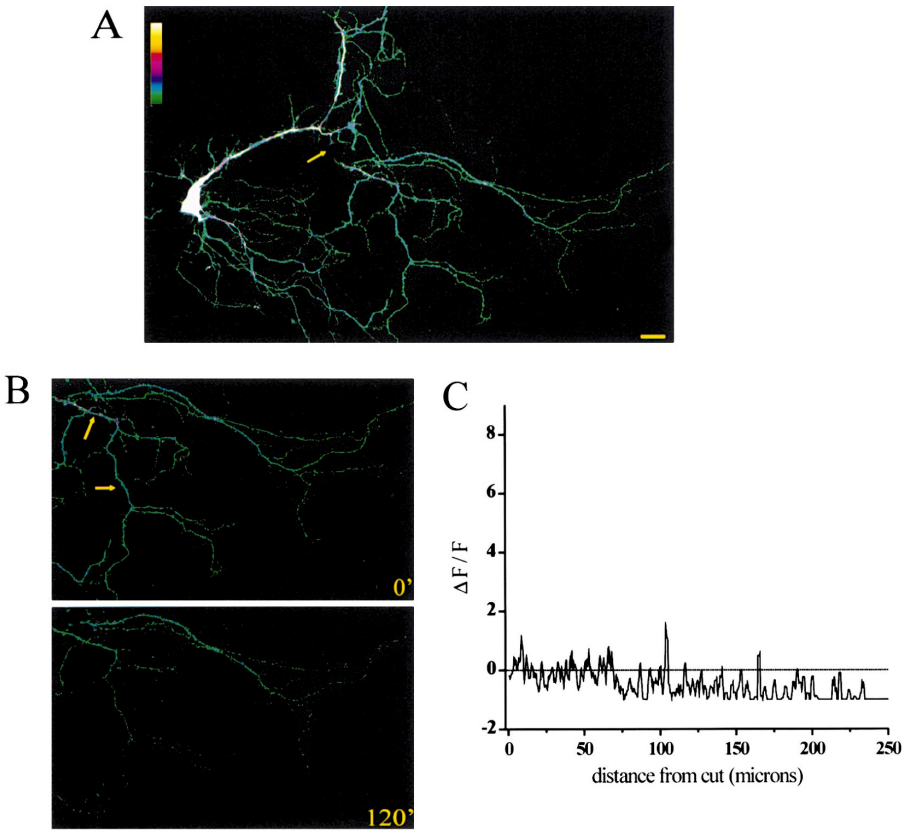


Figure 3. Untreated, Transected Dendrites Do Not Show Increases in Protein Synthesis

(A) Image of an infected neuron; arrow points to the region of transection. Scale bar = 15 μm.

(B) Images of the isolated region of the dendrite immediately following transection and 120 min later. The fluorescent signal in the dendrite decreases over time. Arrows point to the dendrite chosen for analysis in (C). The top dendrite was also analyzed and included in the group analysis (Figure 5).

(C) Analysis of the transected dendrite shown in (A) and (B). ΔF/F was calculated using the data from the 0 and 120 min images (see Experimental Procedures).

most unambiguous proof of local protein synthesis. As before, neurons were infected with Sin-5′dGFP3′. Transected dendrites that were not treated with BDNF usually showed declining fluorescence when monitored over time (Figure 3). In contrast, transected dendrites treated with BDNF exhibited increases in fluorescence in the isolated dendrites (Figure 4). As would be expected, BDNF-induced increases in fluorescence were also observed in the soma and the intact dendrites. The BDNF-induced increases in GFP fluorescence observed in the dendrites were blocked by cotreatment with anisomycin, indicating that the enhanced fluorescence was due to new protein synthesis (Figure 5). Plotting the distribution of changes in pixel intensity over time demonstrated that most regions of transected dendrites treated with BDNF showed increases in intensity (Figure 5C). In contrast, most regions of untreated dendrites or those treated with anisomycin plus BDNF tended to decrease in intensity. (Note that the small number of pixels that increased in intensity in the presence of anisomycin must represent the redistribution of pixels from adjacent areas of the dendrite or the contribution of synthesized, but not yet fluorescent GFP [e.g., Cubitt et al., 1995].) Taken together, these data clearly show that BDNF can stimulate protein synthesis in isolated dendrites. The local dendritic protein synthesis we observed was robust and stable over time.

### A Membrane-Anchored GFP Reporter Exhibits Extremely Limited Diffusion

Because of technical difficulty and the potential for compromising long-term neuronal health, the transection experiments are not a viable option for extensive explorations of local protein synthesis. We reasoned that modifications to the protein synthesis reporter that limited its diffusion would also decrease the potential contribution of somatically synthesized GFP to the signal observed in dendrites. Toward this end, we conferred membrane localization to the reporter by adding a myristoylation consensus sequence (Patrick et al., 1999) at

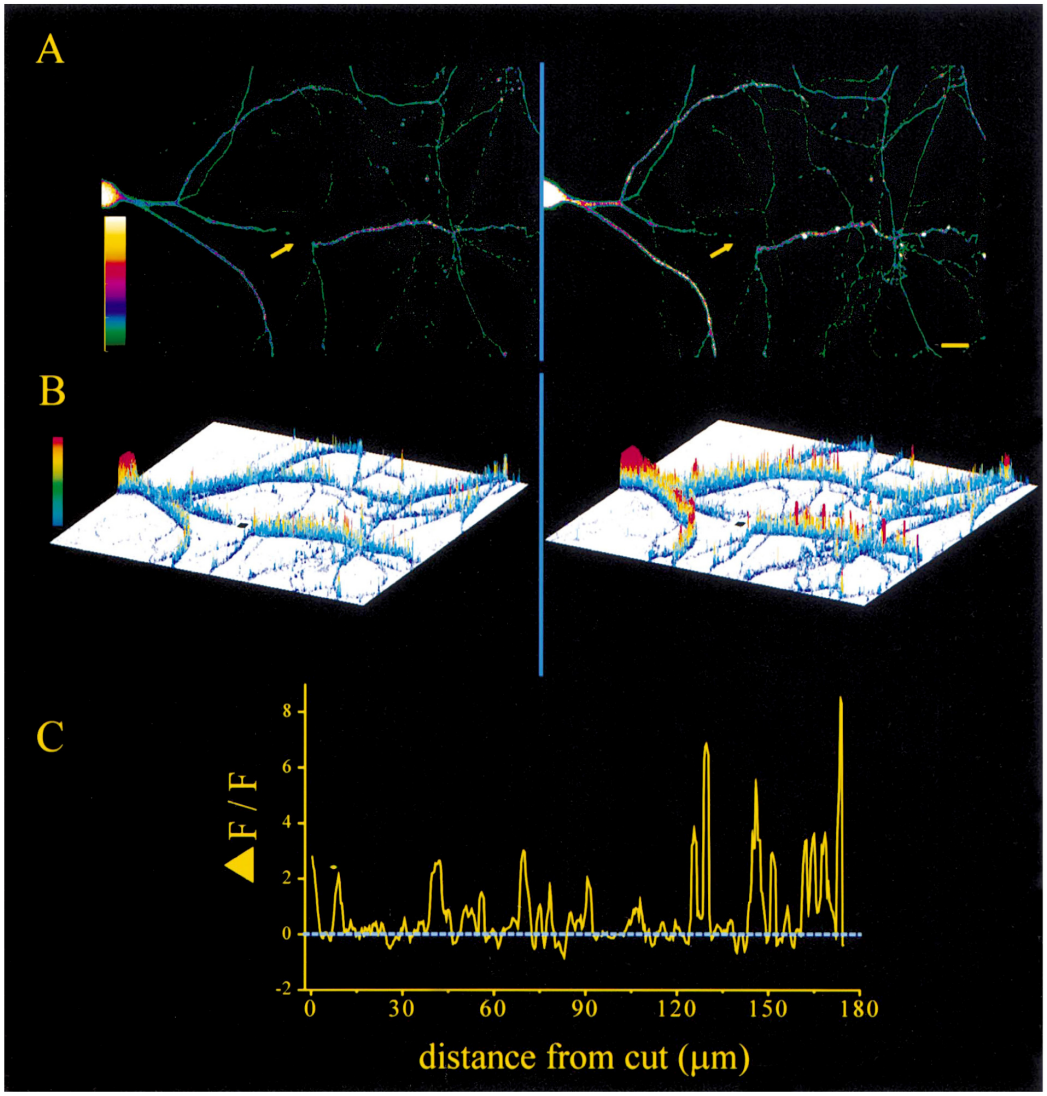


Figure 4. BDNF Stimulates Protein Synthesis in Healthy, Mechanically Isolated Dendrites

(A) Images of transected neuron before (left) and 120 min after (right) BDNF treatment; arrow points to the region of transection. The fluorescent signal in the transected dendrite increases following BDNF treatment. Scale bar = 15 μm.

(B) X-Y-Z plot of the neuron shown in (A) in which changes in fluorescence are indicated by both changes in color and changes in the height of the pixels shown.

(C) Analysis of the transected dendrite shown in (A) and (B). ΔF/F was calculated using the data from the 0 and 120 min images (see Experimental Procedures).

the N terminus of the GFP molecule and expressed this construct, Sin-5′$_{myr}$dGFP3′, in neurons using Sindbis virus. We compared the diffusion of Sin-5′dGFP3′ and Sin-5′$_{myr}$ dGFP3′ by conducting FRAP (fluorescence recovery after photobleaching) experiments in dendrites. Note that the recovery of reporter fluorescence in dendrites following photobleaching is due to both diffusion from the adjacent (nonbleached) compartment as well as new synthesis of the reporter in the bleached domain. To monitor the contribution of diffusion exclusively, we included anisomycin in the bath. In the nonmembrane anchored version of the reporter (Sin-5′dGFP3′), there was substantial recovery of fluorescence in the bleached dendrite within 60 min (Figure 6A). We found that the addition of the myr sequence, however, severely retarded the diffusion of the modified (Sin-5′$_{myr}$dGFP3′)

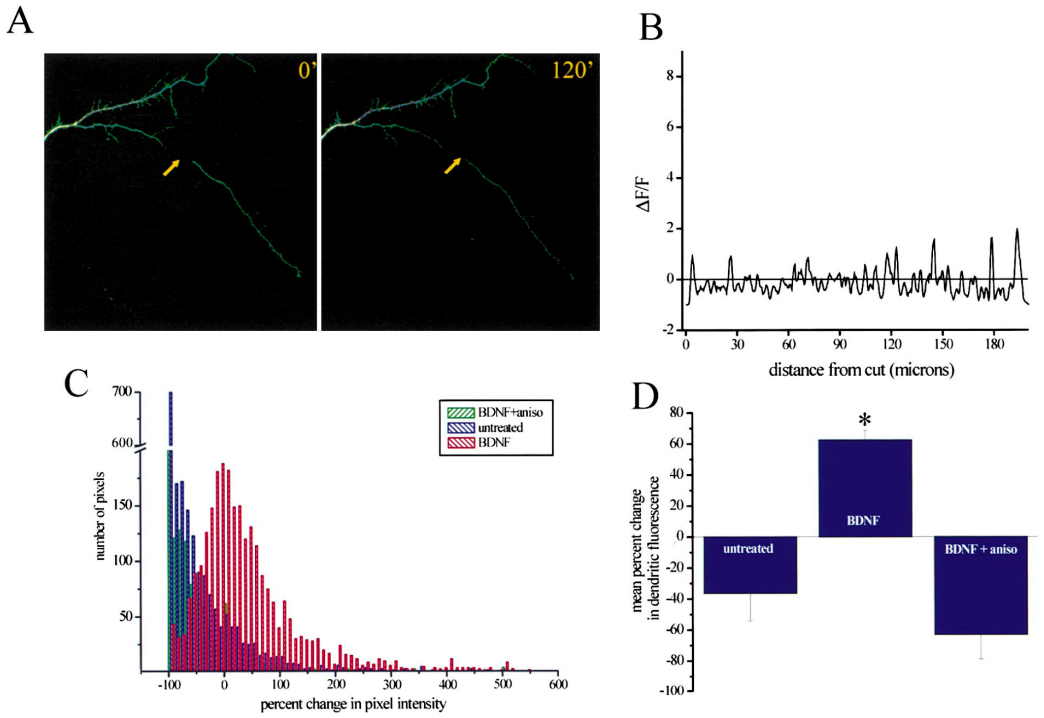


Figure 5. Anisomycin Prevents BDNF-Induced Increases in Protein Synthesis in Transected Dendrites

(A) Images of a transected dendrite before and 120 min after coapplication of BDNF and anisomycin; arrow points to the region of transection. The fluorescent signal in the transected dendrite decreased over time. Arrows indicate the site of transection. Scale bar = 15 μm.

(B) Analysis of the transected dendrite shown in (A). ΔF/F was calculated using the data from the 0 and 120 min images (see Experimental Procedures).

(C) Summary histogram indicating the pixel intensity distributions for all untreated, BDNF-treated, and BDNF plus anisomycin-treated transected dendrites.

(D) Summary diagram indicating the mean percent change in pixel intensity for the three groups. Only the BDNF-treated dendrites showed a signficant increase in fluorescence intensity over time ($p \leq 0.01$). N (cells, dendrites) for each group are as follows: untreated (3, 4); BDNF (4, 5); BDNF + aniso (3, 4).

reporter (Figure 6A). Negligible recovery from the photobleached state was observed in the 120 min following the photobleaching episode. These data indicate that the myristoylated reporter exhibits limited diffusion (see Experimental Procedures), suggesting that it can be used to faithfully report local protein synthesis in intact dendrites.

### BDNF Stimulates Protein Synthesis in Healthy, "Optically Isolated" Dendrites

We next used the diffusion-restricted reporter (Sin-5′$_{myr}$dGFP3′) in combination with photobleaching to examine dendritic protein synthesis in intact neurons. In these experiments, we continuously photobleached the cell body in order to abolish the contribution of somatically synthesized GFP to the dendritic signal; in this way we "optically isolated" the dendrites of interest. The continuous photobleaching of the soma did not compromise neuronal health: propidium iodide labeling of bleached cells revealed no incorporation of the dye (see Experimental Procedures). When we analyzed untreated, optically isolated dendrites, we found that the fluorescence of the reporter decreased over time at most dendritic sites (Figures 6B and 6C). We occasionally observed small (e.g., 0- to 5-fold) fluorescence increases at some sites. These small increases in signal reflect either the redistribution of GFP from adjacent dendritic sites or bona fide new protein synthesis. The

Figure 6. A Membrane-Anchored GFP Reporter Exhibits Limited Diffusion

(A) Shown are two neurons infected with either 5′dGFP3′ or the membrane-anchored 5′$_{myr}$dGFP3′. Neurons were treated with anisomycin for 1 hr prior to the initiation of photobleaching (boxed region shows bleached area). FRAP was monitored in each neuron over time. The neuron infected with the diffusible reporter (5′dGFP3′) showed significant recovery of fluorescence within 60 min of the photobleaching. In contrast, the myristoylated reporter showed negligible recovery within 2 hr following photobleaching. Scale bars: 5′dGFP3′, 15 μm; 5′$_{myr}$dGFP3′, 10 μm.

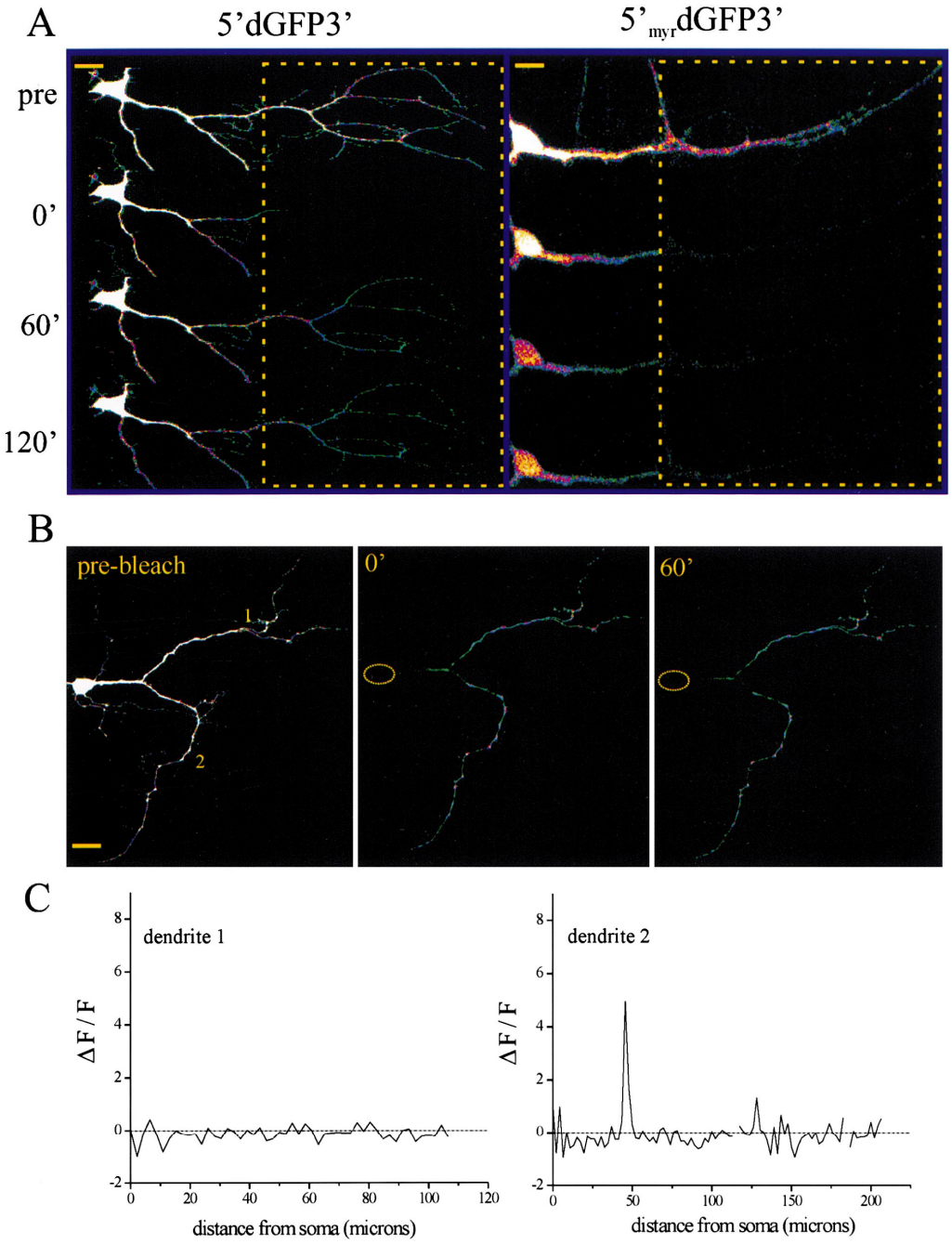


(B) Time-lapse images of a 5′$_{myr}$dGFP3′-expressing neuron that was subjected to somatic photobleaching for the duration of the experiment. The prebleached neuron is shown at the right and two consecutive time points following photobleaching are shown in the middle and left. In this untreated neuron there was an overall decline in dendritic fluorescence during the experiment. Scale bar = 15 μm.
(C) Profile of fluorescence changes between 0 and 60 min for dendrites 1 and 2 (labeled in [B]). In the profiles shown, the mean change in fluorescence between t = 0 and t = 60 was −15.4% and −12.3% for dendrite 1 and 2, respectively.

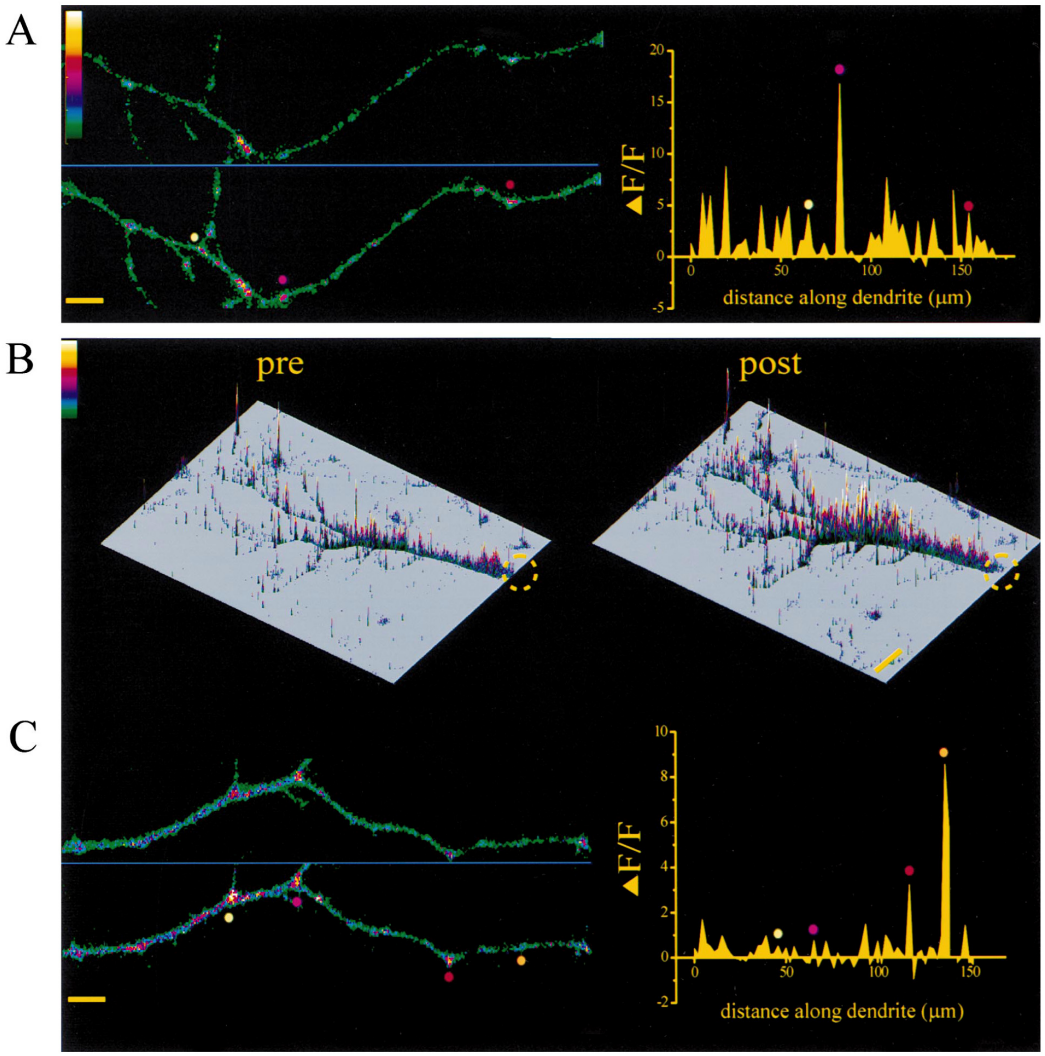


Figure 7. BDNF Stimulates Protein Synthesis in Healthy, "Optically Isolated" Dendrites

(A) Shown is BDNF-induced enhancement of GFP translation in an optically isolated dendrite at two consecutive time points. The profile of fluorescence change between the two time points shown is plotted on the right. Individual hot spots are identified by colored circles on the image and the corresponding profile. Scale bar = 5 μm.

(B) An X-Y-Z plot of a different neuron in which the dendrites were optically isolated. The region of the bleached soma is shown by the dashed circle. The effects of BDNF are evident in comparing the dendritic fluorescence in the pre and post images. Scale bar = 15 μm.

(C) An isolated dendritic segment from the neuron shown in (B) at two different time points. The profile of fluorescence change between the two time points shown is plotted on the right. Individual hot spots are identified by colored circles on the image and the corresponding profile. Scale bar = 5 μm.

fact that both untreated and anisomycin-treated dendrites showed similar average fluorescence change profiles (Figure 8) suggests that most of these small increases reflect redistribution from adjacent portions of the dendrite.

In contrast to untreated neurons, the addition of BDNF to optically isolated dendrites resulted in a robust stimulation of protein synthesis. As shown in Figure 7, increases in reporter translation ranging from 1- to 17-fold were observed at many sites along optically isolated dendrites. Sites of decreased fluorescence were not common in BDNF-treated dendrites. The coapplication of anisomycin completely prevented the BDNF-induced increases in GFP fluorescence, confirming that the observed effects of BDNF were due to new protein synthesis (Figure 8). Dendrites that were treated with aniso-

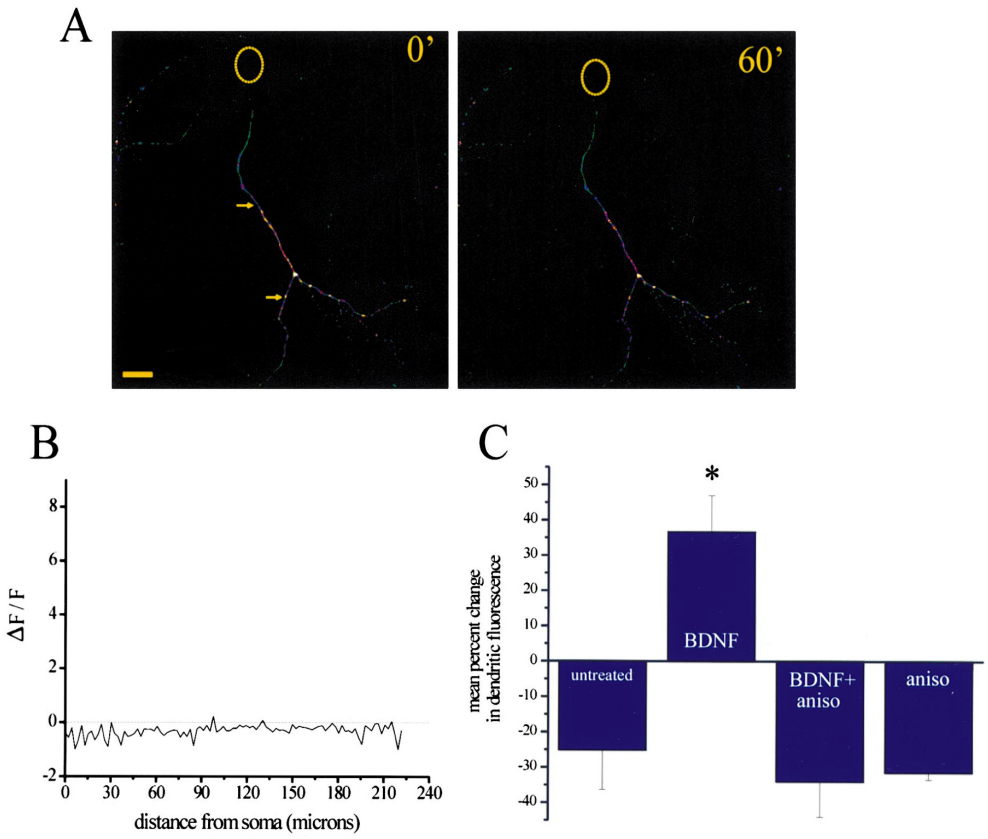


Figure 8. Anisomycin Blocks BDNF-Induced Increases in Protein Synthesis in Optically Isolated Dendrites

(A) Time-lapse images of an optically isolated dendrite that was treated with BDNF plus anisomycin. The optically isolated dendrites are shown at two consecutive time points. There was an overall decline in dendritic fluorescence during the experiment. The area occupied by the photobleached soma is shown by the yellow circle. Scale bar = 15 μm.

(B) Profile of fluorescence changes between 0 and 60 min for dendrite indicated by the arrow in (A). The mean change in fluorescence between t = 0 and t = 60 was −25.7%.

(C) Summary diagram indicating the mean percent change in pixel intensity for all untreated, BDNF-, and BDNF plus anisomycin-, and anisomycin-treated optically isolated dendrites. Only the BDNF-treated dendrites showed a signficant increase in fluorescence intensity over time ($p \leq 0.01$). N (cells, dendrites) for each group are as follows: untreated (4, 6); BDNF (5, 8); BDNF + aniso (4, 5); aniso (3, 5).

mycin alone or anisomycin plus BDNF usually showed decreases in fluorescence along the length of the dendrite interspersed with very small increases that likely represented redistribution of GFP molecules from adjacent regions of the dendrites (Figure 8).

### The Protein Synthesis Reporter Is Concentrated near Sites of Translation and Synapses

Repeated imaging of optically isolated dendrites allowed us to examine the location of GFP signals over time. When the fluorescence intensity profiles derived from time-lapse imaging of an individual dendrite were plotted together, it became clear that the GFP signals appeared to be spatially concentrated at hot spots that were stationary over time (Figure 9). The increases and occasional decreases in GFP signal that were observed over time tended to appear at the same locations along the dendrite. We next examined whether these reporter hot spots were in the vicinity of synaptic sites and/or sites of protein translation. We immunolabeled $5'_{myr}$dGFP3′-expressing cells with an antibody to the postsynaptic marker PSD-95, the presynaptic marker synapsin I, or rRNA (Y10B; Koenig et al., 2000; Lerner et al., 1981). We found that the GFP hot spots often were near ribosomes or synaptic regions as indicated by the proximity of the PSD-95, synapsin, or Y10B signal to GFP (Figure 10). The colabeling for PSD-95 also revealed that the myristoylated reporter appeared not to enter synaptic spines to an appreciable extent and appeared more concentrated in dendritic shafts. As such, we did not expect to observe strict "colocalization" of the GFP signal with the synaptic markers. We did observe, however, that GFP was, much more often than not, in the vicinity of ribosomes and synapses. To quan-

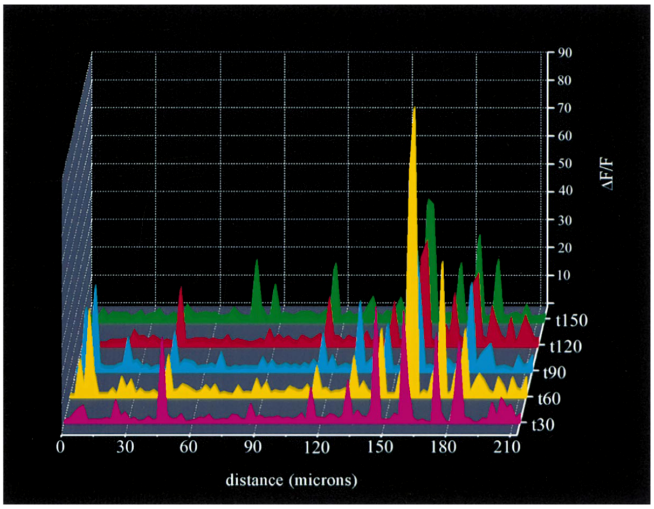


Figure 9. GFP Reporter Signals Are Spatially and Temporally Persistent

Shown are the ΔF/F profiles for a single optically isolated dendrite at several time points. The increased GFP signal is concentrated at relatively stable sites along the length of the dendrites. These sites also appear to be temporally stable over a 2 hr time period.

tify this relationship, we calculated the mean fluorescence for each signal across the dendritic width (thus obtaining mean fluorescence values for the entire length of each dendrite), and calculated the pairwise cross-correlation of GFP and PSD-95, synapsin, or Y10B. A cross-correlation measures the spatial coincidence of the two signals, with the lag value representing the distance one signal must be shifted in order to spatially correlate with the other signal. Analysis of the GFP/Y10B, GFP/synapsin, or GFP/PSD-95 (data not shown) signals revealed a significant cross-correlation between the two signals (Figure 10). The peaks at zero lag for both the GFP/Y10B and GFP/synapsin analysis (Figures 10F and 10G) indicate that the two signals are highly correlated. The observation that locally synthesized GFP is concentrated in the vicinity of ribosomes and synapses suggests that there are local hot spots of translation that are near synaptic sites. These data are predicted to some extent by previous anatomical observations of ribosomes at or near the bases of dendritic spines (Steward and Levy, 1982). The spatially and temporally stable sites of translation that we have identified provide evidence for a central tenet of the local protein synthesis hypothesis—the notion that locally synthesized proteins might be selectively made available to their associated synapses, thus providing a mechanism for synapse specificity (Schuman, 1999a; Steward, 1997; Steward and Schuman, 2001). Whether these observations hold true for other types of locally synthesized proteins (e.g., nonmyristoylated) is an important issue for future studies.

## Discussion

We have described the visualization of dendritic protein synthesis in mature cultured hippocampal neurons. We report a robust stimulation of local protein synthesis by the growth factor BDNF. In the last 5 years, several studies have used clever applications of protein synthesis inhibitors to demonstrate roles for locally synthesized proteins in different forms of synaptic plasticity (Casadio et al., 1999; Huber et al., 2000; Kang and Schuman, 1996; Martin et al., 1997). In *Aplysia* sensory neurons, serotonin application to isolated neurites results in detectable protein synthesis (Casadio et al., 1999). Direct demonstrations of protein synthesis in mature mammalian dendrites are scarce, however. Using radiolabeling, Feig and Lipton (1993) showed that newly synthesized proteins could be detected in dendrites of hippocampal slices—the timing was such that the cell body was unlikely to be the source of protein synthesis. Nevertheless, the difficulty associated with the radiolabeling procedure as well as the troublesome identification of dendritic compartments limits the appeal of this approach. In contrast, the approach we have developed allows the visualization of dendritic protein synthesis in living neurons over time. Ultimately, we combined the use of a membrane-anchored, destabilized GFP with somatic photobleaching to be sure that reporter signals observed in the dendrite were synthesized in the dendrite. Given the limited diffusion of the myristoylated dGFP (e.g., Figure 6), a case could certainly be made for using the myristoylated reporter alone (without somatic photobleaching) in future investigations of dendritic protein synthesis in slice preparations as well as in vivo.

The BDNF-induced increases in GFP fluorescence we observed were completely blocked by anisomycin. Since BDNF does not slow the degradation rate of the GFP reporter (our unpublished data), these data indicate that the fluorescence increases were due to new protein synthesis. In addition, BDNF-induced dendritic protein synthesis was not accompanied by any obvious or systematic changes in cell morphology. We observed increases in GFP reporter within 45–60 min of BDNF application (e.g., Figure 2). Preceding its ability to fluoresce, GFP possesses posttranslational requirements for cyclization and oxidation (Cubitt et al., 1995). As such, GFP is not an optimal reporter for addressing how quickly protein synthesis can occur in dendrites. Previous studies using developing neurons reported that a combination of BDNF and NT-3 (Crino and Eberwine, 1996) or a

metabotropic receptor agonist (Kacharmina et al., 2000) could stimulate translation of a myc epitope in transected growth cones between 1 and 4 hr after transfection. In addition to participating in synaptic plasticity, a role for BDNF-stimulated dendritic protein synthesis might also be imagined in other contexts where BDNF clearly plays an important neurotrophic role in development and the morphology of neurons (McAllister et al., 1999; Schuman, 1999b).

The regulated synthesis of our reporter may mimic the translation of endogenous CAMKII-α since our reporter contains both the 5′ and 3′UTR from the CAMKII-α gene. Indeed, a stimulation of dendritic CAMKII-α translation by LTP has been suggested by immunohistochemical studies (Ouyang et al., 1997, 1999). The 5′UTR may contain translational regulatory elements: we noticed that GFP fluorescence in neurons transfected with a construct lacking the 5′UTR (GFP3′) appeared to be greater than that observed in cells expressing a construct containing both the 5′ and 3′UTR (data not shown). The 3′UTR was included primarily to confer dendritic localization of the GFP mRNA (Mayford et al., 1996; Mori et al., 2000), although this was likely not necessary in the present study given the abundance of the mRNA produced by viral infection. The 3′UTR of CAMKII-α also contains elements for regulation of translation, namely the CPE (cytoplasmic polyadenylation element) and polyadenylation signal (Wu et al., 1998). We have not addressed whether the BDNF-stimulated translation we observe requires these elements, although others have clearly shown regulation of CAMKII-α translation via these and other regulatory elements (Sheetz et al., 2000; Wu et al., 1998).

In addition to its effects on hippocampal slices, BDNF can also facilitate synaptic transmission in cultured hippocampal neurons (Levine et al., 1995; Li et al., 1998a, 1998b). Both pre- and postsynaptic (Levine et al., 1997) mechanisms have been proposed for BDNF's actions on synaptic transmission. In the present experiments, the stimulation of protein synthesis could be due to activation of postsynaptic TrkB receptors and subsequent stimulation of local translation machinery, potentially through the rapamycin-sensitive M-TOR kinase pathway (e.g., Brown and Schreiber, 1996; Casadio et al., 1999; S.J. Tang et al., 1998, Soc. Neurosci., abstract). Alternatively, BDNF could enhance glutamate release from presynaptic terminals (e.g., Li et al., 1998a, 1998b), which could then stimulate postsynaptic protein synthesis through glutamate receptor signaling.

In sum, these data clearly show that dendrites of mammalian neurons can synthesize proteins. The demonstration that dendrites that are in a synaptic network can synthesize proteins provides support for the idea that locally synthesized proteins contribute to synaptic function. The observation that there are spatially and temporally consistent hot spots for translation suggests that local synthesis might play a role in maintaining the specificity of synaptic connections.

## Experimental Procedures

### Cultured Neurons

Dissociated hippocampal neuron cultures are prepared from postnatal 2- and 3-day rat pups as described (Banker and Goslin, 1990). Neurons are plated at a density of 15,000–45,000 cells/cm$^2$ onto poly-l-lysine and laminin-coated coverslips. The cultures are maintained and allowed to mature in growth medium (Neurobasal-A supplemented with B27 and Gluta MAX-1) for 14–21 days before use. In Biolistic experiments, dissociated P2 hippocampal neurons were transfected with the pcDNA3.1-5′GFP3′ construct according to the manufacturer's protocol (Bio-Rad). DNA-gold complexes were generated with the following parameters: 50 μg plasmid DNA, 17 mg 1.6 μm diameter gold particles, and 0.01% PVP. In viral infection experiments, dissociated P2 hippocampal neurons were infected for 12 hr in growth medium containing the Sindbis virus of choice. Six hours post initial transfection or 10–12 hr post initial infection, growth medium was removed and replaced with HEPES-buffered solution (HBS) (Malgaroli and Tsien, 1992) (without glycine or picrotoxin) for imaging. All neurons used in our experiments had a pyramidal neuron-like morphology with one or two major dendrites emanating from the cell body. For immunolabeling, neurons were fixed at room temperature with 4% paraformaldehyde for 20 min. Fixed cultures were then treated sequentially with PBS, PBT (1× PBS, 2 mg/mL BSA, 0.1% Triton X-100), preblock (20% normal goat serum in PBT), primary Ab in preblock at 4°C overnight, preblock, Cy3-conjugated seconday Ab in preblock, preblock, and PBS. Immunostained specimens were imaged in PBS. The sources of the antibodies were as follows: MAP2 (Chemicon), PSD-95 (Upstate Biotechnology), Y10B (generous gift from Jeff Twiss, UCLA), synapsin I (Novus).

### Constructs

pcDNA3.1-5′dGFP3′: The CamKII-α 3′UTR sequence obtained from plasmid (Mayford et al., 1996) was PCR amplified (forward primer: 5′-ttatatttgcggccgcggtcgctaccattaccagtt-3′; reverse primer: 5′-ggc gctctctcgagtttaaatttgtagct-3′) and cloned into the NotI and XhoI sites of the pcDNA3.1 vector (Invitrogen). The resulting vector was then cleaved with BamHI and NotI for insertion of the destabilized EGFP ORF (from pd2EGFP, Clontech). The CamKII-α 5′UTR was released from a plasmid (obtained from J. Fallon) and inserted at the HindIII-BamHI sites, yielding pcDNA-5′dGFP3′. pSinRep5-5′dGFP3′: The 5′dGFP3′ fragment was released with PmeI-ApaI (blunted) and ligated into pSinRep5 (Invitrogen). pcDNA3.1-5′$_{myr}$dGFP3′: The d2EGFP ORF (from pd2EGFP, Clontech) was PCR amplified (forward primer: 5′-cgactctagagtgagcaagggcgaggagctg-3′; reverse primer: 5′-tctagagtcgcggccgcatctacaca-3′), digested, and inserted into the XbaI-NotI sites of pBSK. To generate the myristoylation signal, two oligos corresponding to the N-terminal 10 amino acids of p10 were annealed (myr1: 5′-gatccatgggcacggtgctg tccctgtctcccagct-3′; myr2: 5′-ctagagctgggagacagggacagcaccgtg cccatg-3′), digested, and inserted into the BamHI-XbaI sites of pBSK-d2EGFP. The $_{myr}$dGFP was subcloned into the BamHI-NotI sites of pcDNA3.1-5′dGFP3′. pSinRep5-5′$_{myr}$dGFP3′: The 5′$_{myr}$3 dGFP3′ fragment was released with PmeI-ApaI and subcloned into the StuI-ApaI sites of pSinRep5 (Invitrogen). Sindbis viroids were produced according to the Experimental Procedures provided by Invitrogen. Contrary to observations in other cell types, it appears that single-stranded RNA viruses of the α family do not shut down protein synthesis in neurons (K. Lundstrom, personal communication, Hoffmann-LaRoche, Basel, Switzerland).

### Microscopy

Confocal images were acquired in 0.3 μm sections; image analysis was conducted on z-compressed image stacks that contained the entire neuron of interest. GFP was excited at 488 nm and emitted light was collected between 510–550 nm. Images were acquired with parameters that maximized the dynamic range of pixel intensity for the dendritic signal. Using these parameters, the cell body fluorescence intensity was necessarily, occasionally, saturated. In all experiments, identical acquisition parameters and settings were used for both control and BDNF-treated dendrites on a given experimental day. In time-lapse experiments, the cultured neurons were maintained in an incubator (36.5°C) between image acquisition episodes. Images were acquired at room temperature. The acquisition of images at individual time points took less than 3 min.

### Transections

Cells were preincubated in HBS for 2 hr before the start of transection experiments. Transection was carried out as follows: GFP-

Neuron
500

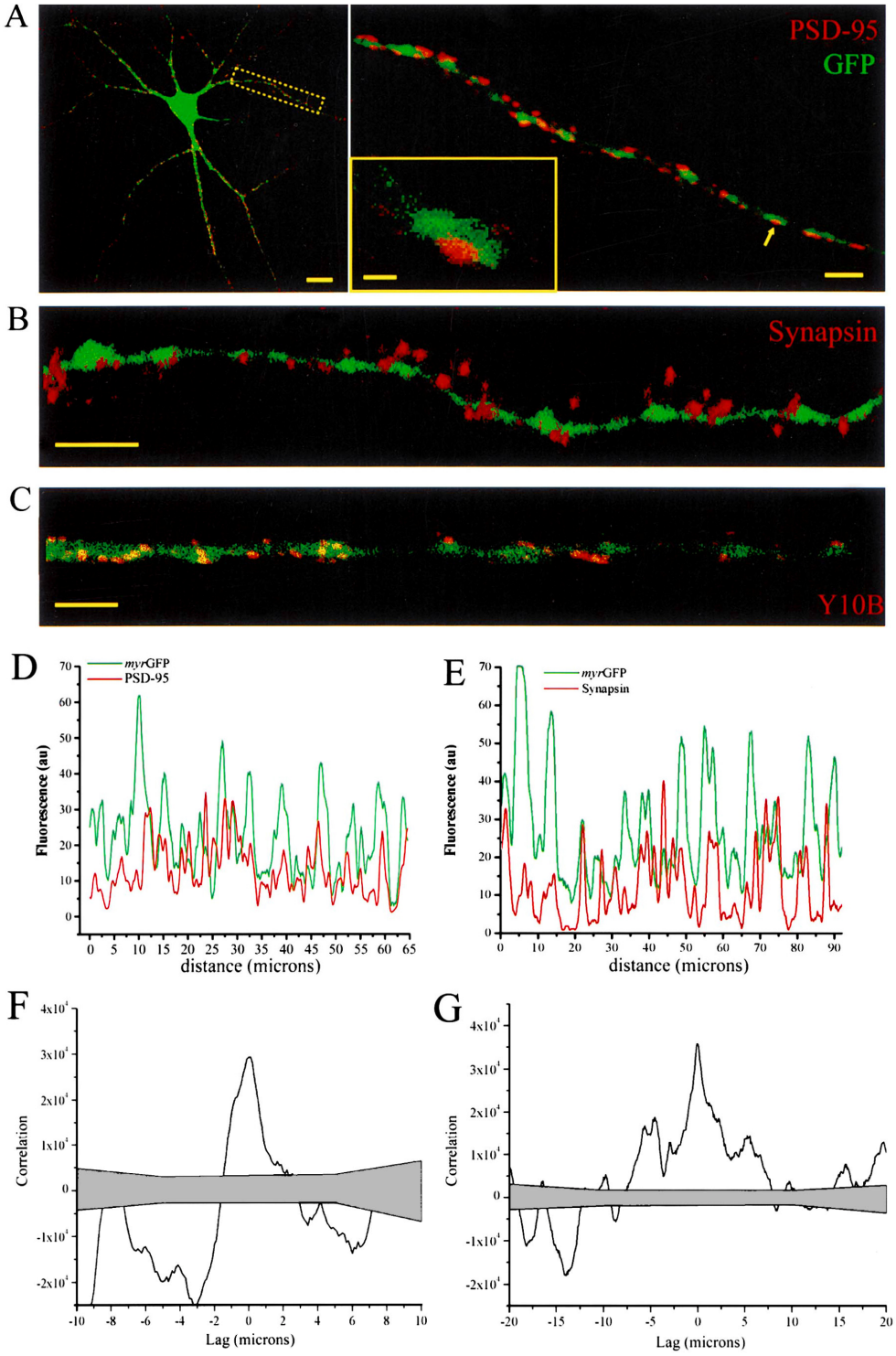
A
PSD-95
GFP
B
Synapsin
C
Y10B
D
myrGFP
PSD-95
Fluorescence (au)
distance (microns)
E
myrGFP
Synapsin
Fluorescence (au)
distance (microns)
F
Correlation
Lag (microns)
G
Correlation
Lag (microns)

expressing neurons were oriented such that the dendritic segment to be cut was in line with the long axis of the microelectrode. The glass microelectrode was then carefully lowered onto the dendrite until a spot of no GFP signal was seen, indicating that the dendrite had been pinched at that point. After allowing the microelectrode to rest in this position for 1-2 min, the electrode was slowly moved down vertically, allowing the tip to flex and push the proximal aspect of the dendrite toward the soma and away from the more distal dendrites. Complete transection of the dendrite as well as the integrity of the dendritic arbor was verified by DIC images. In order to be included in experiments, transected neurons were required to meet the following criteria: (1) both the transected process and the neuron from which it was cut must remain morphologically intact and healthy for the duration of the experiment; (2) no signs of varicosity formation or blebbing; (3) some detectable fluorescence signal must be observed in the transected process 2 hr post transection.

### Photobleaching

In FRAP experiments, an infected neuron was selected and a dendrite from that neuron was scanned for 1 hr with a 488 nm, ~5 mW laser. Complete volumetric data of the dendrite to be studied were acquired at regular intervals before and after the bleaching. In optical isolation experiments, an infected neuron was selected, and its soma was continuously scanned to photobleach the somatic GFP. Propidium iodide (PI) exclusion experiments were conducted to insure neuronal viability during optical isolation experiments. After ~90 min somatic photobleaching, the cell was stained with PI solution (50 μg/ml). The cell was then assessed for PI staining. Positive control experiments utilizing glutamate-induced toxicity (250 μM) were also carried out. No PI staining was evident after somatic photobleaching whereas the glutamate-induced toxicity in the same cells led to strong PI staining. Pilot experiments indicated that complete somatic photobleaching was obtained within 120 min of the initiation of photobleaching. In all experiments, data analysis began with this (complete somatic photobleaching) time point and hence was designated as $t = 0$. Using data from FRAP experiments, we estimate the membrane tethered reporter's diffusion coefficient to be $1 \times 10^{-8}$ cm$^2$/s, which is only slightly greater than the diffusion coefficient of rhodopsin ($\sim 5 \times 10^{-9}$ cm$^2$/s) (Wey et al., 1981) and glycine receptors ($\sim 1 \times 10^{-9}$ cm$^2$/s) (Srinivasan et al., 1990). This difference is expected since rhodopsin and glycine receptors are integral membrane proteins that may be bound to elements in the cytoskeleton and therefore would be more diffusion limited than a myristoylated protein. This estimate of the reporter's diffusion coefficient may include the simultaneous effects of degradation on the reporter. Indeed, there are examples of FRAP experiments where the rate of degradation of the reporter exceeded the rate of diffusion of the reporter.

### Analysis

To analyze the GFP of individual dendrites, we calculated the mean pixel intensity for each dendrite along its length (NIH Image, Scion Image, or Image J), thus controlling for changes in the width of the dendrite. In time-lapse experiments, we calculated a normalized difference score, $\Delta F/F(y - x/x)$, that indicates the change in dendritic fluorescence as a function of time and, when appropriate, treatment with BDNF. In plotting $\Delta F/F$, the data were binned into 1–2 μm sections. In regular time-lapse and dendritic transection experiments, x was the baseline (first) fluorescence measurement and y was the brightest time point following the baseline (typically 120 min). In "optical isolation" experiments, x was chosen as the lowest time point following somatic photobleaching and y was usually taken 60 min later. All untreated cells were "yoked" to experimental cells. That is, they were infected at the same time, imaged at equivalent time points, and the analysis was calculated using the same time points as their BDNF-treated "sister" neurons. For analysis of colocalization, horizontal dendritic segments were analyzed by obtaining the mean fluorescence signal across the width of the dendritic segment. A cross-correlation was calculated for the $_{myr}$dGFP and PSD-95, synapsin, or Y10B: the mean fluorescence across the width of a dendritic segment was calculated, generating a one-dimensional representation of the relative amplitudes of the red and green signals. A cross-correlation was calculated on these two data sets. To calculate the significance of the cross-correlation, one hundred cross-correlations of the randomized data were performed to yield a 95% confidence level. In other experiments, Student's t tests were performed to assess statistical differences between groups. We chose for analysis the brightest (usually principal) dendrite from each neuron in each group. When a single neuron possessed two bright, principal dendrites, both were used in the analysis.

### Acknowledgments

We are grateful to Gilles Laurent and members of the Schuman lab for criticism and discussion. We thank Michael Tsung and Holli Weld for making beautiful cultured neurons. We thank Jeff Twiss for the Y10B antibody. This work was supported by Howard Hughes Medical Institute.

Received February 23, 2001; revised April 17, 2001.

### References

Banker, G., and Goslin, K. (1990). Culturing nerve cells (Cambridge, MA: MIT Press).

Brown, E.J., and Schreiber, S.L. (1996). A signaling pathway to translational control. Cell *86*, 517–520.

Casadio, A., Martin, K.C., Giustetto, M., Zhu, H., Chen, M., Bartsch, D., Bailey, C.H., and Kandel, E.R. (1999). A transient, neuron-wide form of CREB-mediated long-term facilitation can be stablized at specific synapses by local protein synthesis. Cell *99*, 221–237.

Crino, P.B., and Eberwine, J. (1996). Molecular characterization of the dendritic growth cone: regulated mRNA transport and local protein synthesis. Neuron *17*, 1173–1187.

Cubitt, A.B., Heim, R., Adams, S.R., Boyd, A., and Gross, L.A. (1995). Understanding, improving and using green fluorescent proteins. Trends Biochem. Sci. *20*, 448–455.

Feig, S., and Lipton, P. (1993). Pairing the cholinergic agonist carbachol with patterned schaffer collateral stimulation initiates protein

Figure 10. GFP Reporter Signals Colocalize with Ribosomes and Synaptic Markers

(A) Low- (left) and high-power (right) images of a GFP reporter-expressing neuron immunostained with an antibody against the synaptic marker PSD-95. The inset shows the GFP signal that forms a cloud around the punctate PSD-95 signal. Scale bars = 15, 5, and 1 μm, for low-, high-power, and inset images, respectively.

(B) High-power image of a GFP reporter-expressing neuron immunostained with an antibody against the presynaptic protein synapsin I, showing that the GFP signal is often in the vicinity of the presynaptic marker.

(C) High-power image of a GFP reporter-expressing neuron immunostained with an antibody against the ribosomal marker Y10B.

(D) Fluorescence intensity plots for the GFP and PSD-95 signals of the dendrite shown in (A). The mean fluorescence along the width of the dendrite was calculated.

(E) Fluorescence intensity plots for the GFP and synapsin signals of the dendrite shown in (B). The mean fluorescence along the width of the dendrite was calculated.

(F) The cross-correlation functions for GFP and synapsin is shown for the dendrite in (B). The shaded area indicates the results of 100 cross-correlations computed on randomized versions of the data. The upper and lower bounds of the shaded area define the 95% confidence interval.

(G) The cross-correlation functions for GFP and Y10B is shown for the dendrite in (C). The shaded area indicates the results of 100 cross-correlations computed on randomized versions of the data. The upper and lower bounds of the shaded area define the 95% confidence interval.

synthesis in hippocampal CA1 pyramidal cell dendrites via a muscarinic, NMDA-dependent mechanism. J. Neurosci. *13*, 1010–1021.

Frey, U., Krug, M., Reymann, K.G., and Matthies, H. (1988). Anisomycin, an inhibitor of protein synthesis, blocks late phases of LTP phenomena in the hippocampal CA region in vitro. Brain Res. *452*, 57–65.

Huber, K.M., Kayser, M.S., and Bear, M.F. (2000). Role for rapid dendritic protein synthesis in hippocampal mGluR-dependent long-term depression. Science *288*, 1254–1256.

Kacharmina, J.E., Job, C., Crino, P., and Eberwine, J. (2000). Stimulation of glutamate receptor protein synthesis and membrane insertion within isolated neuronal dendrites. Proc. Natl. Acad. Sci. USA *97*, 11545–11550.

Kang, H., and Schuman, E.M. (1996). A requirement for local protein synthesis in neurotrophin-induced synaptic plasticity. Science *273*, 1402–1406.

Kang, H., Shelton, D., Welcher, A., and Schuman, E.M. (1997). Neurotrophins and time: different roles for TrkB signaling in hippocampal long-term potentiation. Neuron *19*, 653–664.

Koenig, E., Martin, R., Titmus, M., and Sotelo-Silveira, J.R. (2000). Cryptic peripheral ribosomal domains distributed intermittently along mammalian myelinated axons. J. Neurosci. *20*, 8390–8400.

Lerner, E.A., Lerner, M.R., Janeway, C.A., and Steitz, J.A. (1981). Monoclonal antibodies to nucleic acid-containing cellular constituents: probes for molecular biology and autoimmune disease. Proc. Natl. Acad. Sci. USA *78*, 2737–2741.

Levine, E.S., Dreyfus, C.F., Black, I.B., and Plummer, M.R. (1995). Brain-derived neurotrophic factor rapidly enhances synaptic transmission in hippocampal neurons via postsynaptic tyrosine kinase receptors. Proc. Natl. Acad. Sci. USA *92*, 8074–8078.

Levine, E.S., Crozier, R.A., Black, I.B., and Plummer, M.R. (1997). Brain-derived neurotrophic factor modulates hippocampal synaptic transmission by increasing N-methyl-D-aspartic acid receptor activity. Proc. Natl. Acad. Sci. USA *95*, 10235–10239.

Li, Y.X., Zhang, Y., Lester, H.A., Schuman, E.M., and Davidson, N. (1998a). Enhancement of excitatory neurotransmitter release induced by BDNF in cultured hippocampal neurons. J. Neurosci. *18*, 10231–10240.

Li, Y.X., Xu, Y., Ju, D., Lester, H.A., Davidson, N., and Schuman, E.M. (1998b). Expression of a dominant negative Trk B receptor, T1, reveals a requirement for presynaptic signaling in BDNF-induced synaptic potentiation in cultured hippocampal neurons. Proc. Natl. Acad. Sci. USA *95*, 10884–10889.

Malgaroli, A., and Tsien, R.W. (1992). Glutamate-induced long-term potentiation of the frequency of miniature synaptic currents in cultured hippocampal neurons. Nature *357*, 134–139.

Martin, K.C., Casadio, A., Zhu, H., E, Y., Rose, J.C., Chen, M., Bailey, C.H., and Kandel, E.R. (1997). Synapse-specific, long-term facilitation of Aplysia sensory to motor synapses: a function for local protein synthesis in memory storage. Cell *91*, 927–938.

Mayford, M., Baranes, D., Podsypanina, K., and Kandel, E.R. (1996). The 3′-untranslated region of CAMKII-alpha is a cis-acting signal for the localization and translation of mRNA in dendrites. PNAS *93*, 13250–13255.

McAllister, A.K., Katz, L.C., and Lo, D.C. (1999). Neurotrophins and synaptic plasticity. Annu. Rev. Neurosci. *22*, 295–318.

Mori, Y., Imaizumi, K., Katayama, T., Yoneda, T., and Tohyama, M. (2000). Two cis-acting elements in the 3′ untranslated region of the alpha-CaMKII regulate its dendritic targeting. Nat. Neurosci. *3*, 1079–1084.

Nguyen, P.V., Abel, T., and Kandel, E.R. (1994). Requirement of a critical period of transcription for induction of a late phase of LTP. Science *265*, 1104–1107.

Otani, S., Marshall, C.J., Tate, W.P., Goddard, G.V., and Abraham, W.C. (1989). Maintenance of long-term potentiation in rat dentate gyrus requires protein synthesis but not messenger RNA synthesis immediately post-tetanization. Neuroscience *28*, 519–526.

Ouyang, Y., Kantor, D.B., Harris, K.M., Schuman, E.M., and Kennedy, M.B. (1997). Visualization of the distribution of autophosphorylated calcium/calmodulin-dependent protein kinase II after tetanic stimulation in the CA1 area of the hippocampus. J. Neurosci. *17*, 5416–5427.

Ouyang, Y., Rosenstein, A., Kreiman, G., Schuman, E.M., and Kennedy, M.B. (1999). Tetanic stimulation leads to increased accumulation of Ca(2+)/calmodulin-dependent protein kinase II via dendritic protein synthesis in hippocampal neurons. J. Neurosci. *19*, 7823–7833.

Patrick, G.N., Zukerberg, L., Nikolic, M., de la Monte, S., Dikkes, P., and Tsai, L.H. (1999). Conversion of p35 to p25 deregulates Cdk5 activity and promotes neurodegeneration. Nature *402*, 615–622.

Rao, A., and Steward, O. (1991). Evidence that protein constituents of postsynaptic membrane are locally synthesized: analysis of proteins synthesized within synaptosomes. J. Neurosci. *11*, 2881–2895.

Schuman, E.M. (1999a). mRNA trafficking and local protein synthesis at the synapse. Neuron *23*, 645–648.

Schuman, E.M. (1999b). Neurotrophin regulation of synaptic transmission. Curr. Opin. Neurobiol. *9*, 105–109.

Sheetz, A.J., Nairn, A.C., and Constantine-Paton, M. (2000). NMDA receptor-mediated control of protein synthesis at developing synapses. Nat. Neurosci. *3*, 211–216.

Srinivasan, Y., Guzikowski, A.P., Haugland, R.P., and Angelides, K.J. (1990). Distribution and lateral mobility of glycine receptors on cultured spinal cord neurons. J. Neurosci. *10*, 985–995.

Stanton, P.K., and Sarvey, J.M. (1984). Blockade of long-term potentiation in rat hippocampal CA1 region by inhibitors of protein synthesis. J. Neurosci. *4*, 3080–3084.

Steward, O. (1997). mRNA localization in neurons: a multipurpose mechanism? Neuron *18*, 9–12.

Steward, O., and Levy, W.B. (1982). Preferential localization of polyribosomes under the base of dendritic spines in granule cells of the dentate gyrus. J. Neurosci. *2*, 284–291.

Steward, O., and Schuman, E.M. (2001). Protein synthesis at synaptic sites on dendrites. Ann. Rev. Neurosci. *24*, 299–325.

Torre, E.R., and Steward, O. (1992). Demonstration of local protein synthesis within dendrites using a new cell culture system that permits the isolation of living axons and dendrites from their cell bodies. J. Neurosci. *12*, 762–772.

Torre, E.R., and Steward, O. (1996). Protein synthesis within dendrites: glycosylation of newly synthesized proteins in dendrites of hippocampal neurons in culture. J. Neurosci. *16*, 5967–5978.

Weiler, I.J., and Greenough, W.T. (1991). Potassium ion stimulation triggers protein translation in synaptoneurosomal polyribosomes. Mol. Cell. Neurosci. *2*, 305–314.

Weiler, I.J., and Greenough, W.T. (1993). Metabotropic glutamate receptors trigger postsynaptic protein synthesis. Proc. Natl. Acad. Sci. USA *90*, 7168–7171.

Wells, D.G., Richter, J.D., and Fallon, J.R. (2000). Molecular mechanisms for activity-regulated protein synthesis in the synapto-dendritic compartment. Curr. Opin. Neurobiol. *10*, 132–137.

Wey, C.L., Cone, R.A., and Edidin, M.A. (1981). Lateral diffusion of rhodopsin in photoreceptor cells measured by fluorescence photobleaching and recovery. Biophys. J. *33*, 225–232.

Wu, L., Wells, D., Tay, J., Mendis, D., Abbott, M.-A., Barnitt, A., Quinlan, E., Heynen, A., Fallon, J.R., and Richter, J.D. (1998). CPEB-mediated cytoplasmic polyadenylation and the regulation of experience-dependent translation of α-CAMKII mRNA at synapses. Neuron *21*, 1129–1139.

Alu sequences from GC-rich DNA are likely to be harmful and prevented from spreading in the population by natural selection. This implies no functional importance for an Alu sequence itself, but merely that, as the deletions of Alus are very unlikely to be precise, a deletion event removing an Alu is also likely to remove valuable sequences around it, and the chromosome bearing the deletion will be lost by selection.

The explanation favoured by the authors for Alu enrichment in gene-rich regions is that of positive selection in favour of Alus in GC-rich DNA. This theory, however, cannot explain the observations. The data show that Alu sequences up to five million years old are not enriched in GC-rich regions. But in human population genetics, estimated times to common ancestry of typical genomic regions show that Alu sequences which are five million years old have already been fixed (found in all individuals) in the population. This observation is also what would be expected from neutrality and genetic drift, given the human effective population size. (Alu sequences which are truly advantageous will spread to fixation much more quickly.) Earlier human ancestors would also be expected to have had similar fixation times for Alu insertions. Yet it is only during the spread to fixation of Alu sequences that positive natural selection has any opportunity to act. Thus, an increasing abundance of Alu sequences in GC-rich DNA as they age beyond five million years cannot be the result of natural selection for positive functions of Alu insertions.

**References**

1. International Human Genome Sequencing Consortium: **Initial sequencing and analysis of the human genome.** *Nature* 2001, **409**:860-921.
2. Baltimore D: **Our genome unveiled.** *Nature* 2001, **409**:814-816.

Address: Institute of Genetics, University of Nottingham, Queens Medical Centre, Nottingham NG7 2UH, UK.
E-mail john.brookfield@nottingham.ac.uk

**Primer**

# Local protein synthesis in neurons

W. Bryan Smith, Girish Aakalu and Erin M. Schuman

The processing power of the mammalian brain is derived from the tremendous interconnectivity of its neurons. An individual neuron can have several thousand synaptic connections. While these associations yield computational power, it is the modification of these synapses that gives rise to the brain's capacity to learn, remember and even recover function after injury. Inter-connectivity and plasticity come at the price of increased complexity as small groups of synapses are strengthened and weakened independently of one another (Figure 1). When one considers that new protein synthesis is required for the long-term maintenance of these changes, the delivery of new proteins to the synapses where they are needed poses an interesting problem (Figure 1). Traditionally, it has been thought that the new proteins are synthesized in the cell body of the neuron and then shipped to where they are needed. Delivering proteins from the cell body to the modified synapses, but not the unmodified ones, is a difficult task. Recent studies suggest a simpler solution: dendrites themselves are capable of synthesizing proteins. Thus, proteins could be produced locally, at or near the synapses where they are needed. This is an elegant way to achieve the synapse specific delivery of newly synthesized proteins.

Local protein synthesis is not unique to neurons. It is one of the primary mechanisms that organisms use to determine cell fate and generate differences among cells.

**Figure 1**

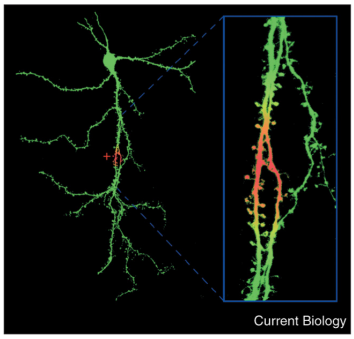


Specificity of synaptic enhancement in neurons. Shown is a single pyramidal neuron with its cell body and dendrites filled with GFP. The small protrusions that occur along the dendrites are the spines, the postsynaptic compartment onto which synapses are made. Highlighted in red is a putative area of synaptic enhancement with the adjacent yellow area depicting regions that might show a lesser amount of enhancement. During long-lasting synaptic plasticity, the spines in the enhanced area of the dendritic tree, but not the adjacent green areas, need to receive newly synthesized proteins.

For example, to achieve cellular differentiation, the *Drosophila* oocyte creates a polarized distribution of mRNA species. The mRNAs are localized and anchored to different poles of the cell *via* motifs in their 3′ untranslated regions (UTRs). The mRNAs are then locally translated to create different regions of the cell and later different daughter cells. Local protein synthesis is even used by unicellular organisms such as *Saccharomyces cerevisiae* to determine cell fate. mRNA for a factor that regulates mating type is shipped from the mother cell to the budding daughter cell, once again based on *cis*-acting elements in its 3′ UTR. The protein product restricts only the daughter cell's mating type.

Local protein synthesis is also used to create functional micro-domains within cells. Myelinating cells such as oligodendrocytes produce processes that function as

**Figure 2**

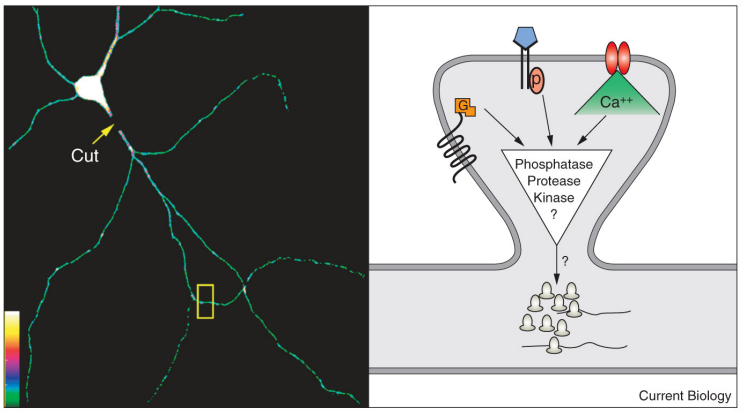


The physical isolation of dendrites from the cell body provides a definitive demonstration of local protein synthesis. Left panel: Shown is a hippocampal neuron expressing a dendritic protein synthesis reporter. A small cut isolates the cell body from the dendrites. In this cell, the application of a growth factor to the isolated dendrite resulted in dendritic protein synthesis. Right panel: Biochemical cascades that may result in protein synthesis activation. A single dendritic spine is illustrated with ribosomes at the base of the spine. Synaptic activation of metabotropic (black), growth factor (blue) and ionotropic (red) receptors may lead to dendritic protein synthesis activation through unknown intermediates.

lipid sheaths to electrically insulate axons. They do this by producing a protein called myelin basic protein that collapses the oligodendrocyte cell membrane, thus squeezing the cytoplasm out of the region where it is expressed. If myelin basic protein were produced in a cell-wide manner it would be toxic. Therefore, restricted translation of myelin basic mRNA is carried out in the oligodendrocyte processes.

Microdomains are useful not only for avoiding toxicity, but also for allowing distributed control of cellular function. Axonal growth illustrates this principle quite well. The growth cone of a developing axon must sort through a dizzying array of attractive and repulsive cues to determine how to reach the appropriate target tissue. To accomplish this task, the growth cone requires specific proteins based on environmental cues it encounters. However, the growth cone is frequently millimeters away from the soma. To solve this problem, the growth cone might locally synthesize the required proteins when it needs them. Several recent studies suggest that this is the case.

What is the evidence that distributed protein synthesis might occur during long-lasting plasticity? An early hint that local protein synthesis might occur within the dendritic compartment of neurons was the anatomical observation of synapse-associated polyribosome clusters at the base of the dendritic spine apparatus (Figure 2, right). Since those ultrastructural studies, an entire complement of translational machinery has been detected in dendrites. Additionally, several mRNA molecules are localized to the dendritic domain of neurons. Although these studies show that the components for local protein synthesis are present, they do not show that this synaptic translational machinery is actually used in response to synaptic activity.

Direct evidence supporting the local synthesis hypothesis was reported in a study by Feig and Lipton. The authors used [$^3$H]-leucine incorporation to show that new proteins were synthesized in the dendritic regions of hippocampal slice tissue following electrical stimulation. The stimulation protocol used in these studies, however, did not alter the strength of synaptic connections. In experiments using growth factor application to hippocampal slices, Kang and Schuman showed the first causal link between local protein synthesis and synaptic enhancement. In this study, brain-derived neurotrophic factor (BDNF) or neurotrophin-3 (NT-3) application to hippocampal slices was shown to elicit a long-lasting synaptic enhancement that was blocked when the tissue was pre-incubated with protein synthesis inhibitors.

In all local protein synthesis experiments, the burden of proof is to show that new proteins are made in the dendrites, not the cell body. Due to the laminar structure of the hippocampal slice, the authors were able to make microlesions that physically separated the cell bodies from the dendrites. Interestingly, even when the dendritic region was isolated, the growth factor-induced enhancement was still sensitive to protein synthesis inhibitors. Although consistent with a dendritic source of protein synthesis, this study could not distinguish between protein synthesis in dendrites, axons, glial cells or local interneurons — all of which are found within the isolated 'dendritic' laminae of hippocampal tissue.

Further evidence of activity-dependent local protein synthesis within neuronal processes has since been reported. In hippocampal slices, one form of long-term depression requires local synthesis. In the marine mollusk *Aplysia*, serotonin application results in a long-term synaptic facilitation that requires protein synthesis in the

neurites. Other studies have detected local synthesis of proteins such as calcium/calmodulin-dependent protein kinase (CamKII) following synaptic plasticity. While the data from these experiments are compelling, they lack the temporal resolution to actually watch the protein synthesis occur over time. In our recent work, we used green fluorescent protein (GFP) in combination with time-lapse microscopy to investigate local protein synthesis in dendrites of cultured hippocampal neurons. In order to rule out the cell body as a potential source of the GFP signal measured in the dendrites, we used two distinct methods of isolating the dendrites from the cell bodies. The first set of experiments employed dendritic transections, in which the dendrites were physically cut away from the cell bodies (Figure 2, left). In a less-invasive approach, the GFP in the cell body was continuously photobleached, and fluorescence was monitored in the distal dendrites. We showed that BDNF application in both experimental preparations resulted in increased GFP production in the isolated dendrites. These experiments provided the first dynamic visual proof of local protein synthesis in dendrites.

An important aspect of local protein synthesis within a micro-domain of any cell type is the transport of mRNA to the appropriate location within the cell. In the case of CamKII, *cis*-acting elements have been identified within the 3′ UTR of the mRNA molecule that are necessary and sufficient to target the message to the dendritic region of hippocampal neurons. A consensus targeting sequence has yet to be identified, but it does appear as though targeting sequences reside in the 3′ UTRs of other messages as well. Several studies show that the mRNA-binding protein Staufen, which is critically involved in mRNA localization in the *Drosophila* embryo, may also participate in mRNA trafficking to neuronal dendrites.

In addition to specific transport requirements, if a message is to have a local effect only at its destination — often a distance of several hundred microns from the nucleus — there must be control over translation of the mRNA. Without translational regulation, the protein could be produced *en route* to its destination, thereby negating any specificity that arises as a result of local synthesis. It has been recently shown that a host of mRNA binding proteins work in concert to restrict translation of certain mRNA species until the appropriate time when the protein is to be produced. Central to this process is the cytoplasmic poly-adenylation element (CPE) found in the 3′ UTR of many messages. The CPE is bound by CPE-binding protein, which forms a complex with other RNA binding proteins thus regulating translation of these messages. As the 3′ UTR sequences of more mRNAs become available, it will be interesting to discover the role the CPE and other mRNA elements play in controlling local mRNA translation.

If dendritic protein synthesis is a requirement for long-term synaptic enhancement, to what extent is activity-induced protein synthesis restricted to activated synaptic sites? In order to answer this question of synapse specificity, experiments that address the precise spatial limits of protein synthesis induction during synaptic activation must be carried out. With such information, we will begin to understand the contribution of locally synthesized synaptic proteins to the subcellular specificity of neuronal communication.

Ultimately, the upstream biochemical signaling events that lead to protein synthesis activation need to be elucidated (Figure 2, right). By understanding the transduction mechanisms that various extracellular signals use to regulate protein synthesis machinery and how differences in these signaling cascades result in translation of distinct subsets of mRNA species, a defined role for activity-dependent local translation in mature dendrites will begin to unfold.

## Key references

Aakalu G, Smith WB, Nguyen N, Jiang C, Schuman EM: **Dynamic visualization of local protein synthesis in hippocampal neurons.** *Neuron* 2001, **30:**489-502.

Bassell GJ, Zhang H, Byrd AL, Femino AM, Singer RH, Taneja KL, Lifshitz LM, Herman IM, Kosik KS: **Sorting of beta-actin mRNA and protein to neurites and growth cones in culture.** *J Neurosci* 1998, **18:**251-265.

Engert F, Bonhoeffer T: **Synapse specificity of long-term potentiation breaks down at short distances.** *Nature* 1997, **388:**279-284.

Huber KM, Kayser MS, Bear MF: **Role for rapid dendritic protein synthesis in hippocampal mGluR-dependent long-term depression.** *Science* 2000, **288:**1254-1257.

Kang H, Schuman EM: **A requirement for local protein synthesis in neurotrophin-induced hippocampal synaptic plasticity.** *Science* 1996, **273:**1402-1406.

Martin KC, Casadio A, Zhu HEY, Rose JC, Chen M, Bailey CH, Kandel ER: **Synapse-specific, long-term facilitation of aplysia sensory to motor synapses: a function for local protein synthesis in memory storage.** *Cell* 1997, **91:**927-938.

Ouyang Y, Rosenstein A, Kreiman G, Schuman EM, Kennedy MB: **Tetanic stimulation leads to increased accumulation of $Ca^{2+}$/calmodulin-dependent protein kinase II via dendritic protein synthesis in hippocampal neurons.** *J Neurosci* 1999, **19:**7823-7833.

Schuman EM, Madison DV: **Locally distributed synaptic potentiation in the hippocampus.** *Science* 1994, **263:**532-536.

Steward O, Schuman EM: **Protein synthesis at synaptic sites on dendrites.** *Annu Rev Neurosci* 2001, **24:**299-325.

Steward O, Levy WB: **Preferential localization of polyribosomes under the base of dendritic spines in granule cells of the dentate gyrus.** *J Neurosci* 1982, **2:**284-291.

Wells DG, Richter JD, Fallon JR: **Molecular mechanisms for activity-regulated protein synthesis in the synapto-dendritic compartment.** *Curr Opin Neurobiol* 2000, **10:**132-137.

Address: HHMI/Division of Biology, Caltech, Pasadena, California 91125, USA.
E-mail: schumane@its.caltech.edu

# Activation-dependent changes in receptor distribution and dendritic morphology in hippocampal neurons expressing $P2X_2$-green fluorescent protein receptors

**Baljit S. Khakh*, W. Bryan Smith, Chi-Sung Chiu, Donghong Ju, Norman Davidson, and Henry A. Lester**

Division of Biology, 156-29, California Institute of Technology, Pasadena, CA 91125

Contributed by Norman Davidson, February 21, 2001

**ATP-gated $P2X_2$ receptors are widely expressed in neurons, but the cellular effects of receptor activation are unclear. We engineered functional green fluorescent protein (GFP)-tagged $P2X_2$ receptors and expressed them in embryonic hippocampal neurons, and report an approach to determining functional and total receptor pool sizes in living cells. ATP application to dendrites caused receptor redistribution and the formation of varicose hot spots of higher $P2X_2$-GFP receptor density. Redistribution in dendrites was accompanied by an activation-dependent enhancement of the ATP-evoked current. Substate-specific mutant T18A $P2X_2$-GFP receptors showed no redistribution or activation-dependent enhancement of the ATP-evoked current. Thus fluorescent $P2X_2$-GFP receptors function normally, can be quantified, and reveal the dynamics of $P2X_2$ receptor distribution on the seconds time scale.**

ion channel | ATP | filopodia

Cationic P2X receptors mediate the "fast" milliseconds time scale actions of ATP in the nervous system (1, 2). The identity of most natively expressed P2X receptors is unclear, but many neurons express $P2X_2$ mRNA, $P2X_2$ proteins, and functional $P2X_2$-like receptors (2). For example, ATP mediates synaptic transmission in a portion of CA1 neurons (3), and postnatal hippocampal neurons express P2X receptors, which include $P2X_2$ subunits (3–7). Moreover, cytosolic ATP concentration is 1–5 mM, and ATP released during tissue damage activates neuronal P2X receptors in the periphery (1). ATP released as a synaptic transmitter and during ischemia of brain neurons may contribute to pathophysiology, but there are no available data on the cellular consequences of $P2X_2$ receptor activation or on the dynamic aspects of $P2X_2$ receptor distribution in brain neurons.

This study used $P2X_2$ receptors tagged with green fluorescent protein (GFP) in a quantitative method to study receptors expressed with recombinant Sindbis virus in embryonic hippocampal neurons. We report (*i*) the properties of functional GFP-tagged $P2X_2$ receptors, (*ii*) an optical and electrophysiological approach to measuring receptor numbers in living cells, and (*iii*) the cellular effects of P2X receptor activation.

## Materials and Methods

**Molecular Biology.** By PCR the $P2X_2$ stop codon was removed and the FLAG (f) epitope was inserted in frame with the $P2X_2$ cDNA cDNA (9). In the same PCR we inserted an *Xho*I site in the DNA. We generated GFP37 (10) with a *Xho*I site before the start codon and subcloned it into $P2X_2$-f between the *Xho*I site 3′ of the FLAG epitope and *Hin*dIII in the pcDNA3 polylinker to yield $P2X_2$-GFP. The $P2X_2$-f-GFP fragment was inserted into pSinRep5 between the *Stu*I and *Apa*I sites, and infective Sindbis particles were generated with the use of the Sindbis Expression System (http://www.invitrogen.com/). Site-directed mutagenesis was performed on the cDNAs with the use of synthetic oligonucleotides to generate K69A and T18A mutants (Quick Change; Stratagene).

**Electrophysiology and Imaging.** All cell preparations, two-electrode voltage-clamp recording of oocytes, and whole-cell patch recording of hippocampal neurons were performed by previously described methods (5, 11). Puffs (5 ms) of ATP (100 $\mu$M) were applied directly by pressure microejection to dendrites, soma, or neurites of the cell under voltage clamp (5–20 psi; 1 psi = 6.89 kPa) from 7- to 10-M$\Omega$ pipettes, with the use of a Picospritzer II (General Valve, Fairfield, NJ). We imaged hippocampal neurons with an Olympus Fluoview confocal microscope and software (http://www.olympus.com), but all analysis was performed with NIH IMAGEJ (http://rsb.info.nih.gov/ij/) and with the Fluoview software. We used an Olympus $\times$40 oil-immersion objective with a numerical aperture of 1.3. We applied test solutions to cells during imaging by switching among an array of parallel quartz tubes (320 $\mu$m i.d. and 450 $\mu$m o.d., ending $\approx$0.2 mm from the cell).

**Data Analysis.** Data were analyzed with CLAMPFIT (Axon Instruments) or ORIGIN 5.0 (Microcal Software, Northampton MA; http://www.MICROCAL.com/). Data in the text and graphs are shown as mean $\pm$ SEM from $n$ determinations as indicated. We estimated the size of the somatic compartment by applying $-5$ mV voltage jumps to neurons under voltage clamp ($-60$ mV) and with the use of the following relations: $R_s = \delta V / I_{in}$ and $C_m = \tau / R_s$, where $R_s$ is the series resistance, $\delta V$ is the change in voltage (5 mV), $I_{in}$ is the amplitude of the instantaneous current, $C_m$ is the capacitance, and $\tau$ is the time constant for the relaxation of the capacitive transient; we assumed a membrane capacitance of 0.92 pF/100 $\mu m^2$ (12). We measured the number of receptors in the somatic compartment by using the relation $I = n \cdot i \cdot p_o$, where $I$ is the peak of the macroscopic current, $i$ is the unitary current at $-60$ mV ($\approx$1 pA), $p_o$ is the open probability (0.6), and $n$ is the number of receptors open at the peak (13). For the optical determination of receptor density the measured pixel intensity was divided by 4 because the receptors are multimeric (1) and by 2 because $\approx$50% of the neuron surface is attached to the glass coverslip; the receptors here are not expected to be gated by ATP. The adjusted pixel intensity (14) was used to determine receptor numbers from standard curves (Fig. 2*F*). The coefficient of variance = SD divided by the mean for $n$ trials, where the $n$th trial is at most 20.

Abbreviations: GFP, green fluorescent protein; wt, wild type.

*To whom reprint requests should be sent at present address: Medical Research Council, Laboratory of Molecular Biology, Cambridge CB2 2QH, United Kingdom. E-mail: bsk@mrc-lmb.com.ac.uk.

The publication costs of this article were defrayed in part by page charge payment. This article must therefore be hereby marked "*advertisement*" in accordance with 18 U.S.C. §1734 solely to indicate this fact.



www.pnas.org/cgi/doi/10.1073/pnas.081089198

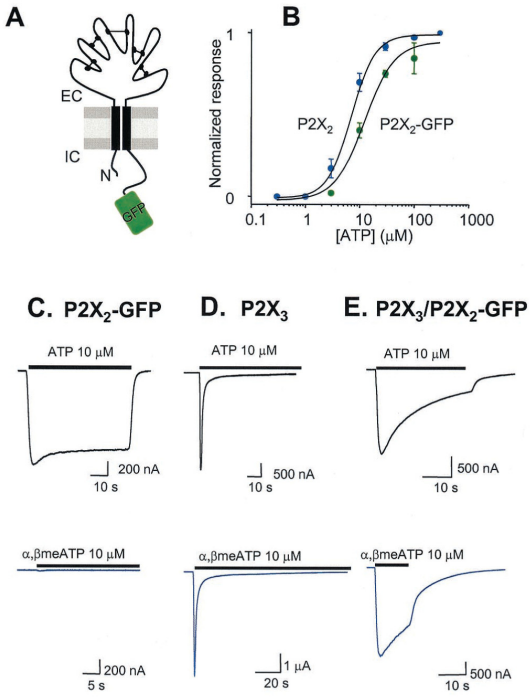


**Fig. 1.** Properties of $P2X_2$-GFP receptors. (*A*) Diagram of $P2X_2$-GFP receptor subunit topology. The folds in the extracellular loop represent hypothesized cysteine-cysteine linkages (1). (*B*) ATP concentration–effect curves for wt $P2X_2$ and $P2X_2$-GFP receptors. (*C–E*) Representative ATP and $\alpha,\beta$-methylene-ATP-evoked current waveforms from cells expressing $P2X_2$-GFP (*C*), $P2X_3$ (*D*), and $P2X_3/P2X_2$-GFP receptors (*E*). The ATP-evoked currents desensitized by 16 ± 1%, 91 ± 1% ($\tau 1 = 0.9 \pm 0.2$ s, $\tau 2 = 9 \pm 2$ s), and 63 ± 3% for $P2X_2$, $P2X_3$, and $P2X_3/P2X_2$-GFP receptors, respectively. The $\alpha,\beta$-methylene-ATP-evoked currents desensitized by 91 + 5% ($\tau 1 = 1.0 + 0.1$ s, $\tau 2 = 13 + 2$ s) and 51 + 6% for $P2X_3$ and $P2X_3/P2X_2$-GFP receptors, respectively.

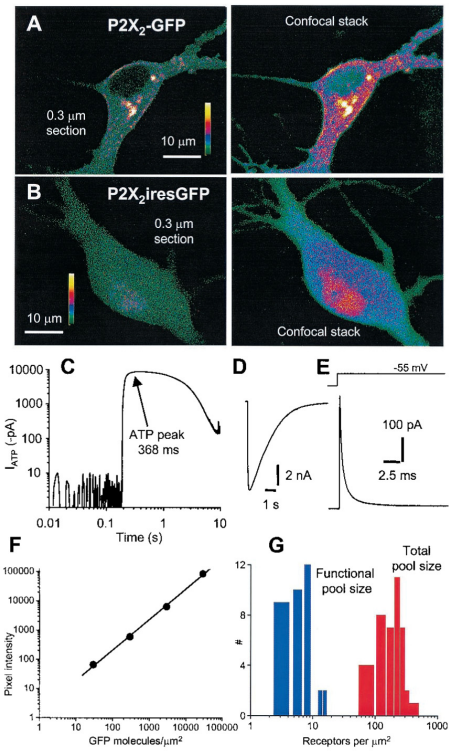


**Fig. 2.** Quantification of $P2X_2$-GFP receptors in embryonic hippocampal neurons. (*A*) (*Left*) An image through the soma of a neuron expressing $P2X_2$-GFP receptors. (*Right*) A confocal stack of 25 optical sections of the same neuron spaced at 0.3 $\mu$m. (*B*) (*Left*) An image through the soma of a neuron expressing GFP from a bicistronic $P2X_2$iresGFP mRNA. (*Right*) A confocal stack of 25 optical sections of the same neuron spaced at 0.3 $\mu$m. (*C*) Representative ATP-evoked current (100 $\mu$M, 0.5 s pulse on to soma) shown on double log scales to show that the peak was calculated at the plateau of the response at 368 ms (peak current −8.5 ± 0.5 nA, 10–90% rise time 82 ± 20 ms, 90–10% decay time 2.9 ± 0.2 s; $n = 36$). (*D*) The same current waveform as in *C*, but on linear scales. (*E*) Representative current in response to a 5 mV step from −60 mV. The trace was analyzed with the use of an equivalent circuit of the neuron somatic compartment, where $V_p$ is the pipette potential (−60 mV), $R_s$ is the series resistance (15 ± 1 MΩ), $R_m$ is the membrane resistance (741 ± 119 MΩ), $V_m$ is the membrane potential, and $C_m$ is the membrane capacitance (24.5 ± 1.6 pF; all $n = 36$). (*F*) Standard curve of GFP fluorescence intensity for agarose beads with various densities of GFP bound to the surface (14). The pixel intensity is the fluorescence intensity per pixel$^2$ of the bead surface. For high GFP densities (>100,000 GFP molecules per $\mu$m$^2$) the intensity was saturating and thus measurements were made with a neutral density filter between the objective and the charge-coupled device, and the absolute values were corrected *post hoc* (14). (*G*) Distribution of numbers of $P2X_2$ receptors per $\mu$m$^2$.

## Results

**Properties of $P2X_2$ Receptors Tagged with GFP.** We ligated GFP (10) in frame onto the C terminus of $P2X_2$ receptors (Fig. 1*A*). When expressed in *Xenopus* oocytes, $P2X_2$-GFP and wild-type (wt) receptors are similar with respect to ATP $EC_{50}$ (Fig. 1*B*) peak currents, desensitization kinetics, and suramin block {ATP $EC_{50}$ 6.5 ± 0.9 and 13.5 ± 1.5 $\mu$M, Hill slopes 1.7 ± 0.1 and 2.1 ± 0.2, for wt ($n = 8$) and $P2X_2$-GFP receptors ($n = 9$); 30 $\mu$M suramin block was 86 ± 11% and 91 ± 2%, and $k_{+1}$ was 1.2 ± 0.4 and $1.2 \pm 0.2 \times 10^4$ $M^{-1}s^{-1}$ for wt ($n = 3$) and $P2X_2$-GFP receptors ($n = 9$); where $k_{+1} = 1/\tau$[suramin]}. $P2X_2$-GFP receptors also formed a heteromer with $P2X_3$ (15), as indicated by a slowly desensitizing response to 10 $\mu$M $\alpha,\beta$-methylene-ATP, whereas $P2X_2$-GFP receptors did not respond to this agonist and $P2X_3$ receptors responded with rapidly desensitizing currents (Fig. 1 *C–E*). Thus wt and $P2X_2$-GFP receptors are similar, with the exception that $P2X_2$-GFP receptors fluoresce under blue light and thus provide a noninvasive marker for receptor location in living cells (Fig. 2).

**Density of $P2X_2$-GFP Receptors in Hippocampal Neurons.** We used Sindbis virus constructs (16) to express $P2X_2$-GFP, GFP, $P2X_2$iresGFP, T18A $P2X_2$-GFP, or K69A $P2X_2$-GFP receptors in embryonic hippocampal neurons, which are devoid of P2X receptors at this stage of development (5). Confocal laser scanning microscopy revealed that expression of $P2X_2$-GFP resulted in green fluorescence that localized to the plasma membrane and the cytosol (Fig. 2*A*), whereas expression of $P2X_2$iresGFP resulted in cytosolic green fluorescence (Fig. 2*B*). Membrane and cytosolic $P2X_2$-GFP fluorescence was notable in 0.3 $\mu$m optical sections (Fig. 2*A*), demonstrating that some $P2X_2$-GFP receptors are cytosolic, as is the case for natively expressed P2X receptors (17, 18). Capacitance measurements showed that somatic membrane area was 2449 ± 159 $\mu$m$^2$ ($n = 36$), and by measuring the peak currents evoked by a pulse of 100

$\mu$M ATP ($-8.5 \pm 0.5$ nA; $n = 36$, Fig. 2 *C* and *D*) we determined that the Sindbis vector directs the membrane expression of $6.3 \pm 0.5$ $P2X_2$-GFP receptors per $\mu m^2$ (Fig. 2 *G*; $n = 36$; see *Materials and Methods*), thus defining the somatic functional receptor pool size for these experiments.

We next exploited the fixed stoichiometry between $P2X_2$ and GFP in the fusion construct and used fluorescence microscopy to measure the somatic total $P2X_2$-GFP receptor pool size. The characterization used transparent beads with calibrated surface densities of GFP quantified with the use of an epifluorescence microscope (14) (Fig. 2*F*). We compared the fluorescence intensity of the soma with the fluorescence intensity per square micrometer of calibrated bead surface, which served as an optical standard (14). We found a value of $208 \pm 14$ receptors per $\mu m^2$ ($n = 42$) for the total somatic receptor pool size (Fig. 2*G*). Thus most $P2X_2$-GFP receptors are cytosolic, and this pool may be a source and sink for delivery to the plasma membrane.

**ATP-Induced Formation of Varicose $P2X_2$-GFP Hot Spots.** We collected images during a 1–5 min control period, then applied a pulse of either 100 $\mu$M glutamate or 100 $\mu$M ATP (10–30 s) and imaged filopodia with confocal laser scanning microscopy. We observed no change in the distribution of fluorescence with glutamate application, but during ATP application some areas increased in fluorescence; in addition, the apparent size of the fluorescent area increased within 5–10 s (Fig. 3 *A–D*). Thus ATP produced varicose hot spots (Fig. 3 *C* and *D*). The formation of varicosities was supported by similar observations in neurons infected with $P2X_2$iresGFP ($n = 8$), and this provides strong proof for a change in dendritic morphology. To quantify hot spot size we measured the intensity of pixels along a control line, during glutamate application and ATP application. Representative images of filopodia are shown in Fig. 3 *A–C*, and normalized plots for 23 line profiles are shown in Fig. 3*D*. Glutamate caused no change in the fluorescence profiles, but ATP increased the width of $P2X_2$-GFP receptor-expressing areas in regions where hot spots occur ($n = 23$). Hot spot width (at the base of the line profiles) was $1.8 \pm 0.2$ $\mu$m initially and $1.8 \pm 0.2$ $\mu$m with glutamate, but $2.9 \pm 0.3$ $\mu$m after ATP ($n = 23$). Thus the ATP-evoked hot spots in filopodia have a diameter approaching that of the varicosities, at $\approx 3$ $\mu$m.

We next chose regions of interest, *post hoc,* where hot spots formed *de novo*. We compared data on regions of interest for 86 hot spots before and during ATP application. On average there was a net increase in pixel intensity or $P2X_2$-GFP receptors in regions of interest by $66 \pm 6\%$ ($n = 86$), but pixel intensity decreased in other nearby areas within the same filopodium (Fig. 3 *E* and *F*), and there was no net increase in spatially integrated intensity (Fig. 3*E*) over entire dendritic arbors. These data imply that $P2X_2$-GFP hot spots occur because existing receptors redistribute during activation (Fig. 3).

Simple ATP-evoked depolarization is not the cause of redistribution because glutamate (100 $\mu$M) and KCl (15 mM; data not shown) did not affect $P2X_2$-GFP distribution (Fig. 3). Furthermore, we observed no ATP-evoked currents or changes in the distribution of fluorescence in neurons that expressed GFP alone or mutant K69A $P2X_2$-GFP receptors (see *Materials and Methods*; $n = 4$, Fig. 4 *A* and *C*), in which ATP binding is disrupted (19). Therefore there are no native ATP receptors that contribute to either the optical or electrophysiological responses described in this study. This observation adds credence to the analysis used to determine receptor numbers (Fig. 2 and *Materials and Methods*)

P2X receptors have at least two open states ($I_1$ and $I_2$) that differ in their permeability to organic cations. The $I_2$ state is entered in an ATP-dependent manner, has higher permeability than the $I_1$ state to some cations (5, 11, 20–22), and is absent in mutant T18A P2X receptors (23) with a disrupted protein kinase C site in the amino tail (24). In contrast to $P2X_2$-GFP receptors, mutant T18A $P2X_2$-GFP receptors did not redistribute when ATP was applied ($n = 11$, Fig. 4 *B* and *C*). T18A $P2X_2$-GFP receptors displayed rapidly desensitizing ATP-evoked responses ($n = 16$; >95% desensitization, 90–10% decay time $= 0.9 \pm 0.1$ s, and 10–90% rise time $= 59 \pm 14$ ms for a 2.5 s 100 $\mu$M ATP pulse; Fig. 4*C*), whereas $P2X_2$-GFP responses desensitized by <10% ($n = 5$; Fig. 4*C*). T18A mutant receptors are useful because they allow $P2X_2$ receptor responses to be assigned to a particular channel state, and we interpret the rapid desensitization kinetics in T18A mutants as indicative of the presence of only the $I_1$ state (23). Overall these data imply that $P2X_2$-GFP receptor redistribution and varicosity formation require prolonged $P2X_2$ receptor function, for instance, as produced by the $I_2$ state.

**Activation-Dependent Run-Up of the $P2X_2$ Current.** Our imaging experiments show that $P2X_2$-GFP receptor activation causes redistribution of fluorescence and a change in morphology, but it remained unclear whether $P2X_2$-GFP receptors move in the plasma membrane as a result of activation. To address the latter, we tested electrophysiologically for stimulation-evoked changes in functional $P2X_2$ receptors by applying ATP briefly (4–10 ms) to soma and dendrites of hippocampal neurons to approach the brevity of synaptic ATP release (25).

When ATP was puffed at a frequency of less than 0.1 Hz, the measured responses differed only slightly from puff to puff by ≤10% (the coefficient of variance was $8.9 \pm 2.2\%$ within a train of 20 responses at 0.1 Hz, and the peak of the first puff was $560 \pm 371$ pA; $n = 3$). But, remarkably, at a frequency of 1 Hz, the ATP-evoked currents increased in amplitude by $254 \pm 45\%$ from $290 \pm 64$ pA at the first puff (Fig. 5*A*; $n = 12$ of 15 neurons; three neurons showed no run-up) of the initial amplitude within 10 responses. The increase could be described by a rate constant of $\approx 0.7$ $s^{-1}$ ($1/\tau$; Fig. 5*B*). The coefficient of variance for puffs 1 through 10 was $23.5 \pm 3.5\%$ ($n = 12$), reflecting the activation-dependent run-up of the ATP-evoked current, but for trials 11 through 20 the coefficient of variance was $5.5 \pm 2.2\%$ ($n = 12$). Our measurements indicate that ≈300 $P2X_2$ receptors are activated during the first puff and, on average, that the number of functional receptors doubles within 10 repetitive puffs at 1 Hz.

Run-up was not observed when glutamate was similarly applied to hippocampal neurons ($35 \pm 13$ pA at first puff, $n = 3$; Fig. 5*B*), when ATP was applied to superior cervical ganglion neurons ($87 \pm 31$ pA at first puff, $n = 5$; Fig. 5*B*), or when ATP was applied to hippocampal neurons expressing T18A $P2X_2$-GFP mutant receptors ($1018 \pm 121$ pA at first puff; Fig. 5*B*). We also examined $P2X_3$ receptors in small-diameter dorsal root ganglion neurons; as expected, the ATP-evoked currents showed marked desensitization between trials (26) ($426 \pm 86$ pA at first puff, $n = 15$; Fig. 5*B*). Accepting the limitation that the glutamate-evoked currents were smaller than the ATP-evoked currents, we interpret these data to indicate that the ATP response in hippocampal neurons (Fig. 5*A*) was not an artifact of the puffer.

## Discussion

The present study shows that $P2X_2$ receptors tagged with GFP are functional. There were more $P2X_2$-GFP receptors in the cell than functional receptors in the membrane, and we present an electrophysiological and optical approach to measuring the number of functional receptors and the total number of receptors in living cells. We expect that similar approaches that use calibrated beads (14) as standards can be used to quantify the expression of any biologically interesting GFP-tagged proteins or organelles such as synaptic vesicles, in living cells in real time. In a previous study, $P2X_1$ receptors tagged with GFP on the C terminus were reported to internalize during ATP applications

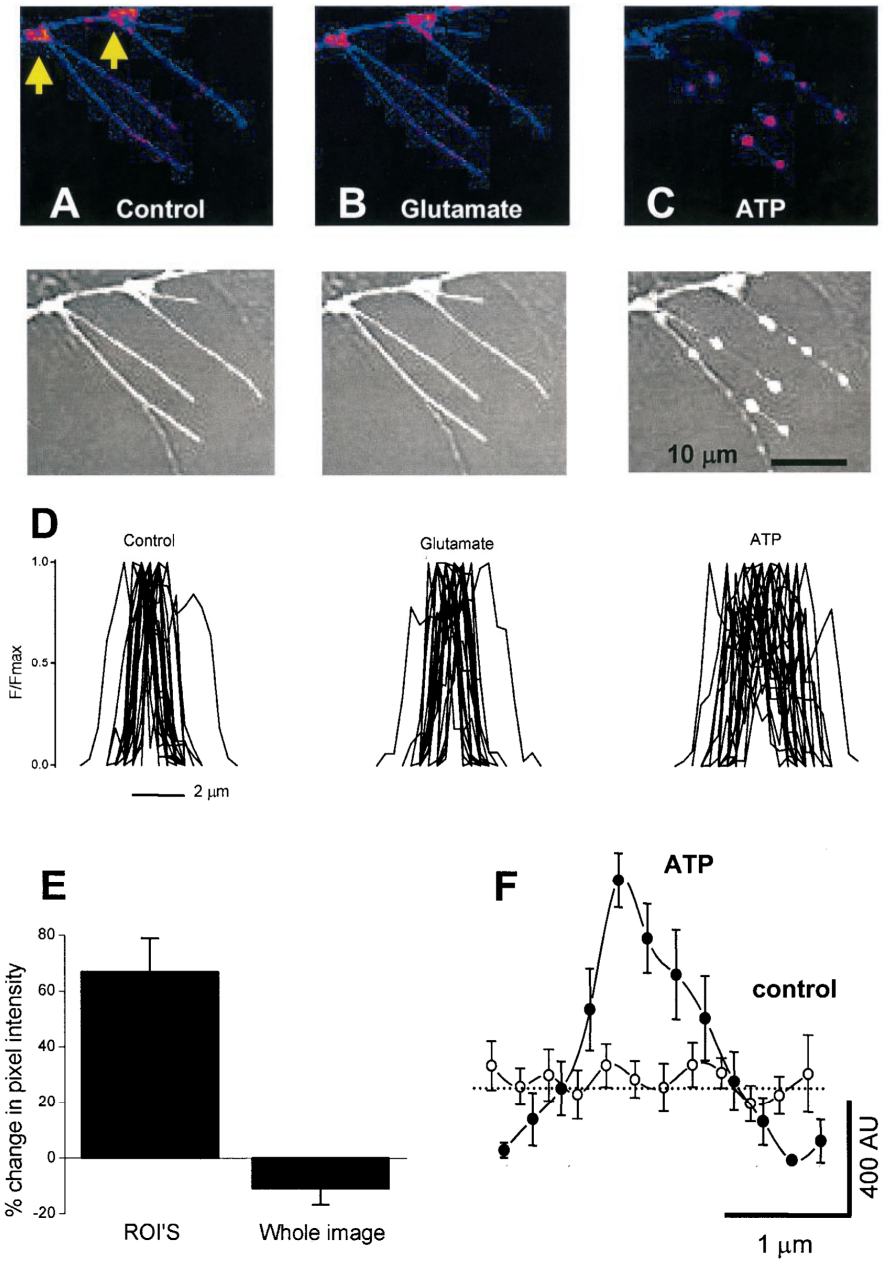


**Fig. 3.** ATP-dependent redistribution of P2X receptors in hippocampal neurons. (*A–C*) (*Upper*) False color images of filopodia from hippocampal neurons expressing $P2X_2$-GFP. (*Lower*) Overlay of gray-scale fluorescence and bright-field images. (*Left*) The control image. (*Center*) With 100 $\mu$M glutamate. (*Right*) With 100 $\mu$M ATP. (*D*) Twenty-three intensity profiles across filopodia for control, in glutamate, and in the presence of ATP. (*E*) ATP-evoked changes in integrated pixel intensity of whole dendritic arbors and regions of interest (ROI's). (*F*) Average line profile along 10 hot spots before and during ATP. AU, arbitrary units. Note the peak of the hot spot has higher fluorescence, but that $\approx$1 $\mu$m from the peak, the intensity falls to values lower than in the control.

(27). In contrast, we found no evidence for net internalization or externalization of $P2X_2$-GFP receptors expressed in hippocampal neurons when ATP was applied.

During $P2X_2$-GFP receptor activation by ATP, we observed (*i*) the formation of varicose hot spots, (*ii*) $P2X_2$-GFP redistribution over micrometer distances, and (*iii*) an activation-

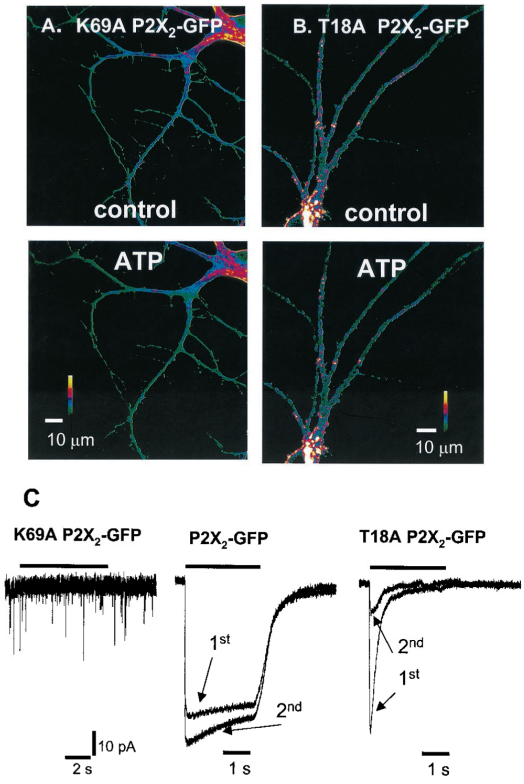


**Fig. 4.** $P2X_2$-GFP hot spots. (*A*) Representative examples of dendrites expressing K69A $P2X_2$-GFP receptors. ATP had no effect compared with the control. (*B*) Representative examples of dendrites expressing T18A $P2X_2$-GFP receptors. ATP had no effect compared with control. (*C*) (*Left*) 2.5s 100 $\mu$M ATP application did not evoke any membrane currents from this representative hippocampal neuron expressing K69A $P2X_2$-GFP receptors. The cells were healthy because glutamatergic excitatory postsynaptic currents were observed (downward deflections). (*Center*) 2.5 s 100 $\mu$M ATP-evoked currents (5 min apart) from a single hippocampal neuron expressing $P2X_2$-GFP receptors. The second response was larger than the first (see Fig. 5 for further experiments), and there was $<$10% desensitization. (*Right*) 2.5-s 100 $\mu$M ATP-evoked currents (5 min apart) from a single hippocampal neuron expressing T18A $P2X_2$-GFP receptors. Note that the second response is smaller than the first (see also Fig. 5). The traces in *Center* and *Right* are normalized to the peak of the first response.

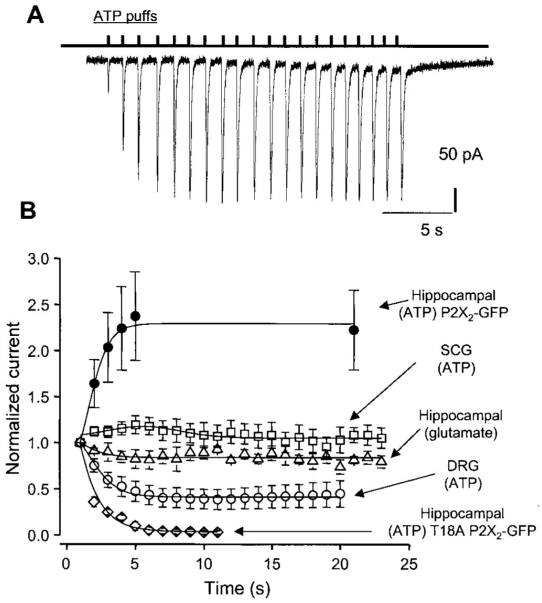


**Fig. 5.** Run-up of the P2X receptor current as a function of activation. (*A*) Representative whole-cell current recording with ATP puffed every second, for a total of 20 puffs. We could not reliably apply ATP at frequencies faster than 1 Hz. (*B*) Effect of repetitive applications of transmitter to neurons, with current normalized to the first puff. The ATP-evoked currents in hippocampal neurons increase as a function of puff number, but glutamate-evoked currents in hippocampal neurons and ATP-evoked currents in superior cervical ganglion (SCG) neurons do not. The ATP-evoked currents in dorsal root ganglion (DRG) neurons show a significant decrease in amplitude as a function of puff number, as do the ATP-evoked currents at T18A $P2X_2$-GFP receptors.

dependent enhancement of the ATP-evoked current. We detected a 66% increase in pixel intensity at the most obvious hot spots after exposure to ATP for 5–10 s. We also detected a 100% increase in ATP-evoked responses after five puffs at 1 Hz. We hypothesize that the clustering (Figs. 3*C* and 5*A*) evoked by the addition of ATP underlies the observed increase in responses to puffs of ATP. There was a difference between the electrophysiology and imaging experiments: whereas the activation-dependent current increase reversed in $\approx$10 s, the increase in pixel intensity and varicosity formation persisted for at least 5 min. Presumably, changes in dendritic morphology (varicosities) that are detected optically, but not electrophysiologically, may explain this difference. Indeed, bright-field images show a change in morphology, and a similar phenomenon was observed with $P2X_2$iresGFP, which directs the expression of cytosolic GFP.

Activation of glutamate receptors results in the formation of varicosities in neuronal processes (28), and the glutamate receptor subunit, GluR1, moves from a cytosolic pool to the plasma membrane during activity in hippocampal neurons (16). These *in vitro* studies are enlightening because glutamate-evoked morphological changes are implicated in the pathogenesis of ischemic neurotoxicity, and GluR1 redistribution may occur during synaptic plasticity (16). The present data are portentous because $P2X_2$ receptor-activation-dependent changes in neuron morphology and receptor distribution may also occur for natively expressed receptors *in vivo*. Indeed, $P2X_7$ receptor-mediated currents in microglial cells show activation-dependent increases (29), and activation of $P2X_7$ receptors evokes changes in cell morphology (30), although changes in $P2X_7$ receptor distribution were not reported. Moreover, changes in superior cervical ganglion neuron morphology occur during P2X receptor activation (11). Interestingly, $P2X_7$ receptors as well as P2X receptors in microglial cells and superior cervical ganglion neurons display the $I_2$ state. The mechanisms underlying P2X receptor-mediated changes in cell morphology are currently unknown, but our data suggest that the higher permeability $I_2$ state of $P2X_2$ receptors is required (5, 11, 20–22) and that perhaps changes previously associated with $P2X_7$ receptors (30) may also occur during activation of neuronal P2X receptors. Fluorescence redistribution and changes in ATP-evoked currents and morphology do not result in cell death because the effects were completely reversible with the brief (up to 10–30 s) applications tested in the present study. Moreover, because the T18A muta-

tion disrupts the protein kinase C consensus site of $P2X_2$ receptors (24), these data are consistent with, but do not prove, the idea that $P2X_2$ receptor properties and redistribution may be shaped by protein kinase C activity.

Native neuronal P2X receptors mediate ATP fast synaptic transmission in the peripheral, enteric, and central nervous systems and presynaptically modulate synaptic transmission (1). In the present paper we have studied $P2X_2$-GFP receptors in hippocampal neurons because these cells are known to express $P2X_2$ receptors (17) and ATP mediates a component of the excitatory postsynaptic current (3). In view of the activation-dependent nature of the redistribution, $P2X_2$ receptor-mediated excitatory postsynaptic currents may undergo short-term modulation, by a postsynaptic mechanism similar to that suggested for glutamatergic synapses (8, 16, 31, 32). Moreover, P2X receptor-mediated changes in neuron morphology may be relevant during stroke when ATP is released. Our data establish redistribution and the formation of varicosities as an interesting functional attribute of heterologously expressed neuronal $P2X_2$-GFP receptors. It remains to be determined whether these effects occur for natively expressed receptors *in vivo*, either physiologically or during disease.

We thank H. Li for preparation of *Xenopus* oocytes and E. Schuman for advice and use of the confocal microscope. This work was supported by a Wellcome Trust (U.K.) Prize Fellowship (to B.S.K.), by a Roche Bioscience Award, and by the National Institutes of Health (NS-11756, MH 49176).

1. Khakh, B. S. (2001) *Nat. Rev. Neurosci.* **2,** 165–174.
2. Khakh, B. S., Burnstock, G., Kennedy, C., King, B. F., North, R. A., Seguela, P., Voigt, M. & Humphrey, P. P. A. (2001) *Pharmacol. Rev.*, **53,** 107–118.
3. Pankratov, Y., Castro, E., Miras-Portugal, M. T. & Krishtal, O. (1998) *Eur. J. Neurosci.* **10,** 3898–3902.
4. Wong, A. Y., Burnstock, G. & Gibb, A. J. (2000) *J. Physiol. (London)* **527,** 529–547.
5. Khakh, B. S., Proctor, W. R., Dunwiddie, T. V., Labarca, C. & Lester, H. A. (1999) *J. Neurosci* **19,** 7289–7299.
6. Collo, G., North, R. A., Kawashima, E., Merlo-Pich, E., Neidhart, S., Surprenant, A. & Buell, G. (1996) *J. Neurosci.* **16,** 2495–2507.
7. Kidd, E. J., Grahames, C. B., Simon, J., Michel, A. D., Barnard, E. A. & Humphrey, P. P. (1995) *Mol. Pharmacol.* **48,** 569–573.
8. Carroll, R. C., Lissin, D. V., von Zastrow, M., Nicoll, R. A. & Malenka, R. C. (1999) *Nat. Neurosci.* **2,** 454–460.
9. Brake, A. J., Wagenbach, M. J. & Julius, D. (1994) *Nature (London)* **371,** 519–523.
10. Grabner, M., Dirksen, R. T. & Beam, K. G. (1998) *Proc. Natl. Acad. Sci. USA* **95,** 1903–1908.
11. Khakh, B., Bao, X., Labarca, C. & Lester, H. (1999) *Nat. Neurosci.* **2,** 322–330.
12. Gentet, L. J., Stuart, G. J. & Clements, J. D. (2000) *Biophys. J.* **79,** 314–320.
13. Ding, S. & Sachs, F. (1999) *J. Gen. Physiol.* **113,** 695–720.
14. Chiu, C.-S., Kartalov, E., Unger, M., Quake, S. & Lester, H. A. (2001) *J. Neurosci. Methods*, **105,** 55–63.
15. Lewis, C., Neidhart, S., Holy, C., North, R. A., Buell, G. & Surprenant, A. (1995) *Nature (London)* **377,** 432–435.
16. Shi, S. H., Hayashi, Y., Petralia, R. S., Zaman, S. H., Wenthold, R. J., Svoboda, K. & Malinow, R. (1999) *Science* **284,** 1811–1816.
17. Rubio, M. E. & Soto, F. (2001) *J. Neurosci.* **21,** 641–653.
18. Gu, B. J., Zhang, W. Y., Bendall, L. J., Chessell, I. P., Buell, G. N. & Wiley, J. S. (2000) *Am. J. Physiol.* **279,** C1189–C1197.
19. Jiang, L.-H., Rassendren, F., Surprenant, A. & North, R. A. (2000) *J. Biol. Chem.* **275,** 34190–34196.
20. Virginio, C., MacKenzie, A., Rassendren, F. A., North, R. A. & Surprenant, A. (1999) *Nat. Neurosci.* **2,** 315–321.
21. Khakh, B. S. & Lester, H. A. (1999) *Neuron* **23,** 653–658.
22. Surprenant, A., Schneider, D. A., Wilson, H. L., Galligan, J. J. & North, R. A. (2000) *J. Auton. Nerv. Syst.* **81,** 249–263.
23. Khakh, B. S., Zhou, X., Sydes, J., Galligan, J. J. & Lester, H. A. (2000) *Nature (London)* **406,** 405–410.
24. Boue-Grabot, E., Archambault, V. & Seguela, P. (2000) *J. Biol. Chem.* **275,** 10190–10195.
25. Zhou, X. & Galligan, J. J. (1996) *J. Physiol. (London)* **496,** 719–729.
26. Cook, S. P., Rodland, K. D. & McCleskey, E. W. (1998) *J. Neurosci.* **18,** 9238–9244.
27. Li, G. H., Lee, E. M., Blair, D., Holding, C., Poronnik, P., Cook, D. I., Barden, J. A. & Bennett, M. R. (2000) *J. Biol. Chem.* **275,** 29107–29112.
28. Emery, D. G. & Lucas, J. H. (1995) *Brain Res.* **292,** 161–173.
29. Chessell, I. P., Michel, A. D. & Humphrey, P. P. (1997) *Br. J. Pharmacol.* **121,** 1429–1437.
30. Virginio, C., MacKenzie, A., North, R. A. & Surprenant, A. (1999) *J. Physiol. (London)* **519,** 335–346.
31. Lissin, D. V., Carroll, R. C., Nicoll, R. A., Malenka, R. C. & von Zastrow, M. (1999) *J. Neurosci.* **19,** 1263–1272.
32. Carroll, R. C., Beattie, E. C., Xia, H., Luscher, C., Altschuler, Y., Nicoll, R. A., Malenka, R. C. & von Zastrow, M. (1999) *Proc. Natl. Acad. Sci. USA* **96,** 14112–14117.